Modelling of a Particle Orientation in Bio-Based Aggregate Concretes

Williams, Joe

Award date:
2017

Awarding institution:
University of Bath

Modelling of a Particle Orientation in Bio-Based Aggregate Concretes

Submitted by

Joseph Peter Williams

For the degree of Doctor of Philosophy

of the

University of Bath

Department of Architecture and Civil Engineering

September 2017

Abstract

The building sector is currently unsustainable in many respects mostly as a result of the material palette used. Bio-aggregate composites such as hemp-lime are high performance and sustainable to produce, meaning they offer a great opportunity to improve the sustainability of buildings in both construction and operation.

The main current obstacles to the more widespread use of bio-aggregate composites is the conservatism of the construction industry and perceived risk of using alternative materials. Improving our understanding of what determines the properties of bio-aggregate composite will lower the perceived risk and help establish them within the sector.

This thesis seeks to achieve an improved understanding of how the properties most relevant to industry, mechanical performance and thermal conductivity, are determined as a result of the inherent constituent and production variables of bio-aggregate composite. The level of understanding targeted is to put bio-aggregate composite on par with more established composite materials by enabling performance criteria led design through behavioural models. Specific focus is directed to the internal structure of the material which is anisotropic to a variable extent and so has a large and directional bearing on the behaviour.

To assess the internal structure of bio-aggregate composites, a novel method was developed using two dimensional image analysis. The method is unique to the study and was able to provide a quantitative assessment of the degree of directionality within bio-aggregate composites allowing the impact of differing variables on the internal structure to be assessed.

An extensive experimental program was undertaken to assess the impact of key variables on the internal structure, thermal conductivity, compressive strength and flexural strength of hemp-lime with a view to linking these behaviours to the production method via the internal structure. All tests were conducted bi-directionally to account for material anisotropy. The constituent variables considered were the aggregate particle size distribution and the ratio of aggregate to binding matrix while the production variables considered were the size of material layering, level of compaction and basic method of

implementation, making the program reflective of the most easily specifiable aspects to industry.

Results for the experimental program demonstrate that the material is highly anisotropic in its internal structure with the degree of directionality determined by both constituents and production. The properties of the composite were found to be bi-directional with variables having a directionally dependent impact on the behaviour as a result of affecting the structure. The findings from the experimental program indicate that there are serval opportunities for optimising the performance of the material within a walling context through manipulating the internal structure.

Based on the experimental findings, a bi-directional model that accounts for the variable anisotropy of the internal structure was proposed and fitted to the experimental data gathered to predict compressive strength, flexural strength and thermal conductivity. The model was able to account for the directional impact of all variables considered with a close fitting to the experimental data sufficient for it to be a viable specification tool.

Acknowledgments

Firstly I would like to thank both of my supervisors for their support and guidance in the production of this work but also more broadly over the last three years. The generosity of time and thought that Mike Lawrence and Pete Walker have shown has been humbling and inspiring. I would also like to thank the wider department and indeed wider university for their support and the friends and colleagues I have worked with along this journey. Finally within the university I would like to extend a special thanks to all of the support staff in the laboratories who essentially facilitated all the experimental aspects of the study. Outside of the university I would like to thank my partner Sophie for her unwavering support and belief over the last three years. Finally I would like to thank my parents for their support and encouragement and particularly my long suffering mother who, I promise, will never have to proof read a thesis again.

Table of contents

List of figures

List of tables

List of Symbols

Upper case Latin

A	Area
C	Compaction of fresh bio-aggregate composite mix
D	Displacement
F	Force / Function
IQR	Inter quartile range of population distribution
N	Total population number
P	Probability
T	Temperature

Lower case Latin

a	Absorption (in situ) / Linear fitting constant
b	Cross section breadth / Linear fitting constant
c	Linear fitting constant
d	Cross section depth
f	Frequency
h	Height of specimen
k	Hydration ratio of binder paste
l	Length
m	Mass / First order moment
n	Number / Power constant
q	Thermal power

s	Shape factor
u	Second order moment
v	Volume
w	Width
x, y, z	Cartesian coordinate descriptors

Upper case Greek

ϕ	Aspect ratio

Lower case Greek

ε	Strain / Peak strain
θ	Orientation
λ	Thermal conductivity
ρ	Density
σ	Stress / Peak stress
φ	Porosity

Subscripts

Used to denote material or property being referenced

p	Particle
px	Pixel
i	Index variable
b	Binder
$b*$	Binder (modified)
a	Air

h	Hemp (solid phase)
c	Composite
w	Water
s	Solid phase
$p1$	Particle primary axis
$p2$	Particle secondary axis
m	Macro scale
$\|\|$	Idealised parallel arrangement
$\perp$	Idealised perpendicular arrangement
C	Compressive
F	Flexural

Superscripts

Used to denote orientation being considered

$\|\|$	Property parallel to casting direction
$\perp$	Property perpendicular to casting direction

1 Introduction

1.1 Wider context of research: Sustainability within construction

Sustainability is a simple principle that must be necessarily adhered to in all aspects of life if our society is to be maintained.

Sustainable as defined by the Oxford English Dictionary: "Capable of being maintained or continued at a certain rate or level." (Oxford English Dictionary)

The implications of applying sustainability to the building industry are however complex and multifaceted due to the number of resources utilised and processes applied in the construction and occupation of a building: for example many insulation materials that improve the sustainability of building operation are not sustainable to produce from a materialistic viewpoint.

In its most basic interpretation, buildings require physical material resources to construct. The scale of this is significant with some 40% to 50% of all natural resource use accountable to the industry (Miller and Ip, 2013). While some of these resources can be procured sustainably, through the use of renewable bio-based materials for example, or through recycling, such as the case of metals, careful management is still required to ensure this occurs. Other materials such as aggregates, the most heavily mined and utilised construction resource in the world (Langer and Arbogast, 2002), are not replenished or always easily recovered for recycling. Use of such resources is therefore not ultimately sustainable despite their apparent abundance. While an apparently inexhaustible supply may be used to diminish the argument against the use of aggregates, slow depletion results in an increase in the cost and impact of extraction, presenting an economic and environmental case to reduce use (Langer and Arbogast, 2002).

Energy is another resource consumed by buildings both in production (material extraction, transport, processing) and operation (heating, cooling, lighting and venting) Energy use is often directly equated to carbon dioxide emissions and consequently tied to global warming, meaning the basic sustainability of energy generation gets overlooked. Considering just energy generation, irrespective of side effects of method, energy sustainability requires us to use less energy than we can indefinitely generate. As our main

energy source, fossil fuels, is forecast to start running out within a few centuries (Shafiee and Topal, 2009), a sustainable level of energy use going forward is considerably less that we currently use. Building operation within Europe is estimated to account for 40% to 45% of total energy use and so is a big part of our current excess demand (Huovila, 2007). Embodied energy associated with the construction of the building is often a lot smaller over a full service life although as buildings are made operationally more efficient, its weighting in our energy use will increase (Franzoni, 2011, Storey, 2008). Reductions in both these demands will be required to bring energy use to a level that is in line with our sustainable production capability.

The higher than natural rate of carbon dioxide emissions into the atmosphere brought about by our high use of fossil fuels is causing an increased greenhouse effect producing climatic changes. These changes are already causing great problems in terms of sea level changes and altering precipitation patterns. This will increase our exposure to natural disaster and impact our food generation capacity and thus our emissions are clearly unsustainable (Field et al., 2014). As a direct function of its manufacture, the production of cement releases carbon dioxide, accounting for 7% of total global carbon dioxide emissions (Meyer, 2009) while indirectly the high energy burden of buildings coupled with a primarily fossil fuel based generation significantly builds on this contribution. The production of buildings is estimated to account for 10% of the world's carbon dioxide emissions alone (Karus, 2005) while almost a half of the UK's total emissions can be attributed to building occupation (Department for Business Innovation and Skills, 2010). The building industry must reduce its energy demand and use of cement in order to help reduce emissions of carbon dioxide to sustainable levels.

A final and often overlooked aspect of building sustainability is the production of waste material. Our ability to dispose of un-recyclable waste is ultimately limited by the capacity of landfill which must be considered finite. Indeed, as is seen with extraction of materials, as the resource depletes, the cost and ecological impact increases and so despite the apparent vastness of the resource there are economic and environmental incentives to reduce landfill use, Figure 1.1. The construction industry accounts for 45% to 65% of all solid landfill waste disposed of by developed countries (Franzoni, 2011) and so is a vast problem for the industry. In a large part this is due to the limited recyclability, reusability and degradability of the materials used which in turn drives a higher demand requirement for extraction of new material. A move towards more recyclable materials would therefore both reduce the development of waste as well as reduce the demand for resource extraction.

In drawing together just these aspects of sustainability, it is apparent that the fabric of a building is of critical importance. The materials used must themselves be as sustainable as possible to source and decommission in all of the metrics discussed to allow for sustainable production. Furthermore, the building fabric must facilitate, when coupled with design, the sustainable operation of the building. This however must not be at the expense of providing a healthy and comfortable space to occupy as it is arguable that producing poor performance buildings that are underutilised is not sustainable regardless of other aspects (Milutienė et al., 2012). If the building industry as a whole is to become sustainable, then renewable, low energy and low carbon construction materials that offer high performance must be employed.

Figure 1.1: Deonar landfill site in Mumbai that is at capacity and competing for space with surrounding grazing land. Photo by Jamie Han (Han, 2015).

1.2 Bio-aggregate composites

A group of materials that goes some way to fulfilling the requirements for the production of sustainable buildings are bio-aggregate composites. Bio-aggregate composites are a mixture of a plant derived aggregate and binding paste that can be monolithically placed in-situ or used to produce building units such as blocks and panels (Bevan et al., 2008). The material is mostly used to provide insulation and bulk to structurally framed walls and roofs but may also be used as a flooring layer. Bio-aggregate composites are generally characterised as possessing low density and high porosity, and exhibiting a low thermal conductivity.

The most common bio-aggregate composite, hemp-lime, was originally developed for the restoration of historic timber framed buildings in France. The first reported use was in the Maison de la Turque in Nogent-sur-Seine during a restoration in 1986 where it was used to infill an oak frame to replace the original wattle and daub (Allin, 2005). As the material was conceived and developed by artisan builders as opposed to large scale industry, the utilisation initially remained relatively small and concentrated in France but has subsequently grown and spread abroad. There are now several hundred examples of hemp-lime buildings in the UK and other countries as well as several thousand in France. The first use of hemp-lime in the UK was in two houses in a housing estate project in Haverhill, Suffolk completed in 2000 (Yates, 2002). Subsequent notable buildings have been the WISE building: Centre for alternative technology, Powys, Figure 1.2; the Adnams distribution centre: Suffolk; the Bright Building: University of Bradford: and the Renewable house: Building Research Establishment, Watford, Figure 1.3.

Being a composite class of materials, the sustainability credentials of bio-aggregate composites is a product of both the separate constituents as well as a combined material.

Figure 1.2: The WISE building, teaching facility utilising hemp-lime external walls, Centre fort alternative Technology, Powys.

Figure 1.3: The renewable house, showcase hemp-lime walled three bedroom house, Building Research Establishment, Watford.

1.2.1 Sustainability of bio-aggregates

Being plant derived, bio-aggregates are theoretically a renewable resource so long as they are grown in a sustainable way. In this respect, the most commonly used plant for bio-composite insulations, industrial hemp, Cannabis Sativa L, Figure 1.4, has particularly beneficial characteristics. Industrial hemp is fast growing and naturally resistant to pests and diseases, allowing it to be used in rotation with other crops and reducing the need for pesticides and herbicides (Miller and Ip, 2013, Decorte, 2011). This allows for high yield at low cost and without encroaching on land otherwise used for food crops; the deep tap root and heavy shading of the plant suppresses weeds and improves soil, making it an actively beneficial crop in dormant fields (Piotrowski and Carus, 2011, Roulac, 1997). Furthermore the reasonably low water requirement and minimal need of fertiliser limits the need for other resources and improves the sustainability of production still further. It has also been suggested that in particular the propagation of hemp may improve local bio-diversity (Piotrowski and Carus, 2011).

Figure 1.4: Industrial hemp being grown for fibre. Photo by Logan Yonavjak (Yonavjak, 2013).

The part of the hemp plant used as an aggregate, as is the case with most bio-aggregates, is the least valuable product of the plant and is a co-product of producing the more valuable aspects such as seeds and fibres (Karus, 2005). This co-product status means that waste from growing hemp and other such bio-aggregate plants is minimised and the cost of the material is lower (Allin, 2005). In the case of the industrial hemp plant it is estimated that almost 100% of the plant is utilisable in a wide range of industries including food, agriculture, and in the automotive, textile and cosmetic industries (Roulac, 1997); Figure 1.5. Not only does this high level of utilisation improve the economic argument for the production of bio-aggregates and industrial hemp in particular, but also means the land fill associated to unused bi-products is effectively zero.

The energy used to produce bio-aggregates is very low. This comes primarily from a combination of low processing energy, the wide distribution of available production sites that can minimise transport energy and the high utilisation factor to the plants (Milutienė et al., 2012). This is particularly highlighted in contrast to some of the materials that bio-aggregate composites could replace within a building such as expanded foam and mineral wool insulations that compared to bio-aggregates have an embodied energy orders of magnitude higher (Hammond and Jones, 2008).

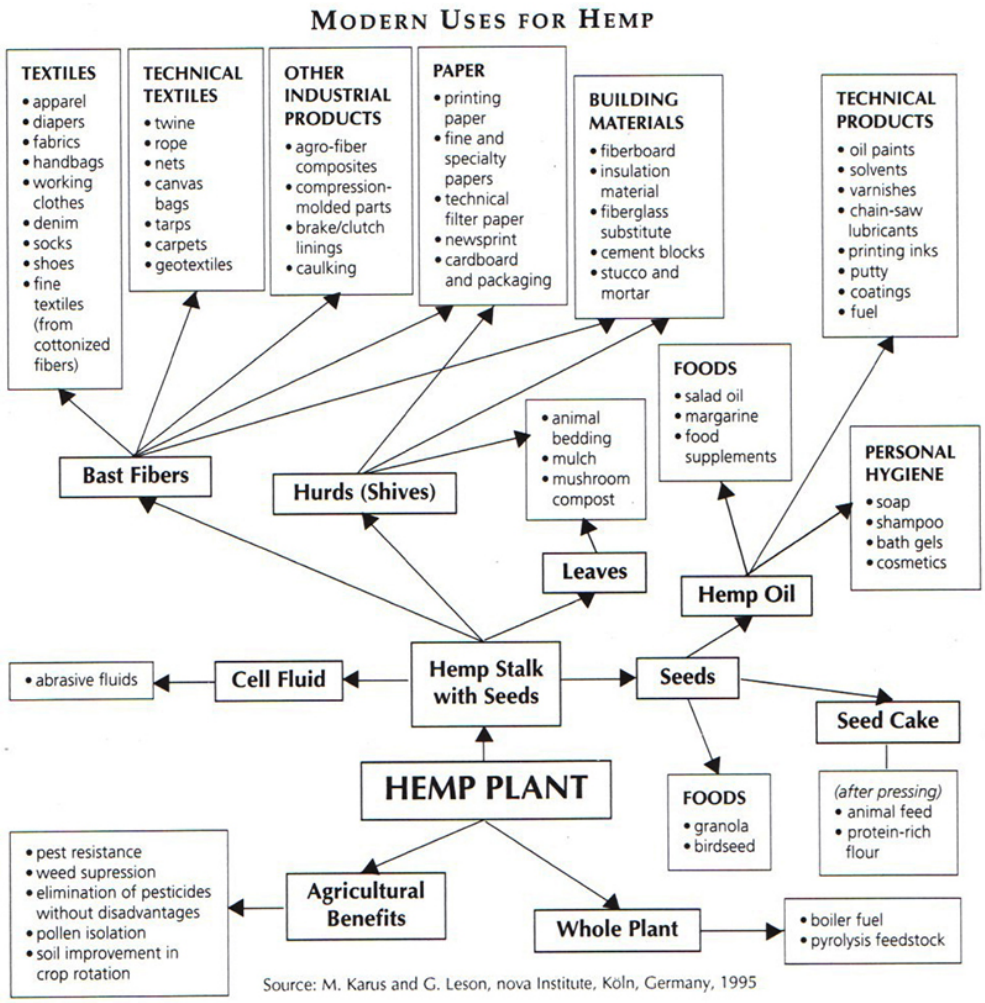

Figure 1.5: The uses of the differing plant of the industrial hemp plant (Roulac, 1997).

As a plant product, bio-aggregates are carbon based with carbon dioxide being sequestered from the air and chemically trapped during growth. Until decomposition, the carbon dioxide remains locked within the material and is effectively removed from the atmosphere for this time. Indeed, so long as the time taken to replenish the resource is significantly shorter than the life of the building, the use of the resource may be considered to remove the carbon from the cycle and be offset against any emissions incurred in the production (Alcorn and Donn, 2010). As a result it may indeed be argued that the production of bio-aggregates has on balance a negative carbon footprint, estimated to be to the extent of -1.4kg of carbon dioxide per 1kg of aggregate produced in the case of hemp (Hirst, 2013). Even if the carbon offsetting of the stored content is not included, the embodied carbon of bio-aggregates remains very low compared to other insulations as a result of the low energy requirements for production mentioned previously.

1.2.2 Sustainability of binders

The binder used in most bio-aggregate composites at the moment is lime. Lime binder is produced from quarried limestone and so is ultimately unsustainable to produce, given our rate of extraction is higher than natural replenishment. Despite this, the quantity of binder used in bio-aggregate composites is low for the volume of material produced, and limestone is a plentiful resource replenished slowly naturally. While the production of lime is not actually sustainable, it may in this context be seen as undepletable. Alternative binders that are truly sustainable to produce such as starch are also being developed (Le et al., 2014, Benitha Sandrine et al., 2015, Le et al., 2015, Balčiūnas et al., 2013).

The energy used to produce the binder depends on the binder in question and may vary considerably; if lime based products are considered then the embodied energy can be quite high. The production of a lime binder requires firing in a kiln at temperatures of around 900°C which is naturally an energy intensive process (Escadeillas et al., 2013). This coupled with the excavation and other associated processing energies results in an embodied energy of 5.3MJkg^{-1} (Hammond and Jones, 2008). While this figure is high, it must be viewed in the context of the small comparable amount used in the formation of composites, around 0.45kg per 1m^2 of a standard wall construction (Pretot et al., 2014). In addition it is notable that the embodied energy figure for lime binder is higher than that of cement, which is 4.5MJkg^{-1}, produced in a similar but higher temperature process using more efficient plant. This indicates that possible reductions to this value are achievable with improved economy of scale and process development.

In terms of emissions, the production of lime binder is again intensive, in part due to the high production energy mentioned but equally due to carbon dioxide being an intrinsic bi-product of the process. In the firing process for both lime and cement, chemically bound carbon dioxide is released as limestone is converted to calcium oxide known as quicklime. This is estimated to account for in the order of 60% to 70% of the total emissions associated with the production of these products (Hammond and Jones, 2008). Some of this carbon dioxide can be reabsorbed in the hardening of lime and secondary phase of cement via carbonation with the whole process being known as the lime cycle, Figure 1.6. With cement it is questionable as to how much of the carbon dioxide may be reabsorbed due to the low porosity of the material. In the case of lime binders, and certainly when used in a bio-aggregate composite, the open porosity is much greater and so it is argued by many that there is more scope for the reabsorption of carbon dioxide. The associated greenhouse gas emissions of lime binders therefore may be considered to be considerably

lower and more sustainable than cement and relatively low in the context of the small amounts used in bio-aggregate composites.

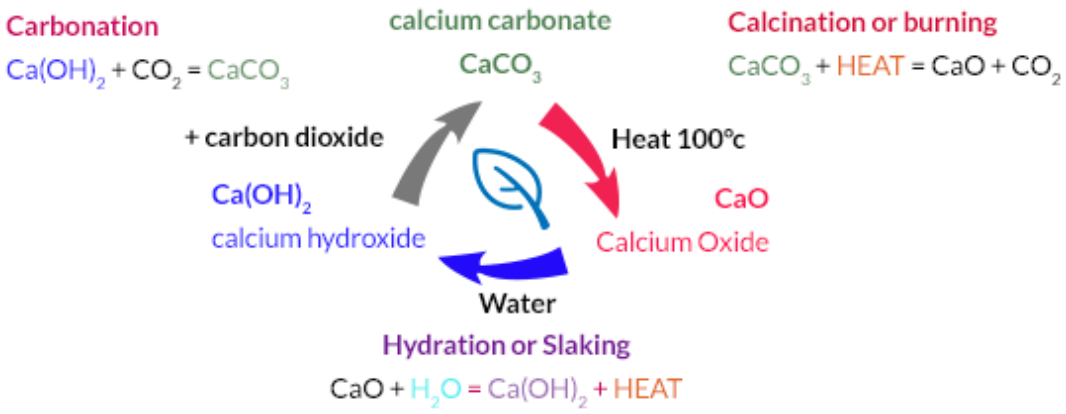

Figure 1.6: The lime cycle. Image from Singleton Birch website (Singleton Birch, 2017).

1.2.3 Sustainability of bio-aggregate composites

As a composite, the overall sustainability credentials are dependent on the individual constituents, their proportioning, the composite performance in the operational phase and the implications of decommissioning. As constituents, bio-aggregates can be considered sustainable to produce in material, energy and carbon terms while a lime based binder is less so. In a composite the ratio of these constituents will then determine the overall sustainability of production. Typically, the volumetric proportion of bio-aggregates dwarfs that of the binder, and so dominates the composite. Resultantly the embodied energy of a standard timber framed hemp-lime wall is estimated to be in the region of 5-6MJ per $1m^2$ of wall (Williams et al., 2017), compared to over $1500MJm^{-2}$ for a traditional cavity wall (Goodhew, 2016). Taking into account the CO_2 sequestration of the bio-aggregate particles, the carbon dioxide emissions associated with the production may be considered negative and in the region of 30kg absorption of carbon dioxide per m^2 of standard hemp-lime wall (Ip and Miller, 2012, Pretot et al., 2014).

As well as being mostly sustainable to produce, bio-aggregate composites have been shown to deliver the levels of performance required for sustainably operating buildings. The most critical aspect of performance for building fabric is the thermal conductivity as this broadly determines the heat loss and thus heating requirement of the building; importantly it is also the basis of most code based thermal design. The thermal conductivity of hemp-lime is generally found to range between 0.07 to $0.11WK^{-1}m^{-1}$ (Benfratello et al., 2013, Collet and Prétot, 2014, Magniont et al., 2012, Sinka and Sahmenko, 2013, Arnaud, 2000, Pierre et al., 2014, Balčiūnas et al., 2013). In comparison

to some insulation materials this is quite high however as hemp-lime is mostly used for a full wall thickness, it remains low enough to provide a wall U-value in compliance with UK building code requirement in a wall of around 200mm in depth (Bevan et al., 2008). These values, as with the embodied energy and carbon, are naturally dependent on the design of the bio-aggregate composite and its constituents although these approximate figures certainly indicate the potential of the materials to deliver the performance required for sustainable heating energy use.

The actual thermal performance of a building is more complex than just the thermal conductivity of the fabric which is a steady state property. In reality buildings exist in a dynamic thermal environment and so the ability of a material to store and release heat during periods of higher and lower temperatures, such as day and night fluctuations, also impacts on the demand for heating (Hasnain, 1998). Unlike many other insulation infills that have limited capacity to store and release thermal energy, bio-aggregate composites, and particularly hemp-lime, have been shown to excel in this respect (Collet and Pretot, 2014, Evrard and De Herde, 2010, Tran Le et al., 2010, Evrard, 2008). As a result of this, hemp-lime buildings tend to outperform other constructions built to the same thermal specifications: a hemp-lime building in the UK was measured to have a similar energy use to a traditionally constructed building of higher U-values while also maintaining a higher and more stable internal temperature over the heating season (Yates, 2002).

Responsible for the dynamic thermal response of hemp-lime is a hygrothermal mechanism that results from the complex, interlinked network of multi-scaled pores present (Evrard, 2008). This structure makes the material highly permeable to the environment around it to which it will constantly equilibrate. Equilibration occurs through the condensation and evaporation of moisture within the pores and through this phase change of moisture, the material is able to store and release latent energy (Hustache and Arnaud, 2008, Evrard, 2008, Arnaud et al., 2013b). The effect of this is to provide an apparent thermal mass that increases the time taken for the material to reach a steady state condition and acts as an effective buffer when in fluctuating temperatures. As mentioned, this, when combined with design that takes advantage of it, may have a significant beneficial impact on the heating and cooling loads of a building as well as increasing perceived indoor comfort. While hygrothermal properties are currently under represented in building codes, the scope for hemp-lime and other similar bio-aggregate composites to provide building that are sustainable to heat and cool is unquestionable.

A further aspect of a building's energy performance and thus operational sustainability is how it handles air. Air refreshment is a requirement of comfort, however it is undesirable

if it is uncontrolled due to the potential loss of thermal energy it may incur (Pérez-Lombard et al., 2008). Relatively airtight building envelopes with controlled ventilation are therefore beneficial and bio-aggregate composites, particularly when produced as a monolithic structure, are able to provide this performance without the need for additional components (Duffy et al., 2014). The main requirement for fresh air is often to handle moisture and indeed this is a key air quality measure (Fang et al., 1998). Due to the complex porosity and interplay with moisture that hemp-lime exhibits, it not only buffers temperature fluctuations but also is effective at buffering moisture. This reduces the need for excessive air refreshment and further reduces a building's energy demand while also helping to produce a stable and comfortable internal environment required for the continued utilisation of a building (Woloszyn et al., 2009, Osanyintola and Simonson, 2006, Evrard, 2006).

The last aspect to consider is the decommissioning and waste generated at the end of life. With a lot of composite materials, a problem exists in separating the components in order to reuse, recycle or effectively dispose of the constituents (Yang et al., 2012). In this respect bio-aggregate composites share this pitfall as it is indeed difficult to separate the binder and bio-aggregates for reuse although it is possible to crush the material to produce binder coated aggregates that could be reused in a similar way to our current use of crushed concrete as concrete aggregate (Wijayasundara et al., 2017). Bio-aggregate composites however may circumvent this through a diminished need to segregate the components. Both constituents within bio-aggregate composites are natural materials that can safely be disposed of in land fill without pre-treatment if required. The bio-based nature of the aggregates furthermore means that they will naturally decompose over time in this environment (Micales and Skog, 1997). As this is the main component this means that the composite as a whole is able to predominantly rot away and may be effectively composted in the correct circumstance. Crushed hemp-lime for example could be spread over fields as a weed supressing mulch or direct replacement for agricultural lime to improve the soil and moderate pH levels.

Overall bio-aggregate composites offer an alternative option to traditional infill insulation materials and associated walling systems that can be produced, implemented and decommissioned in a considerably more sustainable way against all metrics. The properties of the materials are such that they have the potential to produce buildings that are sustainable to occupy and indeed naturally healthy and comfortable. In the context of a building industry that is required to become more sustainable, it is clear that these materials offer very great potential.

1.2.4 The need for research

Despite the notable sustainability credential of bio-aggregate composites, the uptake of them is limited. In part this must be considered as a result of a conservative industry that is traditionally slow to embrace new materials and also due to some of the labelling of natural building materials (Lawrence, 2013). Indeed there is a culture within the UK of being sceptical of anything other than "bricks and mortar" and natural materials are often pigeonholed as "alternative". Deeper than this is a possible general lack of trust about the reliability, performance and durability of natural materials (Nozahic and Amziane, 2013, Duffy et al., 2014). It is possible that some of these views will only change with time, however if the use of bio-aggregate composites is to be increased then it is crucial that their behaviour is well understood and predictable to allow it to be trusted.

In order for a building material to gain traction within the industry, a level of understanding should ideally exist so as to enable reliable design to performance criteria. Such understanding will result in relatively predictable, certifiable performance with limited analysis: for example a reinforced concrete beam may be designed to a loading requirement and predicted to meet that performance without the need for physical testing. This is particularly the case with composite materials where the variation available within specification is large and the performance so dependent upon it. Being able to predict the performance of a specified material is not only necessary to demonstrate code compliance but also to demonstrate understanding of the material sufficient to breed confidence. Given bio-aggregate composites' artisan development and only more recent scientific assessment, there is a lack of effective design principles beyond established rules of thumb and some practical guides that do not currently provide this confidence.

Outside of a basic requirement for a more complete set of design principles and performance predictors, there are additional logistical barriers currently limiting application opportunities. A major one of these is the prolonged hardening and drying time for the material (Bevan et al., 2008, Stanwix and Sparrow, 2014). The lime binder used with most bio-aggregate composites requires the presence of water to set and initially form a workable material. As bio-aggregates also tend to be hydroscopic, it is often the case that an excessive amount of water is necessary meaning the initial moisture content of the cast material is high and is required to reduce considerably prior to the application of finishes (Lanos et al., 2013). If this drying is conducted on site it may not only have a big impact on the critical path of the project but may also dictate seasonal timing (Duffy et al., 2014). The development of binders will necessarily play a big part in

addressing this although these will take time to develop and are not guaranteed to give the same hygrothermal or mechanical properties. The development of new construction methods such as the offsite casting of units and projection forming can already offer plausible solutions but are comparably unstudied within the field. There is only limited assessment of how such methods may alter the properties of the materials, so uncertainty over specification may be greater still. This is limiting the uptake of such methods meaning the logistical problems remain unresolved until confidence and understanding grows.

It becomes clear then that, while the sustainable credentials of bio-aggregate composites are evident and the potential impact is high, take up is hampered by preconceptions and prejudices as well as uncertainty and logistical difficulties. To start to address this it is clear that there is a requirement for a performance-led design framework to be developed for the specification of bio-aggregate composites that will remove some uncertainty and include universal applicability across all implementation methods.

1.3 Aims and objectives

1.3.1 PhD aim

From what has been discussed in the introduction, the aim of the PhD may be distilled as thus:

To develop an understanding of bio-aggregate composites sufficient for performance criteria led specification of products.

A level of understanding of key properties is required whereby performance-led specification of the materials may be undertaken. Such understanding will provide greater access and confidence in specifying such materials in projects by providing a basis for informed design to set performance criteria in a way that the construction industry has adopted for most materials. In addition the understanding brought will enable the informed development of the materials and products, specifically in the precast arena where many of the logistical barriers may also be overcome.

1.3.2 Objectives

A series of objectives were established to guide the study based on a detailed consideration of the project aim within the context of the previous work discussed in the

following literature review. The objectives are a logical progression towards fulfilling the project aim and are thus addressed in sequence presented within the rest of this manuscript: the first objective addressed in section three, the second and third objective addressed in section four, and the last objective addressed in section five.

Objective 1: Establish a method of classifying and numerically analysing the degree of orientation within the internal structure of bio-aggregate concretes.

As will be discussed in the review of literature, there is previous evidence that several of the key physical properties of bio-aggregate composites are directionally dependent. It is widely theorised that this may be the result of an anisotropic internal structure of the materials based on objective speculation about the forming process and qualitative visual assessment. Prior to this study there was no direct assessment or classification of the internal structure and indeed no established method for doing so. As the internal structure is unquestionably a determining factor to the transfer of heat and force, having a fully informed picture of the internal structure of bio-aggregate composites was seen as critical in being able to model behaviour. Furthermore, it was considered likely that the degree of orientation within the material would be determined by mainly controllable factors and thus a quantitative means of comparing directionality and assessing its impact upon key performance criteria was also considered necessary in the context of the project aim.

The planned outcomes of this objective were twofold:

1. to conclusively demonstrate that bio-aggregate composites have an orientated internal structure as a result of the particle nature and production process as speculated in the literature, and
2. to develop a reliable method to numerically quantify the degree of orientation within such materials.

The first part of this is important to building the understanding of the material's structure that may inform modelling as well as future experimental works; as will be shown in the literature review it is often not reported in what orientation tests are conducted. This would not be appropriate if the material is known to be anisotropic. The second part is important for the subsequent experimental works where the aspects that determine this parameter, and indeed if it has bearing on material properties, will be considered.

The criterion for evaluating the successful meeting of this objective was based on the methodology developed. The key measurable factors defining a successful method in this

case were the production of repeatable and insightful results and the applicability to this and other studies in practical aspects such as ease of process, cost and time.

Objective 2: Link the variables associated to production method to the internal structure and key physical properties of bio-aggregate composites.

The production process naturally has an impact on the physical properties of the material. It was observed, as will be seen in the literature review, that several variables within the production process lack a full assessment and that the majority of the previous work was not conducted with respect to a possible orientation within the material. There was no previous study to assess the impact that production variables have on the internal structure of the materials. To fully address the project aim it was thus required to conduct a full, multi-directional assessment of what impact key, specifiable, production variables have on relevant properties used as performance requirements.

The planned outcome of this objective was a complete data set of how key production method variables impact the internal structure of the materials and the major properties in all relevant directions. This outcome was primarily desirable to establish how these aspects impact performance in relation to the direction of applied loading as previous work often assumed a global impact. The data regarding the internal structure was desired to enable a greater understanding of any observed trends that may be later applied to the modelling of such behaviour. As the variables considered are an intrinsic part of current practice and easily altered, the outcomes of this objective were predicted to have immediate relevance to industry in terms of informing process selection.

This objective was measured for success based on the establishment or otherwise of meaningful correlations within the dataset produced. Specifically it was important to establish if the variables had a measurable impact on the internal structure of the material and if this may be related to any change in physical properties in differing directions.

Objective 3: Link the constituent variables to the internal structure and key physical properties of bio-aggregate composites.

It is evident that the constituents of a composite will have an impact on its properties; as indeed has been shown and will be discussed in the review of literature. As with the production variables, the existing knowledge on this topic is limited, mainly for its lack of consideration of a directional dependence. Similarly there is no previous assessment of the

internal structure with respect to the constituent variables that may inform behavioural modelling. To allow for full addressing of the aim it was thus required to conduct a full, multi-directional assessment of what impact key, easily specifiable constituent variables have on relevant properties used as performance requirements.

The planned outcome of this objective was a complete data set of how key constituent variables impact the internal structure of the materials and the major properties in all relevant directions. As with the previous objective, this outcome was desirable to establish how these aspects impact performance in relation to the direction of applied loading, and to enable a greater understanding of any observed trends that may be later applied to behavioural modelling. As the variables considered are again an intrinsic part of current practice and easily altered, the outcomes of this objective were predicted to have immediate relevance to industry. The combined outcome of this and the previous objective were planned to give a detailed and relatively complete picture of how all the variables open to a designer or product manufacturer determine relevant properties and go a significant way to achieving the project aim.

Like the previous objective, this objective was measured for success by determining or otherwise a correlation between the variables considered and the directional performance data gathered.

Objective 4: Model key physical properties of bio-aggregate composites in a directional context based on the internal structure and main design variables.

The previous objectives act as necessary stepping stones to the production of behavioural models that account for any anisotropy and may be used to predict performance, based on the main design variables of the material. A series of behavioural models fulfilling this objective, as will be seen in the literature review, was absent from previous work and would achieve the project's aim of facilitating performance criteria led design of these materials.

The planned outcome of achieving this objective was a number of behavioural models that may be used to predict performance, show compliance to performance criteria and be used to inform design and specification. This would be directly applicable to all facets of industry as well as to future research. By incorporation into an optimisation loop, establishing the performance boundaries of current production methods and identifying possible areas where further development should be focussed were also considered

outcomes. The outcomes will inform directly the recommendations at the end of this manuscript for further research and development opportunities.

This objective was measured for success in several ways. The behavioural models were firstly required to give a level of correlation to the experimentally derived data as to be sufficient for reliable specification to particular design conditions. Secondly, the models needed to be based on the specifiable design variables available within industry currently, to be a useful and accessible tool. Lastly, the models needed to be usable as performance optimisation tools in order to be a useful legacy to further studies.

1.4 Thesis layout

This thesis is comprised of six chapters. Chapter 2 reviews relevant previous published work and sets the finer context of this PhD's contribution to the field. In particular emphasis is given to previous experimental study and theoretical modelling of mechanical and thermal behaviour.

Chapter 3 details the pilot study that was undertaken to develop a new methodology for measuring levels of particle orientation within bio-aggregate composites. The program results and conclusions from this phase of work are presented as well as the resulting methodology taken into the main body of work.

Chapter 4 is comprised of four main sections. The first two sections set out the framework of the experimental work. The procedures and methods are described for conducting of all mechanical and thermal testing and the raw materials used are characterised. The latter two sections detail the specific program of experiments conducted and results obtained for assessing the impact of constituents and production process on the bi-directional properties of hemp-lime respectively.

Chapter 5 presents a theoretical model for the behaviour of hemp-lime that is fitted to the data presented in Chapter 4.

Overall conclusions and reflections on how the thesis meets the aim and individual objectives of this PhD are presented in Chapter 6 alongside recommendations for industry and future work.

2 Literature review

2.1 Introduction

This chapter will critically review the body of available literature relevant to this study. The review commences by considering properties of the individual constituents used to produce bio-aggregate composites as well as variations in implementation and formulation of composites. The main bulk of the review then considers the impacts of these variables on the internal structure, mechanical properties and thermal properties in turn. In each of these cases particular note is also paid to material anisotropy and ways of modelling behaviour, key aspects of this study. As hemp-lime is the most established and studied bio-aggregate composite, the majority of the literature reviewed focuses on this material, however not exclusively. The summary of the review's key outcomes are collated at the end of the chapter where the implications for the study are discussed in terms of experimental design and process.

2.1.1 General comments on the body of literature

The first publications relating to the characterisation of bio-aggregate composites and specifically hemp-lime as a building material come from France in the form of a PhD thesis (Garcia-Jaldon, 1995) and set of technical guidance for implementation (Courgey, 1993). Further published work remained very limited from this first emergence up until around 2005 when seminal works (Arnaud, 2000, Collet, 2004) and reports of building performance (Yates, 2002) identified the hydrothermal attributes of hemp-lime that have generated subsequent interest. As the use of and interest in bio-aggregate composites have broadened, so has the breadth of literature available. The current focus of literature is directed mainly on quantifying and modelling the hydrothermal behaviour (Aït Oumeziane et al., 2017, Mazhoud et al., 2017), and optimisation of the basic structural and thermal properties (Brzyski et al., 2017, Niyigena et al., 2017, Nguyen-Sy et al., 2017).

Study of bio-aggregate composites is now undertaken across the world including Canada (Bütschi et al., 2004) and China (Ning and Bing, 2015) but is still mainly focused in Europe, particularly France, Belgium, Sweden, Ireland, Latvia, Italy and the UK. The main research hubs currently undertaking experimental investigation of hemp-lime and other bio-

aggregate composites are the Université de Toulouse, Université de Bretagne Sud, Université Blaise Pascal and the Université de Rennes in France; Riga Technical University in Latvia; Trinity College in Ireland and The University of Bath and Queens University in the UK.

Alongside the scientific publications and accompanying unpublished work there is an additional body of less scientific literature designed to engage the wider public. The purpose of this literature is often to increase awareness of and promote the material but it also often also covers some of the more practical aspects of using the material. Examples of these publications are the promotional material produced by manufacturers of hemp-lime systems (Tradical®, 2015), general data sheets produced by building institutions such as the BRE (Sutton et al., 2011) and books authored by champions and practicing builders (Bevan et al., 2008, Allin, 2005, Stanwix and Sparrow, 2014). While this grey literature is often less scientific and of less certain reliability, it remains a useful resource for a material that is still mostly used by a small group of knowledgeable crafts people.

2.2 Properties of bio-aggregates

By far the most commonly used bio-aggregate derives from the industrial hemp plant. Other aggregates used derive from rice husks (Chabannes et al., 2014, Chabannes et al., 2015a), flax (Khazma et al., 2014, Rahim et al., 2015), sunflower (Chabannes et al., 2015b, Nozahic et al., 2012) and rape (Laidoudi, 2015, Ning and Bing, 2015) as well as other plants but in comparison to hemp their use is minimal. Hemp aggregates will therefore be the primary focus of this section.

The industrial hemp plant (*Cannabis Sativa L*) is grown across the planet primarily as a source of fibre, seed meal and oil. The hemp derived bio-aggregate, the woody stalk chippings known as shiv, is a less valuable co-product that has alternative uses as animal bedding and biomass fuel (Nozahic and Amziane, 2013). According to the congressional research service, in Europe approximately 40,000 tonnes of hemp shiv is produced per year with the biggest producer being France (Johnson, 2010) although production varies and this figure is possibly now outdated. The growing of hemp plants in rotation with food crops is reported to require limited resources, water fertiliser and pesticide, and has been linked to several benefits including the increase of bio-diversity, aeration of the soil and suppression of weeds (Piotrowski and Carus, 2011, Decorte, 2011). While it is difficult to find direct evidence for some of these claims it remains clear that hemp is a viable and low environmental impact resource.

Hemp bio-aggregate originate from the stem of the hemp plant which is broadly typical of bast fibre plants: tubular with fibres arranged at the outer layers (Picandet, 2013). The xylem of the hemp plant, the woody material providing structure for the stem and transport of minerals, is removed from the rest of the stem and forms the aggregate. The aggregate is cited as accounting for 85% of the plant stem (Picandet, 2013) and 40% to 60% of the plant mass (Evrard, 2003). Traditionally, to separate the fibres and the bio-aggregate, a process of retting is used: lying the cut plant out in the field to allow microbes to break down the bond between fibres to the xylem (Vignon et al., 1996). While this can still be used, the mechanical process of hammer milling is now more common (Picandet, 2013). The outputs of this process are broken up particles of hemp shiv, hemp fibres and dust. In some cases the hemp shiv may be further milled in order to produce finer particles or segregated into a range of grades for differing applications. In all cases the hemp shiv will be bagged on site and undergo no additional preparation prior to use in composites (Vignon et al., 1996).

Due to the range of growing conditions and processing options available, there is going to be inherent natural variability between the product originating from different producers (Picandet, 2013) and indeed this may be considered common to all bio-aggregates. The impact of this variation on the product can be considered at three levels: properties of the particles, the particles' size distribution, and the bulk properties of the material; literature pertaining to which will now be considered in turn.

2.2.1 Particle properties

The chemistry of the bio-aggregate particles is that of the cell walls in the plant from which they come. In the case of hemp this is a combination of mainly cellulose, hemi-cellulose and lignin with additional pectin, ash and waxes (Picandet, 2013). Of the components, cellulose and lignin can be considered the main structural components while soluble elements such as pectin and hemicellulose are considered to influence the hydration of binders (Nozahic and Amziane, 2013, Amziane et al., 2015). The ratio of these and the other chemical components therefore has relevance to both the physical properties of the aggregate and any composites formed. The ratio of these components within hemp samples is reported by several (Table 2.1) and displays variation across the literature.

Table 2.1: Chemical constituents by mass of hemp bio-aggregates presented by different studies.

Study	Cellulose	Hemi-celluloses	Lignin	Pectin	Other
(Garcia-Jaldon, 1995)	48	12	28	6	6
(Vignon et al., 1996)	44	18	28	4	3
(Allin, 2005)	37	16.5	21.8	5	19.7
(Stevulova et al., 2012)	44.3	27.2	22	-	6.2
(Gümüşkaya et al., 2007)	40-48	18-24	21-24	-	21-4
(Evrard, 2008)	50-60	15-20	20-30	-	4-5
(Cigasova et al., 2013)	44.2	30.3	24.4	-	1.1
(Magniont and Escadeillas, 2017)	34.5-52.0	9.0-34.5	18.0-28.0	-	4.0-12.4

The methodologies used for collecting the results in Table 2.1 are consistently not reported and the influence of the method on experimental outcome is unknown. It is not therefore appropriate to apportion the full variation seen across the literature to differences in the material alone however the range reported in individual studies such as the RILEM report of 2017 (Magniont and Escadeillas, 2017) may give an idea of this. The most cited reason for a variation in the reported chemical make-up of hemp aggregates is the differing locations and conditions of production (Bouyer, 2008); it is logical that the conditions plants are grown in and time of harvest will contribute to their chemistry. While data are only correlated here for hemp, it is likely that similar variations are found in the reported chemistry of other bio-aggregates however there is insufficient data available to confirm this.

The micro structure of hemp bio-aggregates has been studied by several using scanning electron microscopy and 3D computer tomography imaging as well as various direct and indirect methods of gauging porosity. Like the chemistry, it can be assumed that the microstructure of bio-aggregates will have bearing on the mechanical and thermal properties of the particles and composites. It is agreed in the literature that hemp bio-aggregates have a highly porous open structure with pores generally aligned along the stem of the plant and thus the long axis of the particle (Hustache and Arnaud, 2008). The range of porosity and size of the pores found in the literature is given in Table 2.2.

As with the chemistry pore size obtained is observed to vary between differing studies. This must be at least in part a result of differing methodologies between studies: scanning electron microscopy allows only for a very limited sample of material and is restricted to measurements in a two dimensional plane whereas 3D computer tomography allows for a larger sample and assessment in any direction. Such differences may account for the identification of larger pores through 3D computer tomography imaging, not observable in scanning electron microscopy, and the absence of smaller pores due to a limit of resolution (Hustache and Arnaud, 2008). It is therefore not reliable to say if the range of pore sizes in hemp particles alters with production at this time. An in depth review of methods of gauging the distribution of pore sizes within the context of bio-aggregates has recently been published (Lawrence and Jiang, 2017) and indicates the possible future use of a number of methods not included in Table 2.2 such as mercury intrusion porosity and dynamic vapour sorption that could provide greater incite.

In the studies reporting values of particle porosity the methods again vary and, in many cases, the methods extrapolate from other parameters making cross study comparisons void. Fortunately the study of Chabriac (Chabriac et al., 2016) used a consistent method across five different producers of hemp as well as five grades of particles from a single producer allowing influence of these variables to be assessed. The method employed did not directly measure porosity but rather inferred it from acoustical parameters; the results were also not calibrated with direct measurements. While it is therefore questionable if the results are truly representative they remain valid for comparison and clearly demonstrate that hemp origin has bearing on the porosity. This is attributed by the authors to both the growth of the plant and the processing and thus it would be feasible to assume such variation is likely in other bio-aggregates although there is not sufficient data available to confirm this. It was also observed that porosity varied with grade of particle, reasoned as finer grades originating from the thinner top of the stem; segregation and processing of particles are therefore also possible contributors.

Table 2.2: The pore size and porosity of hemp bio-aggregates presented by different studies.

Study	Porosity	Pour size (microns)	Methodology
(Nguyen et al., 2010)	-	10-50 wide 80 long	Scanning electron microscopy
(Magniont et al., 2012)	-	10-20 wide	Scanning electron microscopy
(Garcia-Jaldon, 1995)	-	10-40 wide	Scanning electron microscopy
(Ceyte, 2008)	57%	70-400	3D computer tomography
(Cerezo, 2005)	78%	-	Not stated
(Picandet, 2013)	82%	-	Pycnometer and measured particle volume
(Chabriac et al., 2016) (1)	66.2%	-	Extrapolated from sound absorption
(Chabriac et al., 2016) (2)	61.5%	-	Extrapolated from sound absorption
(Nguyen et al., 2016)	78.4%	-	Extrapolates from 96 using thermal conductivity model
(Glé et al., 2012) (1)	50.2	-	Extrapolated from sound absorption
(Glé et al., 2012) (2)	65.9	-	Extrapolated from sound absorption
(Glé et al., 2012) (3)	59.5	-	Extrapolated from sound absorption
(Glé et al., 2012) (4)	46.9	-	Extrapolated from sound absorption
(Glé et al., 2012) (5)	42.6	-	Extrapolated from sound absorption
(Glé et al., 2012) (6)	72.8	-	Extrapolated from sound absorption
(Glé et al., 2012) (7)	66.5	-	Extrapolated from sound absorption
(Glé et al., 2012) (8)	64.9	-	Extrapolated from sound absorption
(Glé et al., 2012) (9)	60.4	-	Extrapolated from sound absorption
(Glé et al., 2012) (10)	51.3	-	Extrapolated from sound absorption

Aside from the chemical profile and porosity of particles, there were very few other parameters reported in the literature although this is an area of rapid development as shown by the recent publication of the RILEM State-of-the-Art-Report: Bio-aggregate based building materials (Picandet, 2017b, Lawrence and Jiang, 2017, Amziane et al., 2017a, Amziane et al., 2017b). The apparent particle density and the skeletal density (density of the solids) are both reported by several studies but in most cases are not

measured directly; only Nguyen (Nguyen et al., 2009) provided a directly measured value of particle density as 256.4kgm^{-3} through the measure of "rod sections of hemp" and a frame density of 1465 kgm^{-3}; further details and the sample size used are not given. Instead, the majority of parameters used to describe the particles are often derived from a few direct measures giving a range of values of apparent particle density between 316 kgm^{-3} and 633 kgm^{-3} and a frame density between 820 kgm^{-3} and 1350kgm^{-3} (Glé et al., 2011, Nguyen et al., 2016, Glé et al., 2012). While values of apparent particle density and frame density are useful parameters for micromechanical models, using values derived by such methods increases interdependence of the results and could lead to the propagation of errors.

2.2.2 Particle size distribution

Particle size distributions of bio-aggregates will logically be an important factor in determining the internal arrangement of a composite and so need to be quantifiable. Particle size distributions have been assessed in the literature by two methods: sieving analysis and two dimensional imaging analysis. Sieving is direct, repeatable and easy to undertake on a well sized sample of material. It is hindered however by the low density and elongated shape of particles and provides only a basic level of data (Picandet, 2013). Consequently most literature now favours the use of two dimensional image analysis that provides richer data. Such methods are more appropriate in the context of bio-aggregates that in general have more elongated forms although are more complex to undertake and have a smaller practical sample size. This section of the review will focus on two dimensional image analysis.

The method of two dimensional image analysis used is relatively consistent across the literature due at least in part to a standard process being provided by the École Nationale des Travaux Publics de l'État (ENTPE) (Ceyte, 2008) and ore recently the outline of a standard methodology by the RILEM TC 236-BBM (Picandet, 2017b). The method itself can be broken into several stages and has significant precedents in wider literature regarding two dimensional image analysis of particles and voids (Nazar et al., 1996, Jiang et al., 2009, Li et al., 2004, Coenen et al., 2012). The stages of analysis used are as follows: arrangement and imaging of a sample of particles, processing of the image, and taking measurement from the image. Given the consistency of this protocol across the literature considered, it is considered acceptable to directly compare data from different studies.

A selection of the particle size distributions for hemp aggregates found in the literature using comparable methods of two dimensional imaging analysis are presented in Figure

2.1. From these compiled data the most obvious aspect is the consistently elongated shape of aggregates found across all studies. This is logically attributed in the literature to the linear form of the stem and so it is often assumed that, in general terms, a particle of hemp will have its longest axis parallel to the stem with the other axes relating to the stem diameter and thickness respectively. While no direct evidence of this proposal exists within the literature it is certainly plausible and strengthens the idea that the particle size distribution of bio-aggregates is influenced by both the processing and the propagation of the plants.

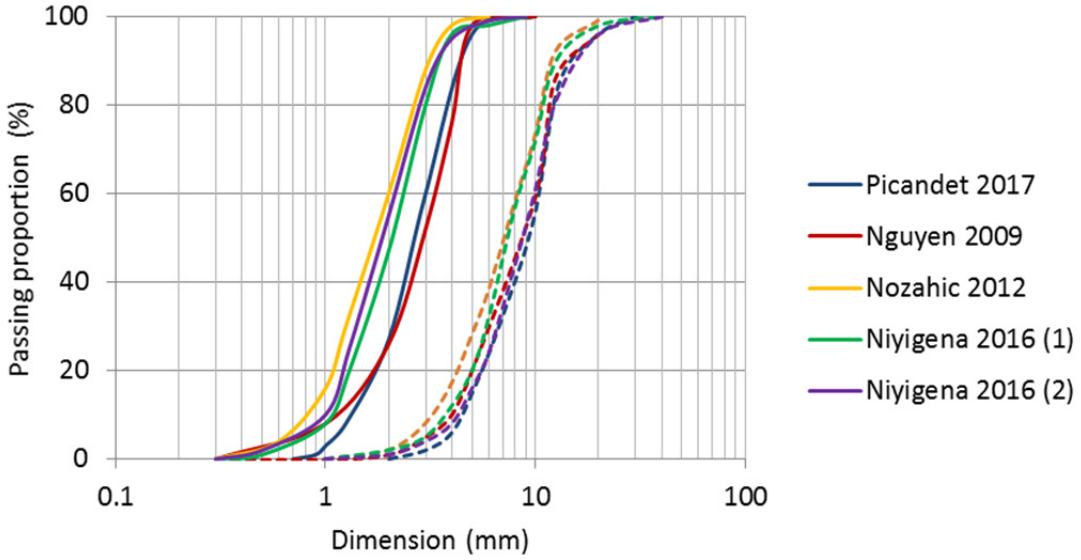

Figure 2.1: Particle size distributions from various studies (Picandet, 2017b, Nguyen et al., 2009, Nozahic et al., 2012, Niyigena et al., 2017) found by image analysis.

The range of distributions presented in Figure 2.1: strongly suggests that different producers of hemp shiv inherently tend to produce different distributions of particles, again a result of different growing conditions and processing (Hirst, 2013). It seems likely that such variations in particle size distributions are repeated in other bio-aggregates for similar reasons. The variations of distributions are noted to be threefold: differing median particle sizes, differing spreads of particle sizes and differing aspect ratios of particle sizes. Given this range of variables available within the distribution it is clear that in order to assess the impact of particle size distribution on composites, a full assessment of the distribution must be undertaken; provision of just a mean particle size or a qualitative comparison such as “coarser” or “finer” as is used in a large number of studies will be insufficient to draw meaningful conclusions.

In terms of what particle distribution of bio-aggregate is appropriate for the production of composites, the French standard suggests the following for hemp-lime: “Particles in a

parallel piped form with widths between 1 and 5mm and lengths of 1 to 30mm. Granulometry (by sieve) with a maximum 5% by mass passing a 0.5mm sieve, around 90% by mass between 1mm and 4mm, and less than 3% by mass exceeding 4mm" (Construire en Chanvre, 2009). It is not clear where these suggestions have come from or even how the former part, "widths between 1 and 5mm and lengths of 1 to 30mm", should be measured. If the particle size distributions acquired by two dimensional image analysis, Figure 2.1:, are assessed against this criterion it can be seen that while most exceed these limits, the bulk of all materials considered falls within them. It seems likely therefore that the limits proposed by the standard have been selected to broadly cover the range of material commonly used at the time as opposed to having a reasoned derivation.

2.2.3 Bulk properties

The bulk properties of bio-aggregates are often studied as they allow for estimation of otherwise hard to measure particle properties through reverse engineering behavioural models and may in turn influence composite behaviour. The bulk properties are logically a result of the particle properties and particle size distribution and so may infer information about both. Of the bulk properties, those most commonly reported and relevant to this study are the bulk density, thermal conductivity, water absorption capacity and restrained compressive behaviour. Due to the relatively recent development of bio-aggregate composites, there is in most cases no established single method used to measure a lot of these properties and so methods between studied tend to vary. To address this there has been two RILEM committees established, TC BBM-236 and TC HDB for characterising bio-aggregates and assessing hygrothermal behaviour respectively, that are beginning to report (Amziane et al., 2017a).

2.2.3.1 Bulk density

The bulk density of bio aggregate particles is found from measures of weight and volume although there is variation in the literature as to the volume used, the shape of container and the method of filling. These aspects will intrinsically alter results on account of bulk bio-aggregates being a compressible material that will consolidate under self-weight and aggravation. The range of reported bulk densities for differing hemp aggregates samples found in the literature as well as a description of the methods used where given are presented in Table 2.3. It is apparent that there is no consensus on methodology and in many cases the method is not reported at all. From those studies that have reported bulk densities for more than one variety of hemp shiv using a consistent method, it is observed

that the variation can be in the region of 76%. This has been attributed to varying particle size distributions and individual particle properties including the roughness of the internal surfaces and surface availability (Picandet, 2017a). In more recent work a standardised method has been proposed for assessing the bulk density of bio-aggregates as an outcome of a multi institutional report (Amziane et al., 2017a) which is similar to the pouring methods described in Table 2.3: and may be considered the preferred method.

Table 2.3: The bulk density of hemp bio-aggregates presented by different studies.

Study	Shiv origin	Bulk density	Method
(de Bruijn et al., 2009)	Sweden	98	Not stated
(Nguyen et al., 2009)	Unknown	113	Not stated
(Gourlay, 2008)	France, Germany, UK, Belgium	62.2-110	Pouring heaped material from a tray into a 5lt bucket and levelling with a ruler
(Picandet, 2013)	Unknown	112	Pouring into a 160mm diameter 320mm tall cylindrical volume

2.2.3.2 Bulk thermal conductivity

The thermal conductivity of bio-aggregates in bulk has been studied only vary sparingly. Arnaud (Arnaud, 2000) took a measure of thermal conductivity for loose hemp particles of 0.058$Wm^{-1}K^{-1}$ using a heat flow meter but with an unreported temperature gradient. The density of the particles quoted was 155kgm^{-3} which, in comparison to Table 2.3:, is high indicating the material might have been compressed rather than loose; no details are given as to the specimen's preparation. In a separate study Cerezo (Cerezo, 2005) obtained a conductivity value of 0.048$Wm^{-1}K^{-1}$ for loose particles with a bulk density of 110kgm^{-3} using a similar method. This density is more in line with the values of loose density in wider literature and thus considered to be a more appropriate value. It has been argued (Nguyen et al., 2016) that loose hemp should have a differing horizontal and vertical thermal conductivity on account of the particles tending to orientate flat to the horizontal. In both cases mentioned, the orientation of the test is not specified and this prediction is not known to have been validated elsewhere. In considering the values presented in both studies it is reasonable to suggest that bulk thermal conductivity is proportional to bulk density and compaction state for loose bio-aggregates. In more recent

work a standardised method for assessing the thermal conductivity of loose particle has been proposed (Collet, 2017).

2.2.3.3 Restrained compressive behaviour

Bio-aggregates, much like any other particulate material, have an intrinsic cohesion and compressive resistance which is of interest in relation to composite behaviour (Picandet, 2013, Arnaud et al., 2013a, Niyigena, 2015). Results reported by Picandet (Picandet, 2013) Nguyen (Nguyen et al., 2009) and Cerezo (Cerezo, 2005) for the compressive testing of contained hemp aggregates all indicate a ductile and compressible behaviour with increasing Young's Modulus with densification. In the case of Picandet (Picandet, 2013) and Nguyen (Nguyen et al., 2009) tests were conducted on humidified, saturated material in order to replicate the presumed conditions of particles within a hemp-lime composite; there is no clear divergence in behaviour from that conducted by Cerezo (Cerezo, 2005) on account of this. The results of Cerezo are reproduced in Figure 2.2 and demonstrate this standard behaviour. To the author's knowledge it has not been ascertained what variables in the aggregate design may influence the compressive behaviour of loose aggregates although the cohesive properties of particles have been used in some explanations of composite behaviour.

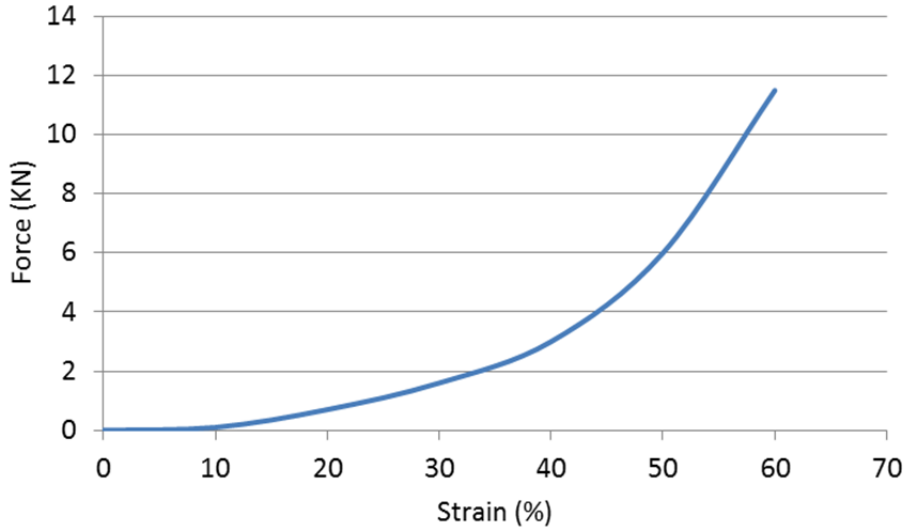

Figure 2.2: Reproduction of compressive testing of restrained dry hemp particles undertaken by Cerezo (Cerezo, 2005)and reported by Hustache (Hustache and Arnaud, 2008).

2.3 Properties of binders

There is a wide variety of binding agents that can be used with bio-aggregates to form composite products, more uncommon examples including starch (Balčiūnas et al., 2013, Benitha Sandrine et al., 2015, Le et al., 2014, Le et al., 2015), earth (Busbridge and Rhydwen, 2010) and magnesium oxide cement (Baghaei et al., 2014, Stevulova et al., Stevulova et al., 2012). Within the majority of literature, the most commonly used binder is lime, used either as a pure aerial lime, a natural hydraulic lime or a specifically formulated blend with additional compounds. As lime based binders are also the most commonly used in practice and what will be used in this study, they will be the focus of this section.

Generally lime is used over mechanically superior cement due to the hydroscopic nature of the bio-aggregate that is reported to produce a competition for water, restricting the ability of hydraulic reactions to take place (Hustache and Arnaud, 2008). While there is limited direct study of such a phenomenon, the preference for lime over cement is definitely noticeable in literature produced by practitioners who believe cement gives a less reliable set (Bevan et al., 2008, Allin, 2005). An occurrence known as “flouring” reported in the study of Hirst (Hirst, 2013), and described as a lack of setting under the surface of hemp-lime, was also attributed to a competition for water when using binders with a higher cementitious content. A second reason for the preference of lime is the higher porosity (Escadeillas et al., 2013). The hygrothermal attributes of such composites as hemp-lime have been attributed to the storage and rerelease thermal energy and water vapour as a result of a multiscale porosity in which the binder plays a part (Collet and Pretot, 2014, Lawrence et al., 2011, Evrard and De Herde, 2010). The porosity of the binder is therefore considered integral to the hygrothermal behaviour of the composite as well as the vapour permeability, both considered major benefits of the material over some traditional constructions (Woloszyn et al., 2009, Evrard, 2006).

As well as practical and physical reasons, lime is also used preferentially to cement for reasons of historical context since lime is common in conservation where bio-aggregate composites were developed. In addition, there is the environmental impact argument: lime is often cited and marketed as having a lower embodied energy and lower embodied carbon compared to cement. This is claimed on the basis of a lower kiln temperature (Kioy, 2013, Bevan et al., 2008, Pritchett, 2009) and a re-absorption of chemically released CO_2 (Nordby and Shea, 2013, Ip and Miller, 2012) and is often an aspect used to support the marketing of hemp-lime and other lime products. While both statements are

evidenced in literature, there is additional evidence that the lack of an economy of scale in the production of lime means that at least the benefit of a lower kiln temperature is currently negated (Hammond and Jones, 2008). It is evident from this that care must be taken with commercially provided information regarding the benefits of different binders.

2.3.1 Properties of lime binders

The two types of lime used as or in most binders are aerial and natural hydraulic and are both produced in a similar way. Generally, raw material is extracted and crushed to suitable sized particles that are then calcined in a kiln at around 1000°C (Escadeillas et al., 2013). Following calcination they are crushed to the desired granulomety and finally dry hydrated in a hydrator. The main difference between the processes is the raw material used: aerial lime uses a pure source of lime or lime that has been washed of contaminants while natural hydraulic lime contains silicate or aluminate compounds as impurities. These hydraulic compounds have the effect of providing an additional hydraulic setting phase to the binder alongside the carbonation setting process observed in both. The chemical and physical structure as well as mechanical and thermal properties of building limes is therefore broadly dependent on the quantity of the hydraulic compounds present.

The internal structure of set aerial limes is reported as highly porous with a large degree of interconnectivity. The actual degree of porosity will alter with specific lime used and the setting conditions, however it is generally reported that aerial lime mortars have an open porosity of around 25% (Lanas and Alvarez-Galindo, 2003, Mosquera et al., 2006) depending on the ratio of constituents ranging between 20% and 30% (Lawrence et al., 2007). Natural hydraulic lime mortars in contrast have a lower reported open porosity, around 20% (Escadeillas et al., 2013, Mosquera et al., 2006). In general terms porosity of lime mortars may be considered inversely proportional to hydraulic content but also dependent on the initial water content and proportion of binder to aggregate (Lanas and Alvarez-Galindo, 2003); the porosity of a set lime paste may be assumed to be higher on account of an omission of aggregates.

Aerial lime mortars and natural hydraulic lime mortars are observed to have a broadly equivalent thermal conductivity in the range of $0.3 Wm^{-1}K^{-1}$ to $1 Wm^{-1}K^{-1}$ (Escadeillas et al., 2013, Vejmelková et al., 2012) again dependent on the specific lime, the water content and the ratio of constituents. The similar thermal conductivities are likely to result from the only small variations in porosity and the large number of other variables. It is considered likely that pure binder paste would exhibit a greater difference in thermal conductivity although this is not verified within the literature considered here.

The mechanical strength of aerial lime develops over considerable time due to the slow rate of the carbonation reaction. The hydraulic reaction by contrast is much faster and so the main benefit of an increased hydraulic content within building lime is the early stage development of strength. The compressive strength of aerial lime mortars could reach 3-5MPa after 6 months of curing in a CO_2 rich environment (Nguyen, 2010) but could be as low as 0.5MPa (Lawrence, 2006) while hydraulic lime can reach 3-5MPa within 28 days under "normal" curing conditions (Escadeillas et al., 2013). As with the porosity and thermal conductivity, it must be remembered that such observations are for mortars as opposed to pure binder paste. Given the more complex chemistry and internal structure of bio-aggregates as opposed to traditional aggregates, such observations of lime mortars may not be relatable to behaviour of bio-aggregate composites. It is believed for example that highly hydraulic binders may have a weaker set when used with bio-aggregates due to the aggregate absorbency and a resulting lack of available water for hydration (Pavia et al., 2015).

2.3.2 Properties of pre-formulated binders

Most binders used in industry and the study of bio-aggregate concretes are formulated blends of lime (aerial and/or hydraulic) and other mineral compounds. These mixtures are formulated in order to maximise the mechanical strength and increase the speed of strength development while not compromising the other advantageous properties of lime binders. In some cases these formulations have been developed by manufacturers specifically for the purpose of use with bio-aggregates while other formulations have been proposed by individual studies. Table 2.4: gives the composition of the formulated binders used for the production of hemp-lime where stated in the literature; in all cases often very little information is given about the properties of cured binder paste in isolation.

Within the literature, Tradical PF70 is the most commonly utilised binder with reported components of primarily aerial lime with additional natural hydraulic lime and pozzolans although the exact ratios reported vary as do the detail of the pozzolans (Cerezo, 2005, Evrard, 2008). Experimental values for the thermal conductivity and compressive strength of cured Tradical PF70 paste produced to a water binder ratio of 0.5 at 28 days are given by Nguyen et al (Nguyen et al., 2010) as 0.373$Wm^{-1}K^{-1}$ and 10 MPa respectively. These results would indicate that the pre-formulated binder exhibits comparable thermal conductivity but improved compressive strength over natural hydraulic limes, quoted in the same study as having a compressive strength between 3.9MPa and 5.9MPa.

Table 2.4: The composition of pre-formulated binders presented by different studies.

Study	Binder	Aerial lime	Hydraulic lime	Cement	Pozzolans	Other
(Elfordy et al., 2008, Nguyen et al., 2010, Nguyen et al., 2009, Kioy, 2013, Kashtanjeva et al., 2015, Youssef et al., 2015, Tronet et al., 2016)	Tradical PF70	70-75	15	0	10-15	0-0.5 (additives)
(Cerezo, 2005, Evrard, 2008, Collet et al., 2008)	Tradichanvre	55-58	10-22	0	0	20-35 (sand)
(Hirst, 2013)	Batichanvre	70	30	0	0	0
(Hirst et al., 2010, Hirst, 2013)	Tradical HB	50-80	10-70	0	5-10 (unspecified)	0
(Walker et al., 2014, Pavia et al., 2015, Kidalova et al., 2012)	Cement blend	50-70	0-20	10-50	0	0
(Walker et al., 2014, Magniont et al., 2012, Walker and Pavia, 2012, Sinka et al., 2015, Dinh et al., 2015)	Metakaolin blend	30-80	0	0	20-70 (metakaolin)	0
(Walker et al., 2014, Walker and Pavia, 2012)	Ground granulated blast furnace slag (GGBS)	70	0	0	30 (GGBS)	0
(Nozahic et al., 2012, Amziane et al., 2015)	Pumice sand blend	10-19	0	0	77-90 (Pumice sand)	0-4 (Na2SO4)
(Balčiūnas et al., 2013)	Clay blend	33	0	33	0	33 (clay)

2.4 Formulation and implementation of bio-aggregate composites

There are many variations in bio-aggregate composites outside the selection of the constituents. These may be broadly classed as either formulation or implementation induced.

2.4.1 Methods of implementation

Bio-aggregate composites are implemented on-site in one of three ways: in-situ casting, arrangement of precast units, or spray applied (Bevan et al., 2008). The most commonly used of these methodologies due to simplicity is in-situ casting. To produce a wall by this method, material is placed by hand in layers into vertical formwork and compacted by vertical tamping (Stanwix and Sparrow, 2014). This methodology can be time consuming and the cast material often then takes a long time to dry to required levels for finishing and habitation (Duffy et al., 2014). The majority of literature into the performance of hemp-lime and other bio-aggregate composites considers material that is cast vertically into cubes or cylinders in a way that replicates this form of on-site placing. Generally the only variables within the process are the number of layers the material is built up in and the level of compaction applied through the tamping.

Pre-casting offers a way of removing drying times from the critical path of a building project but requires a unitised design and may not be applicable to all projects. As pre-casting methodology is often identical to on-site casting in all but location, literature referencing a cast method is generally applicable to both but with a few exceptions regarding compaction. Two common methods of compaction uniquely available to precast placement are vibration compaction and high pressure static loading that are impractical in an in-situ context. In addition pre-casting also facilitates alternative directions of compaction to be applied as opposed to simply vertical.

Projection forming or spraying can be used on or off site and is a faster method of placing material on medium or large scale projects (Bevan et al., 2008). As the method of placing and indeed mixing of components in this case is different it is appropriate that there have been separate studies into the behaviour of material produced this way, all be it not many. The variables inherent to this methodology are the distance of sprayer to substrate, the depth of material within the build-up and the direction of projection. Due to the more artisan and craft development of bio-aggregate composites the machines and processes

used are also known to vary, however there is no known study of these yet. The main two systems of projection are an airflow carrying aggregate and binder meeting jets of water at the lance (Elfordy et al., 2008) and an airflow carrying aggregates meeting jets of binder/water slurry at the lance (Duffy et al., 2014).

2.4.2 Formulation of bio-aggregate composites

Alongside the variations available in the binder and the particles used to produce bio-aggregate composites as previously discussed, there is also variability in the ratios the constituents are combined within both the scientific literature and in practice. Traditionally the formulation of the composite is selected based on intended use: roofing insulation, wall infill, floor slab or render. The Regles Professionelles d'Execution d'Ouvrage en Betons de Chanve (Construire en Chanvre, 2009) indeed provides mixing ratios of hemp-lime for these applications, Table 2.5:. The impact of the aggregate to binder ratio on the mechanical and thermal properties of bio-aggregate composites has been widely studied and will be discussed in later parts of this review.

The amount of water to be used in the production of bio-aggregate composites and particularly hemp-lime varies widely within the literature although unlike the aggregate to binder ratio it is not considered a design variable, alterable for requirement, but rather a parameter that must be correctly set. From the more practical focused literature as well as manufactures' guidelines, the amount of water is often specified in proportion to the aggregate rather than binder (Bevan et al., 2008, Allin, 2005, Tradical®, 2015). The logic stated behind this is that while the binder needs the presence of water to set, the highly hydroscopic nature of the shiv means that it will govern the formulation required. This is supported by more scientific literature that has indeed shown the high water absorption of hemp shiv (Magniont et al., 2012, Gourlay, 2008, Hirst, 2013, Walker and Pavia, 2012, Tronet et al., 2016).

Table 2.5: The use and mixing ratio of different hemp-lime variants as presented by the Regles Professionelles d'Execution d'Ouvrage en Betons de Chanve (Construire en Chanvre, 2009).

Mix reference	Use definition	Aggregate by mass (%)	Binder by mass (%)	Water by mass (%)
Roof	Insulation only for protected areas	25	25	50
Wall	Applications where a degree of durability and mechanical strength is required	15	31	54
Floor	Applications of higher and more regular wear and loading	11	31	58
Render	Surface finishes	10	45	45

While basing the proportion of water used in the formulation on the quantity of hemp alone is a simple and effective system for on-site production, it is clear that if the binder to hemp ratio is changed, then the binder to water ratio will also alter. As the water to binder ratio is known to impact the properties of binder paste as previously discussed, then a dilemma arises in how best to study the impact of the binder to aggregate ratio in isolation. Arguably the large number of studies considering the impact of binder content that have determined the quantity of water based purely on the amount of aggregate alone have not eliminated the water to binder ratio as a variable.

In situations where a large amount of static compaction is applied to composites, an alternative approach has been taken (Youssef et al., 2015, Tronet et al., 2016). In this case an assumption is made that under high compaction, water will be forced out of the aggregate particles and thus the amount of water required may be determined by the binder alone. This assumption allows for a consistent binder to water ratio to be applied at a range of binder to aggregate ratios and in theory removes this as a variable. While a useful concept, this assumption will clearly not be applicable across the full range of possible composites and indeed, even for highly compacted material, its validity must be questioned; there is no experimental evidence to validate complete extraction of water for the particles at high compaction.

In order to have a more consistent way of deriving the water content that may be applied globally, Lanos has proposed a theoretical approach (Lanos et al., 2013). The model assumes that to mitigate absorption of hemp aggregates, particles of binder must be

arranged to have comparable spacing to the pore sizes of the hemp. This scenario is theorised to equate the capillary action of both and thus provide an equilibrium water to binder ratio under which the hemp will not absorb water from the binder paste. Above this value it is suggested that the aggregate will absorb water sufficient to return the water/binder ratio to the equilibrium state. The proposal put forward is thus a window of water contents based on both the binder content and the absorption capacity of the aggregate that will provide a consistent effective binder to water ratio. This is based on an assumption that no absorption by the aggregates will occur under a certain water to binder ratio and thus suggests that any water content will be sufficient within a standard binder to water ratio of mortars. This seems at odds with some of the grey literature that has arrived at much higher quantities of water compared to mortars and the assessment made in highly compacted materials that compression will release water in the aggregates. While nearly all literature reviewed uses a water content within the window proposed by Lanos it remains less clear if this controls the effective water to binder ratio in the setting composite.

2.5 Internal structure of bio-aggregate composites

The internal structure of composites refers both to the quantity of the constituents and their arrangement. In the case of bio-aggregate composites these constituents are the hardened binder paste, the plant solids and voids. As with other composites it is generally stated within the literature that an understanding of the internal structure can be used as the basis of predicting the physical properties and is often the basis of mathematical models. The mass of binder, water and aggregate used to produce bio-aggregate composites is nearly always known from production. The quantity of air and the topology of the material structure are then the primary parameters of interest.

2.5.1 Porosity

The porosity of hemp aggregates and lime based binder paste has been discussed previously and was shown to vary depending on aggregate production, binder chemistry and water ratio. The constituents of hemp-lime as well as other similar bio-aggregate composites can therefore be considered individually porous over a range of scales. It is clear from visual inspection of bio-aggregate composites that they exhibit porosity at a large scale, the imperfect arrangement of the often elongated particles producing inter-particle voids. In consideration of this, as well as the known porosities of the constituents,

it is reported across the literature that hemp-lime and other bio-aggregate composites are multi-scaled porous material with pores ranging in scale from nanometre to millimetre (Collet et al., 2008, Glé et al., 2011, Hustache and Arnaud, 2008, de Bruijn and Johansson, 2013).

The porosity of hemp-lime has been examined in several ways within the literature. The standard approach is to give a value for total porosity which encompasses the inter-particle pores as well as all pores contained within the constituents. Table 2.6: shows values of directly measured porosity for hemp-lime found in the literature and the methods used. It is observed that the range of porosity reported varies with method of assessment (Collet et al., 2008). The most applicable method for determining total porosity is considered to be pycnometry as it allows for testing of a representative sample size and is suitable for measuring porosity on a wide range of scales, unlike mercury intrusion that may not identify large pores (Hustache and Arnaud, 2008). It is most appropriate therefore to only compare results from similar methods or within the same study.

Table 2.6: Porosity of hemp lime and method of data collection as presented by different studies.

Reference	Porosity	Method	Density (kgm^{-3})	Hemp : Binder ratio
(Collet et al., 2008) (1)	76.5	Pycnometry	664	1 : 2.08
(Collet et al., 2008) (2)	64.4	Mercury intrusion	664	1 : 2.08
(Glé et al., 2011) (1)	75	Not stated	390	1 : 2
(Glé et al., 2011) (2)	75		420	1 : 2
(Glé et al., 2011) (3)	74		330	1 : 1.94
(Glé et al., 2011) (4)	67		400	1 : 2
(Glé et al., 2011) (5)	68		390	1 : 1.94
(Glé et al., 2011) (6)	75		310	1 : 2
(Glé et al., 2011) (7)	68		420	1 : 2
(Glé et al., 2011) (8)	73		420	1 : 1.94
(Glé et al., 2011) (9)	72		420	1 : 2

The results obtained by (Glé et al., 2011) come from a range of three binders and three aggregate producers that, on the face of it, might provide explanation for the observed

variations in porosity. Contrary to this, no such pattern between constituent origin and porosity was observable with the variation appearing to be random. This might indicate that the specimen sizes used within this study were insufficient to account for natural variation inherent in the material; it is claimed by both (Evrard, 2008) and (Collet et al., 2008) that a representative volume of hemp-lime is 100-125cm^3 whereas a volume of 83cm^3 was used. The study is therefore neither able to confirm nor rule out a link between the binder and aggregate products and composite porosity

From a mechanical and thermal modelling point of view, the distribution of pore sizes and specifically the division of inter-particle, intra-particle and intra-binder is of more use than the total porosity. To produce a more detailed distribution of pore sizes within the material, mercury intrusion or an interpretation of acoustical or moisture absorption characteristics can be used to provide a pore size distribution although seemingly this is not often undertaken, possibly the result of small specimen sizes and inherent unreliability in the results. An alternative way to establish the ratio of these porosities would be to apply known values of porosity for the aggregates and binder to evaluate the inter particle porosity from total porosity. A limitation of this concept, as noted by Glé, is the assumption that the intra particle porosity of an aggregate is not affected when mixed with the binder (Glé et al., 2011).

2.5.2 Internal topology

The internal topology of bio-aggregate composites is considered to be anisotropic with the particles tending towards planes. The reason for this view is the elongated form of the particles coupled with a compacting force applied during the placement influencing arrangement. In its simplest form this compacting force may be just gravity but nearly always an additional degree compaction from either tamping, pressing, the spray process or vibration compaction is applied. It is considered universally that these factors in combination will tend to align the particles in a perpendicular direction to the force applied (Elfordy et al., 2008, Nguyen et al., 2010, Gross, 2013, Pierre et al., 2014, Picandet, 2015). There is a considerable amount of qualitative evidence for an anisotropic structure within the literature. This often comes from a visual assessment of the materials where particles would appear to be tending towards a certain alignment such as in Elfordy et al (Elfordy et al., 2008). This combined with the persuasive logical argument of the formation process have primarily led to the adoption of this theory. Nevertheless it should be noted that such evidence is not quantitative and thus more open to misinterpretation. There is a

current lack in the literature of any repeatable, quantitative assessment of anisotropy in the structure of the material.

Outside of direct observations of the internal structure it has been observed that hemp-lime exhibits anisotropic physical properties such as compressive behaviour (Youssef et al., 2015, Amziane et al., 2015, Centre scientifique et technique du bâtiment, 2011) and thermal conductivity (Nguyen et al., 2010, Pierre et al., 2014). In all cases such observations are limited to a parallel and perpendicular loading case with respect to the compacting force and the influence of differing production methods on the degree of anisotropy has not been assessed. Additional details in the literature pertaining to the anisotropic mechanical behaviour and thermal conductivity will be discussed fully in later sections of the review.

Looking more widely, comparison may be drawn between bio-aggregate composites and other binder/aggregate composites and compacted particulate material, to see if precedents exist in the wider literature. The most apparent comparisons are with asphalt concrete, wood particle board and fibre reinforced composites that all have a compacting force applied in production. In all cases these materials have exhibited anisotropic material behaviours and consequently techniques have been developed to assess the topology of the internal structure (Coenen et al., 2012, Kutay et al., 2010, Badel et al., 2008, Gong et al., 2004, Nishimura and Ansell, Kaouache et al., 2013, Liu et al., 2013). Such methods applied to these materials are likely to be applicable to bio-aggregate composites but as yet no such application is known about.

The material with possibly the most synergy and most useful body of literature is asphalt, a composite of aggregate stones and bitumen binder that is compacted when cast. As the stones are often angular and tend naturally to have a prevailing axis then it follows that these should align under compaction in a similar way to that assumed to happen in bio-aggregate composites. Within the literature the most common way of assessing the orientation of the aggregate in asphalt has been via image analysis of sliced faces (Coenen et al., 2012, Bessa et al., 2012, Hamzah et al., 2013, Roohi Sefidmazgi and Bahia, 2014, Yue and Morin, 1996) although three dimensional scanning has also been used (Kutay et al., 2010). The general method of image analysis employed is common to nearly all cases and can be described as follows:

- Enhancement of the images. Image filters are used to remove noise and smooth anomalies from the image at the expense of some detail. The most common enhancement used is a median filter that replaces a pixel with the median value of those within a radius.

- Segregation of constituents. This is achieved through a threshold method where a limiting value is used to segregate the image into a binary image of two constituents, typically aggregate and non-aggregate. Selection of the threshold value is critical for accurate interpretation.
- Binary cleaning. This can be achieved by an opening algorithm or erosion algorithm. In each case the process is designed to remove any remaining noise and separate touching particles by removing pixels that have a low degree of connectivity to those surrounding it.
- Identification and measurement. The discrete binary objects within the image are measured for orientation. There are several ways of defining the orientation of the object that may be used and will have impact on the results, the most common being an ellipse fitting method.

Following the analysis of individual particles, the population can be statistically assessed to identify trends in the orientation. This approach has been shown to be effective but may also be considered to have several flaws. Firstly it is likely that the results are sensitive to the variations in the image processing. Sensitivity analyses within the literature are very limited so the extent of this is rather unknown. Secondly it is arguable that a simple population based frequency analysis is unrepresentative given the likely range of particle sizes; it is conceivable that a trend in orientation of larger particles may be missed if there is a large number of randomly orientated smaller particles. Despite these flaws, such analysis would be very useful in the assessment of bio-aggregate composites and the lack of use of such techniques so far represents a large gap in the study of these materials.

2.6 Mechanical properties of bio-aggregate composites

The most commonly reported mechanical behaviour is that of the material in compression as this is considered to be a general indicator of durability. More appropriate possibly in the context of a primarily non-structural walling material is the flexural behaviour in order to convey horizontal loads to the structure. Literature referring to both of these aspects will be considered in this section.

2.6.1 Parallel and perpendicular loading behaviour

It was alluded to in the previous section on internal topology that bio-aggregate composites are widely considered to have an anisotropic internal structure. As the

manufacturing process is directional, it is indeed logical for the material to be assessed in two directions: parallel to the force applied and perpendicular to it. Despite this, the majority of studies until recently have only assessed the material parallel to compaction.

The first known report of the compressive strength of hemp-lime being assessed in multiple orientation is in a 2002 report covering the construction of a housing estate (Yates, 2002). In this report, it is commented that during testing of the walling material, cast hemp-lime of undisclosed design, tests were carried out both parallel and perpendicular to compaction. The report notes that in parallel loading conditions the material demonstrated high compressibility and ductility to the point where no stress plateau was detectable and thus records a compressive strength at a point of 10% strain as is standard for compressible insulations (British Standards, 2013a). In the parallel orientation it is reported that specimens failed by "bursting of the layers" causing a distinct point of collapse. Unfortunately no additional details are given regarding stress at this point or the relative stiffness in each direction.

The next, similarly un-detailed, assessment of directional compressive behaviour is found in a 2007 report from the French Scientific and Technical Centre for Building (Centre scientifique et technique du bâtiment, 2011) (reviewed in English by (Evrard, 2008)). In this instance it is noted that testing of projection formed hemp-lime conducted parallel to the direction of projection yielded a higher initial stiffness and a more brittle failure mode at lower strain than perpendicular testing. It is stated that such differences are less pronounced for manually cast material although no data are presented to justify this statement. In general limited details are given about the testing method or the material used, casting some questions over the repeatability and applicability of the results.

More recently, several studies reported in The First Annual Conference on Bio-based Building Materials of 2015, have provided more complete assessments of the parallel and perpendicular compressive performance of hemp-lime (Kashtanjeva et al., 2015, Youssef et al., 2015, Amziane et al., 2015). In (Youssef et al., 2015), cast material compacted with a high static force were tested while in (Kashtanjeva et al., 2015) and (Amziane et al., 2015) more typical levels of compaction were used applied by tamping. In all cases it was found that the material exhibits anisotropic behaviour under compression and supports the general observations made in the previously considered studies that the material has a stiffer and more brittle behaviour in the perpendicular direction (Figure 2.3). This observation is seen to be observed at a range of aggregate to binder ratios and is attributed across the studies to directionally specific failure mechanisms resulting from an orientated internal topology.

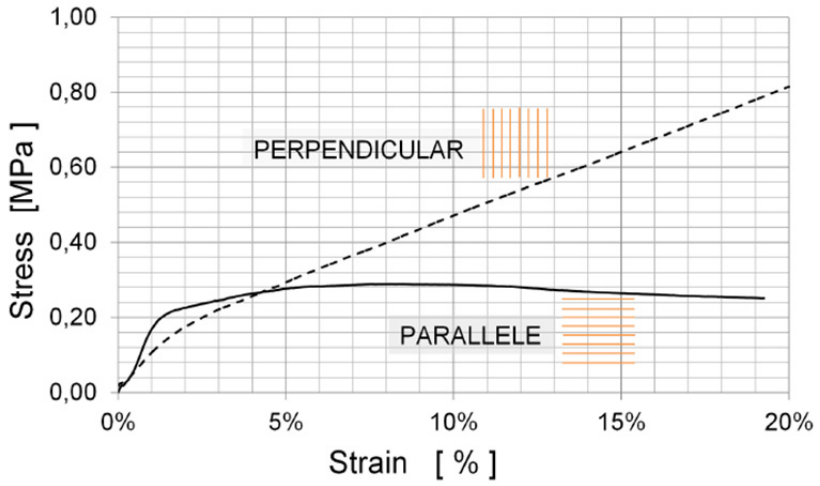

Figure 2.3: Parallel and perpendicular to compaction loading of hemp-lime as presented by (Kashtanjeva et al., 2015).

Taken together, the studies considered can be used to indicate that anisotropy is present in compressive behaviour of hemp-lime in both highly compacted cast material, moderately compacted cast material and projection formed material. Due to differences in testing methods and materials it is not valid to compare across studies and so it is unclear if the degree of compressive anisotropy is increased or decreased by other factors such as compaction or application method. Outside of hemp-lime, the same observations have been made for composites of sunflower and lime (Nozahic et al., 2012) and may be assumed to apply to other bio-aggregate composites although there is insufficient literature available to confirm this.

Multi directional flexural testing of bio-aggregate composites is very sparse in the literature. For projection formed material it is noted in (Hustache and Arnaud, 2008) in a brief review of several sources that, in projection formed hemp-lime, there is a difference in flexural behaviour and strength of material tested parallel to the projection and perpendicular to it. In this case the details of the study are not presented and critically the exact definition of perpendicular loading is not given, which could be in any direction on a perpendicular plane. Beyond there being a difference in differing loading directions, no further conclusions can therefore be drawn.

The only other known example of multi directional flexural testing is in part of the thesis of Gross (Gross, 2013). In this case panels of hemp-lime were tested in three point bending in the two orientations (Figure 2.4). The results indicated a low flexural strength compared to the compressive strength for similar material and, in the direction indicated in Figure 2.4 as horizontal casting, a significantly lower flexural strength than the direction indicated as vertical casting. The two findings were attributed to the lower flexural strength of binder compared to compressive strength and the occurrence of bedding

layers produced by casting. The study goes short of suggesting an orientated internal structure alone could produce similar results if the panel was cast in a single layer. Currently orientated flexural testing in the literature is limited and in need of addressing.

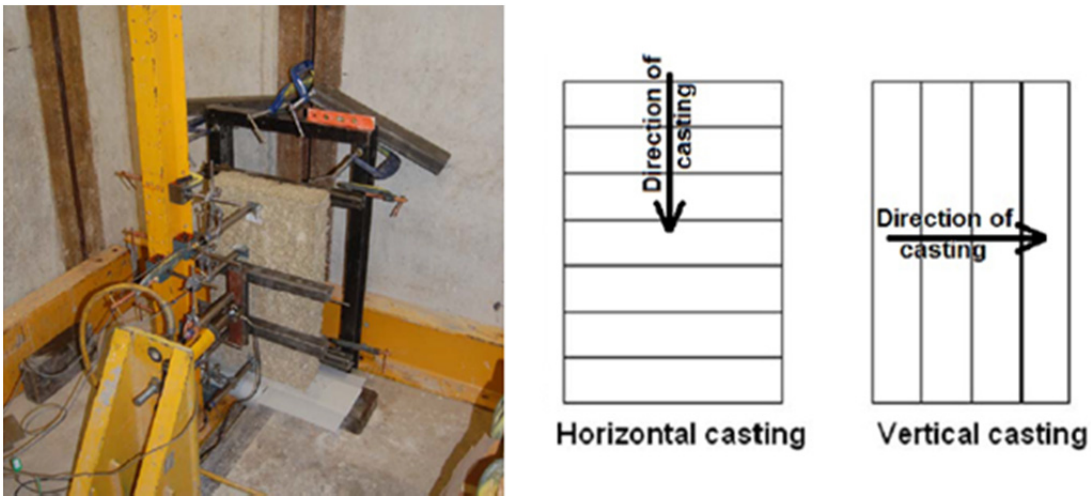

Figure 2.4: Flexural testing of hemp-lime panels in two orientations as presented by (Gross, 2013).

2.6.2 Influence of the constituents

The influence of the constituents can be attributed either to the properties of the constituents or the ratio in which they are combined.

2.6.2.1 Binder to aggregate ratio

The ratio of aggregate to binder is the most obvious variable to change in the production of bio-aggregate composites with a view to altering the mechanical properties. It is logical that increasing the amount of binder will improve the mechanical performance towards that of pure binder paste via the law of mixtures (Askeland and Phulé, 2006). Indeed it is likely that during the early artisan development of bio-aggregate composites, different typical ratios of the constituents arose for differing mechanical requirements (Lanos et al., 2013). In more recent times these typical rules of thumb remain in the prescribed guidelines of the French association of hemp-lime production, Table 2.5: (Construire en Chanvre, 2009). More objective appraisal of the impact of the aggregate to binder ratio on the compressive properties of hemp-lime has since been considered by a large number of studies although the literature relating other bio-aggregate composites is more limited.

At the lower end of binder contents, Hirst has studied the impact of aggregate to binder mass ratios between 1:1.125 and 1:2.25 on minimally compacted hemp-lime made with a

pre-formulated commercial binder (Hirst et al., 2010, Hirst, 2013, Hirst et al., 2012). All specimens in the study were 300mm tall, 150mm diameter cylinders and tests were conducted parallel to the direction of compaction 28 days after standardised curing. The study concludes that, within this window, increasing the content of binder increases the parallel compressive peak strength and stiffness of the composite (Figure 2.5). While a high level of repeatability in the results and rigorous repeatable method validate the conclusion, there is uncertainty as to whether the level of compaction was effectively controlled; set densities of fresh material were outlined for each ratio however the selection of these appears arbitrary.

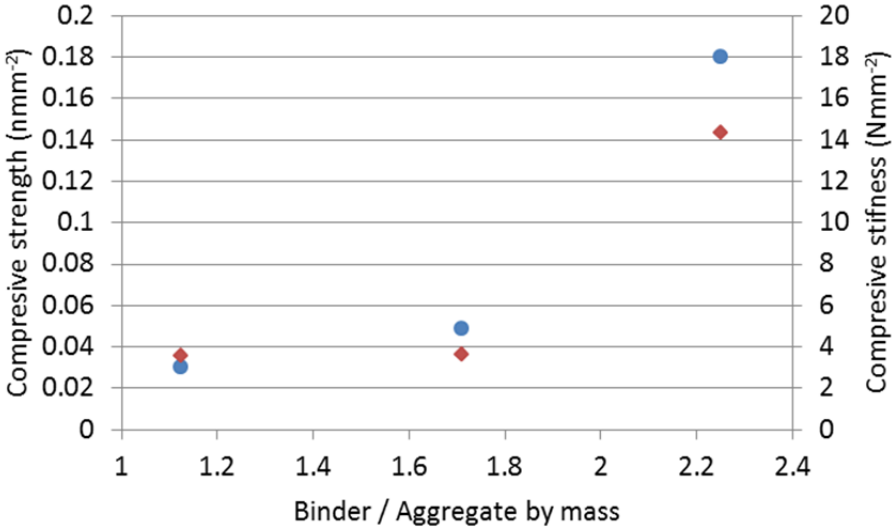

Figure 2.5: The relationship between binder to aggregate ratio and compressive strength (blue circles) and compressive stiffness (red squares) in hemp-lime composites from the results presented by Hirst (Hirst, 2013).

In addition to the studies of Hirst, the work of Sinka (Sinka and Sahmenko, 2013) also considers bio-aggregate composites in a similar aggregate to binder ratio. In this case the binder used was a mix of metakaolin and quicklime as opposed to a pre-formulated commercial binder; the specimens produced were 100mm cubes as opposed to prisms and it is unknown how similar or otherwise the aggregate was. Despite these differences, the same observations of increased parallel compressive strength and stiffness with increased binder content was seen although, unlike the work of Hirst, this relationship was observed to level off at the higher end of binder contents considered. An explanation given was that the interface of aggregate and binder governs behaviour at these ratios and that a threshold therefore exists relating to full utilisation of the surface available. Another difference from the results of Hirst is a noticeably smaller range of densities for produced material, 25kg.m^{-3} compared to 121kg.m^{-3} respectively. This indicates the uncertainty that

compaction was effectively controlled by either study and may be a reason for the levelling off observation not being found in that of Hirst.

At the higher end of binder content, Magniont (Magniont et al., 2012) used aggregate to binder ratios between 1:3.4 and 1:5.5, producing material of between two to three times the density of those studied by Hirst and Sinka. The processes used in the study are otherwise comparable to those previously discussed and it again believed that compaction may not have been effectively controlled. As with the studies on lower binder contents, the observed pattern was again one of increasing compressive strength and stiffness with increasing binder content in parallel compressive loading. The increases in strength and stiffness in this study were observed to be significantly more pronounced at the top of the range of binder contents considered. In this respect there is some coherence with the work of Sinka that noted a levelling of strength and stiffness at the top of the range they considered. Together the results are suggestive of a non-consistent relationship between binder content and compressive performance: generally a positive correlation but seeming to plateau roughly between binder to aggregate ratios of 1:2.25 and 1:4. The explanation of the results provided by Magniont is expressed as fundamental changes in the load transfer and structure of the material at certain binder contents which accords with the explanation of Sinka.

Supporting the findings and assessment of Magniont, the work of Cerezo (Cerezo, 2005) found that for high binder contents, the parallel compressive behaviour of hemp-lime can be effectively modelled as a continuous structural matrix of binder with inclusion of hemp. This work goes on to surmise that at lower binder contents this is not the case and that bio-aggregate composites might have multiple phases of structural behaviour at increasing binder contents characterised by three models: a loose mix of aggregate connected by binder only at touching points; a loose mix of fully coated aggregates with improved mechanical properties and adhesion; and a continuous binder matrix with aggregate inclusions (Figure 2.6:). This theory has been endorsed by others (Hustache and Arnaud, 2008, Escadeillas et al., 2013) and certainly may explain the non-consistent relationship between binder content and parallel compressive properties observed.

Thus far only the studies where the level of compaction applied may be regarded as light, i.e. manually applied tamping, have been discussed. While influence of compaction will be examined fully in a forthcoming section, the effect of binder ratio on heavily compacted bio-aggregate composites will be considered briefly here. Such work has been carried out by Nguyen (Nguyen et al., 2010) who studied material with binder to aggregate ratios of between 1:1.1 and 1:3.44 and formed using a high level of static compaction. All the

specimens were cylindrical, tested in parallel compression and produced to the same cast density across all binder ratios. In contrast to the previously discussed literature regarding less compact material, the findings of Nguyen indicate an inverse relationship between binder content and parallel compressive stiffness and little or no correlation to strength. This was attributed to the higher density of binder compared to hemp resulting in a higher effective compaction for material with lower binder content but similar density. It is impossible thus to make comparisons between this study and those previously considered that allowed the density to fluctuate. Again the importance of defining and isolating compaction as a variable is indicated.

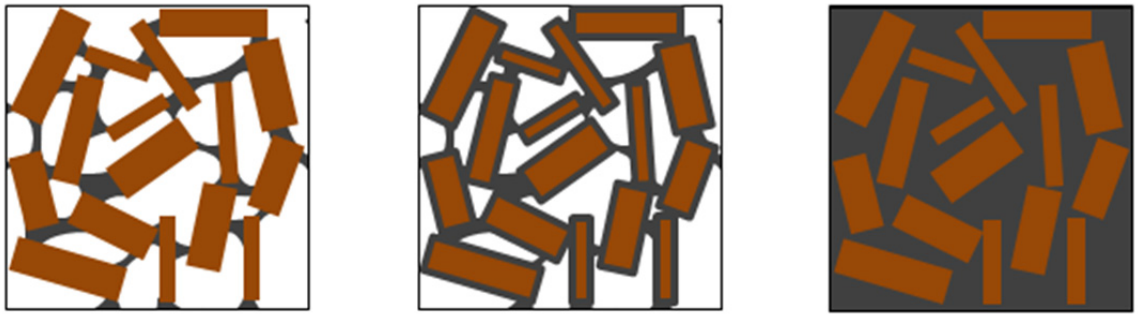

Figure 2.6: Diagrammatic representation of the three phases of structure at differing binder concentrations as proposed by Cerezo (Cerezo, 2005).

The influence of the binder to aggregate ratio on the flexural behaviour of bio-aggregate composites has also been studied although considerably less than the compressive behaviour. Murphy (Murphy et al., 2010) studied prisms of hemp-lime in flexure although the exact method is not specified and the orientation of loading is not known. The specimens considered were produced using volumetric ratios of constituents that approximately equate to mass hemp to binder ratios of 1:3, 1:13 and 1:90. From the result it was found that the flexural strength and stiffness of hemp-lime positively correlate to the binder content of the composite in a similar way to compressive behaviour; it can be assumed that the density of the material also followed this trend however data were not provided. In a second similarity with compressive behaviour it was also observed that the failure mode altered from ductile at a low binder concentration to brittle at high binder concentrations.

Similar supportive results are presented for hemp-lime by Cerezo (Cerezo, 2005) and for composites of hemp-magnesium oxide cement and hemp-starch by Sassoni (Sassoni et al., 2014) and Le (Le et al., 2015, Le et al., 2014) respectively. As with the work of Murphy, the results identify a consistent failure of the tensile face and a global increase in flexural strength and stiffness with binder concentration. Given the range of binders used in the differing studies but similar observations, it may be speculated that this trend as well as

the observations of compressive behaviour are broadly independent of the type of binder used. In respect of failure mode it is speculated in Cerezo's work (Cerezo, 2005) that tensile load transfer may be governed by a complicated combination of tension in continuous binder and shear at the bonded interface of particles; it is assumed that the particles are superior in tension and will themselves not fail. The ratio of aggregate to binder could therefore be considered in part to govern the proportion of load transferred in shear and in tension and thus explain the observed changes of failure mode. There have been no known direct assessments to explore this concept further and validate the proposal.

Outside of hemp as an aggregate, the only found studies to consider the effect of aggregate to binder ratio on a non-hemp aggregate composite were by Chabannes (Chabannes et al., 2015b) and Ning (Ning and Bing, 2015) considering sunflower and rape stalk respectively. In the study of sunflower and lime composites (Chabannes et al., 2015b) only two ratios of aggregate to binder ratio were considered, 1:1 and 1:2, limiting the validity of identifying trends. The material was lightly compacted and the results can be considered in line with those of hemp-lime: an increasing binder content providing an increasing parallel compressive strength and stiffness. In the study of rape stalk (Ning and Bing, 2015), a large range of aggregate to binder ratios, 1:3.3 to 1:20, was considered and again in parallel compression the same overall trend was observed. It seems likely therefore the general relationship between binder content and compressive strength and stiffness is common to all bio-aggregate composites although the nature of the relationship is not simple.

2.6.2.2 Aggregate properties

As discussed in previous sections, the variation possible within bio-aggregates encompasses the chemical make-up and porosity of particles as well as the distribution of particle sizes and shapes. The particle chemistry and porosity are a result at least in part of the plant source and growing conditions rather than a controllable industrial process; the opportunity to control these variables outside of selecting the aggregate is thus limited. In terms of the mechanical characteristics there are two possible ways for such variables to impact on the mechanical performance: firstly altering the mechanical resistance of the individual particles, and secondly the chemical constituency may impact the curing of the binder and interface bonding of binder and aggregate. Outside of hemp, rape and sunflower have also been considered in mechanical studies but there is no study known to date that directly compares composites made with these differing aggregates. No studies comparing the compressive strength of loose aggregates to that of composites

were found and so the focus of this section will be the chemical composition and the particle size distribution.

There has been some earlier work that has considered the impact of the chemistry of hemp on the hardening of lime based binders. Diquélou (Diquélou et al., 2015) looked specifically at the impact of hemp aggregate soluble extract on the setting of cementitious binders and found that such extracts retard hydraulic setting and reduce the compressive strength of binder paste. In addition the study showed that in the case of a composite material, a reduced or nullified setting of binder may be observed at the interface with aggregates. It is not explicitly clear if this phenomenon is a direct result of the hemp extracts and results were limited to considering only hydration setting. No direct compressive assessment of composite material was reported but the study certainly implies that the chemical constituency of the aggregate could impact composite compressive strength.

Only one previous study has been identified to directly attribute a difference of compressive behaviour to a difference of chemistry. In this work (Cigasova et al., 2013), two separately sourced hemp aggregates were used to produce 100mm cubes for compressive testing, assumed to be in a parallel direction. The binder used, magnesium oxide cement, was consistent as was the methodology, and the aggregate particle size distribution was similar for both sources of aggregate. In this instance the main variations in the hemp chemical make-up, obtained by an unspecified chemical analysis method, was in the amount of lignin and toluene ethanol extract. The difference in compressive strength of the material was found to be near to a factor of two and attributed by the authors to the chemical variation retarding the set at the interface. Variation in the density and thus assumed compaction level were considered negligible although other possible aggregate variations such as the porosity were not assessed.

The impact of the particle size distribution on the compressive behaviour of composites has been studied relatively well. Benfratello (Benfratello et al., 2013) considered two "grades" of hemp-shiv, described as having maximum axis lengths of 2mm and 4mm respectively, in composites with hydraulic and hydrated lime binders. All the material was taken from the same source product and composites were made with two aggregate to binder ratios: 1:2.3 and 1:4. The results of the study indicate that at the higher 1:4 binder concentration, the 4mm grade of particles produces a higher parallel compressive strength composite although no explanation is given for the result. This occurrence was found to not be repeated at the 1:2.3 ratio although a likely explanation is the much larger variation of density of these specimens suggesting inconsistency of the compaction used. This,

alongside only two grades of particle being studied, limits the validity of any conclusion obtained from the study. Furthermore as limited detail is provided about the exact nature of the particle distributions it is unclear how they may compare in terms of spread and aspect ratio that may also be important.

Another study with similar findings to that of Benfratello is that of Ceyte (Ceyte, 2008). In this instance a similar method and binder concentration was used however three variations of aggregate particle size distribution were considered allowing for more convincing conclusions to be drawn. The three grades of hemp used in the study were obtained pre-graded from the same manufacturer and described as having increasing "fineness" although no empirical evidence is given to support this statement leaving the definition open to interpretation. The results obtained, if taken at face value, are in agreement with those of Benfratello: a more "coarse" grade aggregate giving improved parallel compressive strength at a comparable binder concentration. Like the work of Benfratello, the lack of specific data about the particle size distributions means other factors such as particle aspect or spread of sizes were not considered and should not be discounted.

A more complete picture of the impact of particle size distribution was obtained by Arnaud (Arnaud and Gourlay, 2012). Within this study three differing grades of the same aggregate, with average lengths of 3.1mm, 7.6mm and 8.9mm, were used to produce hemp-lime composite materials for parallel compressive testing. The conclusions of the study indicated that at 28 days age and an aggregate to binder ratio of 1:2, the longer aggregates provided superior compressive strength. In addition to tests at 28 days, further tests were conducted on material at greater ages wherein the correlation of particle length to compressive strength was found to reverse, Figure 2.7. The explanation given for this is the "finer" grade material producing a more consolidated, stronger internal structure but limiting the carbonation rate and thus rate of setting through restricting CO_2 ingress. This view is supported by an observation of greater initial density for composites made with finer aggregates. Two dimensional imaging was used to analyse the particle distribution in this study and additional data are presented for aspect ratio of particles for the differing grades of aggregate. The aspect ratio of the aggregates was found to increase with increasing average length and thus the data, while not acknowledged by the study, could be used to support a relationship between compressive strength and particle aspect ratio, leaving the results of the study inconclusive.

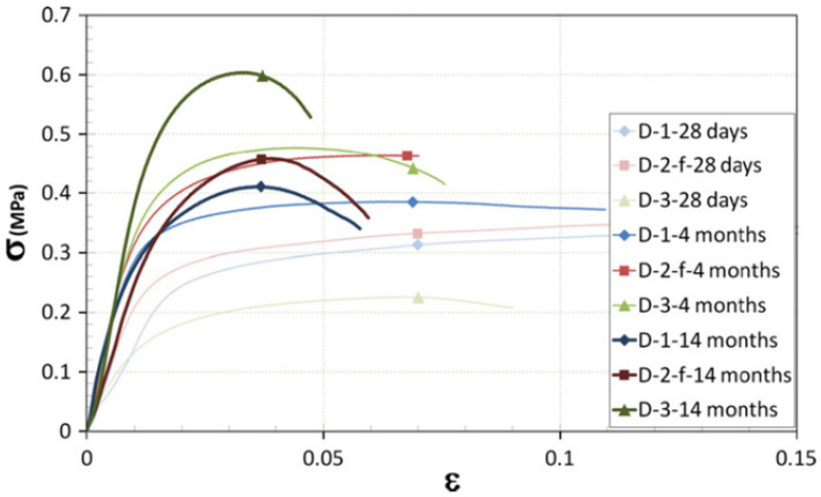

Figure 2.7: Hemp-lime strength with age for differing grades of aggregate (D-1, D-2 and D-3 denoting increasing coarseness)a as presented by Arnaud (Arnaud and Gourlay, 2012).

In contrast to the studies previously mentioned is the work of Cigasova (Cigasova et al., 2013). Cigasova considered hemp aggregates obtained from two sources and each divided into two fractions by means of sieving. Alongside the two fractions of each aggregate, specimens were also made with the original products. Despite limited data of the particle size distribution being presented it may be deduced that original products must have a mean particle length between that of the two fractions but also a much wider spread. The results, contrary to previous studies, found a negative correlation with aggregate particle length and parallel compressive strength at an aggregate to binder ratio of approximately 1:7 and 28 days age. The results were attributed to closer packing occurring with composites made with smaller aggregates although the final density range of the differing materials is small, suggesting this may not have been the case. Possible reasons for the discrepancy between these apparent findings and those of the previous studies are the higher binder concentration considered, although it is not clear why this may be the case, and the volumetric ratios used instead of mass, meaning differing bulk densities of the grades would alter the mass aggregate to binder ratio. It may also be possible that the differing spreads of the distributions is a contributing factor alongside the length of particle thus altering the results.

The impact of the particle size distribution on the flexural behaviour of bio-aggregate composites has been studied by Benfratello (Benfratello et al., 2013) Sinka (Sinka et al., 2015) and Le (Le et al., 2015) and the results are generally inconclusive. Benfratello (Benfratello et al., 2013) studied hemp-lime composites quoted as being made with 20% by mass of aggregate; it is unclear if this refers to the ratio of aggregate to dry binder or aggregate to binder slurry. The flexural tests were conducted on square prisms of 4:1

aspect in three point bending and assumed to be in the direction of casting although this is not specifically stated. The two grades of hemp aggregate were separated from the same product by means of sieving with a 2mm and 4mm sieve respectively. The results presented indicated that the larger particle sizes gave a superior flexural strength approximately 1.4 times higher. This result was attributed to a superior anchorage of long particles allowing for the tensile forces to be taken in the particles and the binder in shear. Such an explanation is in keeping with previously discussed work on the impact of binder concentration (Cerezo, 2005) that suggested a similar shear mechanism to explain differences of failure mode.

In direct contrast to the results of Benfratello, it has been observed by others (Sinka et al., 2015, Le et al., 2015) that smaller aggregates produce weaker composites in flexure. Sinka (Sinka et al., 2015) considered hemp-lime with an aggregate to binder ratio of 1:1.7 by mass and used a greater range of aggregate sizes. In this case the differing grades of aggregates were not fractions of a single product but rather from differing sources which adds additional variables and uncertainty to the results. Despite the possible impact of other variables it was observed that hemp with a higher percentage of larger particles exhibited consistently lower flexural strength. In addition to these results, similar results were found by Le (Le et al., 2015) in composites made with hemp and starch. While it is not clear why these observations differ from Benfratello's, one possible explanation is differences in the particle size distribution that are not commented on such as the spread of the distribution. It is inconclusive from the literature what impact particle size distribution may have on the flexural strength of bio-aggregate composites and additional work in this area is required.

2.6.2.3 Influence of the binder

While many variations of binder have been considered within the literature, given the wide range of other variables, only studies with direct comparisons are considered here. In addition it is noted by Arnaud (Arnaud et al., 2013a) that due to the complex interplay of binder and aggregate, the possible retardation of particular binders in the presence of certain aggregates and the differing setting times, it is hard to categorically define a binder as superior outside of the specific context in which it is tested.

In comparing lime based binders there is a substantial number of studies that are compiled in Table 2.7:. From the studies it can be seen that even within just lime based binders the results are varied across studies and generally inconclusive: Hirst (Hirst, 2013) finds no correlation between binder compressive strength and composite parallel

compressive strength while other studies find a direct correlation in theory but are missing data. A possible reason for this, proposed by Pavia (Pavia et al., 2015), is the differing strength development times of binders and differing testing ages of composites used in studies. A more complete explanation could be to include that while mechanically stronger binders can increase the mechanical performance of bio-aggregate composites, the strength development of binders in a standard mortar may not reflect that in the context of bio-aggregate composites. Specific rheology of binder pastes and soluble chemicals in aggregates may undermine strength development and it is appropriate therefore that lime based binders are assessed on an individual basis in the context of the aggregate they are proposed for.

Outside of lime based binders, both starch and magnesium oxide cement have been considered as alternative binders for use in bio-aggregate composites. It has been found in a study of composites made using both starch and cement binders that starch is able to provide a higher parallel compressive strength than pure cement binders at equivalent binder to aggregate ratio (Balčiūnas et al., 2013). No details are given as to the relative strengths of the binders outside this context and so the explanation of this result is not clear. Likewise elsewhere it has been shown that composites made using a magnesium oxide cement binder can obtain higher parallel compressive strength than those made with equivalent masses of hydrated lime and pure cement binders (Kidalova et al., 2011). Again no details are given as to the relative strengths of the binders outside this context. It cannot therefore be ascertained if indeed such binders provide this apparent superior mechanical strength in composites as a result of being mechanically superior in themselves or by being more suited to application in bio-aggregate composites. A greater understanding of the failure modes of such materials on a micromechanical scale may help to develop this area of study.

Table 2.7: Impact of differing lime based binders on composite mechanical behaviour as presented by different studies.

Study	Binders compared	Observations
(Kioy, 2013)	Tradical PF70 and Natural Hydraulic lime NHL3.5	Commercially formulated Tradical PF70 found to give superior parallel compressive strength and bending strength in composites. Tradical PF70 is assumed to be mechanically superior in a standard mortar but no data provided to confirm.
(Hirst, 2013)	Tradical HB-42.5N, Tradical HB-52.5R, St Astier Batichanvre and Natural Hydraulic lime NHL5	While the weakest binder as a standard mortar, NH5, produced the weakest composite, there was otherwise no correlation between standard mortar compressive strength and composite parallel compressive strength. The strongest composite at 28 days was produced by the second weakest binder in a mortar.
(Murphy et al., 2010)	Hydrated lime CL90 and unspecified commercially formulated binder	The unspecified commercially formulated binder was found to give superior parallel compressive strength. The commercially formulated binder is assumed to be mechanically superior in a standard mortar but no data were provided to confirm.
(de Bruijn et al., 2009)	Various mixtures of hydrated lime CL90, hydraulic lime NHL5 and cement CEMII	Composite parallel compressive strength found to increase with cement content of binder. Strength of mortar may assumed to be similar but no data were provided to confirm.
(Pavia et al., 2015)	Mix of cement CEMII and hydrated lime CL90 and natural hydraulic lime NHL3.5	The mixed cement and hydrated lime binder found to give superior parallel compressive strength in composites. The mixed binder is assumed to be mechanically superior in a standard mortar but no data were provided to confirm.

2.6.3 Influence of the implementation

There are two basic implementation methods for forming bio-aggregate composites that will be considered in turn.

2.6.3.1 Hand casting variations

In hand casting, precast or in-situ, the constituents are first combined within a separate container that may be a simple bucket or more advanced mechanical mixer. The mixture

then is transferred into moulds or shuttering where it is compacted by means of tamping, static compression or vibration. The material is often built up in one or more distinct layers with the compaction being applied between the placing of each layer. The two main variables in hand casting processes are therefore the layer size and level of compaction.

The impact of compaction on compressive behaviour has been studied considerably by Nguyen (Nguyen et al., 2010, Nguyen et al., 2009) in a series of two papers reporting the impact of applying high static compaction force on the parallel compressive strength of hemp-lime composites. All the tests were conducted on cylindrical prisms of material cast in a single layer in a specially created mould. Degrees of compaction varying between two and three times volumetric decrease over loose material were applied using a hydraulic press. Across the full range of aggregate to binder ratios considered, 1:1.11 to 1:3.44, and at 28 days age, increasing the compaction had the effect of increasing the parallel compressive strength and was attributed to a decrease in inter-particle voids; the compressive stiffness of the material was not found to be altered by compaction. Alterations to the binder content were found not to have a consistent impact across the range of compaction forces considered. It is proposed by Nguyen therefore that differing optimum binder contents may exist at differing static compaction forces and that impact of the two variables may be interdependent.

In a separate study to that of Nguyen, Cerezo (Cerezo, 2005), found comparable results: increasing parallel mechanical strength with compaction for a set ratio of aggregate to binder. This was again attributed to a decreasing porosity of the material, an assessment strengthened by the coinciding results. While this assessment is sensible and considered accurate, it is incompatible with the assessment of some of the previously discussed work that attribute larger aggregates as providing a more openly porous structure and resultantly higher compressive strength due to improved setting (Arnaud and Gourlay, 2012). It might be considered possible therefore that these observations would not be observed in bio-aggregate composites formed with a binder that sets through carbonation alone.

In more recent work Tronet (Tronet et al., 2016) has studied the interaction of compaction and binder content at very low aggregate to binder ratios of between 1:1.8 and 1:0.41. Based on the work of Nguyen, an equivalent method of producing and testing specimens was used. In this instance all material produced was of a similar green density of 816kgm^{-3} with compaction and binder content being varied respectively to achieve this, compaction being defined as the volume of the solid phase over the total composite volume. The results indicate that the findings of Nguyen, parallel compressive strength increasing with

increasing compaction, extend into the range of very lower binder concentrations. Where this work goes further is to note that, as the binder is significantly denser than the aggregate, the compaction as defined in this study is inversely proportional to binder content at a set density. This implies that obtaining a target density through compaction produces higher compressive strength than through altering the ratio of constituents – challenging the established view that compressive strength is proportional to density. While this result helps to illuminate the complex interplay between ratio of constituents and compaction, the study only presents data for one density of material and only at very high compactions and so it is uncertain as to how applicable the findings would be to less compact material.

To the author's knowledge there is only one study that assesses the impact of compaction on the flexural properties (Sassoni et al., 2014). In this case composites of hemp and magnesium oxide cement in a weight ratio of 1:1 and produced with three levels of compaction were studied. Flexural tests were conducted in four point bending however the size of the specimens was not kept constant across the different compactions, casting some doubt over the method's validity. The results indicate that increasing the compaction in casting resulted in an increased flexural strength; the flexural stiffness is not reported. By changing the compression ratio (defined as the ratio of compacted volume to initial volume) from 1:1.7 to 1:4 the flexural strength was increased by a factor of eleven while the density increased by a factor of three. The current literature is considered limited in its consideration of the impact of compaction on the flexural properties as well as compressive behaviour in perpendicular loading.

Layer sizes used on-site for in-situ cast material are reported to vary between 150mm (Bevan et al., 2008) and 200mm (Lanos et al., 2013). Precast block or panels (laid flat on the ground) tend to be cast in a single layer and therefore the layer size is dependent on the application but normally ranges between 100mm and 200mm. In contrast to this, in a relatively recent study into the sensitivity of hemp-lime to common testing variables (Niyigena, 2015), it was claimed that a range of layer sizes representative of that used in current research is 30mm to 65mm indicating a distinct discrepancy between the research and real world application. To the author's knowledge there has not yet been a study that directly assesses the impact of layer sizing on the compressive behaviour of bio-aggregate composite materials and therefore any insight from preceding work must be inferred and treated with appropriate caution.

In a study of cylindrical specimens of hemp-lime highly compacted by static compression, (Nguyen et al., 2010), Nguyen observed that within a single 200mm thick layer, the density

of the material varied inversely with depth, Figure 2.8:. It was proposed by Nguyen that this may be as a result of frictional forces along the sides of the mould creating a stress state during compaction that decreased with depth. This hypothesis was later confirmed when a specially produced casting die was used to measure the strains at the mould surface at differing depths during compaction of similar specimens (Tronet et al., 2014). The inference of these results is that the depth of layer size used in statically compacted material will determine the lowest level of compaction applied across the layer and thus the compressive performance at that position.

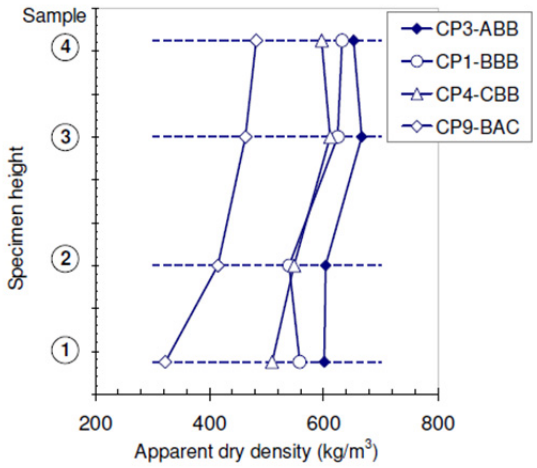

Figure 2.8: density distribution within statically compacted hemp-lime as presented by (Nguyen et al., 2010).

In less compact material, the impact of layer size may be inferred from the work of Hirst (Hirst, 2013). In this study 160mm diameter, 320mm long prisms were built up in levelled "handfuls" giving estimated layer thicknesses of 20mm with minimal compaction. When tested in compression it was observed that the specimens consistently failed in the top third of the specimen. The testing method was ruled out as a possible explanation by observations of inverted specimens then failing in the lower third. It was thus proposed that the material is more compact with depth when produced in this way. The explanation is logical in as an increasing pressure with depth from supported material should increase compaction but is in seeming contrast to the proposal of Nguyen. In consideration of both studies an appropriate conclusion to draw may be that the impact of layer size will be dependent on the amount of compaction. In cases of significant compaction being applied, larger layer sizes may prevent the full depth of the layer reaching the same compaction state due to wall friction; smaller layers would arguably produce more even compaction and better compressive strength. In the case of low level compaction, it can be inferred that the layer sizes have a lesser or no impact as compaction is determined by self-weight

below the level where sufficient wall friction is generated. Currently neither of these theories is supported by direct evidence.

To The author's knowledge there has been no previous direct study of the impact of layer sizes on the flexural capacity of bio-aggregate composites. The only reference to the impact of layering on the flexural properties in any form is considered to be by Gross (Gross, 2013) where it is noted that in flexural loading across layer joints, these may act as a weakness limiting capacity. In general, the mechanical impact of layer sizes is considered to be insufficiently studied in the literature, particularly in light of the discrepancy between experimental and in practice values.

2.6.3.2 Projection casting variations

The only known study to directly consider the impact of projection forming and variables therein on the mechanical performance of bio-aggregate composites is (Elfordy et al., 2008). The specific process of projection in this instance was of an air stream carrying mixed aggregate and binder, 1:2.13, being projected through a spay nozzle where the water is introduced. Large specimens of hemp-lime, 300mm by 600mm by 200mm deep were produced using this method from a range of projection distances: 0.5m, 1m, 2m and 3m. Subsequently 50mm cubes were removed for compressive testing parallel to the direction of projection. The study does not present the compressive strength vs projection distance directly but rather gives the density distribution of material, produced by different projection distances and taken from differing parts of the block, and the relationship of compressive strength to density, Figure 2.9:. From these two results it may be inferred that a projection distance of 1m gives the highest density and thus compressive strength as a result of most effectively compacting the material. The spread of densities found at each distance was greater than the variation in mean densities found between them and so the validity of this inference is weak. In addition only one orientation of testing was considered and no comparison to cast material was made. The available literature on the impact of the projection process is considered very limited.

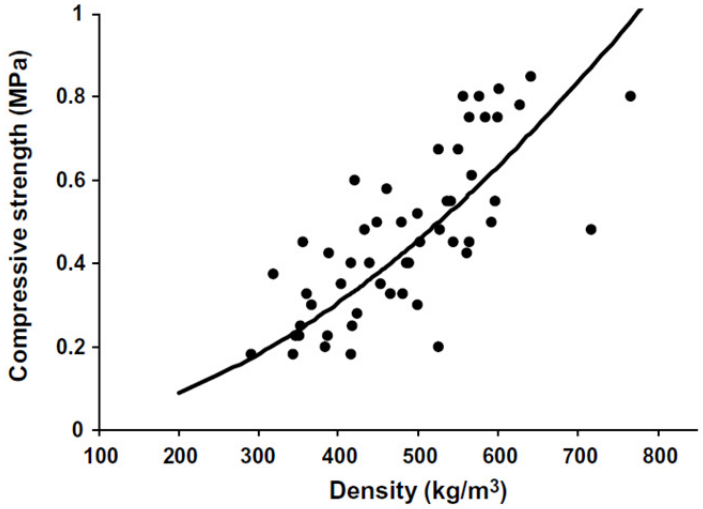

Figure 2.9: Density variation in projection formed material and impact on compressive strength as presented by (Elfordy et al., 2008).

2.6.4 Other factors

Alongside those aspects already discussed there are several other variables that have been shown in the literature to influence compressive behaviour. The most notable of these, the age of the material and the curing conditions, impact the state of the binder at the point of testing. As this impact is specific to the binder and broadly outside of the main scope of this work, the review of this will be limited to provide context and an overview only.

In a number of studies it has been shown that compressive strength and stiffness are influenced by the age of the material; strength is acquired rapidly in the early stages of curing followed by a gradual levelling over a prolonged time. This may be associated with the setting mechanisms of lime based binders: hydraulic set in around 28 days and carbonation possibly across several years (Escadeillas et al., 2013). The age development profile of binders will therefore depend on the constituents of the binder itself and, in the case of carbonation, the ability of the material to permeate carbon dioxide. In the context of construction, 28 day strength is used in design of concrete and subsequent strength gain not considered. In consideration of this, mechanical properties of bio-aggregate composites are often given at 28 days in literature (Arnaud et al., 2013a). The use of 28 day strengths specifically for hemp-lime is considered more appropriate on the grounds of the high hydraulic content of many pre-formulated binders; Hirst found no significant increase past 28 days for hemp-lime made using Tradical PF70 (Hirst, 2013).

The curing conditions will influence the level of set achieved and thus mechanical behaviour of composites. In previous work it has been demonstrated that in the case of

hemp-lime, both the temperature and humidity of the curing conditions may impact the compressive properties. It has been observed that extremes of temperature and humidity are detrimental to the setting of common lime based binders and that optimum conditions are in the order of 20°C and 50% relative humidity (Arnaud and Gourlay, 2012). As the carbonation reaction requires the permeation of carbon dioxide into the material, the impact of a carbon dioxide rich atmosphere has also been studied and has been shown to also improve later stage compressive strength development (Chabannes et al., 2015a).

2.6.5 Modelling mechanical behaviour

Given the importance of being able to model and thus predict and optimise materials it is of no surprise that there are a variety of models of compressive strength of bio-aggregate composites although only one for predicting flexural strength. In general, models for mechanical behaviour may be grouped into two categories: empirical models and micromechanical models (Arnaud et al., 2013a).

The most simple empirical relationship, predominantly found in early studies (Mounanga et al., 2009, Cerezo, 2005, Nguyen, 2010), is a linear relationship between compressive strength and density of the material. This relationship is broadly seen across nearly all published results and may in general be explained by an increase in density indicating more structural material per unit area. As the binder content, aggregate particle size distribution and level of compaction all impact the density, this empirical relationship works reasonably well for a large variety of bio-aggregate composite designs and variations but does not offer the best fit to experimental data when a larger range of densities is considered.

To improve upon the simple linear relationship, Elfordy (Elfordy et al., 2008) proposed power law relationships between density and compressive strength and density and flexural strength. These were based on precedents from other porous media where the physical properties may be estimated by adaptation of the properties of a theoretical material with zero porosity. When adapted for use with density as opposed to porosity, Elfordy established equations for the estimation of compressive and flexural strength of hemp-lime concretes, Equations 2.1 and 2.2:

$$\sigma_{compresive} = A_1 . \rho^n \qquad 2.1$$

$$\sigma_{flexural} = A_2 . \rho^n \qquad 2.2$$

While offering a better fit than a simple linear equation, the model arguably still lacks a physical basis; while A should have a physical basis in the case where porosity tends to zero, there was no attempt to calculate or estimate such a value as opposed to using it as a fitting parameter. In all empirical models a degree of fitting is required which coupled with the lack of theoretical basis limits their applicability to the specific data set they are fitted to - projection formed material in the case of Elfordy. The lack of a physical basis for the models discussed so far is also detrimental to optimisation of individual variables, such as compaction, that are not directly addressed.

In order to provide a mechanical model with greater flexibility, micromechanical models have been developed that look to describe the composite's behaviour in terms of constituent properties and ratio. The basis of such a model is to consider a representative element volume of material made of the same components and arranged in a simply definable arrangement that is representative of the composite on a full scale (Hill, 1965). The first application to bio-aggregate composites, Cerezo (Cerezo, 2005), considered the representative element volume as a cube of binder with a single circular inclusion of non-porous aggregate, containing in itself a singular circular inclusion of air, Figure 2.10. Using this, Cerezo was able to estimate composite compressive stiffness from the ratio of aggregate to binder to air found therein. The model gave a good level of fit to experimentally gathered data but only for binder contents above 10% volume. The was considered to be the representative element volume no longer being representative in this condition where the majority of air voids are intra-particular and the aggregate is fully encased in binder. A further limitation of the model, although not necessarily of the method, is an assumption of isotropic compressive behaviour, shown in work subsequent to the study to not be valid.

To improve on a circular inclusion model and be more representative of the actual micromechanical structure of bio-aggregate composites, more recent work has modelled compressive yield stress utilising a rule of mixtures. This considers both a particle "skeleton" and binder skeleton as separate components, as opposed to assuming an arbitrary arrangement in composite behaviour (Tronet et al., 2016). In this instance the model is directly relatable to both compaction, determining the capacity of the aggregate skeleton, as well as binder content. As a result this model is more immediately useful to industry being theoretically compatible with a full range of binder contents and compactions. While the model seems to fit the data provided in the study very well, the extent of the data is very limited and so it is unclear if the model is valid for the whole range of variables the authors indicate. In addition, as with all the previously discussed models, anisotropic behaviour is not accounted for.

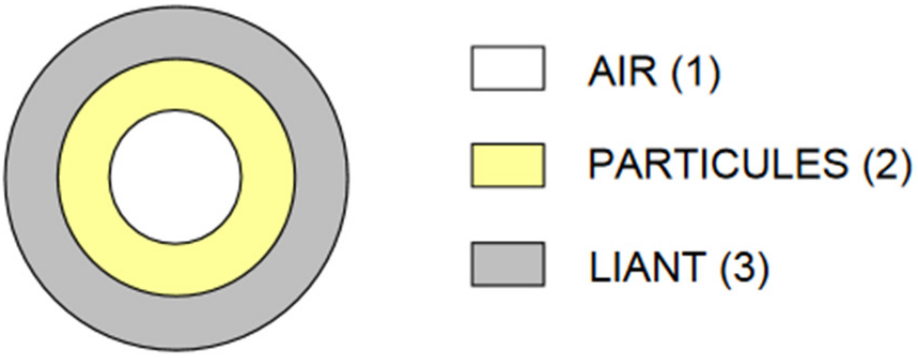

Figure 2.10: Diagrammatic representation of the representative element volume used in the micromechanical model proposed by (Cerezo, 2005).

The only known study to model the mechanical properties of any bio-aggregate composite as an anisotropic material is the study by Mom (Mom et al., 2012). Here a multi scale approach was taken whereby differing scales of inclusion were added to the matrix including both air and rectangular shaped aggregates. As the rectangle has an orientation, the global, directional properties were then considered by applying rotational matrices to the completed representative element volume and taking a weighted average of the results. This approach was applied to results from both Cerezo (Cerezo, 2005), assumed to be relatively isotropic material tested in one direction, and a separate study considering compact anisotropic material tested in two directions (Nguyen, 2010). The model was found to fit experimental results well in both cases including the anisotropic case. The limitations of this model are the complexity of its multiscale design, requiring finite element analysis to solve the reference element volume properties, as well as the acknowledgement that careful fitting was required in the directional weighting in order to get a good fit to the experimental data. This was achieved without an attempt to assess the internal structure of the material directly and presents both a flaw in the model since its dependence on the fitting is not known, as well as identifying the requirement to study the internal structure directly that is not present in the literature.

2.7 Thermal properties of hemp-lime

Generally, in the context of building envelope materials, the most important thermal property is the thermal conductivity as it is used extensively in both environmental modelling and prescriptive building standards (Duffy et al., 2014). The latent thermal storage and effective thermal mass, while often a major attraction of the materials, is undervalued by the current building industry and resultantly of lesser importance to this study. In consideration of this, as well as the additional complications of accessing these

aspects, the main focus of the literature reviewed is on the thermal conductivity. As in the preceding section where the mechanical properties were discussed, the impact of loading direction, constituents and implementation will be discussed in turn.

2.7.1 Parallel and perpendicular loading behaviour

The first known report of bi-directional testing of thermal conductivity was by Nguyen (Nguyen et al., 2010). In this study of highly compacted hemp-lime, thermal conductivity was measured with a heat flow meter on 60mm by 60mm by 30mm plates removed from cylindrical specimens of material. The plates were arranged such that heat flow was tested both parallel and perpendicular to the direction of compaction. The experiment was conducted using material produced to a range of aggregate to binder ratios, 1:1.1 to 1:3.48 and an equivalently varying range of compactions selected to give materials of equivalent density. The results of the study found that thermal conductivity was dependent on the direction of heat flow with respect to compaction orientation: the thermal conductivity parallel to compaction was recorded as approximately one third lower than the perpendicular direction. The author attributes this anisotropy to arrangement of aggregates into planes perpendicular to the casting compaction. Such an arrangement is assumed to allow heat flow more readily across the planes than between them due to a lower degree of continuity of the binder in the latter arrangement. While the specimen sizes used were comparatively small for use in a heat flow meter, the consistency and scale of the difference between the two testing directions gives the authors' conclusions strong justification.

The next study to consider directionality considered projected hemp-lime as opposed to a cast material (Pierre et al., 2014). As a result of the production method, the actual degree of compaction and aggregate to binder ratio are not precisely known however it may be assumed that the "wall mix" used is likely to have a ratio of approximately 1:2 by mass. In consideration of this and the density range reported, 398.7kgm^{-3} to 445.3kgm^{-3}, it is considered likely that the material in this study was less compact that that in the study of Nguyen. The study utilises a transient method of assessing thermal conductivity as opposed to steady state method and while the size of specimen used was larger than that of Nguyen, 100mm by 100mm by 30mm, the method has a localised heating and measurement areas and it is again uncertain if this is representative of the material. The results obtained found an approximately 25% higher thermal conductivity in perpendicular loading and so is in line with Nguyen in suggesting distinct anisotropy. The directional disparity is lower than that found by Nguyen but given the large number of

differences between the studies in terms of both method and material, no meaningful conclusions may be drawn from this.

In more recent work it has been more common to consider the thermal conductivity, as well as some other related properties such as permeability in a directional context (Picandet, 2015). Indeed three studies presented in the 2015 International Conference of Bio-based Building Materials presented directional thermal conductivity measurements for bio-aggregate composites (Picandet, 2015, Amziane et al., 2015, Dinh et al., 2015). This is indicative of a general shift towards acknowledging such materials as anisotropic and identifying the performance implications thereof. In general all three studies had observations similar to those already discussed: a noticeably higher thermal conductivity being found in the perpendicular direction to compaction as opposed to the parallel. In the case of two of the studies, (Amziane et al., 2015) and (Dinh et al., 2015), slightly differing composites were considered, hand cast hemp-lime and vibration compacted hemp and metakaolin composite, while the methodology of testing was similar. The results present a range of directional variation between 13% and 20% which is supportive of thermal conductivity being anisotropic in bio-aggregate composites irrespective of binder and construction method. A further possible implication of this, as well as previously discussed work, is that the degree of anisotropy may vary with other variables in the production of the material.

The only study to consider if the impact of a constituent or implementation variable on the thermal conductivity may be directionally dependent was by Picandet (Picandet, 2015). In this study highly compacted specimens of cast hemp-lime with a range of compaction levels were tested in parallel and perpendicular thermal loading using a heat flow meter. The study in this respect may be thought to be very similar to that of Nguyen (Nguyen et al., 2010) in terms of both material and method used, and indeed identified a similar level of anisotropy in the results. Where this study offers further insight is to note compaction has a directionally dependent influence on thermal conductivity; a similar decrease in porosity through compaction, roughly 0.7 to 0.5, was found to increase the thermal conductivity in the perpendicular direction by a factor of over two while only a factor of 1.5 in the parallel direction, Figure 2.11. The explanation given for this difference is an increasing level of orientation in the higher compacted material, increasing the anisotropy of the properties. While this is a logical explanation and likely to be broadly correct in light of other work (Amziane et al., 2015, Dinh et al., 2015), the study itself cannot fully justify this conclusion as the aggregate to binder ratio is not constant and may have bearing.

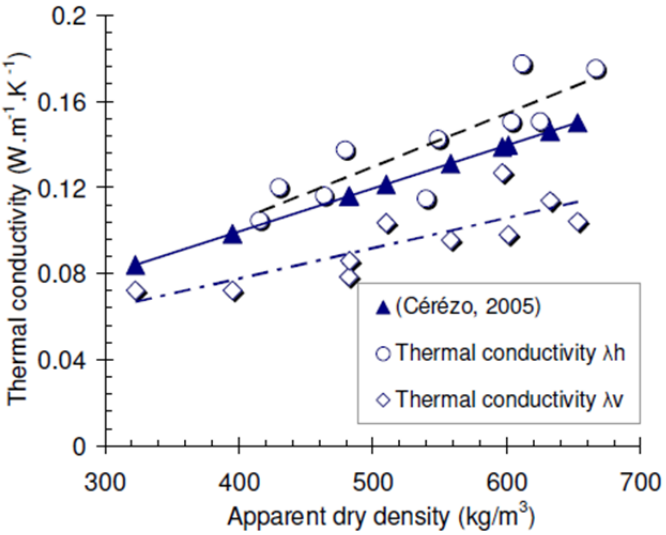

Figure 2.11: The thermal conductivity of hemp-lime at differing apparent densities resulting from compaction in the parallel and perpendicular direction to compaction as presented by (Nguyen et al., 2010).

2.7.2 Influence of the constituents

As with the mechanical properties, the impact of constituents on the thermal properties may be considered to come either from varying the constituents used or the ratio in which they are combined.

2.7.2.1 Binder to aggregate ratio

The impact of the binder to aggregate ratio on thermal conductivity was first considered by Arnaud (Arnaud, 2000). In the study of hemp-lime, three ratios of aggregate to binder were considered between 1:0.85 and 1:4.8 by mass and tests were repeated for two binders (the volumetric ratios of aggregate to binder comparable for both binders used). A heat flow meter was used to obtain the thermal conductivity from 270mm by 270mm by 50mm specimens, considered sufficient in size to be representative. The study reports an increase of thermal conductivity from 0.071$Wm^{-1}K^{-1}$ to 0.114$Wm^{-1}K^{-1}$ for the increase of binder stated attributed to the binder having a quoted thermal conductivity in the order of four to five times that of the bulk aggregate. As it was also noted that the density of the material increased with binder content, a general relationship was thus proposed between density and thermal conductivity for similar bio-aggregate composites of any binder to aggregate ratio. In a separate but similar study, Benfratello (Benfratello et al., 2013) measured the thermal conductivity of hemp-lime produced with similar aggregate to binder ratios and using an equivalent method and obtained results in line with those of

Arnaud. In both studies only a limited number of measurements were recorded however, in combination, the two studies gives both the results and conclusions a high degree of validity. It is not reported in either study in what direction the tests were conducted in, although it may be assumed as parallel from the method descriptions. It is not clear if the results and conclusions presented in these studies are thus valid for perpendicular thermal conductivity.

Outside of hemp-lime, Chabannes (Chabannes et al., 2014) has considered the impact of the aggregate to binder ratio on composites of rice husk and lime. In this study aggregate to binder ratios of 1:1.5, 1:2 and 1:2.5 by mass were considered. This is within the range considered by the previously mentioned studies into hemp-lime but, while not stated, it is likely the compaction was considerably higher given the range of densities reported. In this study tests were conducted using a transient plane source method on circular prisms with a 110mm diameter. Whilst repeated, the size of material sampled by this method must be assumed to be lower than a steady state method and the method and equipment specifically used in this study assumes isotropy in the calculations which, in light of other literature, is likely invalid. Despite a greater variation in results and the diminished validity of the results, the results obtained again indicate a clear trend of increasing binder concentration producing a higher thermal conductivity. In spite of the shortcomings of the method it remains likely therefore that the binder content to thermal conductivity relationship is applicable across all bio-aggregate composites where the binder is denser and more thermally conductive.

In a more recent study the same relationship between aggregate to binder ratio and thermal conductivity has been shown to apply for projection formed material (Collet and Prétot, 2014)(Figure 2.12). The range of aggregate to binder ratio used in this case was between 1:1 and 1:2.5 by mass with a resulting density range of 258kgm^{-3} to 460kg^{-3} - indicating a compaction level similar to that of Arnaud (Arnaud, 2000) and Benfratello (Benfratello et al., 2013). The method used for measuring thermal conductivity in this study was again a transient plane method and so method validity is again questioned despite the averaging of five readings. The results of the study are concurrent with those previously mentioned for cast materials. In light of this and those studies considered already, it may therefore be surmised that in general terms increasing the concentration of binder leads to a higher thermal conductivity in a parallel direction to compaction, irrespective of the aggregate, compaction or implementation method so long as the binder is the denser and more thermally conductive component. Additional work is required to ascertain if this relationship is the same in perpendicular thermal loading.

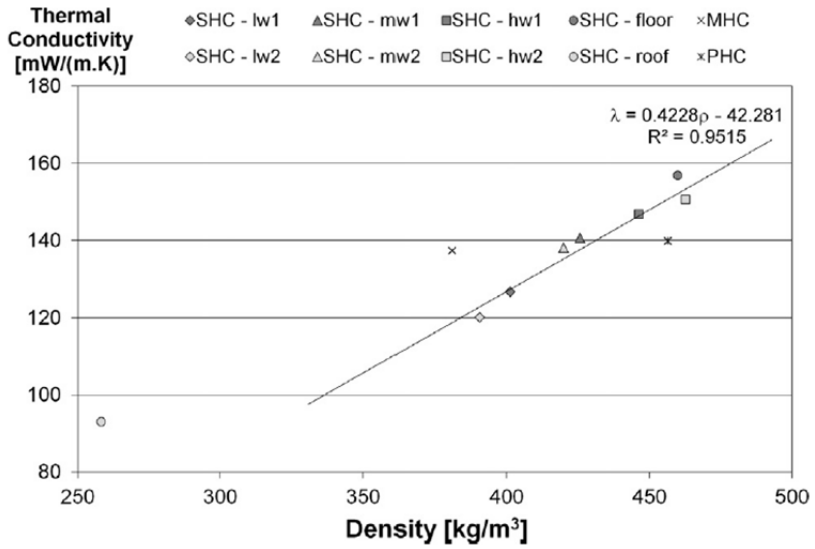

Figure 2.12: Thermal conductivity in relation to density for projection formed material as presented by (Collet and Prétot, 2014).

2.7.2.2 Influence of the aggregates

There are a number of studies, particularly in recent years, which have considered the impact of aggregate variations on thermal conductivity although the impact of using different plant sources other than hemp is only knowingly considered by one (Chabannes et al., 2014). This study used both composites of hemp-lime as well as rice husks and lime across a range of binder to aggregate ratios. The results presented indicate that for equivalent densities, the thermal conductivity of the rice husk composites were in the region of 15% lower than that of hemp-lime. It was also found that for the same aggregate to binder ratio rice husk produced a denser composite and indeed had a marginally higher thermal conductivity. The method of data collection, transient plane source, as discussed previously may be considered unrepresentative and so the accuracy of these measurements is questionable. Nevertheless, the trends observed are strong and lie outside of the natural variation indicating validity of the trends if not the values. The rice husk is reported as having a comparable bulk density to the hemp aggregates but a lower porosity. It is likely therefore that the porosity of hemp-lime is higher than rice lime composites at equivalent binder concentrations. The lower thermal conductivity may be assumed to arise from chemical differences and stacking of particles as opposed to the particle porosity.

In contrast to consideration of different aggregates, studies concerning the particle size distribution of aggregates are more numerous (Sinka et al., 2015, Stevulova et al., Stevulova et al., 2012, Cigasova et al., 2013, Stevulova et al., 2013). The widest range of

particle size distributions considered was by (Sinka et al., 2015) where twelve differing particle size grades were used, four from the same manufacturer. A set ratio of aggregate to binder of 1:1.7 was used for all the tests as was a standard production method and specimen storage removing these as variables; compaction was standardised by using a set mass of wet material that may be questioned given the likely differing bulk densities of the mixtures. The tests were conducted in the same direction as compaction using a heat flow meter with a large representative specimen size. The range of aggregate particle size distributions were described in the study through a sieving analysis and identifies a range of materials that may be labelled as fine to coarse and with a narrow and wide grading. As a sieving method was used, information of particle aspect ratio is not provided which must be considered an unaccounted variable.

The results found a narrow range of thermal conductivities, 0.0718$Wm^{-1}K^{-1}$ to 0.0778$Wm^{-1}K^{-1}$, across the range of aggregate size distributions considered. The results found no conclusive link between the "fineness" of aggregate grade and thermal conductivity although it must be acknowledged that "fineness" is a qualitative observation of a distribution without direct definition. From the data presented, although not commented on by the authors, it could be suggested that a link between the spread of particle sizes and thermal conductivity exists although again this can only be a qualitative observation due to the limited details provided.

In other studies that have considered multiple particle size distributions of hemp aggregates the results have broadly supported those of (Sinka et al., 2015) with no clear trend between mean particle size and thermal conductivity reported by any of (Stevulova et al., 2012, Cigasova et al., 2013, Stevulova et al., 2013). The only reported trend found in literature was (Stevulova et al.) where longer mean particle sizes were found to give higher thermal conductivities, Figure 2.13. In this instance three grades of hemp were used, defined by mean particle sizes: 0.94mm 1.94mm and 3.22mm. These grades were derived by passing a 2mm sieve but not a 0.64mm sieve, passing an 8mm sieve but not a 0.64mm sieve and passing an 8mm sieve but not a 2mm sieve respectively and so the middle grade may also be assumed to be wider. This study differs from the others reported here in that the density of material is high, over 1000kgm^{-3} and so the material must be assumed to be highly compacted. It is not clear if this accounts for the difference in observations of this study from those discussed previously.

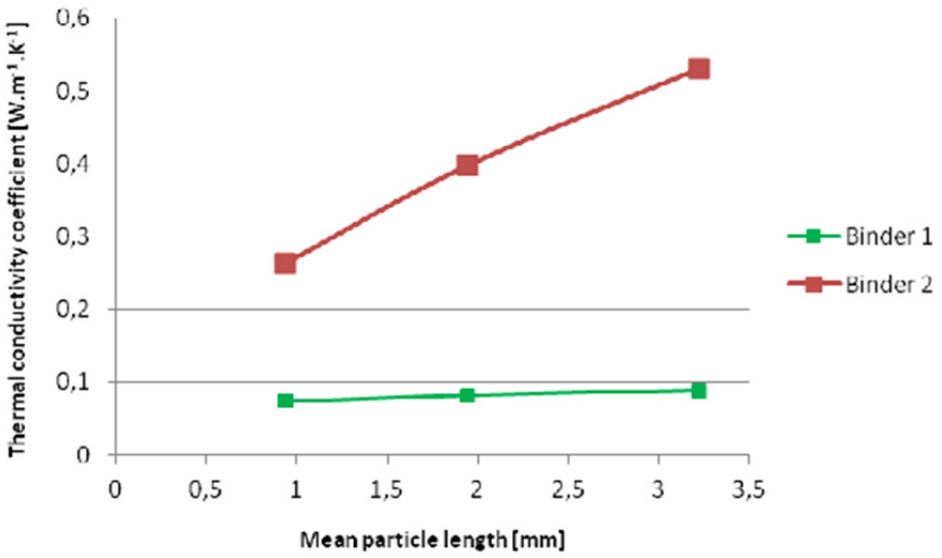

Figure 2.13: Thermal conductivity against mean particle length for hemp-lime composites made with two differing binders as presented by (Stevulova et al.).

2.7.2.3 Influence of the binder

A direct comparison of four lime based binders was carried out by Walker (Walker and Pavía, 2014): a blend of 70% CL90 20% NHL3 10% Portland cement, a blend of 70% CL90 30% GGBS, a blend of 80% CL90 20% metakaolin, and an unspecified commercially blended binder for use with bio-aggregates. In this study material was mixed in an aggregate to binder ratio of 1:2 by mass in all cases and the specimens produced were large, 900mm by 1000mm by 300mm, cast in three layers. All tests were conducted using a "hot box" steady state method one year after casting and after six weeks of conditioning in laboratory conditions. The reported thermal conductivities from the composites made with differing binders had a range of 0.117$Wm^{-1}K^{-1}$ to 0.138$Wm^{-1}K^{-1}$ which, while at face value, may indicate some significant variance dependent on the binder, is not considered so by the authors. Alternatively it is proposed that despite the same cast density of material, the variance in thermal conductivity is a result of density fluctuations and that no binder gives a significant departure from a linear relation between thermal conductivity and density. The impact of binder selection may therefore be considered inconclusive as such density fluctuations may result from the choice of binder or from other natural variation; the initial water content of the mix is also noted to vary to achieve consistent "workability" of the material that would impact cast density.

A similar result to that found by Walker has been found elsewhere (Arnaud, 2000, Nguyen et al., 2010). In both studies, a comparison of commercially available binders is conducted, in the case of (Arnaud, 2000), one noted as providing a 30% increase in thermal

conductivity when used in a standard mortar. The specimen size, method of assessment and curing regime were different to those used by Walker although a steady state method was again used for testing in both cases. Standardised and repeatable methods of compaction as opposed to predetermined densities were used by these studies meaning density fluctuations are a likely result of the binder. In line with the observations of Walker (Walker and Pavía, 2014), the results from both these studies indicate a possible link between binder type and thermal conductivity but are inconclusive. If the effects are assumed to be attributable to the binder variation they are in all cases of low magnitude; binder properties could be considered of marginal consequence in composites due to the low volumetric proportion. As with Walker, no significant deviation from a linear relationship between density and thermal conductivity was observed for any of the binders used. While it is likely that variations in density are a result of the differing binders it is not definite due to some other variations in production, and the results therefore remain inconclusive.

Outside of comparing lime based binders, the thermal performance of composites made using a starch binder has been directly compared to ones made using a cement binder (Balčiūnas et al., 2013). The study considers a range of materials made with differing aggregate to binder ratios and differing particle size distributions of aggregates. The production method implemented was hand casting with compaction applied with a "metal stick" although it is not mentioned how compaction was standardised beyond this. The specimens considered were 500mm by 500mm by 50mm and a heat flow meter was used to measure thermal conductivity; it is not indicated in which direction tests were conducted. In contrast to results comparing different lime based binders, in this study the binder was found to significantly impact the thermal conductivity for material of equivalent density: starch composites found to give a roughly 15% higher thermal conductivity. While no explanation is provided by the authors it is considered likely that the properties of the starch binders are significantly outside the range of properties found in differing lime binders in order to effect such an impact despite the low volume in composites. Further work would have to be conducted in order to confirm this.

Another alternative binder considered has been magnesium oxide cement and as with starch, a comparison between the thermal performance of these composites has been made to those made with more traditional binders (Stevulova et al.). In this study as well as magnesium oxide and a lime based binder, a range of several ranges of aggregate particle size distribution were also considered. The specimens were all produced using equivalent volume ratios of materials as opposed to densities as used in most other studies and the method used to determine thermal conductivity was a localised transient

method which may be less representative. The results presented indicate that the lime based binder gives a lower thermal conductivity than the magnesium oxide binder by a large factor of over three times irrespective of particle size distribution or volumetric proportions. As the reported densities of the magnesium oxide composites are also consistently higher, this is considered to account for the observations. It is not discernible if the higher density is a result of just the binder alone or other factors.

2.7.3 Influence of the implementation

The impact of the implementation variables on thermal conductivity is studied comparatively little within the current body of literature. The compaction of cast material is believed to have been only considered by Nguyen (Nguyen et al., 2010). This study considered composites made using a commercial lime based binder and hemp in a study that considered both parallel and perpendicular loading. The specimens were produced using three levels of compaction defined by differing target densities and produced as 100mm diameter prisms from which the 60mm by 60mm by 30mm were extracted. The specimens were tested via heat flow meter, both parallel and perpendicular to the direction of compaction; the bi-directional testing was a likely reason for the small size of specimens. The thermal conductivity was found to increase with increasing compaction in both the parallel and perpendicular direction, attributed to a reduction in porosity of the material and increased density; the thermal conductivity and density are found to follow a pattern that is equivalent to that found when the binder content is increased. It is not concluded if the impact of compaction is global or directionally dependent despite some evidence in the data that the thermal conductivity in the perpendicular direction is more affected (Figure 2.11).

In support of the general idea that compaction will increase thermal conductivity are results from several other studies considering projection formed material (Elfordy et al., 2008, Pierre et al., 2014). Thermal conductivities presented for a range of projection formed materials were found to vary in relation to density in a similar way to that of Nguyen. As it was observed that density varies with projection distance (Elfordy et al., 2008), and if it is assumed that compaction is similarly related, then these result may be interpreted as displaying a similar trend of increased compaction increasing thermal conductivity. It is of course possible to attribute variations of density to other variables in these studies such as aggregate to binder ratio that may fluctuate given the operator controlled process. In the context of the wider study of the thermal properties of porous media as well as that of Nguyen's work, the conclusion that thermal conductivity will

increase with compaction for bio-aggregate composites in general terms irrespective of implementation is considered justified.

The impact on thermal conductivity of using a projection method over that of casting, vibration compacted and tamped, has been considered by Collet (Collet and Prétot, 2014). The material in all cases was hemp-lime however there are some variations in the binder and hemp aggregates used with each method, due to sourcing logistics, that pose several uncontrolled variables within the study. Alongside this, the study also gives no indication of the direction of testing in relation to the compaction direction in each case and uses a specific transient method of measuring thermal conductivity that assumes isotropy in its calculations. In comparing projection formed and cast material it was found that values for the cast composites, both tamped and vibration compacted, were outliers to the linear trend of density and thermal conductivity for projection formed material. This is suggestive that the implementation process indeed has some bearing on thermal conductivity but given the uncontrolled variables and unknown testing directions, more work will be required in this area to verify the nature of this impact.

2.7.4 Other factors

Outside of the constituent and implementation variables, the moisture content of bio-aggregate composites and its impact on thermal conductivity has also been considered in the literature and has relevance in terms of both experimental protocol and behavioural modelling. Specimens of hemp-lime have been tested for thermal conductivity at a range of moisture contents using both transient source methods within a conditioned environment (Pierre et al., 2014, de Bruijn and Johansson, 2013) and steady state methods on preconditioned specimens (Arnaud et al., 2013b). In all reported cases an increase in the humidity of the environment and thus moisture content of the material leads to an increase in the thermal conductivity. This was also shown in one study to be a globally applicable effect with an equivalent change being displayed in both the parallel and perpendicular directions (Pierre et al., 2014). The importance of controlling this variable if others are to be studied is very apparent in consideration of these results.

2.7.5 Modelling thermal conductivity

A basic model for the thermal conductivity of hemp-lime was first proposed by Cerezo (Cerezo, 2005). The model proposed was based on an empirical relationship between thermal conductivity and density observed in experimental results from a range of hemp-

lime variations made with differing aggregate to binder ratios. This relationship has shown to be accurate for a large range of densities, 200kgm^{-1} to 800kgm^{-3}, where material is produced with a consistent method and constituents but varied binder concentration (Hustache and Arnaud, 2008). In more recent work the same linear equation form has been applied to experimental results produced with differing particle size distributions of hemp aggregates (Benfratello et al., 2013), as well as to composites made with rice husk aggregates (Chabannes et al., 2014) with good levels of fit to the experimental data. For projection formed material, a similar empirical relationship between density and thermal conductivity has been proposed using a power law, again with good correlation to experimental data (Elfordy et al., 2008). These empirical models are both simple and fit experimental data well in most cases but are limited in use by a lack of a physical basis and requirement to be re-fitted for differing materials. Subsequently it has been acknowledged that such empirical relationships are not globally applicable to bio-aggregate composites but rather a particular set of constituents, implementation and orientation (Hustache and Arnaud, 2008), limiting their use in optimisation.

To better generalise thermal conductivity models, micromechanical models have been proposed and broadly superseded empirical relationships in literature. Proposed by Cerezo (Cerezo, 2005) and reproduced in both major reviews of work in the field (Hustache and Arnaud, 2008, Arnaud et al., 2013b) the most widely applied model of thermal conductivity is a self-consistent tri-composite model: spherical inclusions of air within spherical non-porous aggregates, themselves encased in matrix of binder. Such a model allows the individual properties of the components to be accounted for as well as their respective ratio, a result of both the ratio of aggregates to binder as well as the compaction. This not only makes such a model a more appropriate tool for optimisation but also widely applicable to a large range of bio-aggregate composite varieties without refitting. This form of model has been shown to predict the thermal conductivity accurately for cast and tamped, projected and vibration compacted hemp-lime (Collet and Prétot, 2014) as well as material produced to a range of aggregate to binder ratios (Arnaud, 2000). While in theory such a model should be able to account for differences in compaction, there is no known application of it to an appropriate data set and so it is unknown if the simplification of the representative volume element is able to account for the changing internal topology which compaction causes. In addition, a spherical inclusion model is based on an assumption of isotropy that must be considered the biggest shortcoming of this approach that must be addressed.

As yet all the models of thermal conductivity considered within this review have had an incorrect assumption of an isotropic material. Based on qualitative observations of bio-

aggregate composites structure as well as experimental results this is now known to be incorrect. To address this, an alternative model was proposed by Pierre (Pierre et al., 2014) based on the Krischer model (Krischer and Kast, 1978) for the conductivity of composite media, Figure 2.14. This model puts forward that the thermal conductivity of a composite may be described by a weighted mean of theoretical parallel and perpendicular arrangements of the constituents (Maroulis et al., 2002). The constituents considered by Pierre were a solid phase (comprising both hemp and lime), water and air, the first flaw of the approach therefore being the inability to consider varied aggregate to binder ratios without re-establishing the properties of the solid component. In general it was shown that the model was able to provide a good fit to the experimental data gathered by the study for both parallel and perpendicular thermal conductivity. To apply the model several parameters with a physical basis such as porosity were adjusted using a least squares reduction as opposed to being measured. This resulted in differing porosities being proposed for the same material in differing directions and thus highlights an additional flaw in the method: such values become in effect empirically derived fitting factors as opposed to being physically representative. The applicability of the model in this occurrence must be considered to be diminished as a result.

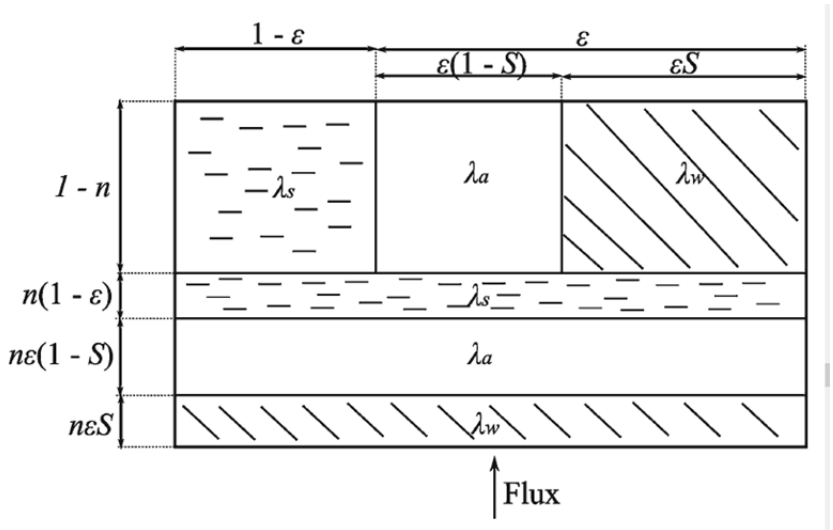

Figure 2.14: Diagrammatic representation of a three phase Krischer thermal conductivity model as presented by (Pierre et al., 2014).

Outside of bio-aggregate composites there have been a number of models proposed for the thermal conductivity of composite materials that have not yet been considered in the context of bio-aggregate composites. Of most interest and relevance to this work are possibly the parallel and series models, the Maxwell-Eucken models, and the effective medium theory (EMT) model (Wang et al., 2006). These models are considered both simple and effective at representing multi-phase materials that and are comparable to the

model employed by Cerezo. Where the internal structure can be considered more complex and indeed anisotropic, combination models can provide a better representation by providing a closer physical basis to the material (Wang et al., 2006). This concept was indeed tried by Pierre (Pierre et al., 2014) using the series and parallel models. Although there were some shortcomings in the application of a combined model in this instance, the approach is likely to be the strongest basis for improved models moving forward.

2.8 Summary of findings

The review undertaken identifies several important gaps within current knowledge that may be synthesised and coherently ordered as follows:

- Anisotropic behaviour has been exhibited in the key mechanical and thermal properties of bio-aggregate composites although modelling of the materials does not sufficiently account for this.
- A lack of a direct and quantitative method for the investigation of the internal topology of such materials has limited the scope of behavioural understanding and effective micromechanical modelling.
- Several important factors have been identified in determining the physical properties of such materials although their impact has not been sufficiently studied within a directionally dependant context resulting in insufficient current data for the effective fitting and validating of directional models.
- The flexural behaviour and impact of variables thereon is underrepresented in the literature despite the importance of this behaviour to current applications.
- The impact of layer sizing has not been considered despite anecdotal indications of importance.
- The body of literature considering projection formed material is comparably small and the impact on properties of producing material in this way has not been sufficiently studied and not at all in a directionally dependant context.
- The current modelling of bio-aggregate composites is limited in it applicability to the development of materials and processes the biggest flaws to address being:
    - Not modelling in a directional context.
    - Not being generalised for use with all material varieties.
    - Related to secondary control variables such as density rather than primary ones such as constituent ratios.
    - Not modelling flexural strength

The aims of this thesis have been proposed as means to fill these gap and in so doing achieve the greater objective of the work.

3 Pilot study: A method for assessing orientation within bio-aggregate composites

3.1 Introduction

Previous work (Chapter 2) has shown that bio-aggregate composites exhibit anisotropic mechanical and thermal behaviour. Such behaviour is widely assumed to originate from an aligned internal structure, with the elongated bio-aggregate particles tending to align perpendicular to the applied direction of compaction (Elfordy et al., 2008, Nguyen et al., 2010, Gross, 2013, Pierre et al., 2014, Picandet, 2015). Despite this, there has been no previous attempt to directly and quantitatively assess the internal structure of bio-aggregate composites. The primary aim of the first experimental phase (pilot study) of this PhD was to determine a method to assess the internal structure, presented in this chapter. The work presented in this chapter has been previously presented as a journal paper: "A method for the assessment of the internal structure of bio-aggregate concretes" (Williams et al., 2016b) which is presented in full within the appendices.

3.2 Precedents within the literature

No previous studies that directly measure the internal topology of bio-aggregate composites in any form have been found in the literature review. Any precedent for a methodology must therefore be sourced from the assessment of other materials, such as other composite materials that have some inherent directionality within the production process that may influence structure. Examples include asphalt (Coenen et al., 2012, Bessa et al., 2012, Kutay et al., 2010), wood particle/fibre board (Badel et al., 2008, Gong et al., 2004, Fan et al., 2004, Kazemi Najafi et al., 2007, Standfest et al., 2010) and fibre reinforced plastics/concretes (Kaouache et al., 2013, Liu et al., 2013, Akkaya et al., 2001, Michel and Billington, 2014, Baghaei et al., 2014). It is noticeable from the literature that a similar core approach has been used to examine the internal structure and to measure orientation (Coenen et al., 2012, Hamzah et al., 2013, Yue and Morin, 1996, Liu et al., 2013, Kastner et al., 2011, Kutay et al., 2010, Lux et al., 2006, Badel et al., 2008, Fliegener et al., 2014, Kang and Kim, 2011, Nishimura and Ansell). This approach is based on the identification and measurement of individual particles using methods that were

established in the development of computerised image analysis and may be summarised according to the following steps (Nazar et al., 1996):

1. Image acquisition.
2. Image processing and segmentation.
3. Data extraction and representation.

To assess bio-aggregate composites it is therefore logical to follow the same approach given their similarity to the other particulate composite materials. While the structure is consistent, the exact nature of the processes to fulfil each of the three stages vary in the literature, and so appropriate methods must be determined. One of the objectives of this pilot study was therefore to assess the different process options and identify a suitable single method to be used with bio-aggregate composites going forward.

3.3 Experimental approach

Three variations of the bio-aggregate composite, hemp-lime, were used, the specifications of which are given in Table 3.1**.** These mixes were chosen to reflect the range of material initially considered likely to be used in the main study, at the time of the pilot study, as well as reflecting industry practice (Bevan et al., 2008, Stanwix and Sparrow, 2014). The standard mix represents a typical commonly used ”wall mix”; the light-weight mix represents a lower binder concentration material of interest to industry and research (due to the lower embodied energy); and the compact mix represents material formed using standard mass ratios but with a high compaction as has been the focus of several recent studies (Tronet et al., 2016, Nguyen et al., 2010, Nguyen et al., 2009). Specifically relevant to this pilot study, these materials represent a median material and the two variations that may cause issues for analysis of the internal structure. For example, the light weight mix has poorer strength making handling and assessment harder.

The specimens were all 150mm cubes, produced in three 50mm layers with light tamping between layers with the material weighed out directly into the mould to ensure consistent density. This size and form were selected based on three criteria: their established use for wider testing of the material (Amziane et al., 2015, Le et al., 2014, De Bruijn, 2008, Magniont et al., 2012, Collet and Pretot, 2014); being larger than the size of the representative volume as quoted in wider literature (Evrard, 2008, Collet et al., 2008); and being symmetrical in three axes allowing for assessment in multiple directions. After casting, the specimens were stored in controlled conditions of 50% relative humidity and

20°C for a period of 28 days to allow them to sufficiently harden; moulds were kept on for the first 6 days and removed thereafter.

Table 3.1: The bio-aggregate composite mix designs used within the pilot study.

Mix	Constituent percentage mass (%)			Mass of wet specimen (kg)	Average dry density (kgm^{-3})
	Bio-aggregate	Binder	Water		
Standard	16	36	48	2.00	284
Light weight	21	36	43	1.48	353
Compacted	16	36	48	2.41	422

Mixing of the constituent materials was conducted in a revolving pan mixer where the binder and water was first mixed for two minutes to form a slurry prior to adding the bio-aggregate and mixing for a further two minutes. The bio-aggregate used in this study was from a UK producer and marketed as Hempcore®; the binder used was a pre-formulated lime binder produced by Lhoist and marketed as Tradical HB (Tradical®, 2015). The bulk density of the hemp was determined as $108kgm^{-3}$ determined via weighing a 3l volume of loosely poured particles. The particle size distribution of the bio-aggregates, Figure 3.1, was found through a standardised method of two dimensional image analysis as presented by (Picandet, 2013).

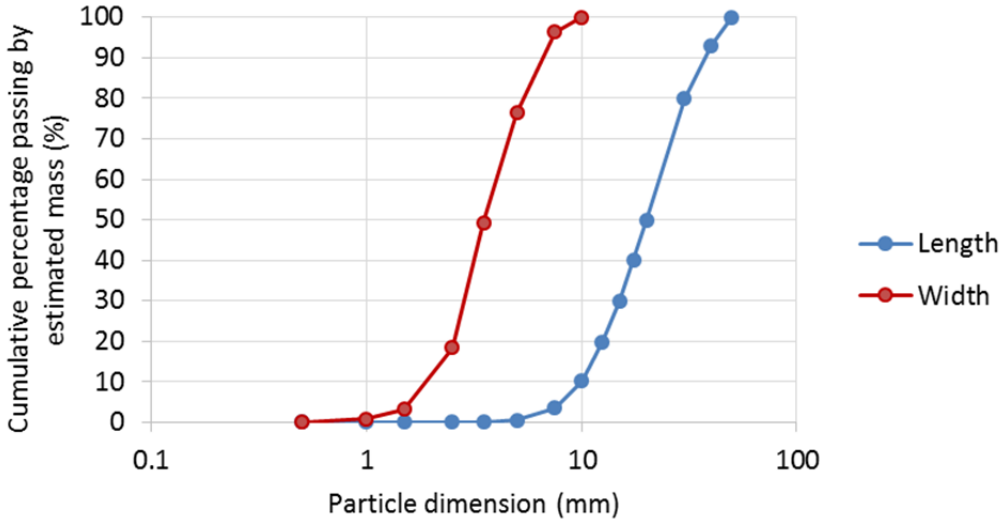

Figure 3.1: The particle size distribution of Hempcore® bio-aggregate composite as established by two dimensional image analysis.

The results of the image analysis show the magnitude distribution of the particles two major axis by cumulative mass in a similar way to standard sieving derived distributions.

From Figure 3.1 the generally elongated particle form can be identified by the discrepancy in the distribution of particle length and width. As it is the elongation of the particles that is assumed to be the cause of anisotropic composite behaviour as observed by others then this analysis confirms that the aggregate used here is appropriate for use in the pilot study.

3.3.1 Imaging

Two methods of imaging were commonly found, and identified as potentially applicable in the context of bio-aggregate composites: two dimensional digital imaging of cross sections and three dimensional computer tomography x-ray imaging (CT scanning). Both methods were applied at this stage of work.

3.3.1.1 Two dimensional digital imaging

Two dimensional digital imaging of sections was established mainly in the study of asphalt (Coenen et al., 2012, Yue and Morin, 1996, Bessa et al., 2012) and soil (Jiang et al., 2009, Li et al., 2004, Shi et al., 1998, Velde et al., 1996). In this approach the material is sliced to produce a cross section that is then imaged using either a fixed digital camera or a flat-bed scanner. The method has the advantage of being comparatively cheap and simple to use. Disadvantages, however, include its destructive approach and the limited amount of data it collects: data are only collected from a single section with each scan and so multiple sections in multiple directions are required to establish a three dimensional interpretation of the material. Additional disadvantages, which appear to be specific to application with bio-aggregate composites, are the similar colouration of bio-aggregate and lime binder, making interpretation of images harder, combined with the fragile nature of the material, which means cutting can cause degradation of the face to be imaged.

To collect data using this method in this study, two hemp-lime specimens were produced for each mix design. Each individual specimen was sliced into 150mm square, 25mm deep sections using a band saw; one section was sliced parallel to the direction of compaction and one perpendicular. The size of the slices was chosen following trial and error to optimise the number of slices, and thus data gathering potential, for each cube whilst maintaining sufficient durability for handling. The cut faces were imaged using a flatbed scanner at a resolution of 2400dpi, used in preference over a digital camera due to a better consistency of framing and lighting. The resolution of the scanner gives an effective pixel size and thus smallest definable detail size of 0.000113mm^2.

An initial visual assessment of the basic digital image set showed that there were three possible issues that may later impact the image processing and analysis. The first noticeable concern was the similarity in colouring of the binder paste and the bio-aggregate particles, Figure 3.2. This poses an issue for the segregation phase where a clear visible contrast is beneficial for accurate segregation via the analysis software. To overcome this, an additional set of specimens were produced where a red pigment was added to the binder to colour the binder paste, Figure 3.3. This process has precedent in the study of soils by similar means (Li et al., 2004) and enhances the visual contrast between the elements. In achieving a better contrast it was predicted that a more accurate identification of constituents and thus more representative result would be achieved.

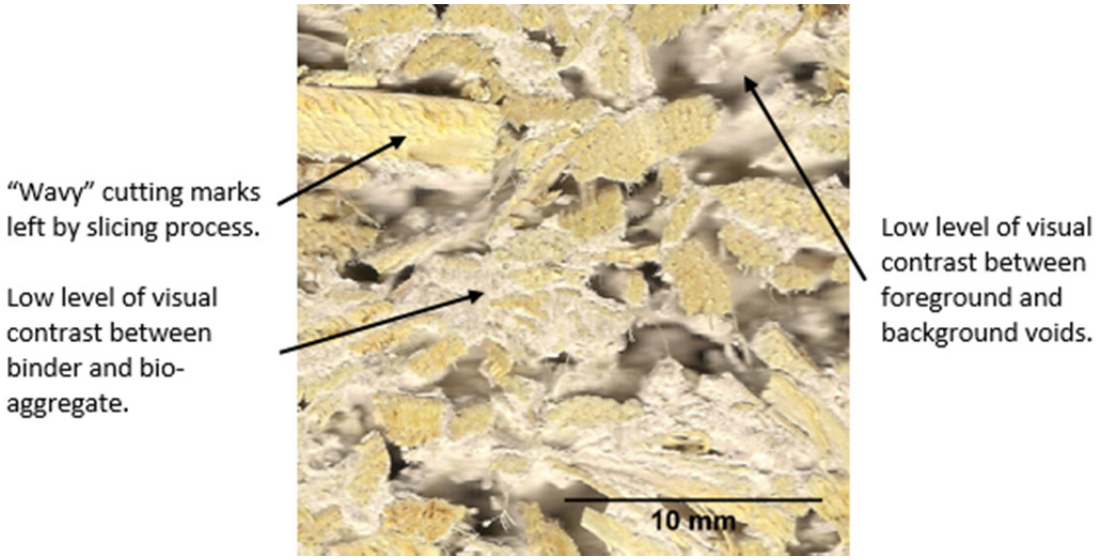

Figure 3.2: Possible image contrast issues identified within digital images with no pre-treatments.

Other noticeable issues with this method were the difficulty in differentiating foreground from background (and thus a difficulty in establishing what constitutes the voids), and the visibility of cutting marks on the material, Figure 3.2. It was considered possible that these taken together may undermine the identification of constituents and the subsequent analysis. To overcome this, an adapted digital imaging method was devised, whereby the cut faces were impregnated with a low viscosity coloured resin and then sanded back to reveal the face for scanning. This was considered to be a possible way of simultaneously providing a clear visual difference between the foreground and voids within the material and also stabilising the delicate surface to allow for removal of cutting marks via sanding. The use of a resin in this way has precedent within the wider literature (Li et al., 2004, Jiang et al., 2009, Velde et al., 1996) of image analysis where it has been employed for similar reasons. The resin used in this instance was a blue casting resin, Sika Bi-resin 27, with 100ml being used for each slice giving an approximate penetration of 5mm, Figure

3.3. The sanding was conducted using an industrial belt sander fitted with 120 grit paper. Due to the vastly improved quality of the image set produced using both the pigmented binder and resin impregnation of the face, only this set of images was considered for further processing. A full appraisal of the image qualities achieved from using one, both or none of these specimen preparation methods is presented in the results and justifies this decision.

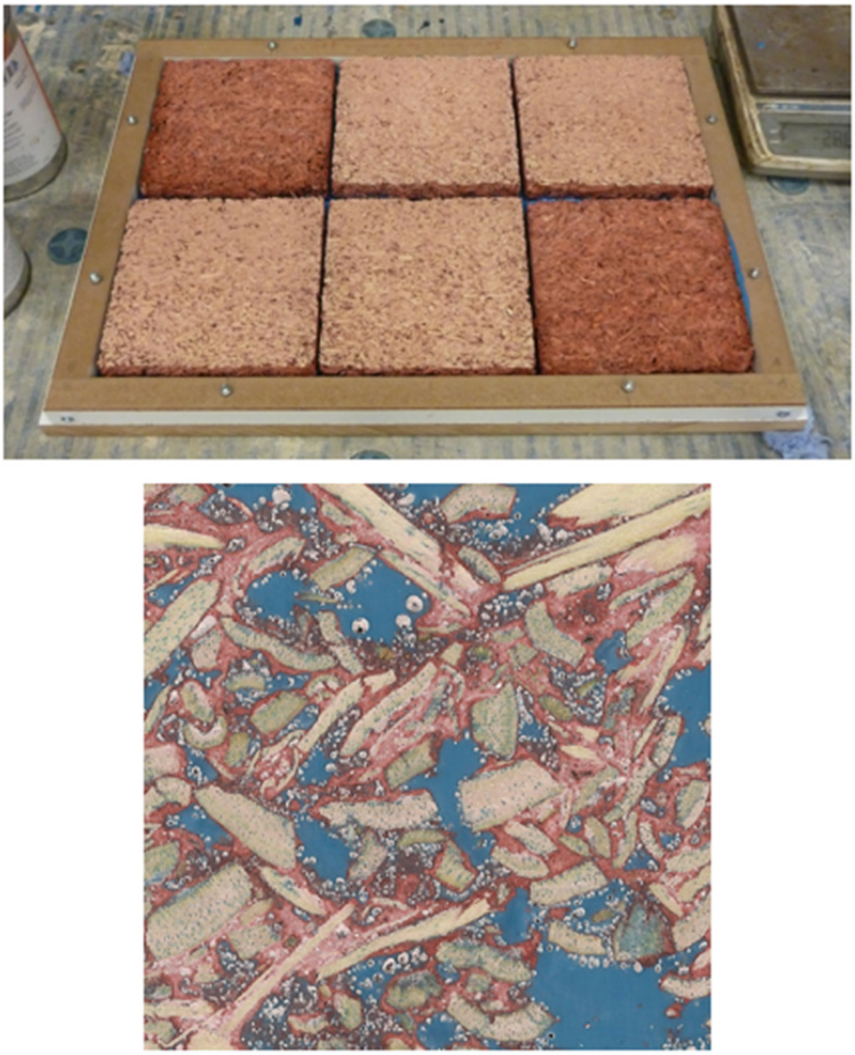

Figure 3.3: The resin impregnation process being applied to specimens dosed with red binder pigment (top) and the resultant improved contrast images produced using these pre-treatments (bottom).

3.3.1.2 Three dimensional computer tomography imaging

Three dimensional computer tomography imaging uses a large number of two dimensional x-ray images taken in differing orientations to reconstruct a three dimensional map of x-ray absorption within the specimen (Standfest et al., 2010, Wehrhausen et al., 2012). As x-ray absorption is closely linked to density, the images

produced from CT scanning will have high contrast between distinct materials within a composite so long as the densities are distinct (Kastner et al., 2011). As with two dimensional digital imaging, CT scanning has been used previously for the study of aggregate orientations within composite materials (Fliegener et al., 2014, Badel et al., 2008, Liu et al., 2013) as well as for the identification and measurement of material defects (Wehrhausen et al., 2012); while there was a reference found to using CT scanning with a bio-aggregate composite, no quantitative data seems to have been extracted in this instance (Picandet, 2015). CT scanning has the advantage of being non-destructive and collects a much larger quantity of data compared to two dimensional digital imaging (Wehrhausen et al., 2012). The major disadvantage of the method is the high cost as well as the high computer processing requirement to analyse the images.

In this study a single specimen was produced to each mix in Table 3.1 and was scanned using a Nikon XTEK, XTH 225 ST CT scanner set to 165kV and 165uA, Figure 3.4. The settings of the scanner while input by the user, are largely dictated by the material and specimen size required as well as the scanning time available. The settings used were therefore determined by an experienced technician to give the best resolution for the size of specimen within a reasonable scan time window of four hours. The images produced by three dimensional computer tomography had a voxel size of 0.00049mm^3.

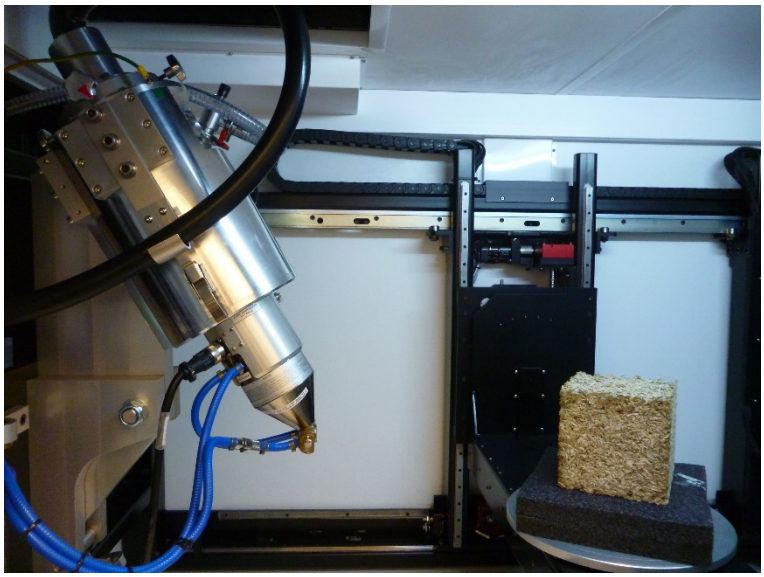

Figure 3.4: CT scanning of a hemp-lime block.

3.3.2 Image processing and segregation

Given the two different types of image produced by the imaging methods used, different software was used on the respective image sets: ImageJ (Schindelin et al., 2012) and

Avizo® Fire 8 (FEI Visualization Sciences Group, 2007) were used for two dimensional digital images and three dimensional CT scanned images respectively. Despite the different software, as close as possible the same approach was taken in each case to ensure comparability of the methods. A series of processing and segregation stages were selected based on the precedents within other materials previously discussed where a prevailing set of processes are heavily favoured, although the execution tended to change between materials. The three stages of image processing and segregation applied consistently elsewhere and therefore within this study, were a median filter, a threshold filter, and an opening algorithm. The nature and execution of these processes will now be described in turn with the list of settings trialled presented at the end of the section in Table 3.2.

3.3.2.1 Median filtering

The first process applied was a median filter. This replaces the value of a pixel or voxel with the median of those within a specified surrounding area (Standfest et al., 2010). The effect of the median filter is a slight smoothing or blurring of the image that helps to remove noise, anomalies and features considered of a negligible size such as dust, Figure 3.5. The degree of smoothing is controlled by the size and shape of the specified area as well as the number of times the operation is run on the image. In the case of digital images, a circular shape was used with a range of six radiuses between 5 and 30 pixels. This range was selected based on the physical equivalence of the radius, 0.053mm to 0.32mm being considered to approximate the scale of dust and other anomalies. As the number of iterations was observed to have a lesser impact, a single iteration of the process was run in all cases for simplicity.

For the three dimensional CT scanned images, a ball shape area was applied but as there was no option to control the radius within the program, in this case a sequence of 5 to 7 iterations were trialled. These numbers of iterations were selected so as to give a visually similar degree of smoothing to the range used for the two dimensional images.

3.3.2.2 Threshold filtering

Following smoothing of the image, a threshold filter was applied to segregate the image into a binary image of the constituent of interest, Figure 3.5. This was achieved by comparing a value assigned to each pixel/voxel, such as brightness, to a threshold range where it is either classified as foreground or background. If the values pertaining to different constituents in a composite are relatively distinct from one another, via correctly

setting the threshold range, a single constituent may be segregated to form a binary image (Nazar et al., 1996). For the two dimensional digital images, the best results were obtained by thresholding the images according to the 8-bit hue values due to the clear distinction in colouring of the aggregates, binder and voids as a result of the pre-treatments used. While selection of the upper threshold value was arbitrary in this case due to the significant distinction in values, selection of the lower value was identified as critical due to the closer colouring. A range of five values was selected around the perceived optimum in order to assess the impact of the value selection.

For the CT scanned images, the voxels only have a single value attributed to them corresponding to their relative x-ray absorbance compared to the specimen average. It was noted that the different phases on this scale were hard to identify visually. This was assumed to be a result of the high level of porosity of both the binder and hemp resulting in the values varying, increasing crossover of the ranges. There is no apparent way to improve this apart from using the median filter as was applied in this study and may well be a limitation of this imaging method with bio-aggregate composites. A range of three upper and three lower values for the threshold were considered, to total nine threshold ranges, to assess the sensitivity and again values were selected around the perceived optimum. Whereas a single set of threshold values was applicable to all the two dimensional digital images, it was discovered that this was not appropriate for the three dimensional CT images and so individual ranges were selected for each variation of material. It is not clear why this was the case and possible explanations will be discussed in the results and discussion sections.

3.3.2.3 Opening algorithm

An opening algorithm is a binary operation whereby pixels are added and removed depending on the values surrounding them and is actually a combination of an erosion process (sequential removal of pixels based on surrounding connectivity) followed by a dilation process (sequential addition of pixels based on surrounding connectivity), Figure 3.6 (Badel et al., 2008). For erosion of a binary image, a pixel/voxel is replaced with the background if it borders a background pixel/voxel within a 3x3(x3) surrounding area. Dilation is the opposite whereby a background pixel/voxel is turned to foreground if it borders an existing foreground pixel/voxel. The combined process of opening has the effect of cleaning the edges of discrete binary objects and removing small objects without being as destructive as the use of an erosion algorithm on its own. In the context of particle based image analysis the main rationale for use is to help separate what should be discrete particles that are narrowly overlapping and helping to remove small extrusions

on the edge of particles that may lead to misinterpretation of their defining shape (Lux et al., 2006, Li et al., 2004), Figure 3.5. Unlike the median filter and threshold filter, the application of an opening algorithm directly changes the topology of the image and so has the possibility of changing the parameter you are measuring. Because of this, the results obtained are highly sensitive to the selection of variables made within this algorithm.

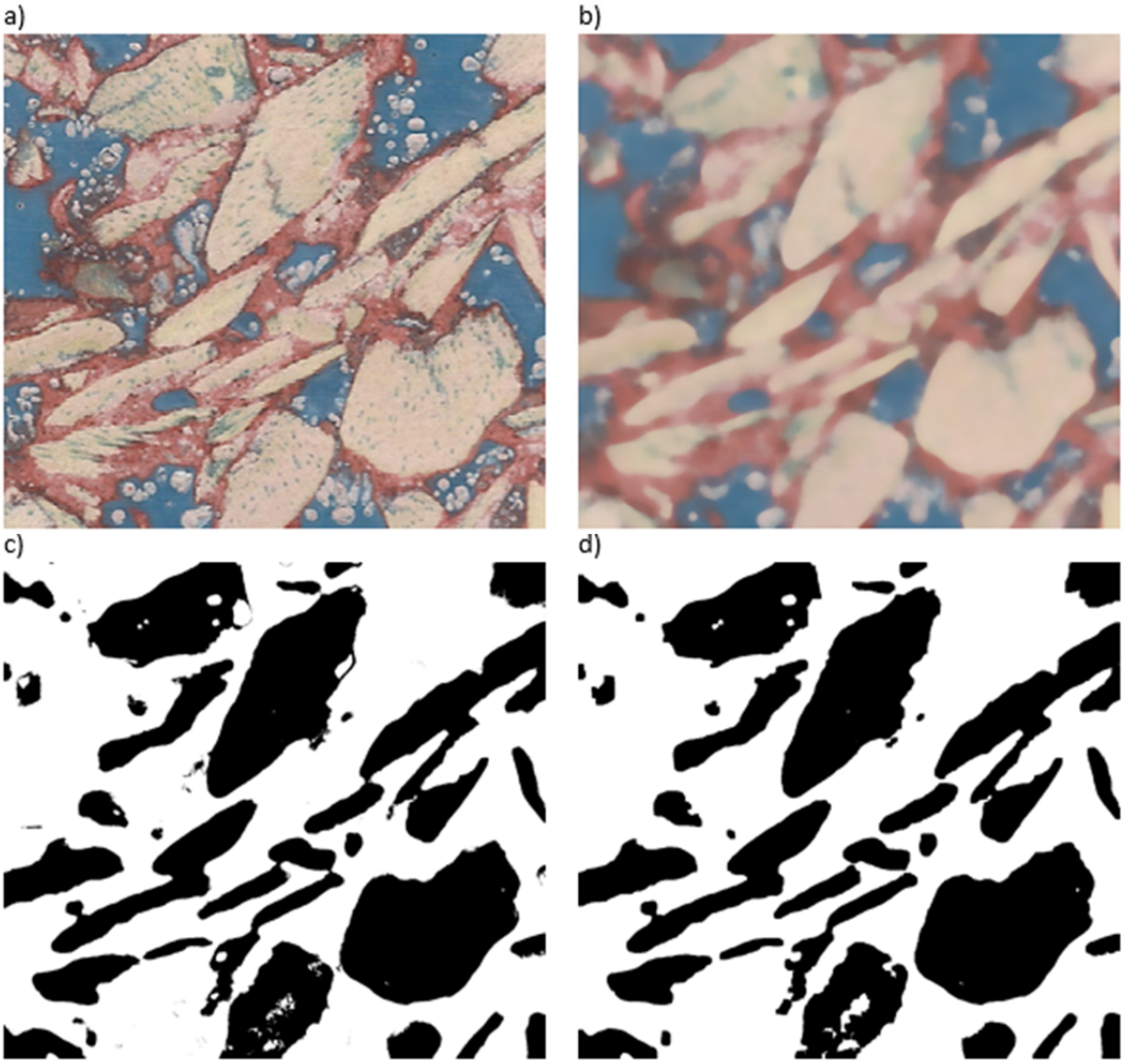

Figure 3.5: Stages of image processing. a) raw image b) median filtered c) threshold filtered d) opening algorithm.

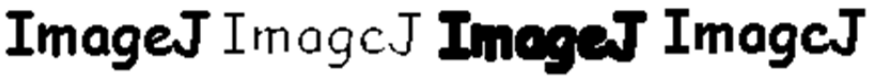

Figure 3.6: Binary image operations as given by the ImageJ user manual (Ferreira and Rasb, 2012). Left to right: original image, eroded image, dilated image, opened image.

For the two dimensional digital images, the opening algorithm used was applied iteratively and a range of iteration counts were considered in the study (Ferreira and Rasb, 2012). The range was selected in order that, at a minimum, the alteration from the

original image was just perceivable and at a maximum it was clear that the topology of the image was significantly altered. For the CT scanned images the control of the opening algorithm within the program is achieved through setting a radius, although the literature for the program operation is unclear as to exactly what this refers to (FEI Visualization Sciences Group, 2014). In light of this, a range of values were selected again to reflect a perceived similar level of impact to that observed in the two dimensional images for the range of iterations used there.

Table 3.2: The range of values for defining the median filter, threshold filter and opening algorithm used for the digital and CT scanned images within the pilot study.

Image set	Image processing and segregation parameters trialled			
	Median filter	Threshold lower	Threshold upper	Opening algorithm
Digital	5,10,15,20,25,30	10,12,14,16,18,20	50	1,2,3,5,10,15,20,25
CT scanned:	5,6,7			1,2,3
Light weight		4,5,6	28,29,30	
Standard		4,4.5,5	8,8.5,9	
Compacted		6,7,8	28,29,30	

3.3.3 Data extraction and representation

The main requirement of the method is to identify if there are trends within the orientation of the bio-aggregates, therefore the orientation of an aggregate particle must be defined. If a single particle is considered to be of elongated but unspecific form, then the orientation may be considered that of the major axis and so a definition of the major axis is required. In its simplest form, the major axis may be the line between the two perimeter points that are furthest separated, Figure 3.7. The distance between these two points is often referred to as the Feret or calliper diameter and the orientation of this axis within a plane, the Feret orientation (Dražić et al., 2016, Ferreira and Rasb, 2012). The limitations of using this method are the sensitivity to projections away from the main form that may sway the result, Figure 3.7. Indeed, in the case of bio-aggregate particles that tend more towards rectangular forms, it is unlikely that the measure would be an accurate representation, as the major axis of a rectangle being defined in this way as along the diagonal (Picandet, 2013).

A more appropriate method, and therefore one which was implemented in the pilot study, is to define the major axis as the line about which the second moments of area are minimised. This in effect replaces each distinct grouping of pixels/voxels with an ellipse/ellipsoid (two dimensional and three dimensional images respectively) of the same second moments and volume and returns the orientation of this shape where the major axis is obviously apparent, Figure 3.7. This method overcomes the limitations of the Feret orientation, not being sensitive to small projections from dominant form making it more appropriate for the random array of shapes presented by bio-aggregates.

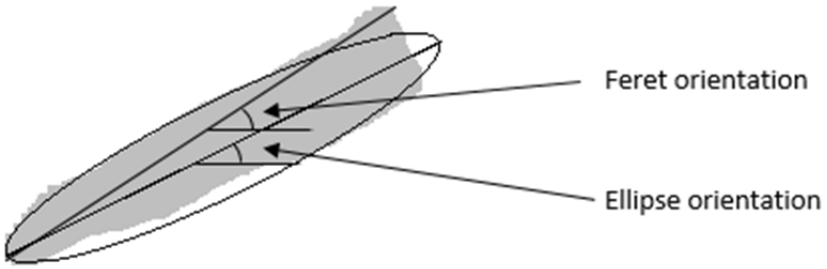

Figure 3.7: The definitions of Feret and ellipse orientations of a particle.

In order to measure the ellipsoid orientation of groups of n connected pixels /voxels, in a Cartesian coordinate system where all pixels/voxels may be assumed to have the same density, for each group of n connected pixels/voxels making a particle, the global first and second moments (m_{000}, m_{001}, m_{010} and m_{100}) may be calculated from Equation 3.1:

$$\mathrm{m_{pqr}} = \sum_{\mathrm{i=1}}^{\mathrm{n}} \mathrm{x_i^p y_i^q z_i^r} \qquad 3.1$$

From these, the central second moments (u_{200}, u_{020}, u_{002}, u_{011}, u_{101}, and u_{110}) and the centroid coordinates of the particle ($\bar{x}, \bar{y}$ *and* $\bar{z}$) can then be determined from Equations 3.2, 3.3, 3.4 and 3.5:

$$u_{pqr} = m_{pqr} - \frac{m_{100}^{p} m_{010}^{q} m_{001}^{r}}{m_{000}} \qquad 3.2$$

$$\bar{x} = \frac{m_{100}}{m_{000}} \qquad 3.3$$

$$\bar{y} = \frac{m_{010}}{m_{000}} \qquad 3.4$$

$$\bar{z} = \frac{m_{001}}{m_{000}} \qquad 3.5$$

An ellipse or ellipsoid form is then considered of equivalent central second moments, area/volume and centroid coordinates. The orientation of the principal axis of the ellipse/ellipsoid may then be found in each 2D plane from Equations 3.6, 3.7 and 3.8:

$$\theta_{xy} = \frac{1}{2} tan^{-1}\left(\frac{2u_{110}}{u_{200}u_{020}}\right) \quad 3.6$$

$$\theta_{yz} = \frac{1}{2} tan^{-1}\left(\frac{2u_{011}}{u_{020}u_{002}}\right) \quad 3.7$$

$$\theta_{zx} = \frac{1}{2} tan^{-1}\left(\frac{2u_{101}}{u_{002}u_{200}}\right) \quad 3.8$$

A mathematical derivation for Equations 3.6, 3.7 and 3.8 has been presented by others previously (Teague, 1980, Ming-Kuei, 1962, Mulchrone and Choudhury, 2004).

An important difference between the data outputs from CT scanning and two dimensional digital imaging is the reference plane used for measuring orientation. In CT scanning the full particle is measured and therefore its orientation in three dimensions is known. The generated measurements from the software can therefore describe the orientation of the true particle axis from or in any given reference plane; a plane perpendicular to compaction in the context of this study, XZ in Figure 3.8. In the two dimensional digital imaging, the angle measured is for an effectively random particle cross section within a physically cut plane; in the context of this study planes physically cut parallel and perpendicular to compaction, Figure 3.8. Resultantly the CT scanning data can be thought of as representing a true particle orientation while the two dimensional digital scanning is a representative value. There is therefore an inherent degree of error in individual particle data from two dimensional imaging and a key aspect of this comparative study was to ascertain if this is significant when a large population of particles is considered.

With an individual particle's orientation defined within a plane, it only remains to define the degree of orientation within the population present in that plane. There are several ways to assess the population, the simplest and that which was reported in the paper covering this work (Williams et al., 2016b), is to compile a frequency analysis over the population. Using a frequency analysis of the population allows for the identification of population-wide trends to be identified as well as the form of such patterns. The shortcoming of this approach is the questionable representativeness of assessing a population of particles of varying sizes in a way that they all contribute with an even weighting. It is a logical argument that a bigger particle should have a bigger weighting in terms of defining the overall orientation of the material in a similar way to which a

standard particle size distribution curve presents not the number of particles within each size range but their mass (British Standards, 2012).

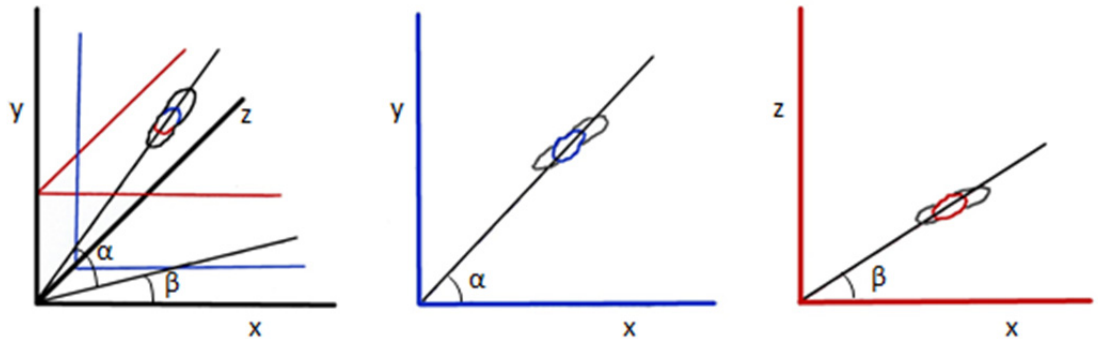

Figure 3.8: The orientation of a particle parallel, α, and perpendicular, β, to compaction in the Y axis as measured in CT images, left, and 2D cross sections, centre and right.

An alternative way to represent the population that may be considered more representative of the material globally is to present a mass distribution, and a similar methodology to that used to interpret a particle size distribution from two dimensional image analysis of bio-aggregate particles, may be used in this respect. In particle size distribution assessment via two dimensional imaging, image data are used to estimate the mass of particles to produce a particle size distributions of effective mass passing (Picandet, 2013). In the case of three dimensional images, assuming the density of particles is homogenous then volume may be used to provide an estimated mass and may be used as an alternative presentation to frequency. In the case of two dimensional images the volume is not known but may be approximated if the additional assumption of a constant aspect ratio between the three axes of the particles is made. In this case an estimated particle mass may be found from the area of the particle in the two dimensional analysis, Equation 3.9:

$$m_p = A^{\frac{3}{2}} \qquad 3.9$$

Results obtained both with a frequency as well as an estimated mass were produced in order to compare the two representations.

The orientation of the particle in three dimensions is presented by the program as its orientation within a horizontal plane and vertical orientation as measured from this plane; providing a measure or orientation viewing parallel to the compaction force and perpendicular to it respectively. In the two dimensional digital images the orientations provided were in the cutting plane which was set to be parallel to compaction and

perpendicular to compaction in pairs of specimens, allowing comparable results to be presented for both methods: a distribution when viewing parallel to casting compaction and a distribution when viewing perpendicular to casting compaction. The populations of particles considered in each case was the whole population of particles above $1mm^2$ or $1mm^3$ for the two and three dimensional images respectively, and comprised the accumulation of all six images taken for each two dimensionally assessed specimen. Due to the lack of a discernible front or end of a given particle, the orientation range was reduced to between 0° and 90°, indicating the major axis in alignment with the horizontal and vertical axis of the image respectively.

3.1 Results

As previously stated, the aim of this pilot study is not to compare the materials selected but rather to establish a methodology. Appropriately then the results are presented in a number of ways applicable to this. Firstly the two methods of imaging are appraised objectively from a usability and practicality viewpoint with respect to application within the main project. Secondly a sensitivity study is presented for the different variations within image processing in order to assess the impact these variables have on the orientation distributions produced. Lastly, following selection of the image processing considered to give the most reliable identification of particles for each imaging method, the results from the two imaging methodologies were compared and weighed against the previously considered usability and practicality implications. While not an objective of this part of the study, results are also presented comparing the distributions of bio-aggregate orientations produced viewing parallel and perpendicular to the applied compacting force.

3.3.4 Applicability of the imaging methods

Table 3.3 compares the five imaging methods against a number of key features regarding the applicability of the imaging method for the main study. The defining features of the main study that are considered in this comparison are the resource restraints: cost, time, raw materials and availability of equipment.

Table 3.3: Usability and paracticality observations of the differing imaging methods considered.

Method	Cost	Time	Raw material use	Availability of equipment
Digital imaging	Very low ≈ £0 per specimen	Low but human input intensive ≈ 20m per specimen	Destructive method, no additional materials required for specimen preparation	Flatbed scanner – consistent availability and reliability
Digital imaging with pigmented specimens	Very low ≈ £1 per specimen	Low but human input intensive ≈ 20m per specimen	Destructive method, additional pigment required but of minimal quantity for specimen preparation	Flatbed scanner – consistent availability and reliability
Digital imaging with resin impregnated specimens	Low ≈ £5 per specimen	High and human input intensive ≈ 60m per specimen	Destructive method, additional resin required in reasonable quantity for specimen preparation	Flatbed scanner – consistent availability and reliability
Digital imaging with pigmented and resin impregnated specimens	Low ≈ £6 per specimen	High and human input intensive ≈ 60m per specimen	Destructive method, additional resin and pigment required for specimen preparation	Flatbed scanner – consistent availability and reliability
CT scanning	High ≈ £100-200 per specimen depending on scan time	Very high but not human input intensive ≈ 240-480m per specimen	Non-destructive method, no additional raw materials required for specimen preparation	CT scanner – high user demand and questionable reliability - prolonged periods of maintenance

As the two dimensional digital imaging methods produce images of the same format, it was straightforward at an earlier stage to identify the best of these methods in terms of image quality without the need for time consuming processing of all the images; Figure 3.9 shows typical images produced by four two-dimensional imaging methods and illustrates this point. From these it is immediately evident that the resin impregnated specimens

provide the best visual contrast between the foreground and background. A significant improvement in handling durability of the specimens was also noticed, leading to a less damaged face being imaged. Additionally, it is noticeable that the pigmented binder gives a clear improvement in the visual distinction between the binder and the bio-aggregates that are otherwise similarly coloured. Given the obvious advantages of using both the pigment in the binder and resin impregnation for image quality, it was decided that only this approach would be followed in the latter stages of the pilot study, as has been previously mentioned. The modest associated cost in money, time and materials associated with using these pre-treatments was considered insignificant compared to the gains in this instance.

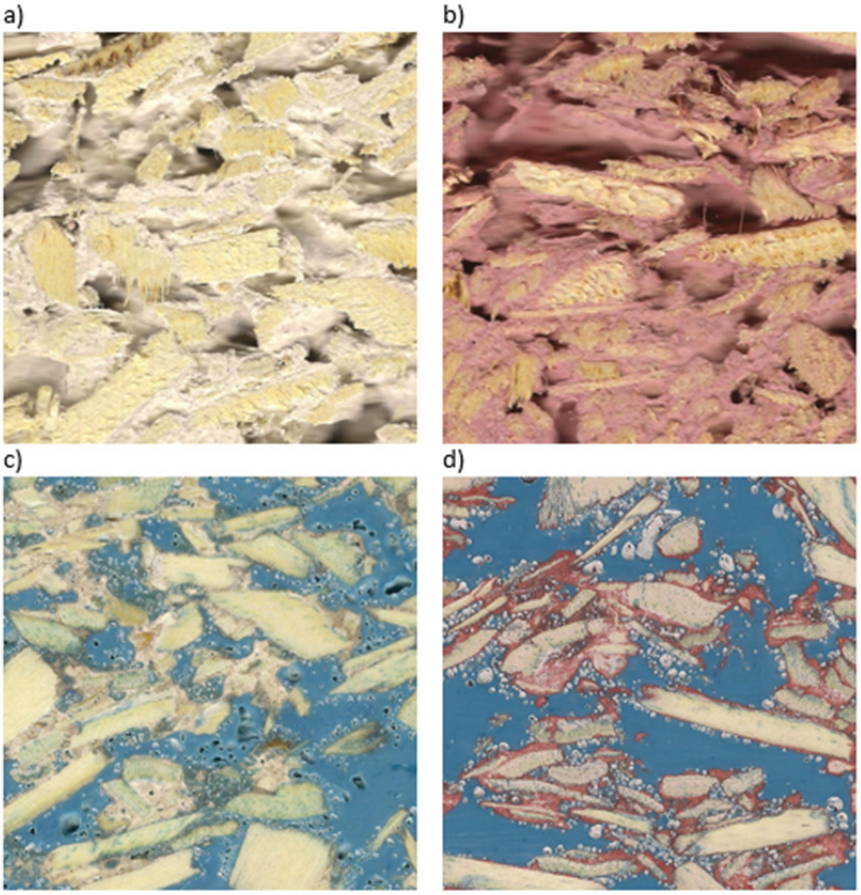

Figure 3.9: The variety of two dimensional imaging trialled a) no pre-treatments, b) red pigment added to binder, c) resin impregnation, d) red pigment added to the binder and resin impregnated.

3.3.5 Sensitivity to image processing

Figure 3.10 shows the window of orientation frequency distributions produced in a perpendicular viewpoint for the same two dimensional digital image of standard mix hemp-lime but with range of image processing values presented in Table 3.2. An important

initial observation is that the distribution is extremely swayed when observed transverse to compaction, something not observed viewing parallel. This sway is repeated across all mixes, imaging methods and processing procedures used within the pilot study and is indicative of there being a directionality within the structure of the material. The implications of this observation will be discussed in considerably more detail in the main study but within the context of developing the method, it is apparent that the perpendicular viewpoint is what must be used in order to compare and observe the impact of the imaging processing conducted.

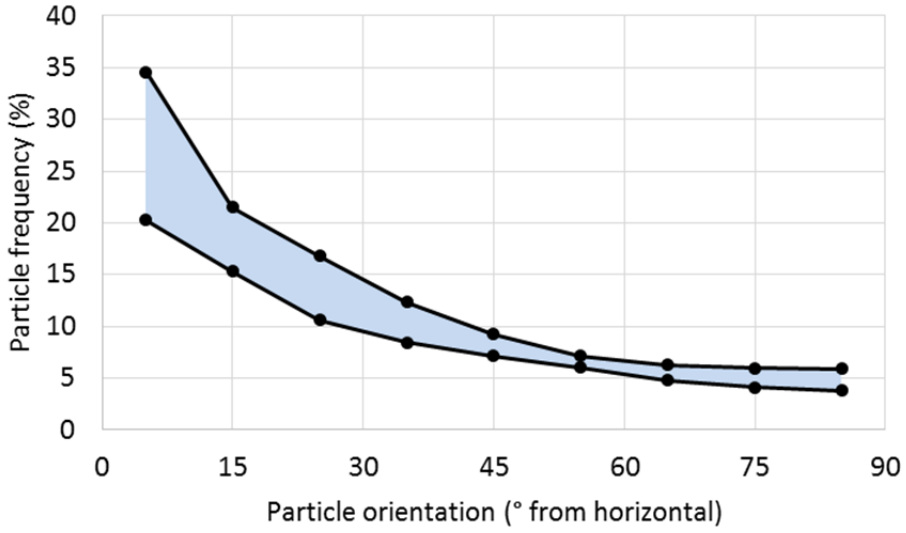

Figure 3.10: The window of frequency orientation plots obtained using the range of image processing on perpendicular, two dimensional digital images of pre-treated standard mix hemp-lime.

When considering the window of distributions produced, the impact of the image processing settings is noticeable and may be regarded as significant within the range of values considered. The window of frequency values found within to 0°-10° grouping was 15% indicating the results are highly sensitive to the settings used during processing. In order to explore this and identify any particularly onerous processes, a quantitative approach to describing the distribution is required. This may be achieved through fitting an idealised equation to the data; the fitted constants of which may then be compared and used to gauge the sensitivity of the results to the image processing variables.

The form of the equation fitted to the data was the Hankinson's formula, Equation 3.10. This equation was developed and is primarily used for the estimation of the properties of timber at different angles to the grain (Hankinson, 1921). It was derived purely empirically but has been shown to accurately predict experimental results for both solid timber (Holmberg) and manufactured orientated materials such as orientated strand

board (Nishimura and Ansell) and wood particle board (Fan et al., 2004, Kazemi Najafi et al., 2007). Bio-aggregate composites are very similar to these materials and while the Hankinson formula is mostly used to model physical properties, previously the Hankinson's formula has been used successfully to model the orientation distribution of a particle population within the context of paper production (Schulgasser). Given the particulate construction and directional manufacturing process, this may be seen as a direct precedent for use here. Several other possible equations forms were considered including a sinusoidal curve and a quadratic form however the Hankinson's form was found to be significantly closer to the experimental results.

$$f = \frac{f_0 f_{90}}{f_0 sin^n\theta + f_{90} cos^n\theta} \qquad 3.10$$

Equation 3.10, may be fitted to the orientation distributions through a method of solving for the least squares condition. Through this, the constants: f_0, f_{90} and n can be found where n represents the shape function, and the values of f_0 and f_{90} are the bounding maxima and minima values of the distribution. The value of the shape function, n, and the difference between f_0 and f_{90}, indicative of the degree of sway in the distribution, may therefore be used as useful metrics to compare distributions. The values of $(f_0 - f_{90})$ found when one image is processed using all possible variations of image enhancement settings in Table 3.2 are plotted in Figure 3.11 and Figure 3.12 for a two dimensional digital imaged and a three dimensional CT image respectively. In both cases the data are plotted in triplicate (two dimensional digital images) and quadruplicate (three dimensional CT images) so to identify specific sensitivity to each of the image processing stages.

In order to determine the best set of parameters to use with each method, a quantitative approach is not practical as the "best" identification of particles is impossible to quantify. Instead a simpler approach was adopted whereby an overlay of the ellipsoids found using each permutation of enhancement parameters was compared to the original image by eye. This was conducted in a "winner stays on" approach, whereby two overlays were evaluated against each other visually and the one considered to be less representative discarded and replaced. This process was continued for all permutations. While this method is based on human perception and therefore may be considered of less rigour, the human eye is exceptionally attuned to the identification of objects within an image (Ranasinghe, 2008) and thus offers the best form of calibration available within the context of the study.

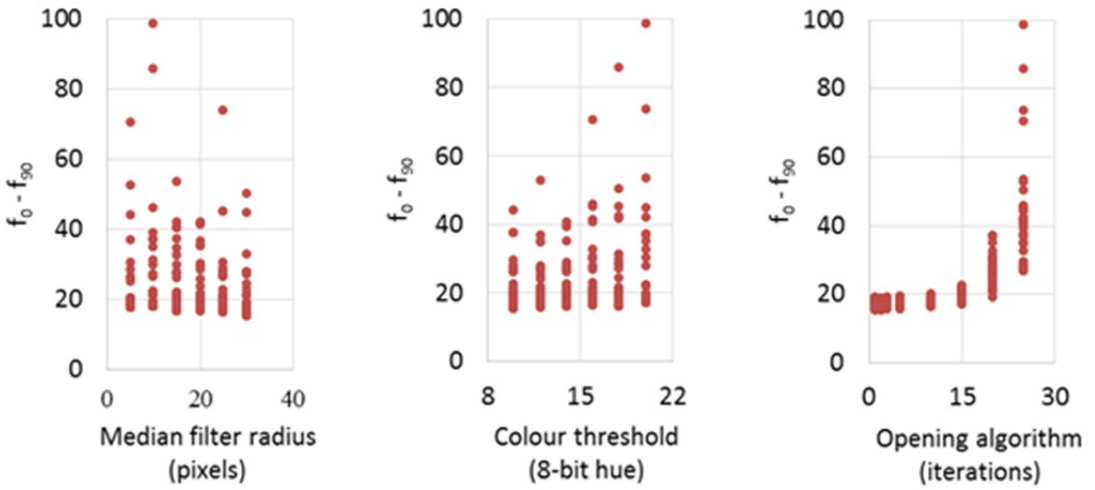

Figure 3.11: The sensitivity of $(f_0 - f_{90})$ to image processing criteria of median filter, colour threshold and opening algorithm settings (left to right) obtained for orientation frequency distributions of the same two dimensional digital image of standard mix material.

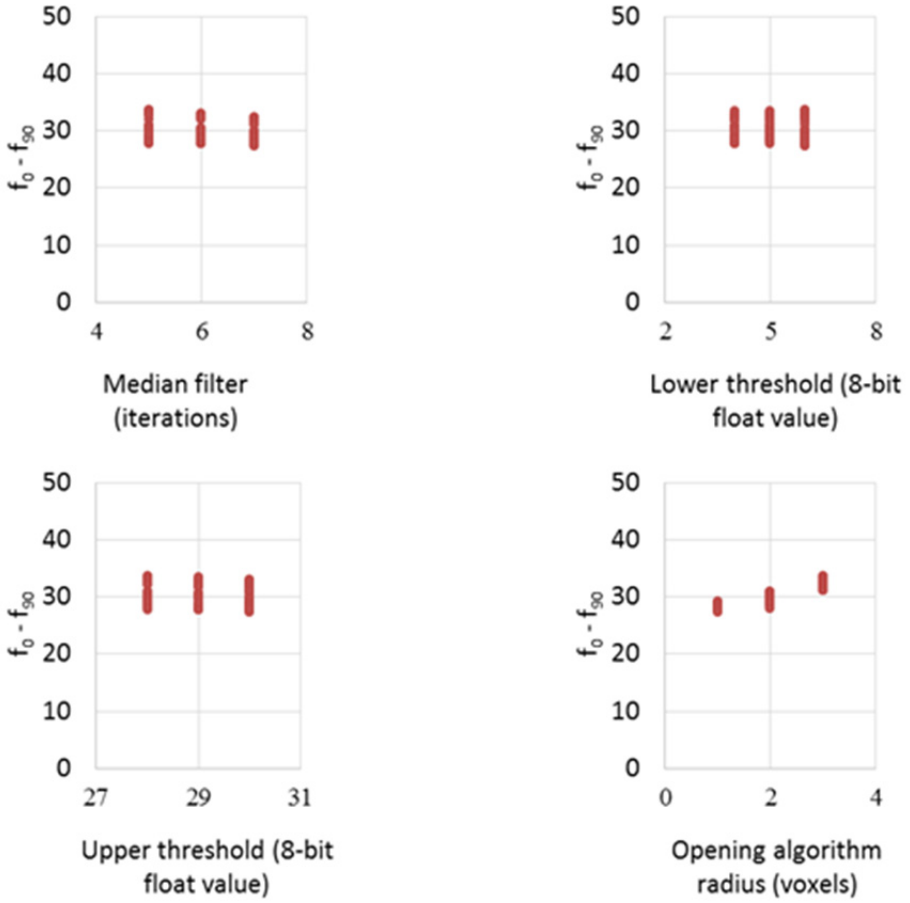

Figure 3.12: The sensitivity of $(f_0 - f_{90})$ to image processing criteria of median filter, colour threshold and opening algorithm settings obtained for orientation frequency distributions of the same three dimensional CT image of standard mix material.

3.3.6 Orientation distributions

The orientation distributions of both estimated mass and frequency, for all three mixes and produced using the optimally considered image processing, are presented in Figure 3.13 and Figure 3.14 for two dimensional digital and three dimensional CT images respectively. In all cases the Hankinson's formula, Equation 3.10, has been fitted to the data to aid visual comparison with the derived values listed in Table 3.4.

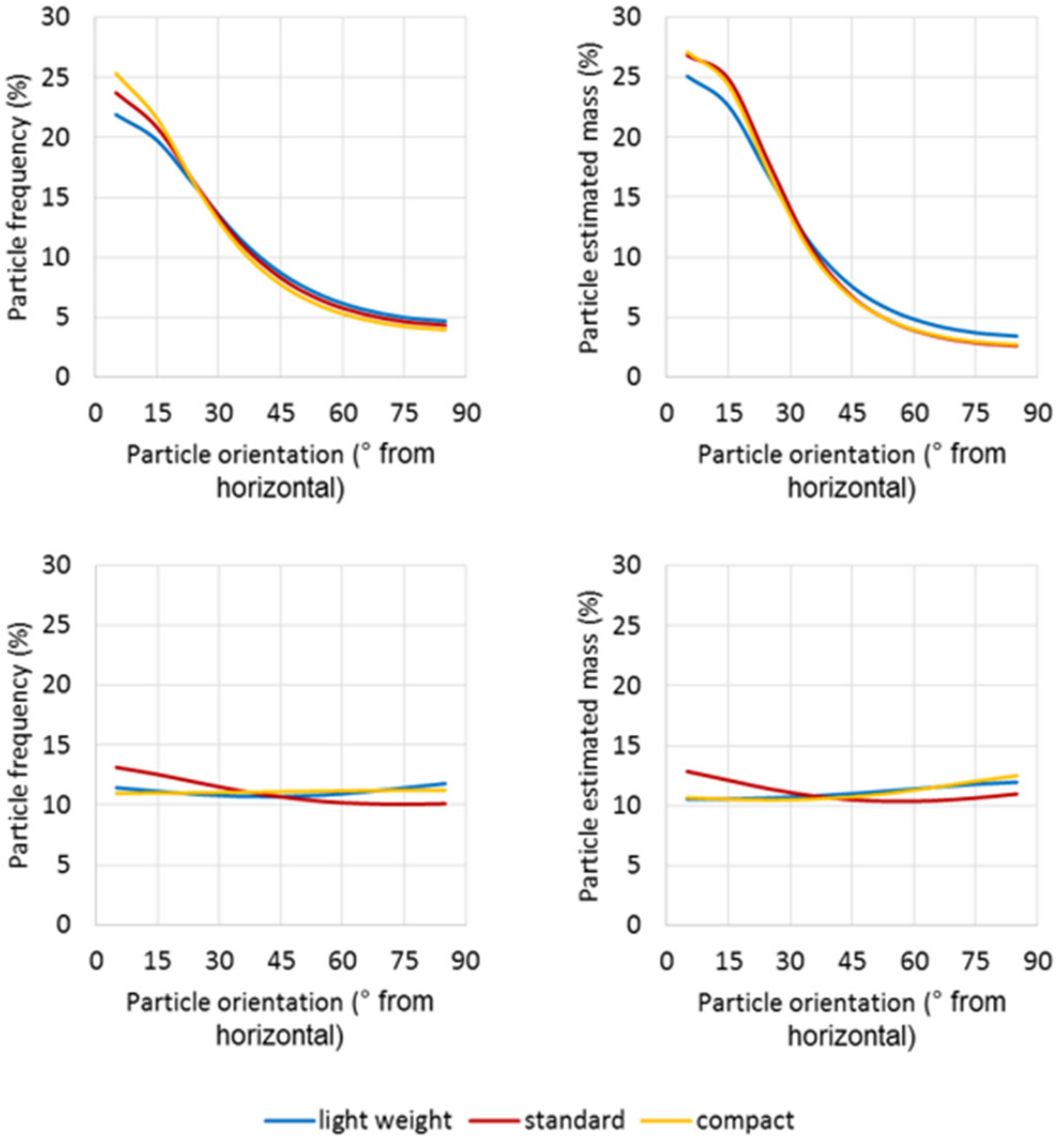

Figure 3.13: Particle orientation distributions obtained by two dimensional digital image analysis presented by particle frequency (left) and estimated mass (right) and for perpendicular to compaction and parallel to compaction viewpoints top and bottom respectivly.

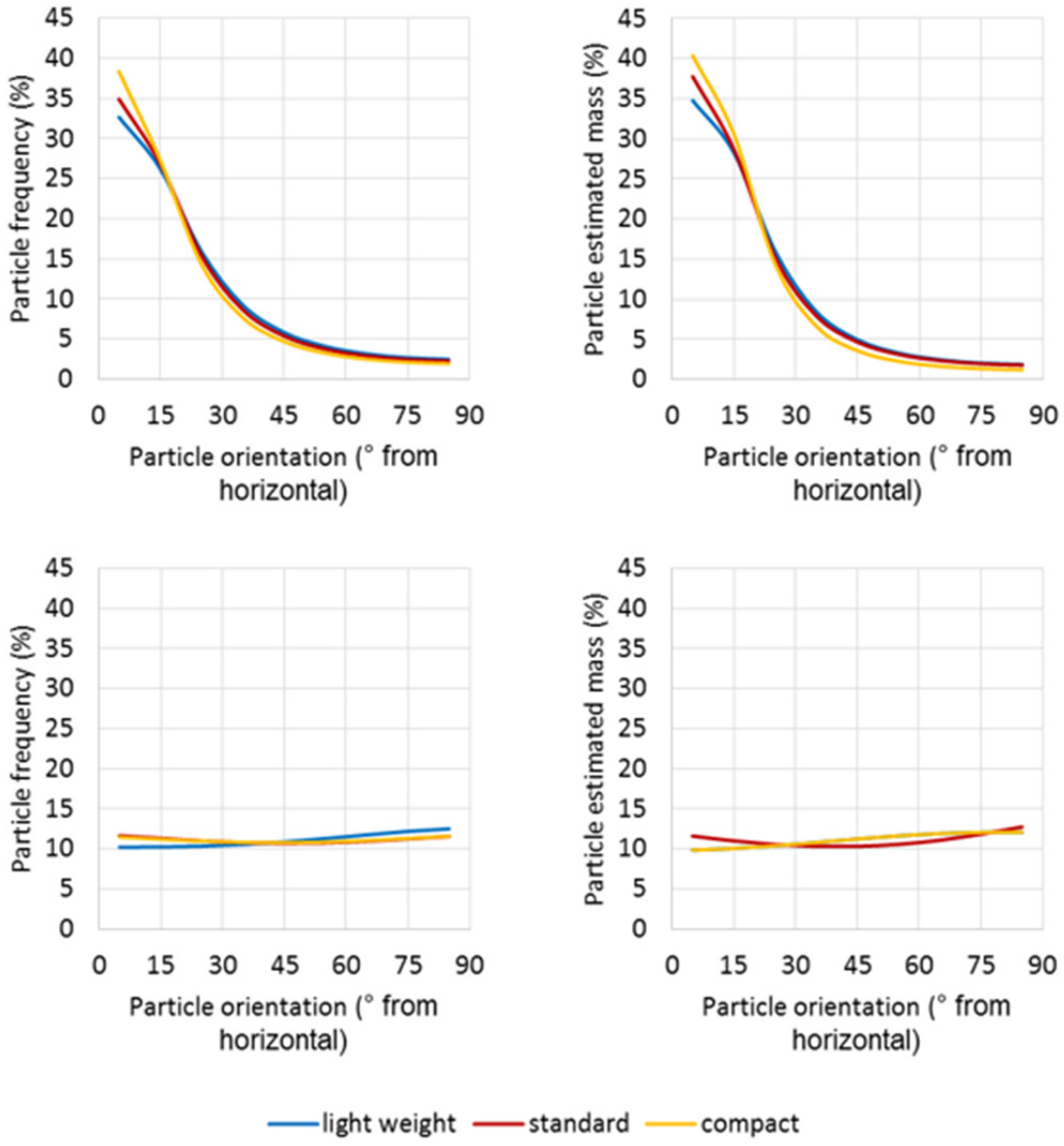

Figure 3.14: Particle orientation distributions obtained by three dimensional CT image analysis presented by particle frequency (left) and estimated mass (right) and for perpendicular to compaction and parallel to compaction viewpoints top and bottom respectivly.

Table 3.4: The fitted Hankinson's values for particle orientations perpendicular to compaction from two dimensional digital imaging and three dimensional CT imaging.

	Two dimensional digital imaging				Three dimensional CT imaging			
	Frequency		Mass		Frequency		Mass	
	n	$(f_0 - f_{90})$	n	$(f_0 - f_{90})$	n	$(f_0 - f_{90})$	n	$(f_0 - f_{90})$
Light weight	2.36	17.39	2.67	21.72	2.71	30.45	2.99	32.97
Standard	2.51	19.40	3.02	24.11	2.70	33.04	2.90	36.23
Compact	2.33	21.76	2.88	24.37	2.70	37.01	3.23	39.18

3.4 Discussion

3.4.1 The imaging method

From Figure 3.9 it is evident that optimal two dimensional imaging of hemp-lime requires the addition of two pre-treatments to the specimens to overcome an inherent lack of contrast between the constituents. It is possible that the use of other bio-aggregates and binders may make these stages unnecessary, although due to the general similar colouration of most bio-aggregates as well as the predominance of lime based binders, this is considered unlikely. These processes must therefore be accepted as necessary requirements for the two dimensional assessment of most bio-aggregate composites. As mentioned previously, the small increase in cost, time and resources required, Table 3.3, to carry out these pre-treatments is considered acceptable against the significant increase in image quality. While considered unlikely, due to the low concentration used, it is possible that the pigmentation of the binder could impact the material properties of the composite which may be an issue in certain cases. For rigour, separate physical tests were subsequently carried out using all three mixes on pigmented and non-pigmented materials and no discernible difference was found in the compressive strength, compressive stiffness and thermal conductivity.

Three dimensional computer tomography imaging is very time intensive compared to two dimensional digital imaging, but critically less labour intensive due to no requirement to pre-treat the specimen, Table 3.3. While this is beneficial, a lack of pre-treatment options may equally hamper applicability; with hemp-lime it was observed, as will be discussed later, that selection of the threshold values was difficult due to the lack of a clear distinction in the x-ray absorbance of the constituents. For other bio-aggregate composites

it is possible that this may even be worsened due to altering densities, limiting applicability of this method unless a solution for increasing contrast is found. The other major problem with the method, at least within the context of this study, is the cost of the process which is considerably higher than two dimensional digital methods, Table 3.3. This is as a result of the more specialised equipment required to undertake the imaging and is a major consideration for projects where a large number of material variants are to be considered; the poor availability of the equipment is also a disadvantage for this reason.

From Figure 3.13 and Figure 3.14 it is apparent that three dimensional and two dimensional methods provide distinct results from one another. In general terms the three dimensional computer tomography results provide a smoother distribution that is closer to the fitted Hankinson's formula. The difference is considered to be due to the comparably larger population of particles assessed by this method. This is the biggest perceived benefit of this method over the digital imaging method as it makes for a more representative and reliable result. The lower level of smoothness obtained in the two dimensional data may be improved upon by increasing the number of sections analysed however this has an associated financial, time and resource cost that must be considered.

The main difference to emerge between the distributions is a consistently higher value of $(f_0 - f_{90})$ from those obtained from CT scanned images, Figure 3.13, Figure 3.14 and Table 3.4. A likely reason for this is the subtle difference in what is measured by each method described previously. CT scanning allows each particle to be measured in their entirety and at an orientation from the horizontal plane, while conversely digital imaging measures a random section through each aggregate within the plane of cutting, Figure 3.8. The implication of this difference is effective overlay of a random, even, distribution in the results from two dimensional digital images to account for the random section orientation. While this seemingly does not overwrite the trends visible in orientation, it does have the effect of dulling the trend, causing the lower values of $(f_0 - f_{90})$ and higher values of n, reducing the perceived level of orientation. This does not invalidate the method as a comparative tool as long as the differences between different composites remain detectable which can be seen to hold true when frequency distributions were considered. This indicates that within the context of the materials being assessed in this project, the digital imaging method is an appropriate tool for assessing and comparing the orientation of the bio-aggregates. It should however be acknowledged that as the distributions are altered in both degree of orientation and shape depending on the method, two dimensional digital imaging would not be a valid tool for applications requiring a true description of topology, such as computational thermal and mechanical properties, without some form of correction.

3.4.2 The processing method

From Figure 3.11 and Figure 3.12 it is firstly evident that the image enhancement settings have a significant impact on the results. For the two dimensional method, this was found to be up to a 175% variation in the value of $(f_0 - f_{90})$ for the range of parameters used within this pilot study. The variance in the three dimensional images was found to be of significantly lesser magnitude, 25%, considered to be a result of a narrower variety of image processing settings considered and the differences between how the processes are carried out by the respective programs used. In all cases it is evident that consistency must be maintained in image processing in order to ensure comparability of the results.

In both the three dimensional and two dimensional images it is the opening algorithm that is observed to have the biggest impact; when this is controlled the variation in $(f_0 - f_{90})$ for two dimensional images drops to around 23%. The reason for this significant impact is considered to be the nature of the algorithm directly altering the topology of the image. The best perceived identification of particles was obtained when the value of the opening algorithm was set to three iterations for two dimensional images and a radius of three voxels for three dimensional images. At these values the algorithm may be considered to provide the optimal balance between segregating lightly touching aggregates and removing outliers, and altering the shape of the aggregates and measured orientations. Above this value the impacts of this process are seen to drastically increase as the particles become eroded to the point of losing their defining shape.

It can be seen from Figure 3.11 and Figure 3.12 that both the median filter value and the threshold value have less impact on the results than the opening algorithm. The median filter parameters perceived to give the best identification of aggregates were a 20 pixel radius and three iterations for the two dimensional and three dimensional processes respectively. It is considered certain that this is related to the resolution of the image and thus the pixel size and so it may be appropriate to re-establish a value in the event of using images of differing resolutions. In this instance, given the very high value of 20, it is considered that the scanning resolution used of 2400dpi was excessively high and may be reduced to lower file sizes and so reduce analysis time; preceding studies into asphalt that has particles of similar magnitudes have employed lower resolutions, supporting this opinion (Le Troëdec et al., 2011, Yue and Morin, 1996). Given the apparent sensitivity of the result to the median filter a consistent value should be used.

The setting of the threshold filter upper value in two dimensional images was observed to have no impact due to the very clear distinction in hue between the blue resin and the

mostly yellow aggregate, Figure 3.15, and so consideration of a range of values was not required. In contrast the threshold value selected for segregation of the aggregate from the binder is found to have significant bearing as a result of an overlap in the hue values possible in both media, Figure 3.15. In this instance it was observed that the best value was hard to select and while a value of 14 was used, it was noticed that this was a compromise between the three mixes considered and differing values may have actually been more appropriate for these cases; perceived to be a result of natural variation in the colour of the aggregate. To overcome this in the main study, while maintaining a consistency of process, a defined and repeatable methodology for selecting this value is required as the results are again sensitive to the selection of this value.

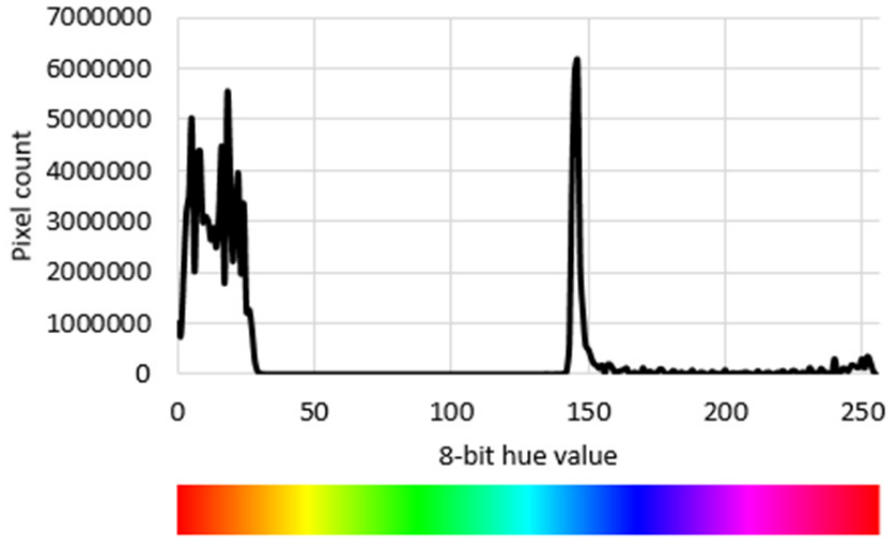

Figure 3.15: The 8-bit hue distribution of pixels in a two dimensional image of fully pre-treated hemp-lime standard mix.

As with the segregation of the aggregate from the binder in two dimensional images, segregation of all three phases (void, bio-aggregate and binder) was not clear cut in the CT images, Figure 3.16. The lack of contrast is likely a result of the large amount of small scale porosity within the aggregates and binder that cause local variation in the x-ray absorbance, creating significant overlap between the value envelopes of the three components. Unlike with the two dimensional imaging, it is not clear if specimen pre-treatments may help improve the contrast and indeed this may be considered a limitation of the method. Appropriate values in this case were so significantly different for each of the three mixes of material considered that a compromise, as used for the two dimensional images, was not applicable. To overcome this, the process must either be conducted by eye, increasing the scope for human error, or, as proposed for two dimensional imaging, selected based on a consistent mathematically applied methodology.

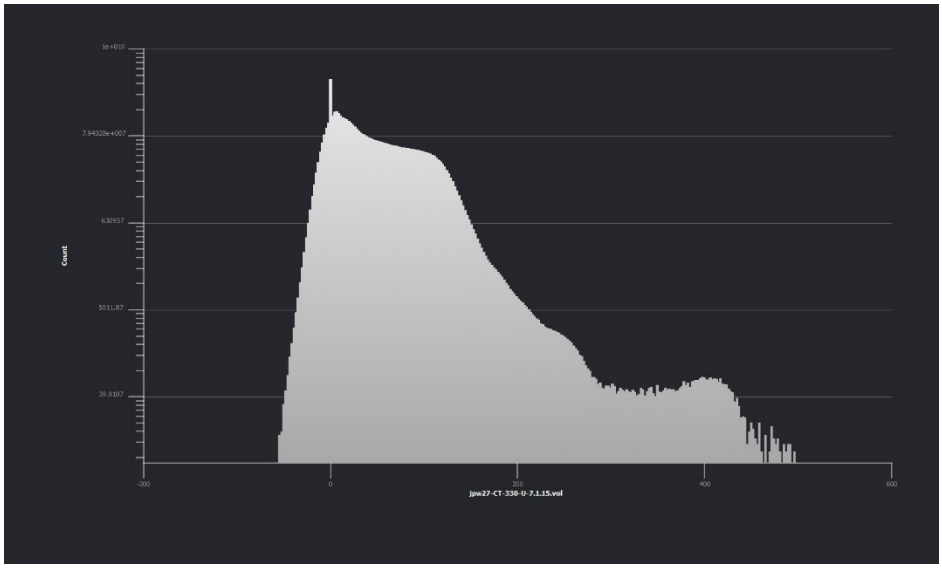

Figure 3.16: The 32-bit float value distribution of voxels in a three dimensional image of hemp-lime standard mix.

3.4.3 The distribution analysis

From the differing methods of presenting the distributions, by frequency and by mass, Figure 3.13 and Figure 3.14, it can be seen in general terms there is limited difference to the forms produced. In the three dimensional imaging this similarity is strongest with both the form of the distributions as well as the perceived order of most to least orientated being the same. This consistency is not fully repeated in the two dimensional image analysis where the same form is observed but the standard mix and compact mix are observed to have similar levels of orientation in the cumulative mass distribution. In light of this it is considered likely that the comparably larger number of particles observed in the three dimensional imaging reduces the sensitivity of the mass distribution to particularly large particles that likely accounts for the results from the two dimensional imaging. While the mass distribution is arguably more representative measure of the materials structure, the seeming increased sensitivity of this method of data processing must be considered in analysis of small particle populations.

In addition it has also been possible to confirm the long standing view within the literature that the material has an anisotropic internal structure. From Figure 3.13 and Figure 3.14 it is observable in all the specimens that there exists a sway in the orientation for the aggregates to align their major axis perpendicular to that of the compaction force applied in casting. Orientation sway of particles is a logical occurrence resulting from compaction and explains anisotropic behavioural patterns observed by others in thermal conductivity and compressive strength. Despite this anecdotal evidence there was no direct evidence to

confirm the concept prior to this study and this formed one of the major findings of the journal paper reporting this part of the project.

3.5 Conclusions

The pilot study was considered very successful as it has shown there are multiple methodologies that may be employed that provide coherent results for the assessment of the degree of orientation within bio-aggregate composites. In addition it has been established that there is a measurable anisotropy within cast bio-aggregate composites due to the directional production process, confirming this long hypothesised condition.

The following key aspects regarding the most applicable processes to be used in the main part of the study and indeed future work have been identified:

- A high level of contrast between the constituents within the image is important for accurate analysis and pre-treatments or processes that enhance this without altering the structure to be measured should be applied where possible.
- Both three dimensional and two dimensional imaging processes are effective, with computer tomography imaging offering a greater level of data capture and more representative values, whereas two dimensional imaging offers a more cost effective process with a greater degree of contrast between constituents.
- A degree of image processing is required prior to taking measurements in order to get the best results. The processes used are applicable both in two dimensional and three dimensional images. Image processing has a significant bearing on the results and so a standardised method must be adopted to ensure fair comparison.
- The most appropriate way to assess the overall distribution of a population of particles is to consider a mass distribution although the results are sensitive to small populations of particles and a frequency distribution may be more applicable in these cases.

Based on the experiences and results obtained from the pilot study, a standardised method is proposed for the assessment of orientation within bio-aggregate composites that was adopted in the rest of this study.

3.5.1 A standardised method for the assessment of orientation within bio-aggregate composites

Two dimensional image analysis was used on account of the high cost of computer tomography scanning and the number of variants being considered in the study. For each variant three 150mm cube specimens were used, increased from the single specimen used in the pilot study to increase the population assessed. These specimens were produced using the normal production process with the single alteration of adding a red lime pigment to the binder at a dosage of 10g per specimen. The pigment used was a powder based, inert, finely ground compound specified for use with lime materials and supplied by Ty-Mawr of Wales, Figure 3.17. As per the manufacturer's recommendations for the production of coloured lime render, the pigment was slaked with a small amount of water 24 hours prior to casting and added to the binder slurry mid-way through mixing.

Specimens were cured for a minimum of 28 days and in the optimum conditions specific to the bio-aggregate composite used in order to develop sufficient strength and durability for cutting. In the case of hemp-lime, conditions of 50% relative humidity and 20°C were used with the moulds removed after 6 days to enable faster removal of excess water and permeation of carbon dioxide. After curing, the specimens were sectioned into six slices using a band saw. The band saw used was fitted with a fine blade of 12 teeth per inch in order to minimise tearing of the material when cut and to preserve the face in a good condition. The casting orientation of the specimen was marked onto each slice.

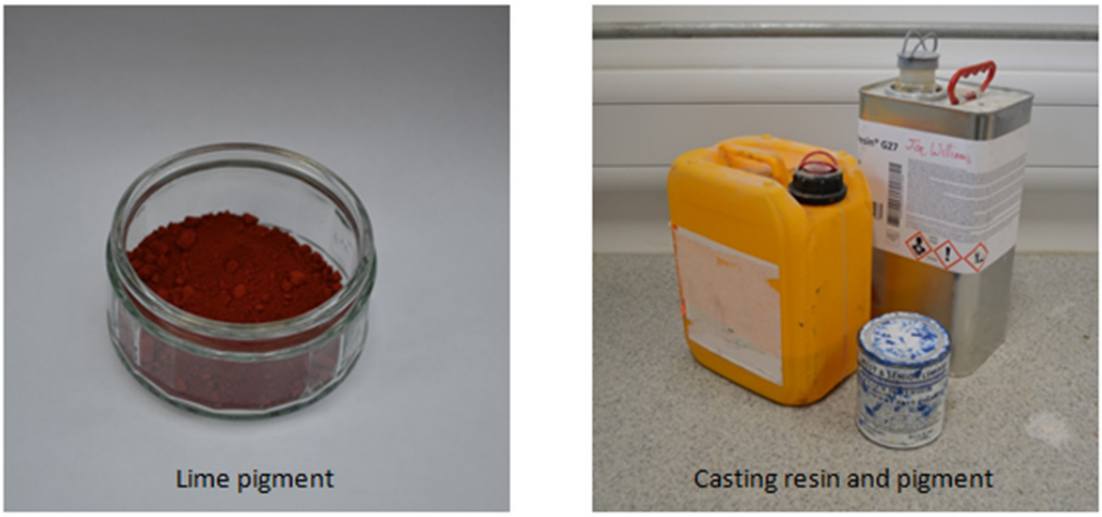

Figure 3.17: Additional materials used for the pre-treatment of hemp-lime for two dimensional imaging.

The faces were prepared for scanning by impregnating with resin and then sanding. The resin used must be distinctly coloured from the binder and hemp and of a low viscosity in

order to be clearly distinguishable from the other constituents and penetrate the full range of visible voids. Sika Bi-resin 27 was used in this case with a blue resin pigment, Figure 3.17. The resin casting process, Figure 3.18, was conducted by preparation of 100ml of resin per slice to the manufacturer's instructions, which was then transferred into a suitable size of prepared tray. The tray used was 330mm X 490mm, sized to accommodate all the slices being cast comfortably but with minimal spare area; it was levelled and applied with a mould release agent prior to use. The slices were individually placed into the resin tray slowly to allow filling of the pores and then held in place until the resin solidified. The resin cast faces were sanded using a belt sander initially with an 80 grit paper to remove excess material and then with a 120 grit paper to remove any marks from the coarser paper.

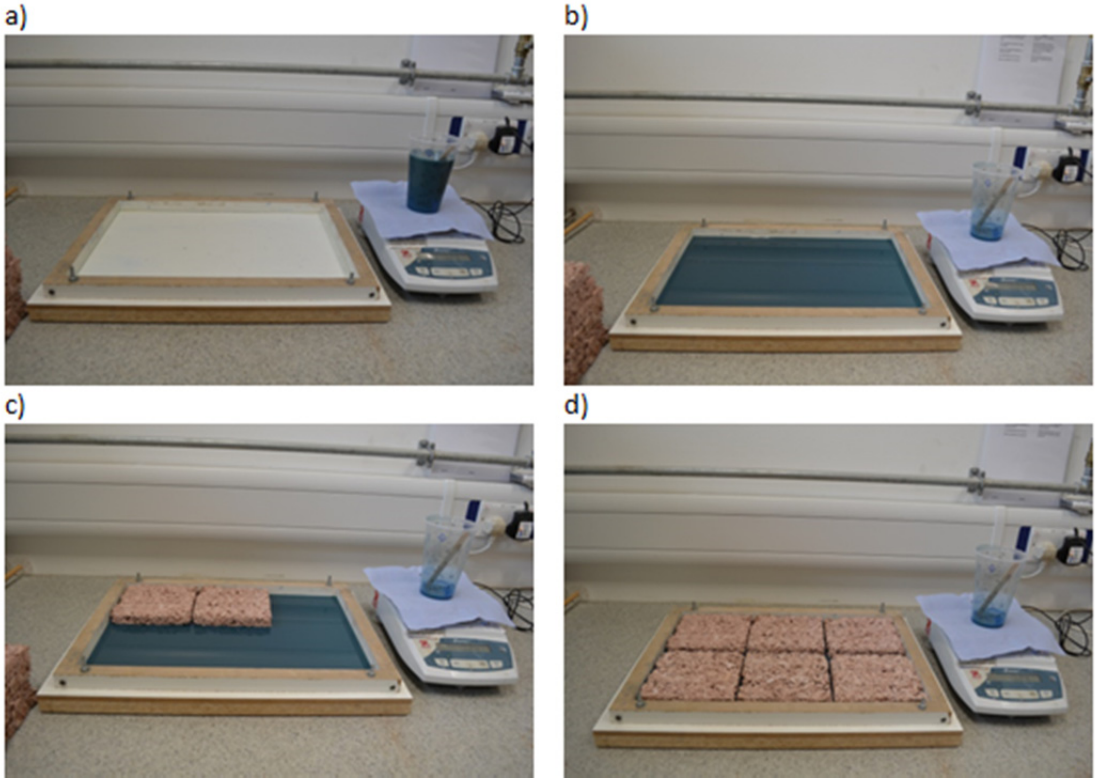

Figure 3.18: Resin impregnation process of hemp-lime specimens.

Scanning was undertaken on a Hewlett Packard A4 scanner at 1200dpi, reduced from 2400dpi due to the excessive detail this gave. Prior to positioning the specimens for scanning, the faces to be scanned were cleaned with water and tissue paper to remove dust. As the scanner digitises a whole A4 area but the size of the cut faces is smaller, a template was used to position the face in a constant location to allow for automated cropping of the images. Each image is cropped using a macro script to give images of 6800 pixels square that were individually inspected by eye for defects such as dust, or other foreign objects, and to establish that the images were correctly framed.

Image enhancement was carried out in the same three stages as used previously. Firstly a median filter with a radius of 10 pixels was applied - reduced by a factor of two from the optimum identified radius in the pilot study to account for the reduction in image resolution of the same magnitude. After each processing stage the images were copied to a new file location to maintain the original versions of each image for reference.

The threshold filter level used to segregate the bio-aggregates from the voids was a set 8-bit hue value of 50 within a hue-saturation-luminosity colour space. The pilot study identified that different values for the threshold value between the bio-aggregates and the binder were appropriate for different material varieties and images in order to get the most accurate perceived segregation. It was also identified that there is a requirement for standardisation within the process, given the impact it can have on results. For this reason an algorithmically determined value for the threshold between binder and aggregates was used. The algorithm used is referred to as IsoData and is an iterative process to find a threshold value that is equidistant from both the average value of the pixels above the threshold and those under it; satisfying Equation 3.11 (Ferreira and Rasb, 2012):

$$Threshold\ value = \frac{average\ value\ above\ threshold + average\ value\ under\ threshold}{2} \qquad 3.11$$

This method was trialled along with a series of other possible algorithms prior to being selected, based on the modest run time and a very good correlation to the optimum threshold value as judged by eye. As well as using these thresholds to identify and segregate the bio-aggregates, by using a third fixed value threshold with an 8-bit hue value of zero, the distinction can also be made between binder and voids. This allows for the measurement of the separate areas of each of the three constituents at this point that was undertaken using the measure tool inbuilt to the program.

Following conversion to a binary image via the threshold, an opening algorithm was applied to clean the images. Based on the pilot study, three iterations of the algorithm were used. The analysis of bio-aggregate orientations was undertaken via the particle analysis tool within the ImageJ software. The orientation reported for each discrete group of pixels is established via the elliptical fitting approach discussed and mathematically detailed previously. In each case, as well as the orientation of the bio-aggregate, the area was also reported. The data collected were presented as a frequency distribution as while the estimated mass distribution is considered more informative the pilot study identified a possibly higher level of sensitivity to certain features of the material resulting in less reliable comparisons when compared to the CT results. In each case the population each variation of material was all of the observed bio-aggregates from all six images from each

of the three specimens. As with the pilot study, the orientation distribution of 0°-180° was manipulated to 0°-90° given the lack of a front and back within the major axis of a bio-aggregate. The resulting plots of estimated particle mass against orientation between 0° and 90° are then presented as the outcomes of the analysis, one plot for imaging in the direction of compaction and one plot for imaging perpendicular to it, Figure 3.19.

In order to more easily compare results and contrast the varying degrees of orientation, the Hankinson formula (Equation 3.10) was fitted to each distribution from perpendicular imaging. This was achieved by finding the least squares fit to the experimental data in each case. The Hankinson plots as well as the values of $(f_0 - f_{90})$ were then used to directly compare variations of material.

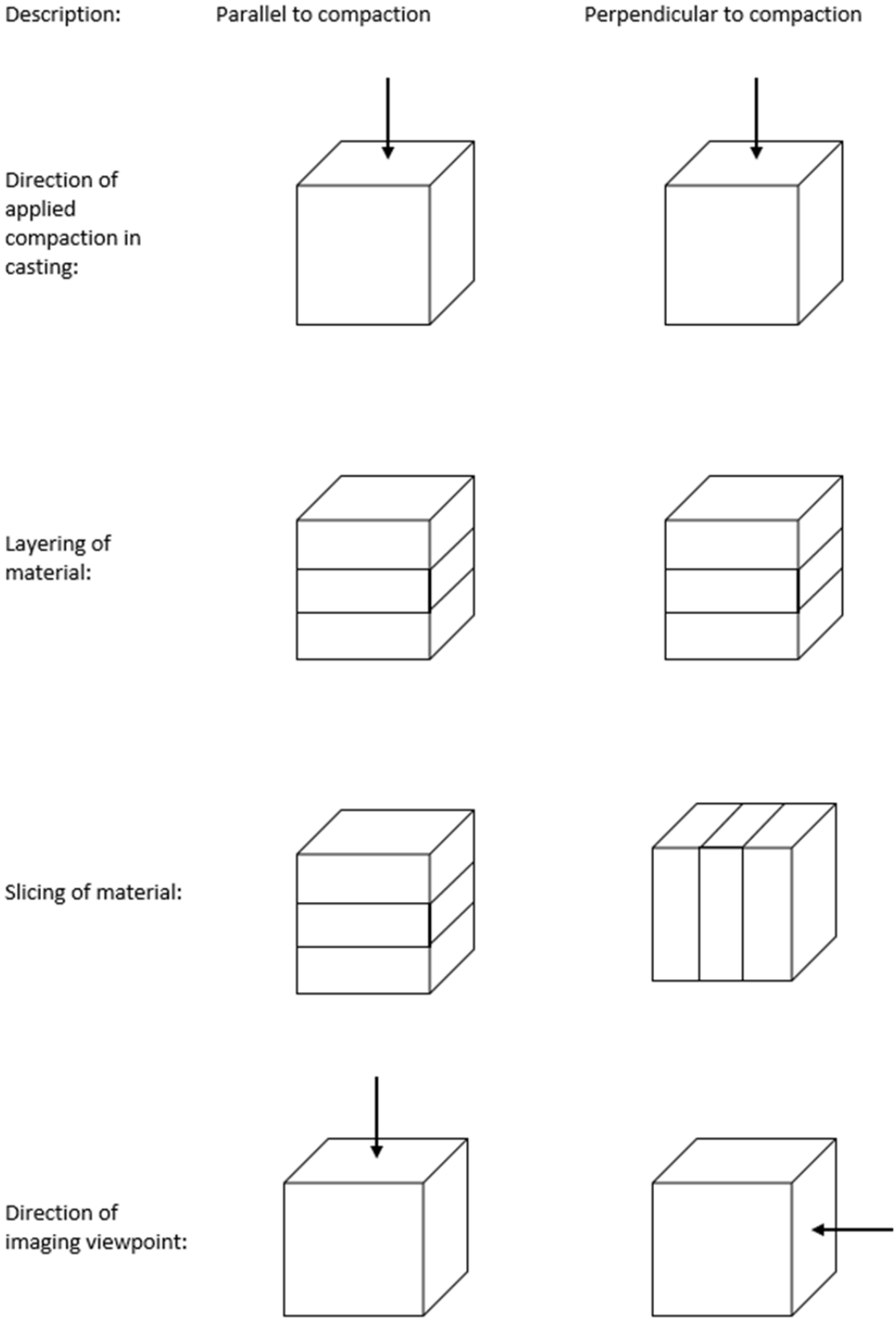

Figure 3.19: The definitions of parallel and perpendicular imaging with respect to compaction direction and material layering as adopted in the study.

4 Experimental study

In this section the main experimental parts of the study will be presented. As the study was split into two distinct phases the results will be considered in separate sub sections while common aspects (classification of raw materials and experimental procedure) will be presented first.

The literature review, Chapter 2, identified that there are a large number of variables that have an established or potential impact on the properties of bio-aggregate composites. The variables in this study have been split into two categories:

Constituents:

- The nature of the bio-aggregates – size distribution
- The ratio of binder to bio-aggregates by mass

Implementation:

- The method of application used – cast or projection formed
- The level of compaction obtained
- The thickness of layers used to build the material

In contrast with other studies, the novel and important distinction of this experimental program was to consider the impact in a directional context. The pilot study confirmed that bio-aggregate composites have an orientated layout of particles and some limited previous work has shown a directional dependence in the properties of the materials in individual cases (Pierre et al., 2014, Nguyen et al., 2010, Nozahic et al., 2012, Youssef et al., 2015). What was yet to be established, and is the intended outcome here, is to identify if the impact of the constituent and the implementation variables is global or directionally dependent with respect to the direction of compaction.

The physical properties measured in this study are:

- Compressive behaviour, ultimate strength and failure mode: used as a general measure of durability and handle-ability, properties required for precast production particularly.
- Flexural behaviour, ultimate strength and failure mode: used as a measure of handle-ability as well as being required in walling contexts to convey horizontal loads to the structural frame.

- Thermal conductivity: used as a measure of thermal performance in an insulating context and used in the majority of building design scenarios to show compliance to thermal regulations.

These properties are those identified as most important for the expanded use of the material and while arguably not representative of some of the material's main benefits, they are important within the current requirements of building regulations and industry. As all these properties are a response to directional action, either via force or thermal gradient, they must be considered both in the direction of compaction and perpendicular to it.

As well as directional physical tests, it is also required to assess the internal structure of the composites produced. This is necessary to aid identification of the mechanics behind how these properties develop and thus inform behavioural modelling. The assessment of internal structure was achieved through the method established in the pilot study to assess the degree of orientation within the bio-aggregates.

In summary, the extent of the required experimental work involves assessing the impact of five variables on four properties and in two directions. In most cases, apart from the method of application, three values for each of the variables are required. If the variables are considered to be interdependent then this would give a total of 162 variations to consider in each direction and for each property. Given the time and resources constraints of this project, such an extensive experimental programme was not feasible. As an alternative, the decision was made to consider each of the variables in turn and thus as independent, reducing the total variations to 10. While it is not clear if it is justifiable to consider these variables as independent, no previous evidence was found for or against this assumption within the literature and as a result, the practical constraints dictate this approach.

4.1 Characterisation of raw materials

Both the bio-aggregates and the binder must be characterised. As well as the thermal conductivity and appropriate mechanical properties it was also prudent to obtain certain other properties that have a bearing on the combining of the materials such as hydration of the binder and water absorption of the bio-aggregate.

4.1.1 Bio-aggregates

The bio-aggregates used in the study were hemp particles sourced from the French cooperative Cavac in 2015 and are assumed to come from that year's harvest. The material is provided in large bags of roughly 20kg, Figure 4.1. Four "grades" of aggregates were provided listed as 7, 8, 12, and 14 relating to a visually noticeable increasing coarseness of the particles. These grades are produced by an air stream separation method with the grading numbers having no known relevance; the pre-graded aggregate is assumed to come from a hammer mill production line. For this study, for reasons that will be discussed subsequently, the varieties of bio-aggregates used were number 7, referred to herein as fine, number 14, referred to herein as coarse, and an equal by mass mixture of numbers 8 and 12, referred to herein as medium.

Figure 4.1: Hemp-shiv particles as supplied.

Alongside thermal conductivity and mechanical properties, the bio aggregates were characterised for particle size distribution, bulk density and water absorption. In several cases the most useful measures from a micromechanical modelling perspective would be for individual particles, however this was not practical to obtain in most cases due to their small size and variable shape. Where particle properties are required subsequently they are therefore either estimated or derived from bulk measurements. For all of the measurements, a representative sample was required and so a process of quartering was used in each case; the underlying assumption was however made that the materials were consistent across separate bags.

4.1.1.1 Particle size distribution

The defining feature of the different aggregates used is the particle size distribution. Based on the literature reviewed it is apparent that the best way to produce a particle size distribution of bio-aggregates is via two dimensional imaging as opposed to sieving due to the significant aspect ratio of the particles. The method used in this study is in essence the same as that documented elsewhere (Nozahic et al., 2012, Nguyen et al., 2009, Picandet, 2013) and has been incorporated into the French hemp-lime professional regulatory code (Construire en Chanvre, 2009). Subsequent to the work being undertaken, a multi institutional report (Picandet, 2017b) has proposed a standardised method for the process that is considered directly comparable to that used here.

The process in this case used a 20g sample of material in each instance. Imaging of the material was conducted on a Hewlett Packard digital scanner whereby the particles were spread out on the surface to avoid touching and overlaps, Figure 4.2. The process was repeated for 10-15 images to account for the full 20g sample. The scans were produced at a resolution of 1200dpi and against a solid blue background to give a high level of contrast to the images.

Figure 4.2: Segregated aggregate particles prior to scanning for two dimensional image analysis.

Once the full set of images for each of the grades of bio-aggregates had been produced they were processed and analysed using the program ImageJ (Kashtanjeva et al., 2015). The images were processed by first applying a median filter with a radius of 3 pixels. The median filter was used to help smooth out the edges of the imaged particles and remove irregularities. This step has not been used in other applications of this method where a lower resolution of image is used, possibly to preserve the level of detail. In this case the

resolution used means that a median filter will not diminish the image quality below that used elsewhere and has the benefit of improving the subsequent steps. Precedent for this exists in the image based particle analysis of other materials (Coenen et al., 2012, Standfest et al., 2010).

Following the median filter a threshold filter was used to segregate the image according to the 8-bit hue value of pixels, the value used selected by eye to ensure the most accurate detection of the particles. This process has the result of producing a binary image of the particles that was then cleaned by the application of three iterations of an opening algorithm (successive use of an erosion and dilation algorithm to remove unconnected pixels and fill voids respectively), used to remove small particles of dust and fibre attached to the bio-aggregates. Finally the bio-aggregates were measured using the particle analysis tool inbuilt within ImageJ (Ferreira and Rasb, 2012).

The measures of length and width extracted by the program and thus presented are those of a fitted ellipse that has the same centroid and area as the particle. This is achieved via the same processes and equations described in Chapter 3 for orientation analysis of particles. It is used here as it is considered more representative than the alternative calliper (or Feret) diameter within the context of irregularly formed particles. While it is noted that this may overestimate the values in some cases, where the shape tends more to that of a rectangle than an ellipse (Picandet, 2013), a similar occurrence would occur using the calliper diameter and is considered inconsequential here where the aim is to compare.

From the particle data collected the area, A_p, and aspect ratio, ϕ_p, may be found for each particle using Equations 4.1 and 4.2. The average values for each 20g sample are given in Table 4.1.

$$A_p = n_{px} \times 0.01058 \qquad 4.1$$

$$\phi_p = \frac{l_p}{w_p} \qquad 4.2$$

To produce a particle size distribution by mass, as is the standard form for other materials, the mass of the individual particles, m_p, must be estimated. Following the procedure laid out by (Picandet, 2013) this was achieved by making two assumptions: that the depth of the particle is related to the width linearly and that the mass is likewise related to volume. From this the estimated mass of a particle may be may be derived from the area and width, Equation 4.3.

$$m_p = A_p \times w_p \times c \qquad 4.3$$

Where c is a constant accounting for the aspect ratio of depth to length and the density of the material. The cumulative mass distribution of particles for length $P_m(L \leq l_n)$ and width $P_m(W \leq w_n)$ may then be found from Equations 4.4 and 4.5.

$$P_m(L \leq l_n) = \frac{\sum_{i=1}^{n} m_i}{\sum_{i=1}^{N} m_i} = \frac{\sum_{i=1}^{n} A_i\, w_i}{\sum_{i=1}^{N} A_i\, w_i} \qquad 4.4$$

And:

$$P_m(W \leq w_n) = \frac{\sum_{i=1}^{n} m_i}{\sum_{i=1}^{N} m_i} = \frac{\sum_{i=1}^{n} A_i\, w_i}{\sum_{i=1}^{N} A_i\, w_i} \qquad 4.5$$

Where n is the number of particles under a given value of length or width out of a total population of N.

The distributions produced by this process are presented in Figure 4.3 and provide a useful visual representation of the particle size distribution for qualitative comparison. In order to extract numerical values that may be then used to quantitatively compare the distributions, median and inter quartile range by mass can be found for length and width of the distributions giving comparable values of particle size and spread. The use of mass weighted median and interquartile range is used to remove sensitivity to the large quantities of fines and to be directly relatable to the distributions presented in Figure 4.3. The median and interquartile range of the width and length of particles from the differing grades of bio-aggregates are presented in Table 4.1 in the summary of the bio-aggregates section.

From Figure 4.3 and Table 4.1 it may be identified that the particle mean area, median particle length and median particle width follow an expected correlation to the apparent coarseness of aggregate: the fine grade and coarse grade having the lowest and highest values respectively. In terms of distribution spread there exists no correlation with coarseness of aggregate grade and indeed, from Figure 4.3, the medium grade of bio-aggregates appears to have the biggest spread. The assessment is supported by the interquartile ranges, especially when considered as a fraction of the median, Table 4.1. This is a purposefully engineered result obtained by the combining of two manufacturer's grades of material to produce this distribution. The reason for this is to separate the two variables of particle size and spread of the distribution that otherwise normally correlate due to the high occurrence of fine particles in all grades and is an aspect previously

unconsidered elsewhere. By splitting the variables it allows for the respective impacts to be considered separately which was identified as lacking in the review of previous work.

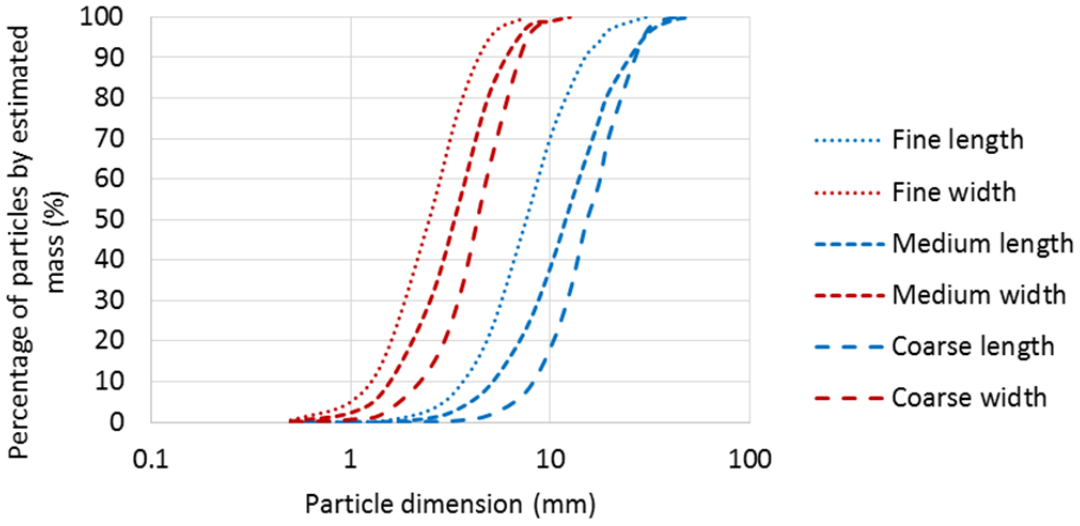

Figure 4.3: Particle size distribution of the three grades of hemp shiv.

From Table 4.1, alongside the size and spread of particles, it is also noted that the average aspect ratio of the three grades differs and broadly speaking correlates to particle length. It is not clear if this is a product of the growth of the plant or the processing method and it is therefore not presumed that a similar correlation may be found in other aggregates from differing suppliers.

4.1.1.2 Uncompact bulk density

The uncompact bulk density of the aggregates in a dry state was found by a method of pouring, based on methods established within the previous literature (Hirst, 2013, Picandet, 2013). To do this, material that had been conditioned in a 105°C oven to remove moisture was transferred into a large container with a pouring lip. The particles were then mixed by hand to ensure an even mix and minimise natural segregation of bigger and smaller particles. From this container the material was poured onto a separate smaller 3L container of which the volume to the brim was determined accurately by water filling. The material was poured in until just proud of the top of the container prior to careful scraping across the top with a metal ruler to remove excess, Figure 4.4. The container was then weighed to establish the mass of the aggregates and the process repeated to give an average of 10 readings.

The results of the uncompact bulk density are presented in Table 4.1 for the differing grades of hemp aggregates and identify a general trend between increasing fineness of

particles and decreasing density as has been found elsewhere within the literature (Hirst, 2013, Hustache and Arnaud, 2008). This is considered a result of an increased level of natural consolidation within the smaller particles due to a lower mean aspect ratio, Table 4.1.

Figure 4.4: The process of determining bulk density of loose hemp-shiv.

4.1.1.3 Water absorption

The water absorption of the aggregates with respect to time was determined in this study by means of timed submersions and weighing. There was no standard method for this procedure but a range of approaches have been tried previously within the literature and were used to guide the process (Hirst, 2013, Dinh et al., 2015, Walker and Pavia, 2012). Subsequently a standard method has been proposed elsewhere (Amziane et al., 2017b) using a slightly differing process but was not available at the time of testing.

A set mass of 50g of oven dried bio-aggregates was used for each test. To contain the particles during submersion a set of two grading sieves were used, Figure 4.5. Sieves were used as opposed to other perforated containers, as used in previous studies, as it enabled various passing sizes to be trialled and thus an optimum compromise between minimal water retention in the apparatus and minimal material escape to be achieved. The sieves used on top and bottom were both of a 425µm passing and oven dried prior to use.

As opposed to weighing the sieves after a period of submersion, instead the process followed was to submerge the sieves for the required time and to weigh the water vessel prior and post removal to measure the uptake by subtraction. This was used to simplify the process and allow for quick measurements to be taken. To account for water naturally retained by the sieves, a standardised process of shaking was used throughout the

experiments and a blank run without aggregates was also conducted to measure the extent of water retention. The submersion times used in the study were based on those in previous literature and were 1 minute, 2 minutes, 5 minutes, 10minutes, 30minutes, 60minutes and 24 hours.

Figure 4.5: Sieves used to measure water absorption of aggregates.

The results of the water uptake experiments are presented in Figure 4.6 for the different bio-aggregates. The results indicate an increasing hydroscopic behaviour with decreasing particle size although there is a suggestion from the medium and coarse grades that the results will converge in a longer period. This is likely to be a result of a larger exposed surface area for finer particles allowing for an increased speed and degree of water absorption in the early stages. In general it can be seen that the water absorption for all the varieties of hemp aggregates considered is very high, in the region of 150% after two minutes, as has been observed elsewhere (Hirst, 2013, Walker and Pavia, 2012).

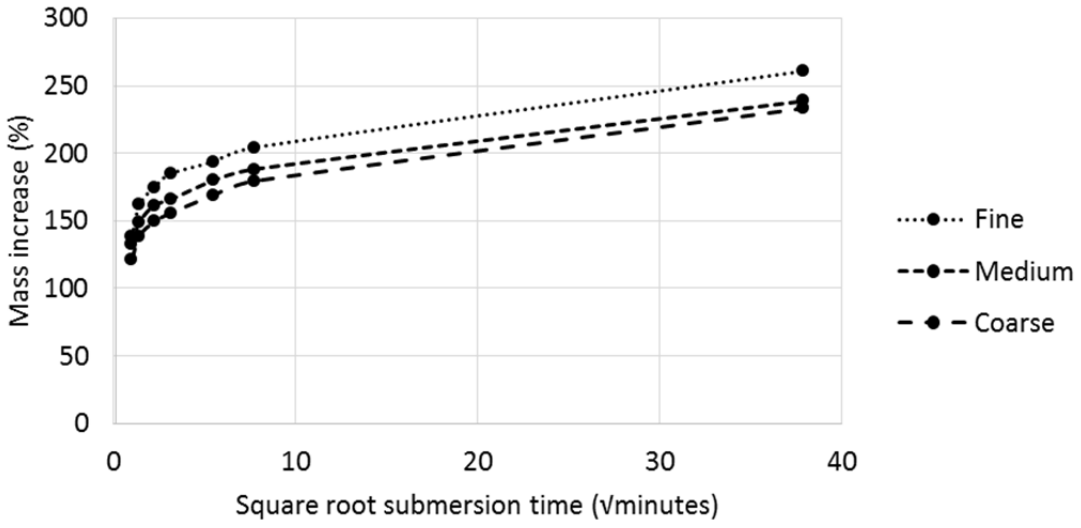

Figure 4.6: The water absorption curves obtained from each of the three hemp aggregates used in the study.

4.1.1.4 Thermal conductivity

Thermal conductivity would ideally be measured at a level of individual particles, however this was not practical to obtain. Thermal conductivity was therefore found as bulk property for each variation of hemp particles considered. As no standard existed for the finding of the thermal conductivity of bio-aggregates specifically at the time of testing, guidance was taken from the British Standard BS EN 12667:200 "Thermal performance of building materials and products. Determination of thermal resistance by means of guarded hot plate and heat flow meter methods. Products of high and medium thermal resistance" (British Standards, 2007) and adapted where necessary. Values were obtained using a Lasercomp Fox 600 heat flow meter, Figure 4.7. Heat flow meters use a manufactured thermal gradient across the upper and lower plates and then measure the energy flow during steady state to measure directional thermal conductivity of the material between the plates. As this apparatus is used in the main set of experiments a full description of the process is given in Chapter 4.2.

To measure the thermal conductivity of bio-aggregates a specific frame was made to contain a layer of the loose material within the machine. This was achieved using an 18mm deep MDF perimeter board and a plastic film Figure 4.7. These were deemed to not impact the results on the grounds of the frame being outside the central measured region of the plate area and the negligible thickness and thus thermal resistance of the plastic film. The required amount of loose material to give the correct uncompact bulk density, Table 4.1, was preconditioned in a 105°C oven to remove moisture and gently poured into the frame and levelled with a straight edge. Thermal conductivity was measured at a temperature gradient of 10°C - 30°C and using a steady state condition defined by section 7.3.5 of (British Standards, 2007).

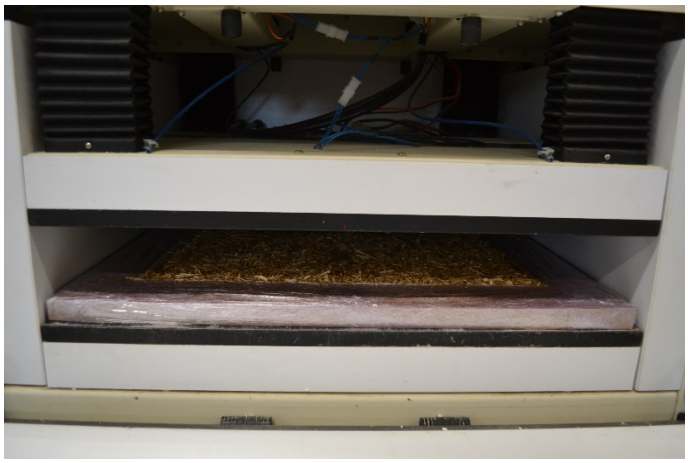

Figure 4.7: Experimental setup for determining the thermal conductivity of bulk hemp shiv.

The results of the thermal conductivity tests are presented in Table 4.1. In general the results can be considered in line with previously obtained values (Arnaud, 2000, Collet, 2004) although the expected correlation between density and thermal conductivity is not present. From the results it can be observed that a positive thermal conductivity to particle size correlation is instead found with the bio-aggregates of larger sizes produced higher thermal conductivity. This is likely due to a greater connectivity in the heat transfer paths produced with bigger particles dominating over the slight decrease in total material presence in this case where the thickness of the test specimen is comparable to the dimensions of the aggregate.

While the particle thermal conductivity is a more useful parameter than bulk thermal conductivity for modelling the composite material's behaviour it was not practical to measure this directly. To overcome this in previous studies, a model for thermal conductivity of bulk hemp-shiv was created and then worked backwards to estimate a value for particle thermal conductivity. Such an approach has not been taken here on the grounds that previously applied models (Nguyen et al., 2016) have related to density whereas no correlation between thermal conductivity and density was observed in these tests and rather the relative particle dimensions were found to dominate. The observation calls into question the use of simple models to estimate the behaviour of bulk hemp shiv identifies this as an area requiring additional study in the future.

4.1.1.5 Mechanical properties

Bio-aggregates as a bulk material may be considered to have some physical resistance due to the cohesion of the particles in a similar way to that of mineral aggregates and soils. A defining difference compared to mineral aggregates however is the deformability of the particles which limits the structural contribution within composites (Arnaud, 2000). That aside, it is still important to examine how the loose particles behave in compression in order to assess what contribution composites might derive from cohesion.

To test the different grades of bio-aggregates in this way, a confined compressive test was conducted on material using a specially produced load cell, Figure 4.8, in a similar way to that of previous studies (Picandet, 2013, Nguyen et al., 2009, Collet, 2004). While no standard method existed during the time of writing, a subsequently published report (Picandet, 2017a) does now provide this and is considered comparable to the method used here. The cell was produced from thick polycarbonate tube with an internal diameter of 88mm. A sealed end was produced from machined steel as well as a free moving polycarbonate punch head used to convey the load. The top of the cell was marked with a

depth line at 150mm to give a capacity of 9.123L when full. The whole cell was positioned within an Instron 50KN mechanical testing frame that was used to both apply the load and measure the displacement and force through the inbuilt instrumentation, Figure 4.8. The polycarbonate punch head and timber extender were affixed to the top platen to remove any unmeasured loading of the material. Tests were conducted on material preconditioned in a 105°C oven to remove moisture. The material was placed into the cell in the same method used to measure the uncompact bulk density, gently pouring from a larger container, and the quantity weighed to ensure it was at comparable density to the loose bulk density determined previously. The loading was applied at 3mm per minute and the tests repeated five times for each grade of hemp.

The results of the tests are presented in Figure 4.9. It can be seen from the results that the stress density relationship from the different bio-aggregates appears to be dependent on the grade rather than the median particle size. It can be observed that the steepest curve, indicating highest rate of resistance gain to increasing density, comes from the bio-aggregate with the smallest range of particle sizes. Likewise the shallowest curve is observed to come from the particles with the largest range of particle sizes, Table 4.1. This indicates the possible importance of particle size spread in the development of inter-particle load paths that may cross over to composite behaviour.

Figure 4.8: The loose hemp load cell installed within the Instron 50KN frame.

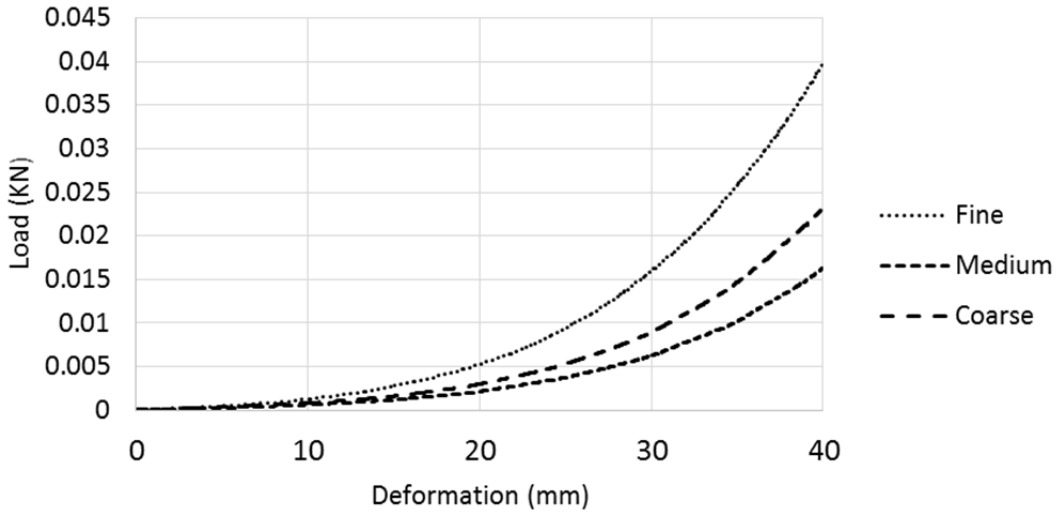

Figure 4.9: The load extension graphs for the three grades of hemp shiv.

4.1.1.6 Bio-aggregates properties summary

A summary of the characteristics of each of the three grades of hemp shiv considered is presented in Table 4.1.

Table 4.1: The key characteristics of the bio-aggregate grades.

	Material Grade		
	Coarse	Medium	Fine
Mean particle area (mm^2)	8.81	4.81	3.11
Mean aspect ratio	3.66	3.27	3.04
Median particle length (mm)	15.27	11.88	7.54
Interquartile range (mm)	9.42	9.80	5.54
Median particle width (mm)	4.30	3.31	2.47
Interquartile range (mm)	2.44	2.26	1.60
Uncompact bulk density (kgm^{-3})	118	122	129
Standard deviation	0.934	1.50	2.07
Uncompact thermal conductivity ($Wm^{-1}K^{-1}$)	0.04821	0.04616	0.04522

4.1.2 Binder

The decision to only use a single binder was based on practicality and the perceived high level of coverage of this aspect within the literature already. It was therefore concluded that by considering multiple binders the scope of the experimental programme would

increase significantly with limited additional original outcome or insight. As lime based binders are the most commonly used binders, it was deemed most appropriate to use a lime based binder in this study.

The binder used is produced by Lhoist group and marketed in the UK as Tradical Thermo. While the exact constituents are not known it is believed to be mostly composed of pure lime and natural hydraulic lime augmented with pozzolanic compounds. This binder was selected due to its availability as well as some setting issues experienced with other binders trialled in the early stages of the project. The seemingly more reliable setting of Tradical Thermo is believed to be a result of the high surface area of the powder and viscosity of the slurry, considered beneficial in retaining water within the binder when used with the highly absorbent bio-aggregates (Sheridan et al., 2017). It is a failure of the binder to retain sufficient water that is often considered the reason for a phenomenon known as “flowering”, reported sporadically elsewhere (Hirst, 2013, Gross, 2013), and experienced in the early stages of this project on a seemingly random basis, Figure 4.10. While it is outside the scope of this study to consider the phenomenon of flowering and the associated setting mechanics of binders when used with bio-aggregates, it can be noted that the use of Tradical Thermo, once adopted within this study, resulted in no issues with setting.

Figure 4.10: Cross section of hemp-lime showing a normal set (top) and a flouring set (bottom).

As with the bio-aggregates it is necessary to classify the binder properties in the key areas relevant to this study. While the chemical make-up and setting processes are of course determinants to many of the binder properties they are not of key interest to this study and so have not been considered. Instead results were obtained to establish the mechanical and thermal properties of the set binder paste as well as those parameters of relevance to the mixing process such as bulk density.

4.1.2.1 Bulk density

The bulk density of the binder power was found using the same process as that used for the bio-aggregate composites and detailed in the previous section. The result obtained as an average of five reading was 685kgm^{-3}.

The bulk density of the set binder was found from the binder prisms used for mechanical testing the production and curing of which will be described in that section. Measurements were conducted at 28 days age and after oven drying at 105° for 48 hours. The results obtained for each of three water to binder ratios considered are presented in Table 4.2 at the end of this section and represent an average of five specimens for each ratio. The bulk density of the binder paste was observed to decrease with increase water ratio as would be expected but this was also observed to come with and increased deviation in values; it is not certain what the cause of this observation is.

4.1.2.2 Hydration ratio

The hydration ratio, k, within the context of this study is defined as the mass change in binder as a result of hydration as described by (Lanos et al., 2013) and given by Equation 4.6.

$$k = \frac{m_2}{m_1} \qquad 4.6$$

Where m_1 is the mass of the binder prior to hydrating and m_2 is the mass after.

In practical terms this was established by producing binder paste mixtures, binder and water only, to several constituent ratios. A small sample of each paste was then weighed and allowed to cure for 28 days within a conditioning room, 20°C and 50% relative humidity. After conditioning, the sample was oven dried at 105° for 48 hours and checked to ensure it was mass stable, defined here as a change of mass of less than 0.1% in 24 hours. The samples were then reweighed to provide a hydrated mass; the un-hydrated mass was established from the original mass of the specimen and known ratio of constituents. It is assumed that the mass increase associated with carbonation will have been negligible due to the maintained high water content reducing permeation of atmospheric carbon dioxide. The three water to binder ratios used were 0.4, 0.6 and 0.8, selected to cover the range of effective water to binder ratios considered plausible for binder paste in-situ incorporated into bio-aggregate composites.

The results are presented in Table 4.2. The average hydration ratio across the three water to binder ratios is 1.086 with no seeming correlation to water to binder ratio. This indicates that the hydration ratio of the binder is comparable to that quoted for a similar pre-formulated binder (Lanos et al., 2013); in general, a value of 1.25 is considered reasonable for Portland cement while pure lime should give a value to near 1 where there is negligible hydration (Escadeillas et al., 2013). The implication of this finding is that the hydraulic content of the binder is low indicating a high pure lime content. The consistency over the three water contents indicates sufficient water is present across this range to enable the full utilisation of the hydraulic content.

4.1.2.3 Thermal conductivity

The thermal conductivity of pure binder paste could be established by steady state methods, as was used for the bio-aggregates, however this was not appropriate in the context of the equipment available: the Lasercomp Fox 600 requiring a minimum specimen size much larger than could be produced from pure binder paste without encountering shrinkage cracking. To overcome this an alternative, transient method was used. Such methods rely on measuring the temperature of the material at a localised position after producing a thermal pulse at the location. By interpreting the temperature decay with respect to time, the thermal conductivity of the material may be calculated (Coquard et al., 2013, Al-Ajlan, 2006, Log and Gustafsson, 1995). This method requires a much smaller specimen size and so is well suited to this context.

Square tablet specimens were produced in pairs, the method requiring encasement of the sensor, with dimensions of 100mm x 100mm x 25mm and for the three water to binder ratios used for the hydration ratio tests: 0.4, 0.6 and 0.8. The specimens were cured for 28 days at 20° 50% relative humidity with mould removal at 6 days age. Prior to testing the specimens were oven dried at 105°C for 48 hours and checked to ensure mass stability. The equipment used to conduct the test was a CT Meter, Figure 4.11, used in with the manufacturer's recommended setting for the type of material. To ensure a good contact to the sensor the specimens were prepared by light sanding to ensure a flat face. A polythene bag was also used to contain the specimens and sensor during the tests to minimise air movement and tests were all repeated five times.

Figure 4.11: Experimental set up for determining the thermal conductivity of binder paste.

The values obtained for thermal conductivity for the differing water to binder ratios are presented in Table 4.2. From these results it may be seen that the thermal conductivity varies significantly with water to binder ratio. This result is none the less intuitive considering the trend in density with water to binder ratio that is also found and in general the values can be considered to be in line with that found for other pre-formulated binders of similar make-up (Nguyen et al., 2010).

4.1.2.4 Mechanical properties

The compressive behaviour and flexural behaviour of pure binder paste were considered in this assessment as these are the most common ways of mechanically characterising cement and lime mortars (British Standards, 2005), and are the properties of interest in the composites themselves. Mechanical test are standardly conducted at 28 days but, due to the high lime content of the binder, it is known that peak strength will not have been reached by this time. The method does however remain valid in the context of industry where scheduling requirements may be critical.

As no specific standard exists for testing binder paste, the British Standard used for testing mortar, BS EN 196-1 2005 (British Standards, 2005), was used and adapted where appropriate. In this approach a single set of prismatic specimens may be used for both the determination of flexural strength through three point bending and then compressive strength of a cube using the retained pieces of material. The prisms produced were all 40mm X 40mm X 160mm in accordance with the standard. Three binder to water ratios were considered: 0.4, 0.6 and 0.8 and all mixing was conducted in an electric mortar mixer using the standard regime (British Standards, 2005, British Standards, 1999). Specimens

once cast were cured in a conditioning room stable at 20° and 50% relative humidity for 28 days with moulds removed after six days.

All mechanical tests were conducted using an Instron 50KN testing frame in combination with specialist jigs for the purpose of testing mortar prisms, Figure 4.12. Tests were conducted in flexure first, using the loading regime as specified by the standard until failure of the specimen. Following the flexural tests, compressive testing of the half pieces was conducted again in accordance with the standard. In both cases five specimens were considered of each water to binder ratio.

The results of the flexural test and compressive tests are given in Figure 4.13; the average peak compressive and flexural strengths are given in Table 4.2.

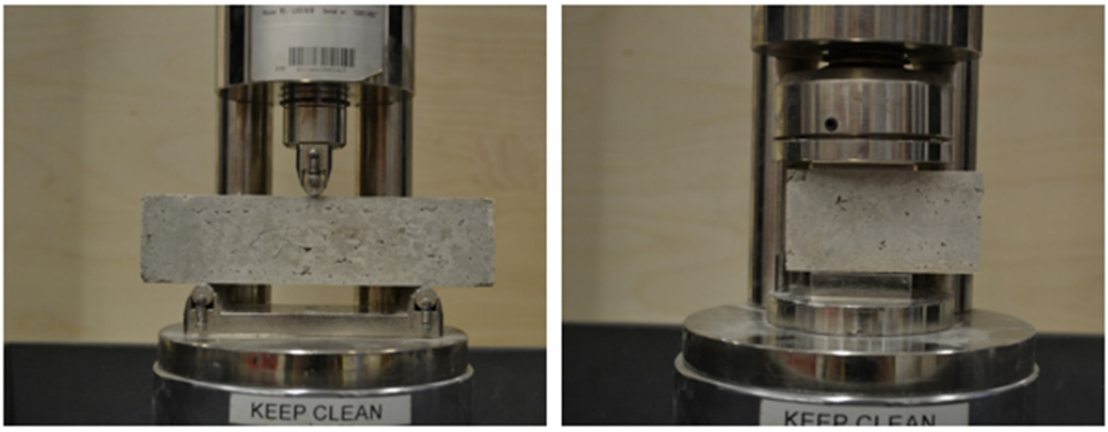

Figure 4.12: Flexural testing (left) and compressive testing (right) of binder paste prisms and half's.

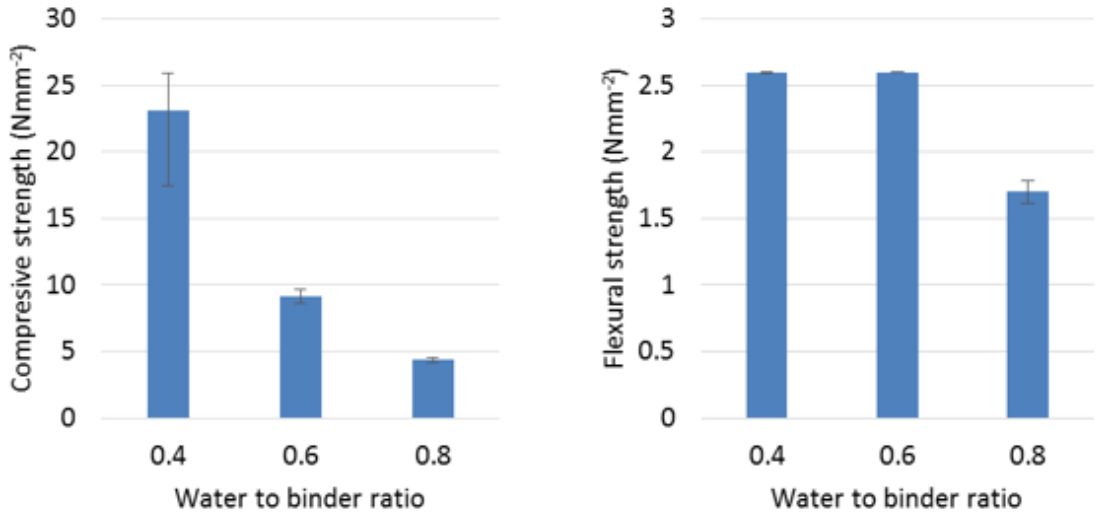

Figure 4.13: The compressive and flexural strength of Tradical Thermo binder at three water to binder ratios at 28 days.

The results from Figure 4.13 and Table 4.2 suggest that the compressive strength is significantly dependent on the water to binder ratio used as would be expected based on other work (Escadeillas et al., 2013). Transversely the deviation in the compressive strength was also found to increase with decreasing water to binder ratio despite deviation in the density decreasing and it is not clear why this is the case. In general the compressive strength of the binder paste is considered to be in line with that reported for another formulated binder (Nguyen et al., 2010) and indicative of a high hydraulic content. The flexural strength in contrast is seen to be less dependent on the water to binder ratio but still significantly so at higher values. In order to obtain consistency in the testing of bio-aggregates it is clearly important to try and isolate the in-situ water to binder ratio as a variable based on these results.

4.1.2.5 Binder properties summary

A summary of the characteristics of each of the three water to binder ratios considered is presented in Table 4.2.

Table 4.2: The key characteristics of Tradical Thermo lime based binder at differing water to binder ratios.

	Water to binder ratio		
	0.4	0.6	0.8
Density	1660	1411	1327
Standard deviation	9.7	20.9	56.7
Hydration ratio	1.072	1.100	1.087
Thermal conductivity ($Wm^{-1}K^{-1}$)	0.497	0.327	0.248
Standard deviation	0.018	0.019	0.023
Flexural strength (Nmm^{-2})	2.60	2.60	1.70
Standard deviation	0.003	0.001	0.061
Compressive strength (Nmm^{-2})	23.1	9.15	4.37
Standard deviation	3.22	0.33	0.14

4.2 Experimental procedures

This section outlines the experimental procedures that are common across all aspects of the main study including the various testing methodologies and equipment as well as the production of the specimens. The range of variables considered and tested using these methods will be discussed separately for formulation variables and implementation variables in Chapter 4.3 and 4.4 respectively.

4.2.1 Testing regime

The properties identified as of relevance to the aim of this study are the compressive behaviour, flexural behaviour, thermal conductivity, and the orientation of the internal structure. The methods used to establish these properties will now be outlined and discussed.

4.2.1.1 Flexural behaviour

Flexural behaviour may be defined by the stress strain relationship of the material under flexure which in turn may be characterised by the flexural failure stress, flexural stiffness, and the failure mode. In the case of hemp-lime these aspects may be relatively easily obtained from a simple three point or four point bending test as has been established in previous literature (Benfratello et al., 2013, Elfordy et al., 2008, Hustache and Arnaud, 2008, Sassoni et al., 2014, Le et al., 2015).

In this case a three point bending test was used. The size of specimen and geometry of the test can have bearing on the results and there was no consensus in the previous literature as to an appropriate testing form for these materials. Based on the maximum layer size to be considered and the requirement to test in two directions, a 150mm square prismatic form was selected. This cross section is both in keeping with previous work and considered of sufficient size to minimise the impact of natural variance in the material based on reported representative volumes (Evrard, 2008, Collet et al., 2008). In deciding the length of span, consideration was given to the storage space available and the considerable number of specimens that were going to be required, both necessitating that specimen sizes be minimised. For this reason a specimen length of 400mm was selected for use in three point bending over a span of 300mm. This represents a relatively stocky form under the standard span to depth ratio used for similar materials of near 4:1 however a series of preliminary test confirmed that this specimen size was sufficient to

give a clear flexural failure in hemp-lime. The use of a higher span to depth ratio would have required a compromise on the 150mm maximum layer that was considered of greater importance. The resulting geometry of the prisms and flexural tests is shown in Figure 4.14.

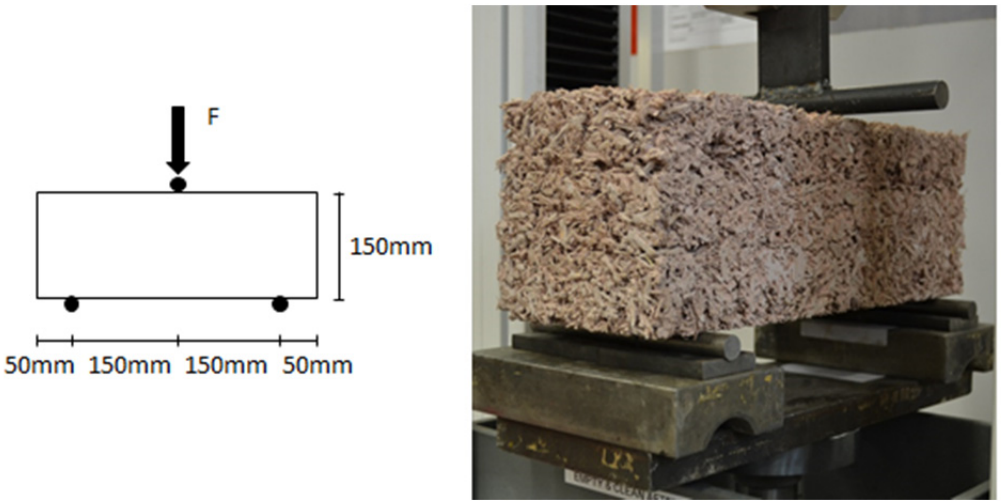

Figure 4.14: Diagrammatic and actual testing of hemp-lime prisms in flexure.

All the flexural tests were conducted using an Instron 50KN testing frame with inbuilt instrumentation to record extension and load to an accuracy of $\pm 1x10^{-8}$m and $\pm 1x10^{-5}$N respectively at a sample rate of 10Hz. The testing frame was fitted with a large metal plate and simple pin supports at the lower surface, the deflection of which was considered to be negligible, and a metal bar in the top jaw to apply a line load across the width of the specimen. In each case the bar was adjusted so that it was resting flat to the top surface of the material to ensure minimal loading concentrations. The tests were run at a loading rate of 3mm per minute and were photographed throughout the test to record the behaviour and mode of failure. Figure 4.14 shows the test setup used.

Prior to each test the specimen was weighed using a mass balance with an accuracy of ±1g and the physical dimensions of the specimen measured using a steel rule, ±0.5mm, to the method presented in the British Standard for the determination of linear dimensions of thermal insulation products, BS EN 12085 2013 (British Standards, 2013b). From the testing frame output and the dimensions recorded, the stress and strain values corresponding to the test data were calculated using the standard relationships, Equation 4.7 and 4.8, assuming idealised elastic beam bending where b, d and l are the depth, breadth and span respectively and D is the central displacement.

$$\sigma_F = \frac{Fl3}{2bd^2} \qquad 4.7$$

$$\varepsilon_F = \frac{6Dd}{l^2} \qquad 4.8$$

It is possible that a better value of flexural strain may have been obtained via the use of surface mounted strain gauges or digital photographic image analysis however this was dismissed due to the complex surface, and thus likely development of localised results, and a lack of precedence respectively.

As the failure point in flexure is clearly defined, the flexural strength of the specimen is simply the peak value of flexural stress obtained. The reported flexural strength of each variation of material is then given as the mean value of the three tests.

The flexural stiffness of the specimen material may be found from the gradient of the stress / strain graph during the linear elastic phase. From the literature review it was anticipated that the results were likely to exhibit an initial settling phase meaning a linear approximation passing through both the datum and peak stress points would be an inappropriate measure. A cyclical loading regime might have been used to overcome this, however as it was assumed that hemp-lime may strain, harden or degrade with loading in a nonlinear elastic way, and as arbitrary strains must be selected for unloading cycles. Ultimately it was decided that the most appropriate way to compare materials would be via visual comparison of the stress/strain plots where relative stiffness may be visually assessed.

To assess the failure mode, the duration of the test was deliberately selected to be significantly beyond the expected failure strains. This allowed additional data to be collected past the peak stress and during the failure of the material. As it was relatively unknown as to how the material would behave post failure, based on a limited body of literature, no preconceived quantitative measures were applied to the data and instead, qualitative comparison of the plots was determined as the best analysis tool. To aid this process and provide more data, images were taken throughout the loading program as previously described as well as additional images taken after the test of the specimen once loading was removed and detailed photos of the area of failure. For comparability the same selection of images were taken for each specimen.

4.2.1.2 Compressive behaviour

Compressive behaviour may be defined by the stress strain relationship of the material under compression which in turn may be described by the compressive failure stress, the

compressive stiffness, and the failure mode. A simple compressive test of cylinders or cubes of material may be used to measure these parameters as was established in the literature review.

There is precedent within the literature for testing both with cylindrical prism specimens as well as cubes. While it has been shown that that the results are independent of the geometry selected it has been noted that cylindrical specimens give a more defined failure point as a result of a greater length to width ratio (Niyigena, 2015). Within the context of this study, where material is to be produced with opposing directions of compaction, cylindrical specimens are not practical to manufacture and so cannot be used. A plausible alternative is square prism of the same aspect ratio but this was discounted based on a lack of precedent within the literature as well as the increased material use and storage requirement compared to cubes. Cube specimens with a size of 150mm X 150mm X 150mm were selected as this is a standard size for the cubic testing of concrete (British Standards, 2009), has significant precedent within the literature (Amziane et al., 2015, Le et al., 2014, Le et al., 2015, De Bruijn, 2008) and is larger than the representative volume of material identified in some previous studies (Evrard, 2008, Collet et al., 2008).

The test set up is shown diagrammatically and physically in Figure 4.15. An Instron 50KN testing rig was used to apply the load and measure the extension and force using the inbuilt instrumentation. The specimen was placed on a 150mm plate on the bottom platen of the machine and a second plate was placed on top. The top platen was then lowered to apply a pre-load of 50N. To ensure an even load transfer the platen at the top is fitted with a gimbal. In some previous work, capping of the specimens in dental plaster has been used as an alternative method of ensuring even load transfer (Hirst, 2013) and while trialled here, was not used due to the potential horizontal restraint it might provide to the surfaces. The loading regime applied was deflection controlled at 3mm per minute and data recorded at 10Hz to an accuracy of $\pm 1 \times 10^{-8}$m and $\pm 1 \times 10^{-5}$N. As with the flexural test photos were taken throughout the loading process.

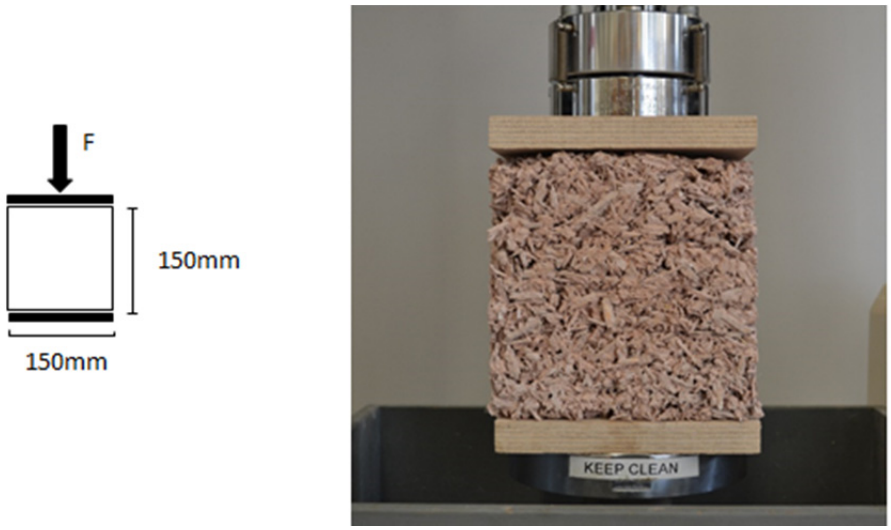

Figure 4.15: Diagrammatic and actual testing of hemp-lime in compression.

As per the flexural test, prior to each test the specimen was weighed using a mass balance with an accuracy of ±1g and the physical dimensions of the specimen measured using a steel rule, ±0.5mm, to the method presented in the British Standard for the determination of linear dimensions of thermal insulation products, BS EN 12085 2013 (British Standards, 2013b). From the testing frame output and the dimensions recorded, the stress and strain values corresponding to the test data were calculated using the standard relationships, Equations 4.9 and 4.10, where d and b are the depth and breadth respectively of the loaded cross section, D is the deflection and h is the specimen height.

$$\sigma_C = \frac{F}{db} \quad 4.9$$

$$\varepsilon_C = \frac{D}{h} \quad 4.10$$

Unlike the flexural behaviour, the failure point in compression is reportedly hard to identify due to an increasing densification and strain hardening reported for parallel loading within the literature (Tronet et al., 2016, Youssef et al., 2015). To overcome this, a definition of compressive failure must be used that accounts for this behaviour and can be applied universally to both directions of loading. In some previous studies this has been achieved by taking the compressive stress at an arbitrary value of strain for comparison (Sinka and Sahmenko, 2013, Sassoni et al., 2014, Youssef et al., 2015), a method also applied in the standard testing of insulation materials (British Standards, 2013a). A perceived problem with this method within the context of hemp-lime was the reported differing stiffness's of the material in differing directions and the prolonged and often

variable settling period in early loading; the representativeness of such values may therefore be questioned.

The method adopted in this study was to define the failure point in terms of a change in gradient of the stress strain relationship, signalling a fundamental change of behaviour in the material. In the case of bio-aggregate composites this change may be considered a failure of composite action leading to a notable reduction in material stiffness. The change in stiffness may be calculated as a percentage drop from the peak stiffness and therefore the failing stress identified by this measure is insensitive to both the material stiffness and the material settling in a way that previous methods have not been. This value is labelled the "compressive rupture strength" and is defined in this study as the stress where the instantaneous stiffness drops to 25% of the peak value using a moving average of 20 consecutive data points. The compressive rupture stress values presented are the mean of three specimens for each variation.

The compressive stiffness, as with the flexural stiffness and for the same reasons, was compared across material via a direct comparison of the stress/strain plots. To assess the failure mode of the materials the compressive testing regime was selected to deliberately go significantly beyond the compressive rupture strain values anticipated. This, as with the flexural test, allowed for additional data collection to assess post failure behaviour. Photos taken regularly throughout the loading of each specimen and additional photos were also taken after loading removal were also used to aid interpretation.

4.2.1.3 Thermal conductivity

Thermal conductivity is a measure of energy flow through a material and may be calculated using several methods. The method selected for this study is a steady state method using a heat flow meter selected for the significant precedent, direct as opposed to indirect measuring of the property and unidirectional application. A heat flow meter uses a pair of thermally controlled plates between which a specimen is placed. The plates are then held at a set temperature gradient until the power required to do so stabilises and steady unidirectional heat flow may be assumed through the specimen. From the heat flux measured in a central portion of the specimen, the thermal conductivity, λ, may then be established from the Fourier-Biot law, Equation 4.11, where dx is the specimen depth, dT the temperature differential of the plates and q the thermal power supplied (Collet, 2017).

$$\lambda = -q\left(\frac{dx}{dT}\right) \tag{4.11}$$

The instrument used in this case was a Lasercomp Fox 600 heat flow meter that is in accordance with and calibrated to the appropriate British Standard for the thermal testing of insulation materials via heat flow meter (British Standards, 2007). The specimen size required for the apparatus requires that the central, measuring, portion of the plate is sufficiently covered and the width of the specimen sufficiently small such that uniform parallel heat flux may be assumed through the material. Within the context of this study and with consideration in mind to limit the total material usage, a specimen size of 400mm X 400mm X 50mm was selected. As the full plate size of the apparatus is 600mm X 600mm a low density polyurethane foam surround was used to insulate around the specimens. The apparatus and experimental set up can be seen in Figure 4.16.

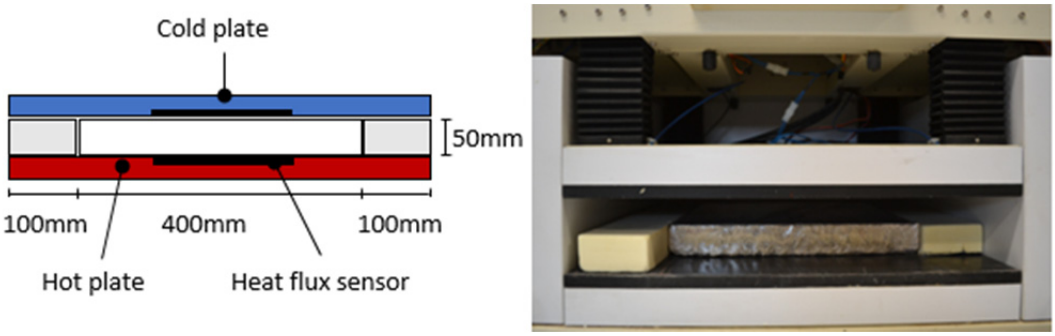

Figure 4.16: Diagrammatic and actual testing of the thermal conductivity of hemp-lime.

Each test in the heat flow meter was run using the apparatus settings prescribed in (British Standards, 2007) that defines the permitted thermal and energy fluctuations acceptable to fulfil the prescribed definition of steady state as well as the required period it should be maintained for. Standardly top and bottom plate temperatures of 0° and 20° are used respectively and are set due to the dependence of thermal conductivity on temperature. In this case values of 10° and 30°were substituted to minimise the potential for condensation within the machine that may be damaging, while still maintaining the same gradient and being reflective of realistic operating temperatures. As an additional precaution to prevent equipment damage, the specimens were wrapped in a single layer of plastic film: considered to have negligible impact on the results due to a negligible thickness.

The test on each specimen was conducted twice: once after conditioning the material in a 105°C oven for 48h, and once after the material had equilibrated in a climatic room of 20°C and 50% relative humidity. Prior to each test the specimen was weighed using a mass balance with an accuracy of ±1g and the physical dimensions of the specimen measured using a steel rule, ±0.5mm, to the method presented in the British Standard for the determination of linear dimensions of thermal insulation products, BS EN 12085 2013

(British Standards, 2013b). As the specimens are large compared to most previous studies within the literature review, the effective size of material sampled may also be considered large. In addition, the testing protocol already incorporates the taking and averaging of several measurements. For these reasons as well as the long duration of the tests, repeated tests were not considered necessary.

4.2.1.4 Image analysis

Image analysis was conducted using the methodology developed in the pilot study and outlined fully at the end of Chapter 3.

4.2.2 Specimen production

The specimen production is directly linked to some of the variables that are considered within this study, most notably the formulation, compaction and layer sizes. Alongside these studied variables however are a number of other variables that require control in order to isolate them from influencing the results such as mixing regime and specimen sizes. Within this section therefore the consistent aspects of the specimen production method are outlined and measures to control these variables noted.

4.2.2.1 Specimen sizing

In order to cover the range of variations and examinable properties this study identified, careful planning of the form of the specimens to be produced was undertaken to help minimise the material use and to ensure the program was achievable within the time available. For each variation of the bio-aggregate composite to be considered, the specific tests to be undertaken were thermal conductivity, flexural behaviour, compressive behaviour and image analysis all in two directions. As this would require around twenty individual specimens to be produced for each material variation, a more efficient way was sought. Taking inspiration from the testing of mortar prisms to British Standard BS EN 196-1 2005 (British Standards, 2005) where flexural test are conducted on prisms and then the half pieces used for compressive tests, it was theorised that a similar approach may be taken with bio-aggregate composites to allow the flexural, compressive and image analysis tests to be all conducted from one set of specimens.

In order to validate the use of a single set of specimens for multiple tests it was required first to confirm that this process would not affect the results. To do this a trial was conducted using hemp-lime made to the specification given in Table 4.3, positioned in the

mid-range of all the variables to be considered in the main study. A series of three 400mm X 150mm X 150mm prisms were produced as well as a set of three 150mm cubes. In all cases the mixing process and curing regime was the same as used in the main study and detailed in the following sections. Compressive tests were conducted at 28 days after casting using an Instron 50KN frame and inbuilt instrumentation using the method described previously. The flexural specimens were first broken using a three point flexure test and the two halves of the specimens retained. One of the halves was tested in compression without additional alteration using a set of 150mm plates to provide load to the required area only, while the other half was resized to a 150mm cube using a band saw and then tested in compression in the same way. Both sets of results were then compared to the results obtained from the 150mm cube specimens.

Table 4.3: Specification of hemp-lime used for validating the use of combined flexural and compressive specimen use.

Mix ID	Constituents (% mass)			Compaction (% density increase)	Fresh density (kgm^{-3})	Dry density (kgm^{-3})
	Bio-aggregate	Binder	Water			
Datum	16	36	48	45	432	358

The results of this test found that using non-resized flexural specimen halves gave higher compressive strength results than the standard 150mm cubes. This was attributed to load being distributed into the extra material, reducing the effective stress at a given loading, Figure 4.17. The resized flexural specimen halves were found to give fully comparable results to the cube specimens with no discernible effect occurring from the resizing process. It was therefore considered justifiable to use a single set of three 150mm X 150mm X 400mm prism specimens for the flexural, compressive and image analysis tests provided that the appropriate 150mm cube specimens are physically extracted from the flexural halves prior to further testing.

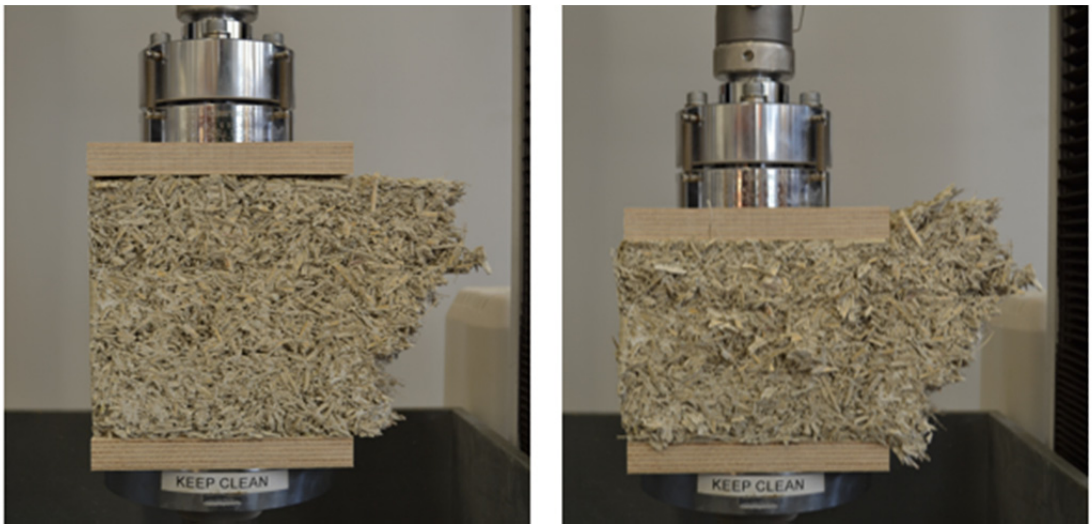

Figure 4.17: Compressive testing of a non-resized flexural specimen half.

4.2.2.2 Formulations

There are three constituents used to produce hemp-lime: hemp aggregate, binder powder and water. Within the context of this study, the binder to bio-aggregate ratio is to be varied while the water content, not being studied and impacting the behaviour of the binder paste as shown previously, Figure 4.13, must be controlled. In the case of traditional concrete the aggregates are not absorbent and so the in-situ water to binder ratio of the paste is determined by the water to binder ratio of the mix. In bio-aggregate composites this is not true and so the in-situ water to binder ratio of the paste is dependent on both the water to binder and water to aggregate ratio; indeed many formulation guides base the water content purely on the aggregate content due to its high absorption (Tradical®, 2015, Stanwix and Sparrow, 2014, Bevan et al., 2008) despite this leading to a varying water to binder ratio. A method of determining the mixture water content that controls the in-situ water to binder ratio based on the ratio of binder to aggregate is therefore required.

From the literature review, the most detailed consideration of the issue of appropriate water content was conducted by Lanos (Lanos et al., 2013) where a window of water contents was proposed which a stable in-situ binder to water ratio could theoretically occupy. As this method provides not a set figure but rather a window of values, a refinement has been sought here.

If it is assumed that the binder and the bio-aggregates develop a state of hydric equilibrium at a given mixture water content and specific pairing of binder and bio-aggregates then this state may be described by Equation 4.12.

$$m_w = a_b(m_b) + a_p(m_p) \quad 4.12$$

Where a_b is the in-situ absorption of the binder and a_p is the in-situ absorption of the bio-aggregate particles when used together.

It therefore stands that a_b may be maintained across differing bio-aggregate to binder ratios provided this equation remains satisfied by varying the water content. As the binder content may be written in terms of the bio-aggregate content and the proportions must add to one, Equations 4.13 and 4.14 may be derived.

$$m_b = \left(\frac{m_b}{m_p}\right)(m_p) \quad 4.13$$

$$m_w = 1 - \Big((m_p) + (m_b)\Big) \quad 4.14$$

The bio-aggregate content, binder content and water content by mass required at any mass ratio of bio-aggregate to binder, to maintain the state of equilibrium and thus in-situ water to binder ratio, may then be found from solving Equations 4.12, 4.13 and 4.14 simultaneously; what remains to be determined are appropriate values of in-situ absorption, a_b and a_p for the materials used in this study.

The binder manufacturer provides a recommended mass ratio, 16% bio-aggregate: 36% binder: 48% water, and so this was used for the basis of establishing the values of a_b and a_p. As it is not possible to separate the constituents, taking individual measurement of the in-situ binder paste and bio-aggregate is not practicable. The approach taken was therefore to compare the feel and appearance of the binder paste in-situ when combined to the manufactures proportions to that of a range of pre-prepared binder pastes in order to estimate a_b. Taking this qualitative approach is possible due to the very noticeable difference in the binder paste workability and appearance between water to binder ratios of 0.4 and 1, Figure 4.18. Based on the absorption time profile of the bio-aggregates determined previously, Figure 4.6, the assessment was conducted 30 minutes after mixing where the water uptake of the hemp particles should be slowing and reflective of an equilibrium state. The process was repeated for all three grades of bio-aggregate.

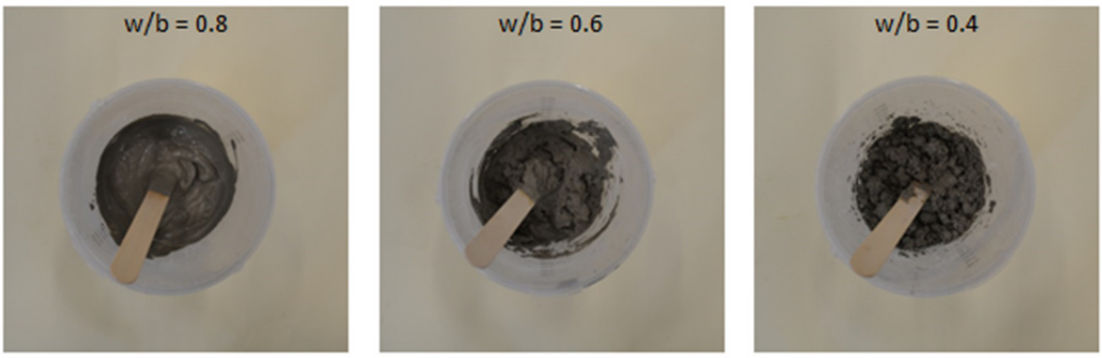

Figure 4.18: The visual appearance of pure Tradical Thermo binder water pastes made with differing water to binder ratios.

From the visual inspection it was estimated that the in-situ water to binder ratio, a_b, in the manufacturer's recommended ratio was 0.5 with no discernible difference between the different grades of aggregates. The value of a_p was then calculated as 1.9 from the known constituent contents of the mixture. By applying these values to the equilibrium equation it becomes possible to determine the required constituent contents to satisfy the same equilibrium state at any bio-aggregate to binder ratio.

The approach is based on the assumptions that water equilibrium occurs and is maintained 30 minutes after mixing, the in-situ absorptions of both binder and bio-aggregates are constant for a selected pairing of materials, and, most critically, a quantitative estimation of the numerical value a_b is accurate. In this respect the method is questionable and so results must be scrutinised with additional care although the approach could be simply and significantly improved by use of an appropriate alternative to visual assessment not considered here. Within the context of the literature where the control of the water content is regularly addressed by using either a constant binder to water or bio-aggregate to water ratio, this approach remains arguably more vigorous in removing the impact of in-situ binder water ratio as an uncontrolled variable. Furthermore this method is based on physical observations rather than the purely theoretical approach which constitutes the only known previous attempt to scrutinise the issue; it is noted that the formulations provided by this method consistently fall within the window identified in the theoretical study (Lanos et al., 2013). It is therefore considered on balance that this provides an acceptable method for the isolation of the in-situ water to binder ratio.

This method was applied throughout the study as a means of controlling the in-situ water to binder ratio and determining the specific contents of bio-aggregate, binder and water to be used for each formulation of material.

4.2.2.3 Production method - cast

There was, at the time of testing, no official standard for the preparation of cast hemp-lime specimens although one has now been proposed since the undertaking of the work (Niyigena, 2015). Resultantly, the production method used for casting material was based on the method in previous studies considered within the literature review. The most notable of these influences was the PhD thesis of Hirst (Hirst, 2013) where a detailed description of a rigorous and well tested method is presented that provided a high level of consistency in results.

The raw materials were first weighed out into separate containers using a mass balance with an accuracy of ±1g. The mixing of the constituents was conducted in a large revolving pan mixer, Figure 4.19. This was enacted by first mixing the binder and water in a process known as slaking. The binder and water were added to the pan and mixed for one minute by hand to wet through the binder while minimising dust generation. This was followed by electric mixing for two minutes with a halt midway to break up pockets of non-dispersed binder that accumulate around the sides and mixing paddles. After two minutes the mixture was checked to ensure it was homogenous and that all of the binder was evenly dispersed in the water and mixing was continued if necessary until these criteria were met. For batches of mixture for making prismatic specimens for flexural, compressive and image analysis experiments, a dose of slaked red pigment was added at this stage of 10g per specimen and mixing continued until this was fully combined, Figure 4.19.

Following the slaking of the binder to form a slurry, the bio-aggregate was added to the mixer and initially folded into the slurry by hand to avoid unnecessary dust production from the hemp. Electric mixing was then conducted for an additional two minutes, again with a break midway to allow breaking of clumps by hand. After two minutes the mixture was checked for a homogenous appearance and even coverage of the bio-aggregate by the binder paste; mixing was continued in the event of this not occurring until the material was judged to be consistent, Figure 4.19.

Figure 4.19: The mixing process. Left to right: the pan mixer, the slaked binder with pigment dose added, the final combined mixture.

To give consistent specimen production it was shown by Hirst (Hirst, 2013) that weighing out the amount of mixture for each layer is the most effective way of controlling the process. Each layer of material to produce a specimen was therefore weighed out directly into the mould and a collar was used where more material that would otherwise fit in the mould loosely was required, Figure 4.20. The layer was then tamped to the required thickness using a wooden tamp, specifically sized to the mould used, to give an even compaction throughout the specimen. All the moulds were specifically produced for the project using plywood with a phenolic finish designed for use in concrete shuttering. The inside surfaces of the moulds were prepared with a mould releasing agent each time they were used and cleaned between uses.

Based on the specimen sizes required for the testing regime, for each variation of material the following set of cast specimens were produced, the moulds of which are shown in Figure 4.20:

- Six pigmented 400mm X 150mm X 150mm prisms for flexural tests, compressive test and image analysis. Three for testing in the direction of compaction, three for testing perpendicular.
- One unpigmented 400mm X 400mm X 50mm specimen cast with layering in the major axis for thermal conductivity testing perpendicular to compaction.
- One unpigmented 400mm X 400mm X 50mm specimen cast with layering in the minor axis for thermal conductivity testing parallel to compaction.

Following the production of the specimens they were transferred to a conditioning room maintained at 20°C and 50%RH. The moulds were removed after six days and the specimens replaced in the room. Due to the limited size of the mixer and storage space, the specimens were produced in batches staggered over the second year of the study.

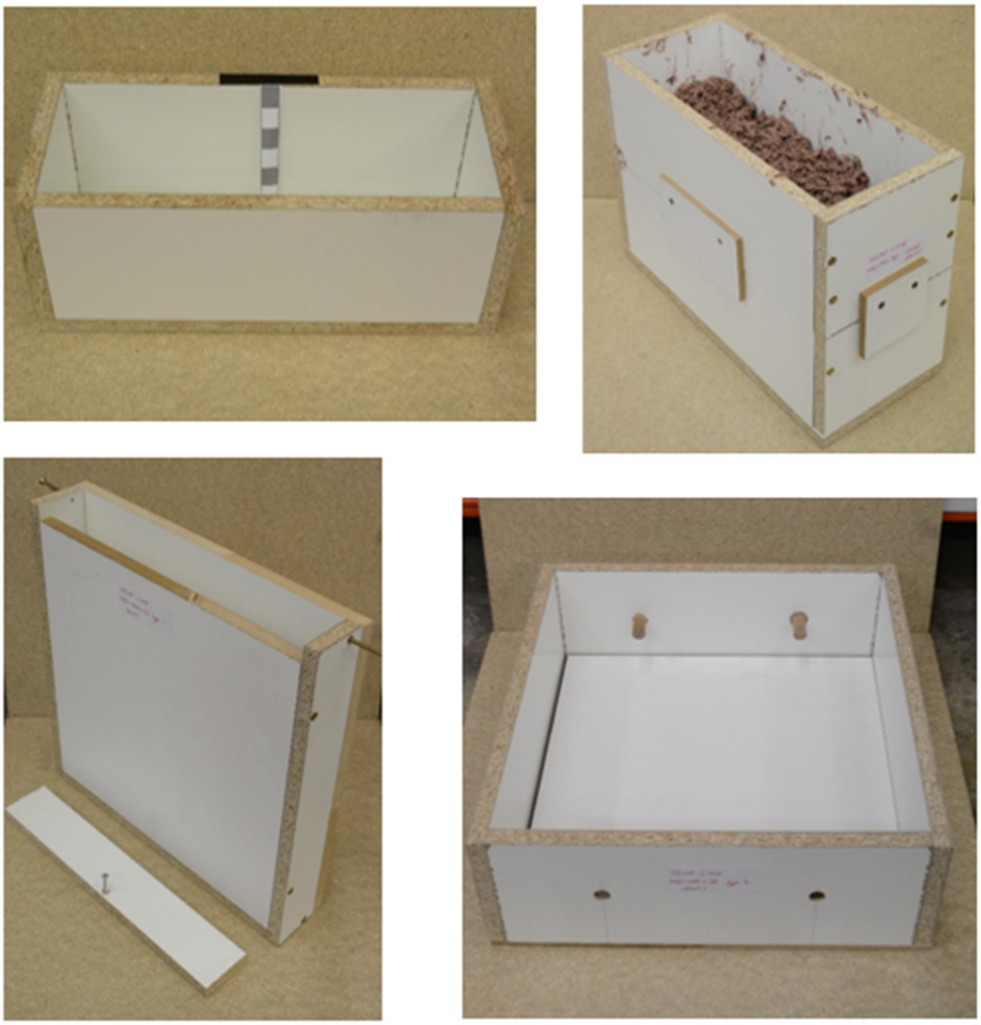

Figure 4.20: The moulds used for differing hemp-lime specimens. 400 X 150 X 150 prismatic mould (top left), prismatic mould fitted with filling collar (top right), 400 X 400 X 50 thermal conductivity mould for perpendicular testing (bottom left), thermal conductivity mould for parallel testing (bottom right).

4.2.2.4 Production method – projection formed

As with cast bio-aggregate composites, there is not a definitive method for the production of projection formed specimens. Furthermore in this case there is a lesser body of literature to use as a precedent and to a great extent the method is determined by availability of equipment. In this study, based in the United Kingdom, the accessibility of the equipment dictated entirely the use of a specific projection methodology due to there only being a single contractor in the market.

The contractor used was Hemp-lime Spray that uses a method of projection using separate streams of slurry and hemp particles that are directed into one another. This method is different to some of those in previous studies, where the binder is incorporated dry into

the air stream and the water alone is added at the lance (Elfordy et al., 2008). The equipment, Figure 4.21, is in three parts:

- A revolving pan mixer, hopper and pump for the mixing, aggregation and delivery of a pressurised binder slurry feed via hose.
- A large hopper with auger fed air stream for delivery of the bio-aggregate via large diameter hose.
- An operator lance where the air steam carrying the bio-aggregates is projected through a central opening while the binder slurry is sprayed through fine openings at the perimeter directed slightly inwards. The regulation of the rate of flow of both the bio-aggregate and the slurry are controlled by the operator via controls on the lance.

Figure 4.21: The three parts of the projection forming equipment. Left to right: the slurry mixer/agitator and pump, the aggregate hopper and air blower, the application lance.

The aim of this part of the study was not to assess the impact of projection variables but rather to assess the impact of the projection process compared to casting. For this reason it was necessary to produce comparable material to that made by casting where possible. The variations in projection formed material, from the literature review, are noted to come from formulation, constituents used and projection distance which alters the compaction. It was therefore desirable to control and regulate these aspects where possible.

The ratio of water to binder was directly controllable due to the nature of the process and so this could be matched to that of the median cast material. The ratio of bio-aggregate to binder and bio-aggregate to water is effectively determined by the operator who regulates the flow of slurry and bio-aggregate. To produce a material as near as possible to that used in the cast material, specimens of cast material were used as a visual reference for consistency. The ratio of slurry was then calibrated in several test specimens to match the consistency and then controlled to this thereafter. The raw materials in all cases were the same as used in the cast material.

The distance between the lance and the substrate, as well as the inherent power of the equipment, determines the effective compaction applied to the material and the movement of the lance arguably determines the layering. The contractor's recommendations for the projection distance and lance movement were a distance of 1m and building the specimen from the lowest part upwards. The 1m distance is in accordance with values proposed in the literature as optimal for density and minimal waste and so was adopted in this instance (Elfordy et al., 2008). Following production, the actual compaction was able to be estimated from other properties. The lance movement used was maintained across all specimens and the process recorded for reference, however the effective layering of the material is not controlled beyond this point and is considered a direct and intrinsic impact of the method.

While the same specimen sizes were used for the testing protocol as previously described, it was not practical to produce regular specimens to this size directly. Instead specimens were produced at a much larger size of 800mm X 800mm X 200mm, Figure 4.22, and then the required prisms and panels as described in the specimen sizing section removed from these at 27 days using a band saw. All the specimens were produced on a working site in Lay Hill, UK, and then taken via road to the University of Bath the same day. Due to the size of the specimens, they were stored in lab conditions as opposed to controlled conditions. Five sides of the moulds were removed after six days in concurrence with the cast specimens; the base was maintained to aid handling.

Figure 4.22: The production of the projection formed specimens by Hemp-lime Spray.

4.3 Experimental study into the directional impact of constituents

4.3.1 Introduction

This section details the experimental outline and results obtained from a study into the impact of constituents on the behaviour of bio-aggregate composites. As has been previously mentioned, the constituent variables considered within this study are the particle size distribution of the aggregates and the binder to aggregate ratio; the classification of all the materials used is provided in section 4.1. The physical behaviours assessed were the flexural behaviour, compressive behaviour and thermal conductivity using the methods previously detailed in section 4.2. In addition to this, results are also presented from two dimensional image analysis of the material in two directions using the method detailed in chapter 3. The results from this study have been presented as a journal paper currently under consideration entitled "The influence of the constituents on the properties of bio-aggregate composites".

4.3.2 Experimental outline

4.3.2.1 Assessed variables

Three variations of each of the two variables considered were used: fine, medium and coarse hemp particles, as were previously defined in chapter 4.1, and three values of hemp to binder ratio. In order to limit the total number of specimens produced not every one of the nine possible permutations of these variable combinations were considered but rather each variable was considered independently, with the specimens of median value being applicable to both as is displayed diagrammatically in Figure 4.23. Consequently five variations of material were considered in this study, the details of which are summarised in Table 4.4 (the nomenclature used to refer to the mixes being of the form: "shiv grade" "binder ratio"). In total 40 specimens of cast hemp-lime - 30 prismatic, 150mm X 150mm by 400mm, and 10 panel, 50mm X 400mm X 400mm - were produced for this study.

To produce the three variations of particle size distributions desirable for this study one option would have been to source a single supply of bio-aggregates and to then produce divisions of this material through sieving. This has been successfully applied previously in the literature (Cigasova et al., 2013) and has the advantage of minimising any natural

variation of material that might occur between differing suppliers identified within the literature review as a potential source of uncertainty. The disadvantages of this approach are its time consuming nature, especially given the quantity of bio-aggregate required in this study, but also the limited benefit any finding might be to industry. Practitioners are likely to have limited interest in producing their own grade of particles since this will involve considerable additional cost and material wastage.

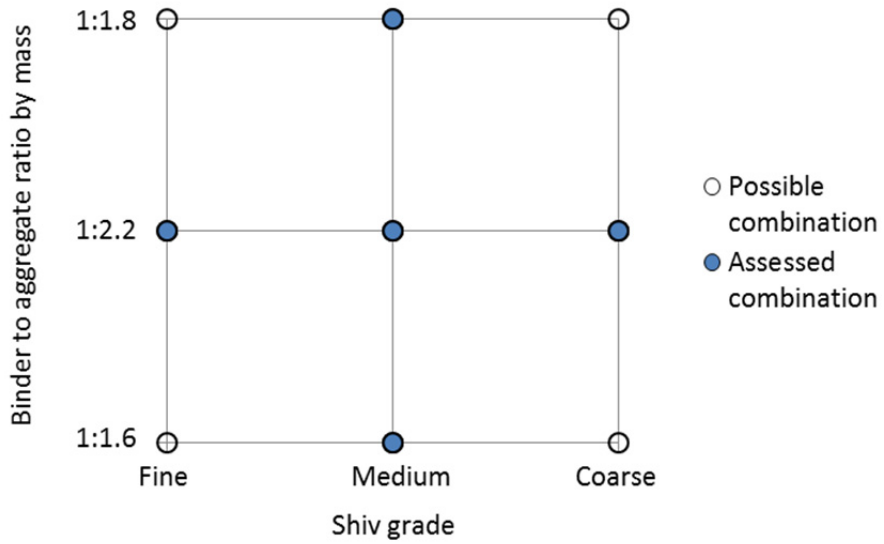

Figure 4.23: Diagrammatic view of the full range of material variations possible and the variations considered.

The alternative approach taken here was to use differing grades produced by the same manufacturer as this hopefully minimises chemical variations in the product while being known to be reflective of products available to industry. Out of four available pre-prepared grades from the manufacturer, two grades were used as provided and a third was prepared by the even weight mixing of the other two grades. The reasoning behind this was derived from the particle size distribution assessment that identified only very slight variation between No 7 and No 8 grades, leading to limited value being ascribed to the testing of both. This presented an opportunity to produce a new grade of material from mixing the two middle manufacturer's grades - 8 and 12 - while maintaining a minimum of three variations of particle size. As was touched on in Chapter 4.1 where the particle size distributions of the grades used are presented, this provided three distinct grades of material in terms of average particle size but also produced the largest spread of sizes in the grade with the median particle size. This segregates out the two variables of particle size and particle size spread that have not been independently assessed effectively within preceding work. The experimentally measured characteristics of the three grades used in this study are presented in Figure 4.3 and Table 4.1.

The ratios of binder to hemp used were selected to give a range of ratios surrounding those commonly used in practice. The literature review indicated that bio-aggregate composites with both higher and lower doses of binder have been considered in the literature. This study may be considered to sit at the lower end of this range as a result of focussing on materials representative of current application.

4.3.2.2 Controlled variables

All the specimens were produced using the basic methodology for cast material production detailed in Chapter 4.2 and cured following the regime outlined within the same chapter relevant to the tests conducted. The production variables that are the focus of the following Chapter 4.4 were controlled within this part of the work.

The layer size used for specimen production was maintained at 50mm for all specimens, being the median value of the range of layer sizes used later and in line with the values used in preceding studies.

The casting compaction is defined in this study as the ratio of compacted to un-compacted density; a definition selected to be independent of the natural level of packing obtained by differing variations of material. The un-compacted densities of each of the mix permutations considered were obtained by gentle sprinkling of the material into a 3L container and then weighing the contents in a similar way to that adopted for the determination of the un-compacted bulk density of hemp aggregates. The process was repeated five times to find an average value that was then used, Table 4.4. This definition of compaction is considered to be more applicable to industry than a fixed level of static loading due to its easy onsite application. In this study the compaction was set at 1.45. This value was selected to be representative of standard compaction implemented on site, estimated from the measured un-compacted density of the median aggregate to binder ratio and the reported wet densities of standard “wall mix” material within grey literature (Bevan et al., 2008, Tradical®, 2015).

It is not possible to control both the water to binder ratio and the water to aggregate ratio for reasons discussed in Chapter 4.2. The water content used for each mix was instead determined by the method and equation outlined previously, in order to give a consistent effective water to binder ratio of the in-situ paste. The percentage ratios of water binder and aggregate as derived by this method for each of the mix variations considered are presented in Table 4.4.

Table 4.4: Mixtures of hemp-lime used in the study of the directional impact of constituents.

Mixture Ref	Grade of aggregate	Binder to aggregate ratio	Mix constituents ratio (%)			Un-compacted wet density of mix (kgm^{-3})	Target wet density, 45% compaction (kgm^{-3})
			Binder	Aggregate	Water		
Fine 2.2	Fine	1:2.2	36	16	48	459	666
Medium 1.8	Medium	1:1.8	32	17	51	407	590
Medium 2.2	Medium	1:2.2	36	16	48	433	628
Medium 2.6	Medium	1:2.6	39	15	46	470	682
Coarse 2.2	Coarse	1:2.2	32	16	48	411	596

4.3.3 Results

4.3.3.1 Flexural behaviour

The measured physical dimensions and mass of each mix are given in Table 4.5 as well as the calculated values of 28 day density; the moisture content determined following compressive testing of a cube removed from each flexural specimen is also given. In each case the mean value of three specimens and uncertainty are presented given.

The stress /strain plots produced using the method detailed in Chapter 4.2 for all specimens tested within this part of the study are presented in Figure 4.24. From the results presented in Figure 4.24, the failure stress in each specimen can be identified and the mean value and uncertainty found - Figure 4.25.

Photograph sequences for the first tested specimen of each variation, used to help ascertain the failure mode and interpret the likely internal flow of forces within the material, are presented for all tests in the appendices while the image sequences for parallel and perpendicular loading for the median material tested, 'medium 2.2', are presented in Figure 4.26.

Table 4.5: Physical parameters of the flexural specimens produced for the study of the directional impact of constituents.

Mixture Ref	Specimen length (mm)	Specimen width (mm)	Specimen depth (mm)	Specimen mass, 28 days (g)	Specimen density, 28 days (kgm^{-3})	Specimen moisture content (%)
Fine 2.2	397.3 ± 0.7	147.9 ± 2.0	149.4 ± 1.5	3712 ± 39	423 ± 9	14.2 ± 1.7
Medium 1.8	396.9 ± 0.7	147.3 ± 1.7	148.7 ± 1.8	3292 ± 110	379 ± 11	16.8 ± 4.4
Medium 2.2	398.2 ± 1.0	149.2 ± 2.7	149.3 ± 1.7	3640 ± 57	411 ± 12	16.6 ± 1.7
Medium 2.6	396.3 ± 0.8	148.0 ± 0.8	148.9 ± 2.3	3762 ± 64	431 ± 12	12.7 ± 2.6
Coarse 2.2	397.5 ± 1.0	148.0 ± 2.0	148.1 ± 2.2	3378 ± 29	388 ± 4	16.1 ± 1.3

From Table 4.5 it can be seen that the consistency of the specimens' physical dimensions, both within sets of similar specimens and differing variations, was reasonably good and imply that dimensionally induced impacts on the results are negligible. In general the dimensions of the specimen were found to be below the proposed dimensions of 400mm X 150mm X 150mm. It is unclear if this may be as a result of slight variations within the moulds from these dimensions although it is considered more likely that this may be as a result of slight material shrinkage during drying or a side effect of the method applied to obtain the results.

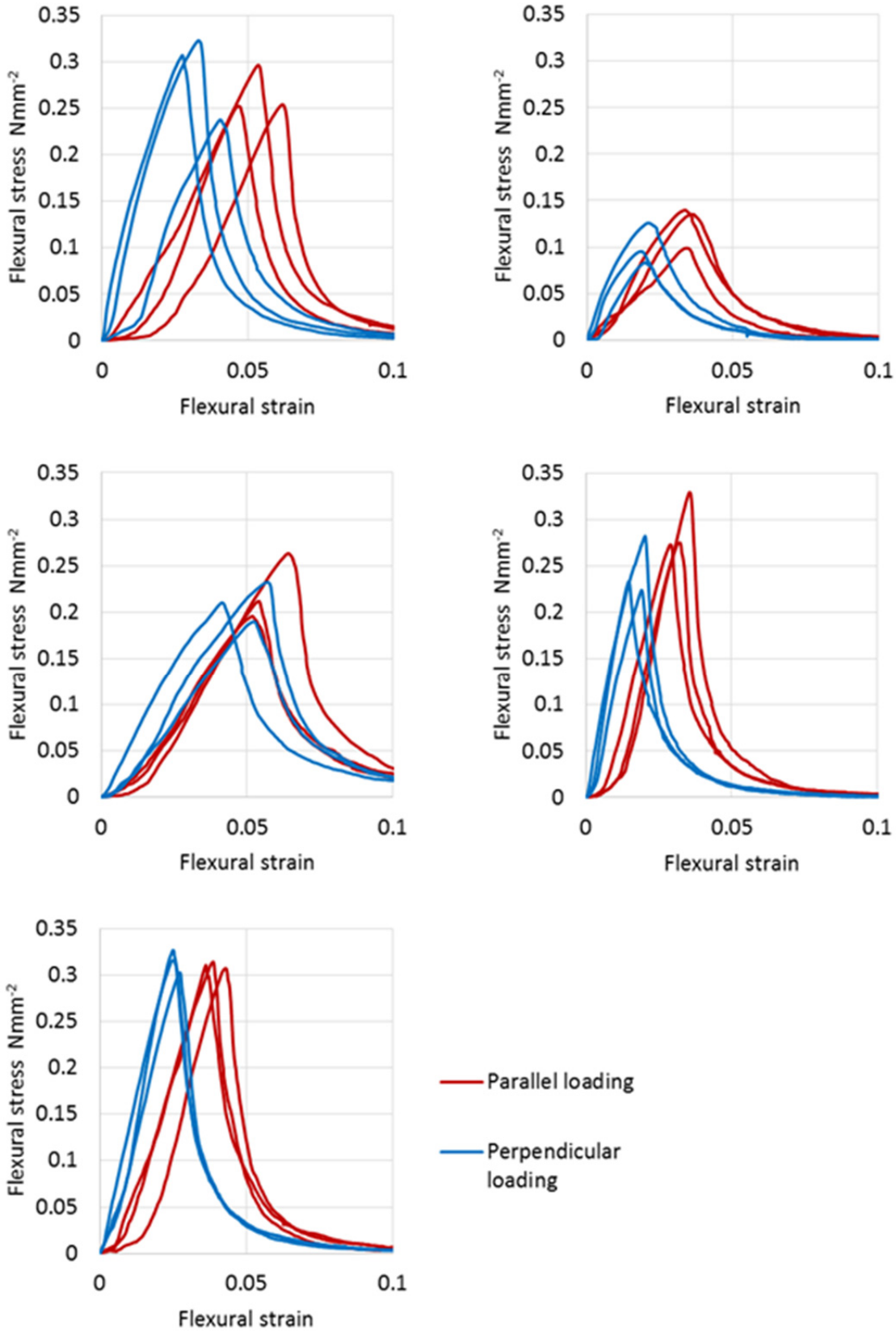

Figure 4.24: The flexural stress/strain plots for fine 2.2 (top left,) medium 1.8 (top right), medium 2.2 (middle leftt) medium 2.6 (middle right), and coarse 2.2 (bottom) mixtures.

The density of similar specimens was found to have an uncertainty of around 2.5% indicating a good level of consistency in the material produced. The mean density of specimen sets seems to be broadly in line with what would be expected from the wet densities, Table 4.4. The moisture content was found to vary more than other parameters and while it is not clear why this is, it may be speculated that differing locations within the conditioning room might be in part accountable as well as natural variations in the material.

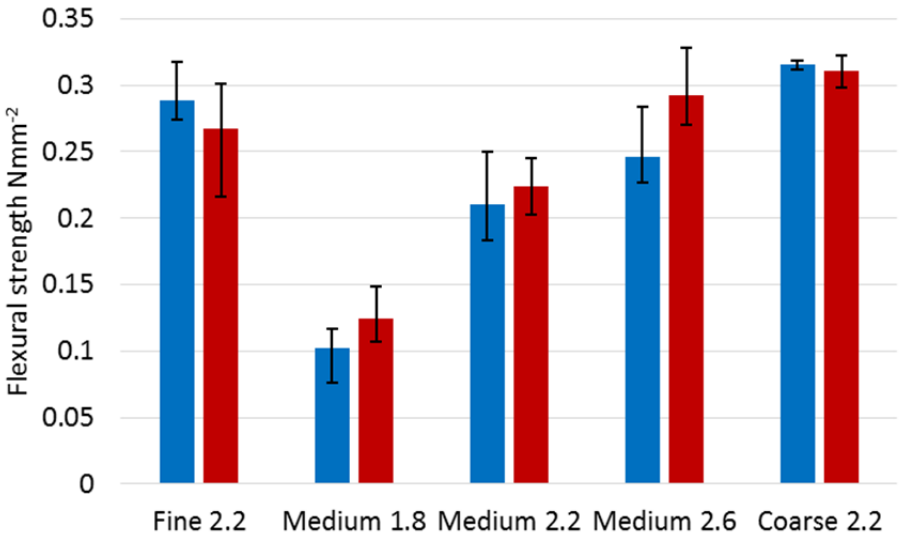

Figure 4.25: The flexural strength of parallel loaded (red) and perpendicular loaded (blue) hemp-lime of differing constituents.

From Figure 4.24 several general observations can be made as to the directional impact of the altered parameters on the flexural behaviour. The general the form of the graphs is similar across all variations and in both loading directions; in all cases a clear peak stress is observed followed by an immediate reduction in load capacity indicating a brittle failure of the material. The main difference in the plots is observed to come from the alterations to the binder to aggregate ratio where a lower binder content is observed to give a lower peak stress, although with seemingly limited impact on failure strain. The grade of aggregate is observed to have a lesser impact than the binder to aggregate ratio for the ranges considered and there is no apparent correlation between size of particle and peak flexural strength, the medium 2.2 mix found to have a lower parallel and perpendicular peak stress than both the Fine 2.2 mix and Coarse 2.2 mix. When loading direction is considered, perpendicular loading appears from visual inspection to give a marginally steeper gradient during loading, which is indicative of higher stiffness.

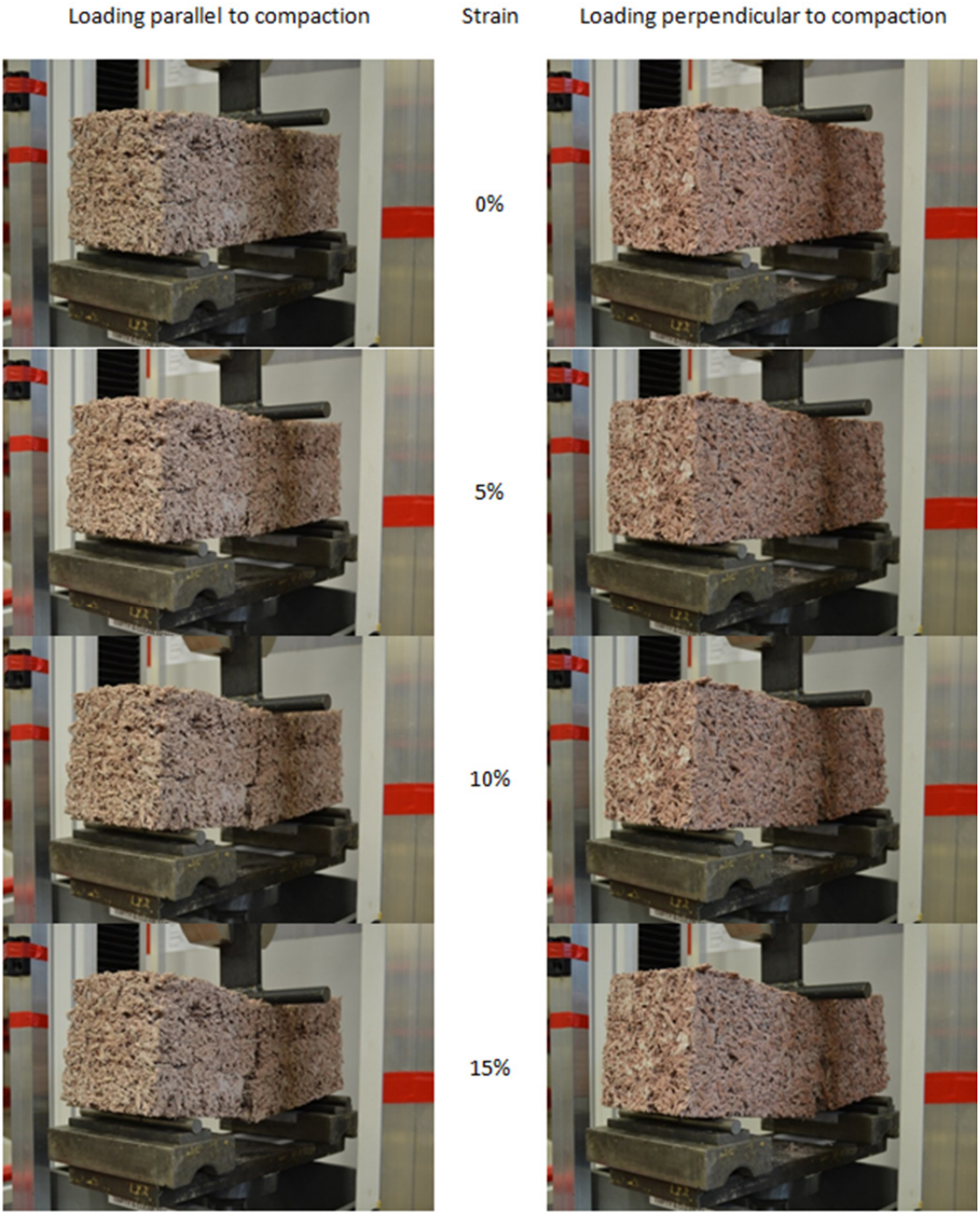

Figure 4.26: Loading image sequenced for medium 2.2 mixture hemp-lime in flexure.

Figure 4.25 confirms two of the interpretations that are drawn from Figure 4.24 limited difference in parallel and perpendicular flexural strength and a clear correlation between the binder to aggregate ratio and the flexural strength in line with what has been reported elsewhere (Sassoni et al., 2014, Le et al., 2014, Le et al., 2015). It may also be seen from Figure 4.25 that while no correlation to particle size is observed, the medium particle grade may be considered to produce a statistically significant decrease flexural strength in both loading directions.

The image sequences in Figure 4.26 appear to show a consistent failure mode in both directions of loading that may be described as a near to vertical crack propagating from the tensile face at the point of material failure. This is consistent with preceding literature that identifies the tensile strength of hemp-lime as significantly lower than the compressive strength (Walker et al., 2014, de Bruijn et al., 2009).

4.3.3.2 Compressive behaviour

The measured physical dimensions and mass of each of the specimens are given in Table 4.6 as well as the calculated values of 28 day density. The moisture content determined subsequently to compressive testing for each specimen is also given, where the values are the same as those presented from the flexural specimens. In each case the mean value and uncertainty for each material variation are presented.

Table 4.6: Physical parameters of the compressive specimens produced for the study of the directional impact of constituents.

Mixture Ref	Specimen height (mm)	Specimen width (mm)	Specimen depth (mm)	Specimen mass, 28 days (g)	Specimen density, 28 days (kgm^{-3})	Specimen moisture content (%)
Fine 2.2	149.5 ± 1.2	149.2 ± 1.7	149.6 ± 1.3	1407 ± 27	422 ± 12	14.2 ± 1.7
Medium 1.8	149.1 ± 2.5	147.2 ± 1.3	148.6 ± 3.5	1213 ± 39	373 ± 13	16.8 ± 4.4
Medium 2.2	149.4 ± 1.0	150.0 ± 0.5	150.0 ± 1.7	1363 ± 49	405 ± 14	16.6 ± 1.7
Medium 2.6	149.1 ± 2.5	147.2 ± 1.3	148.6 ± 3.5	1216 ± 39	432 ± 11	12.7 ± 2.6
Coarse 2.2	149.9 ± 1.2	148.7 ± 1.2	149.2 ± 2.7	1272 ± 37	383 ± 18	16.1 ± 1.3

The stress against strain plots produced using the method given in Chapter 4.2 for all specimens tested within this part of the study are presented in Figure 4.27. From the results presented in Figure 4.27, using the method detailed within chapter 4.2, the compressive rupture stress in each specimen can be found and the mean value and uncertainty calculated, Figure 4.28.

Photograph sequences for the first tested specimen of each variation, used to help ascertain the failure mode and interpret the likely internal flow of forces within the

material, are presented in the appendices while the image sequences for parallel and perpendicular loading for the median material tested, medium 2.2, are presented in Figure 4.29.

From Table 4.6, similar observations as were made of the flexural specimens, Table 4.5, can be made here: reasonable consistency in the dimensions implying little dimensional impact on the results. The dimensions generally are again observed to be smaller than was specified and similar reasons to those discussed previously are likely to apply. The specimen densities at 28 days are in line with what is expected from the wet densities of the mixtures, Table 4.4.

In contrast to the flexural results, the form of the plots produced from parallel and perpendicular loading, Figure 4.27, are of significantly differing form and this distinction is preserved for all variations of material considered. The two major differences are in the gradient of the loading phase and the distinct difference in post failure behaviour, parallel loading exhibiting a reduction of gradient and perpendicular exhibiting a peak. This observation is in line with bi-directional loading results within the literature (Youssef et al., 2015, Amziane et al., 2015). As with the flexural results, Figure 4.24, the main difference between variations of material considered is observed to come from the ratio of binder to aggregate with a seemingly similar trend of increasing global failure strength with increasing binder content; the perpendicular loaded Medium 2.6 result is a notable outlier to this. No obvious correlation is apparent between increasing size of particles and behaviour although the particle size distribution appears to have a significant impact none the less with the fine and coarse grades outperforming the medium grade.

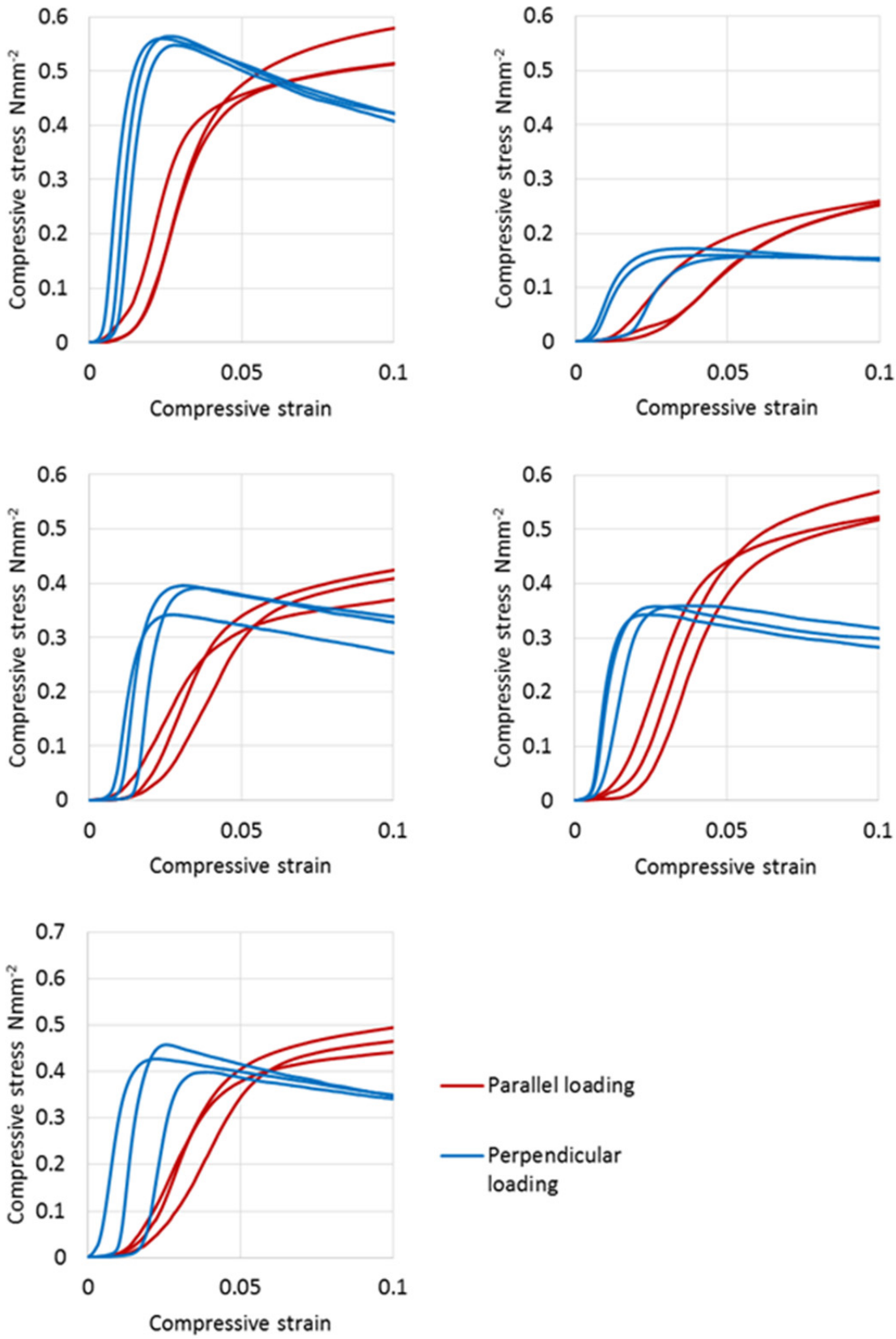

Figure 4.27: The compressive stress/strain plots for fine 2.2 (top left,) medium 1.8 (top right), medium 2.2 (middle left) medium 2.6 (middle right), and coarse 2.2 (bottom) mixtures.

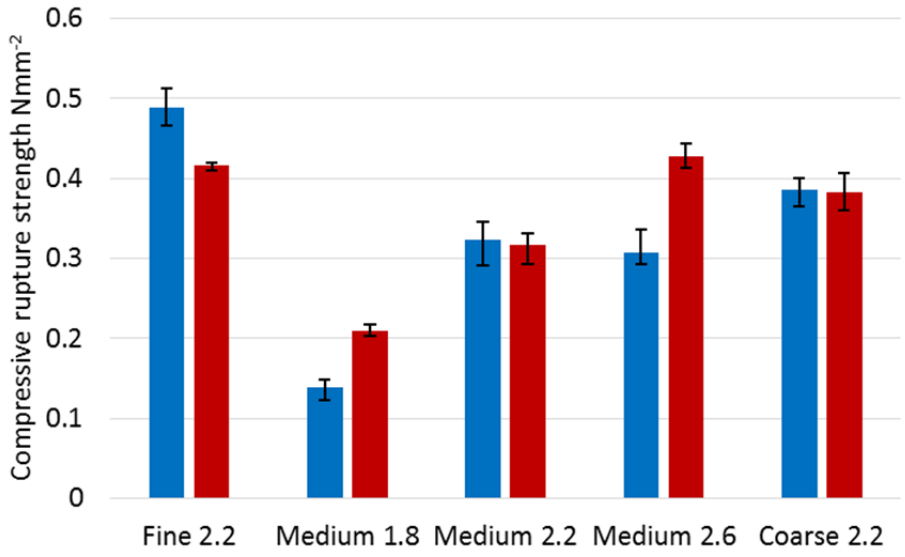

Figure 4.28: The compressive rupture strength of parallel loaded (red) and perpendicular loaded (blue) hemp-lime of differing constituents.

The results presented in Figure 4.28 are for compressive rupture stress, a parameter defined in section 4.2 and used to allow effective comparison between parallel and perpendicular loaded material despite differing stress/strain relationships and failure modes. As this parameter is novel to this study the results may not be directly compared to preceding results elsewhere. The results confirm initial observations of a correlation between binder to aggregate ratio and compressive strength but indeed also highlight the unconformity to this in the parallel loading condition at the highest binder content. Using this definition of compressive strength it may also be observed that the orientation of loading has a bearing on the result; however the nature of this impact is observed to depend on the material variation. As with flexural strength, Figure 4.25, there is evidence of particle size distribution impacting the compressive rupture strength to a significant level but without a seeming correlation to coarseness of aggregate.

The image sequence in Figure 4.29 demonstrates a clear difference in the material's reaction to compressive load along its differing axes. Parallel to the casting compaction the material is observed to compact and bulge evenly as load is applied; almost no material is observed to break off from the specimen. Perpendicular to the casting compaction, the material is observed to break away sideways and sections are observed to rotate out from alignment with the loading path. Loose material is abundant in this case with significant proportions observed to fully detach from the specimen.

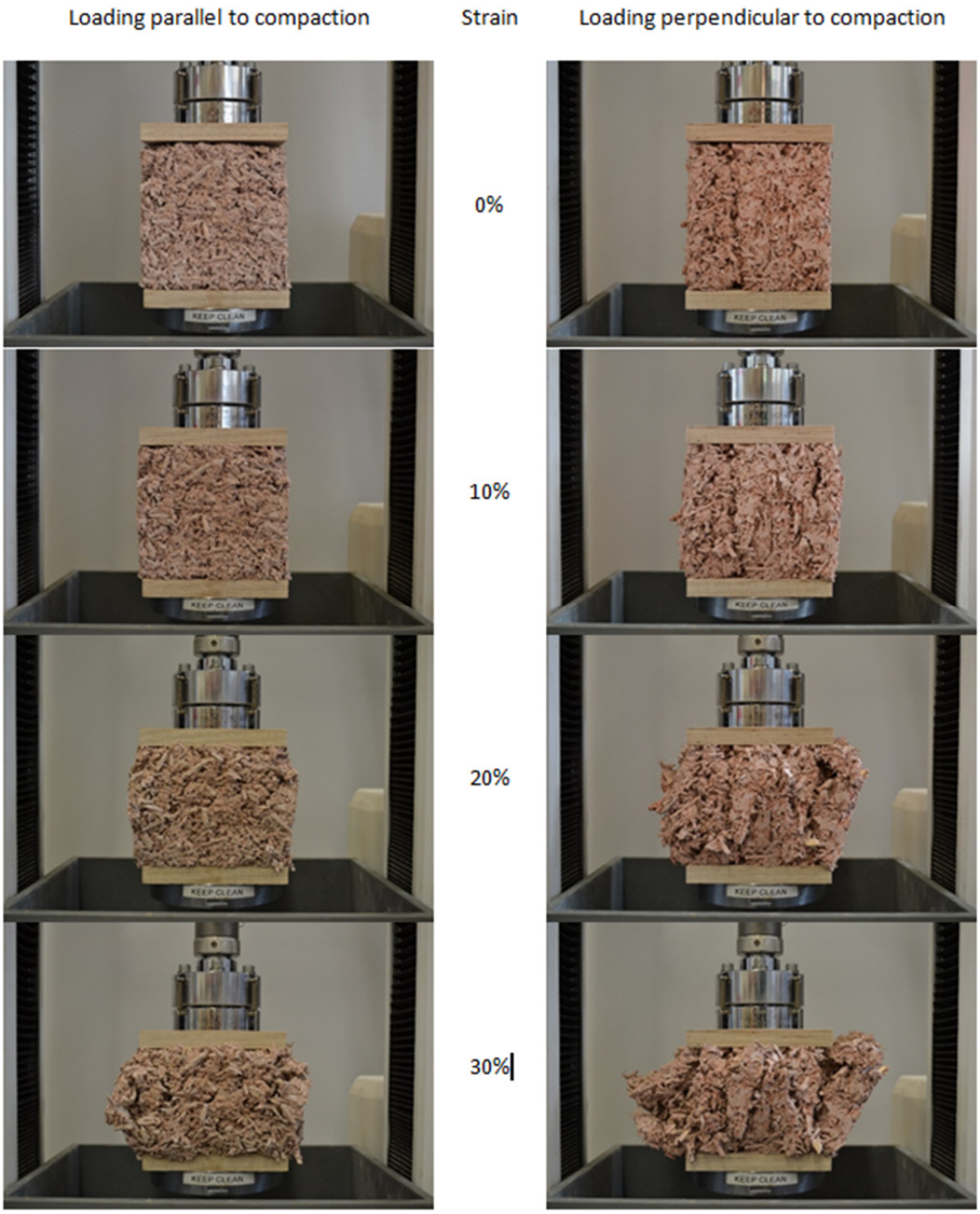

Figure 4.29: Loading image sequenced for medium 2.2 mixture hemp-lime in compressison.

4.3.3.3 Thermal conductivity

The measured physical dimensions, stable density and dry density of each of the specimens are given in Table 4.7. The calculated value of stable moisture content is also given. Both the dry thermal conductivity and stable thermal conductivity for each material variation are presented in Figure 4.30 and Figure 4.31 respectively. In all cases, "stable"

refers to the specimen being of stable mass for a period of 24 hours within a 20°C and 50% relative humidity environment as was defined in Chapter 4.2.

From Table 4.7 it is observed, as has been previously noted for the flexural and compressive specimens, that the dry and stable density generally follows what would be expected from the wet densities in terms of least to most dense materials. It may also be seen that compared to the 28 day densities for the similar flexural and compressive specimens, the stable density is consistently lower; the lower moisture contents in this state tally with this observation and can mostly account for the results. In general the stable moisture content is found to be relatively consistent across all materials.

Table 4.7: Physical parameters of the thermal specimens produced for the study of the directional impact of constituents.

Mixture Ref	Specimen length (mm)	Specimen width (mm)	Specimen thickness (mm)	Specimen density, dry (kgm^{-3})	Specimen density stable (kgm^{-3})	Specimen stable moisture content (%)
Fine 2.2	399.0 ±0.9	399.8 ±1.2	50.0 ±0.9	363 ± 2	385 ± 3	6.3 ± 0.1
Medium 1.8	399.5 ±0.8	400.1 ±1.8	50.6 ±1.1	312 ± 3	333 ± 5	6.5 ± 0.1
Medium 2.2	400.4 ±2.2	398.0 ±1.2	50.1 ±0.5	345 ± 2	366 ± 1	5.9 ± 0.2
Medium 2.6	398.8 ±0.4	399.5 ±0.8	50.0 ±0.6	374 ± 2	397 ± 2	6.1 ± 0.1
Coarse 2.2	399.7 ±1.0	399.4 ±1.1	50.5 ±1.0	326 ± 0	347 ± 0	6.5 ± 0.1

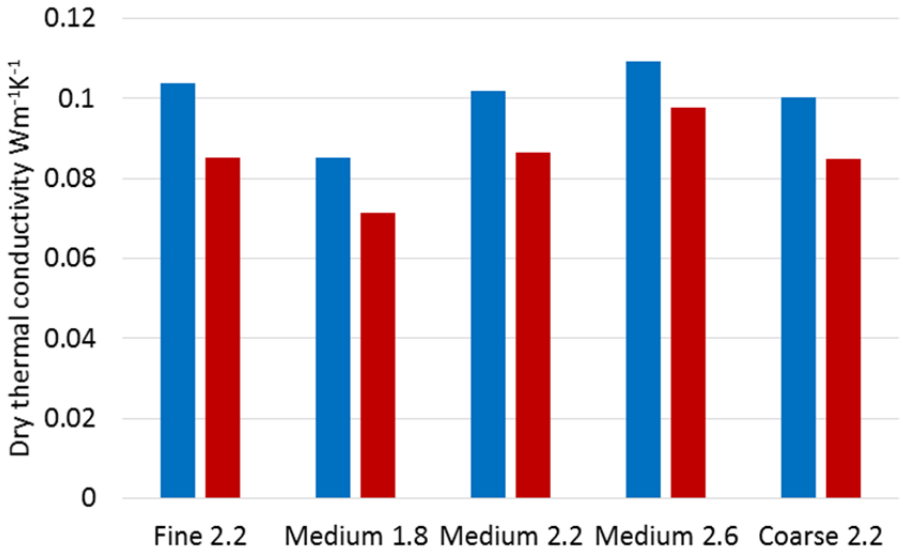

Figure 4.30: The dry thermal conductivity of parallel loaded (red) and perpendicular loaded (blue) hemp-lime of differing constituents.

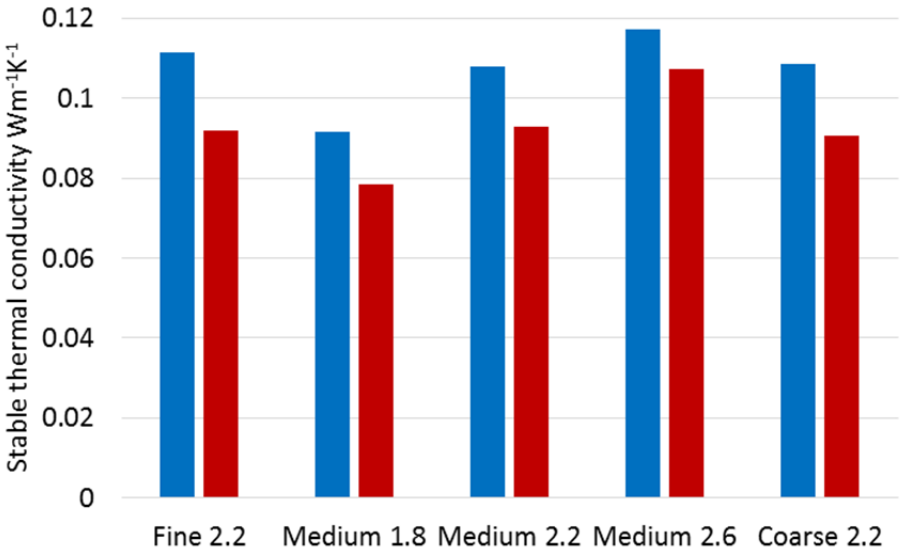

Figure 4.31: The stable thermal conductivity of parallel loaded (red) and perpendicular loaded (blue) hemp-lime of differing constituents.

From Figure 4.30 and Figure 4.31 it is noticeable that increase in moisture content produces a seemingly uniform increase of thermal conductivity. It is also noticeable that there is a consistently higher value of thermal conductivity recorded in the perpendicular to compaction direction irrespective of the variation of material considered or whether or not it has been dried, consistent with previous results that found a similar difference (Nguyen et al., 2010, Pierre et al., 2014). What is originally seen here is a clear variation in the discrepancy between parallel and perpendicular values with mix variation indicating the degree of anisotropy is dependent on these aspects. As with flexural strength and compressive rupture strength, there is evidence of a positive correlation between the

thermal conductivity and the ratio of binder to aggregates but not an obvious correlation to particle size.

4.3.3.4 Two dimensional image analysis

Figure 4.32 presents the frequency distribution of particle orientation for each of the variations of material. In each case the distributions are presented both from the two dimensional images taken parallel to the direction of compaction and images taken perpendicular to the direction of compaction. The distribution in each case represents the total population of particles observed from six cross sections taken from each of the three specimens, totalling 18 images. All the images were produced, processed and analysed using the methodology developed in the pilot study and outlined in Chapter 3. In all plots, a fitted Hankinson form equation is also shown where the equation has been fitted via a least squares fitting approach.

As was touched on in Chapter 3, the image analysis conducted when viewing perpendicular to the casting compaction is of most interest as it is in this direction where the level of orientation within the material can be observed. Accordingly the fitted parameters of the Hankinson equation: f_o, f_{90} and n, for each of the material variations in the perpendicular viewing direction are presented in Table 4.8. Alongside this, the calculated value of $(f_0 - f_{90})$ and the sum of the least squares, indicative of the closeness of fit, are also given.

Table 4.8: Summary of particle orientation frequency distributions from hemp-lime of differing constituents.

Mixture Ref	f_0	f_{90}	n	$(f_0 - f_{90})$	Sum of least squares
Fine 2.2	17.40	6.99	2.03	10.42	0.273
Medium 1.8	19.46	6.07	2.10	13.40	0.199
Medium 2.2	17.98	6.50	2.13	11.48	0.121
Medium 2.6	17.25	6.93	2.08	10.32	0.091
Coarse 2.2	18.94	6.32	2.07	12.63	0.451

From the results presented in Figure 4.32, the clearest result to be demonstrated is the difference between the orientation frequency distribution when viewing parallel and perpendicular to compaction. Imaged parallel to compaction, across all variations of material considered, the distribution is noted to be relatively even and so in planes

perpendicular to compaction the particles may be considered to be evenly distributed in terms of orientation. There is a slight tendency in the particle orientation towards both 0° and 90° in this imaging direction although this is of low magnitude. Imaged perpendicular to compaction, again across all variations of material considered, the distribution is observed to be skewed towards 0°. This indicates that within planes parallel to the direction of compaction the particles tend towards an alignment of their major axis perpendicular to the applied force.

Comparing differing variations of material it is noted that in the analysis of perpendicular images, while the form of the graph remains constant, the apparent degree of sway in the distributions alters with the material considered. This is confirmed in Table 4.8 where the shape function, n, is observed to fluctuate little while the value of $(f_0 - f_{90})$ is found to vary more. From Table 4.8 there is a strong indication that the value of $(f_0 - f_{90})$ (and thus the effective level of orientation within the material structure) is dependent both on the binder to aggregate ratio and the grade of particles: a positive correlation between coarseness of grade and $(f_0 - f_{90})$ is seemingly apparent while a negative correlation between binder to aggregate ratio and $(f_0 - f_{90})$ is seen. It is also seen from Table 4.8 that in all cases the sum of the least squares is low indicating a very accurate fit of the equation to the experimental data, visually confirmed by Figure 4.32.

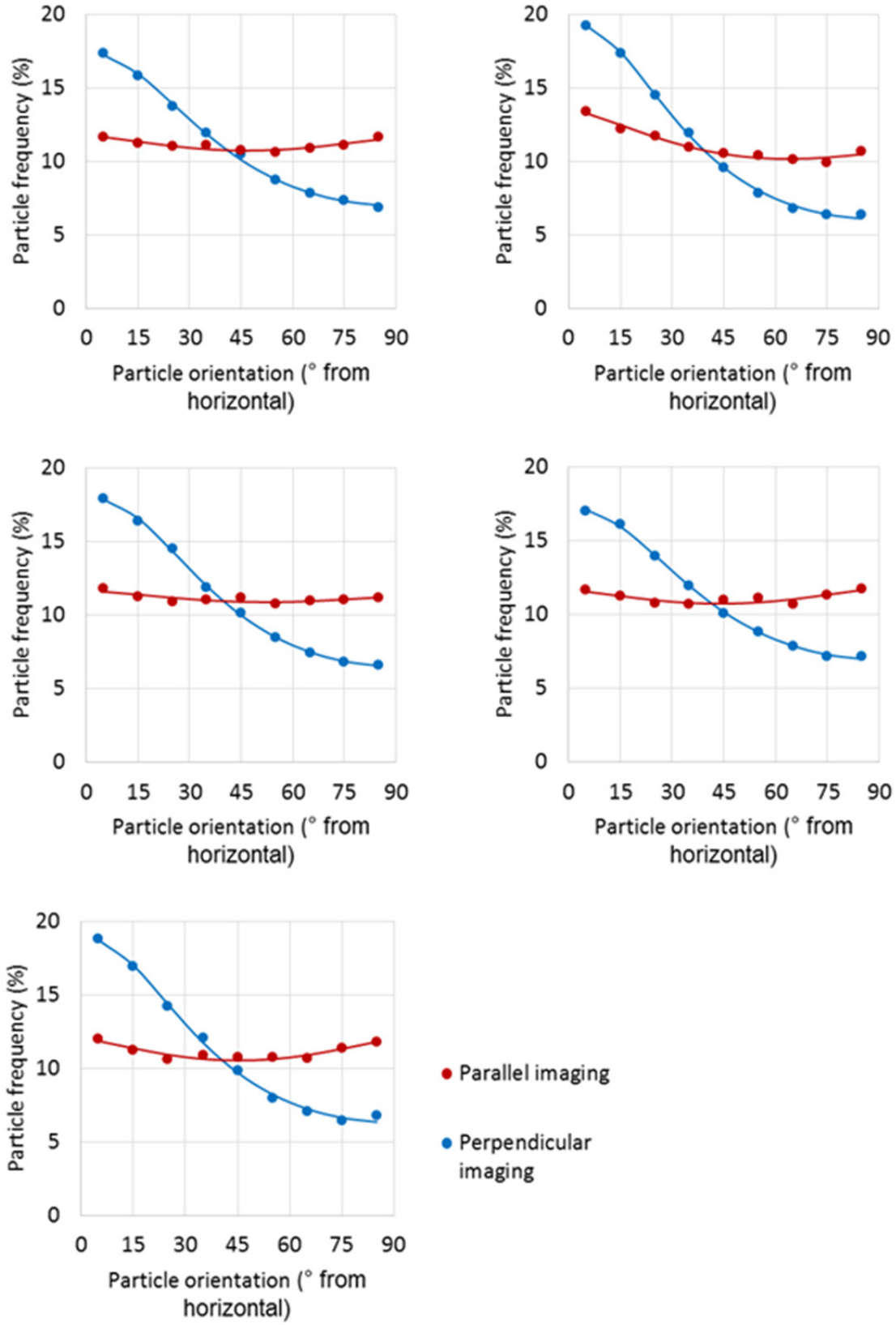

Figure 4.32: The particle orientation frequency distribution for fine 2.2 (top left,) medium 1.8 (top right), medium 2.2 (middle left) medium 2.6 (middle right), and coarse 2.2 (bottom) mixtures.

4.3.4 Discussion

4.3.4.1 Density profiles

Using the data from the compressive and thermal specimens, the density and moisture content of the differing material variations considered can be plotted against one another, Figure 4.33, to assess the consistency of the material produced across these tests.

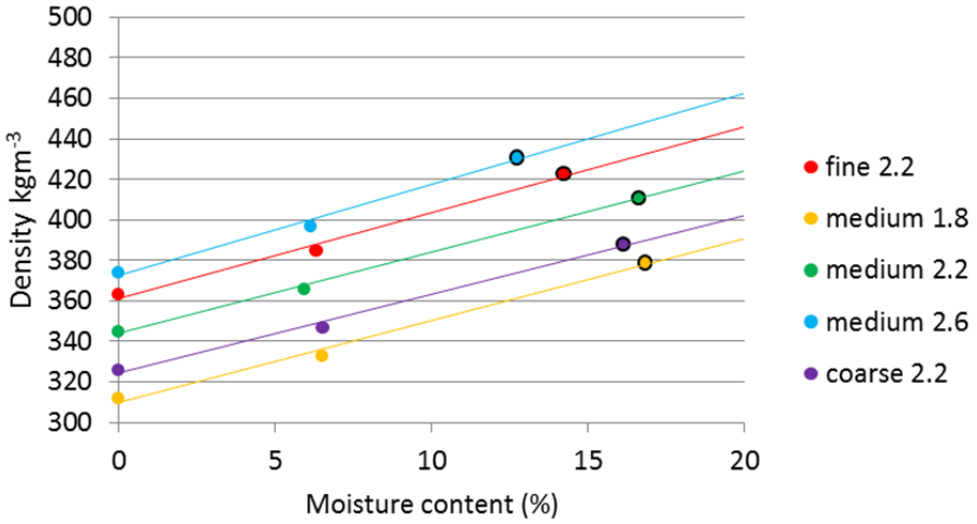

Figure 4.33: The moisture content/density plots for thermal and mechanical (black ringed) specimens of hemp-lime of differing constituents.

From Figure 4.33 it can be seen that the densities of the material vary with the constituent variables of particle size distribution and binder to aggregate ratios across a range of moisture contents as would be expected. More importantly, from Figure 4.33 it is noticeable that there is minimal discrepancy between the achieved densities for mechanical tests at 28 days (black ringed) and what would be predicted from extrapolating the thermal specimen data. This indicates a very high level of consistency in the material produced for these differing tests and in turn indicates the methodology used to produce the specimens may be considered highly repeatable and to have incurred minimal natural variation into the material.

4.3.4.2 The directional impact of binder to aggregate ratio

The impact on the properties of bio-aggregate composites of the binder to aggregate ratio has been studied previously and thoroughly but an important part of undertaking the work in this study was to determine if the findings are globally applicable or if instead the

impact is directionally dependent, something previously not established and of great importance.

Considering first the two dimensional image analysis, Figure 4.32 and Table 4.8, it can be seen when comparing the medium 1.8, medium 2.2 and medium 2.6 materials that there is an apparent increase in the level of directionality with lowering binder contents. This can be most clearly seen in the values of $(f_0 - f_{90})$ where, if plotted against binder to aggregate ratio, a clear negative correlation is observed, Figure 4.34. From Figure 4.34 the relationship between binder to aggregate ratio and f_0 - f_{90} would appear to be reasonably described as linear although it must be acknowledged that the limited number of three data points means that it is not possible to say to what level the result may be extrapolated. Further tests outside the range of the binder to aggregate ratios considered here would be of benefit to refine this assessment.

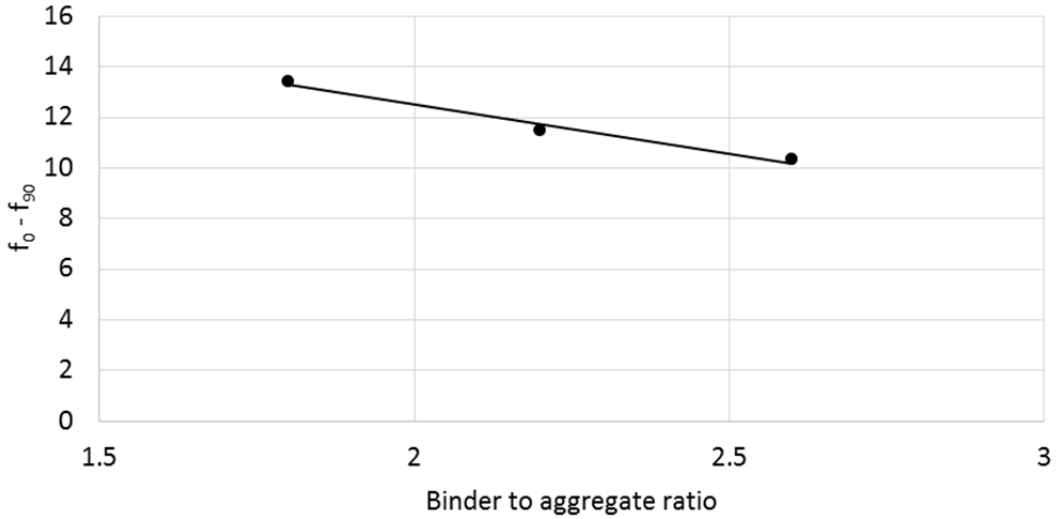

Figure 4.34: $(f_0 - f_{90})$ /binder to aggregate ratio plot based on two dimensional image analysis.

A possible reason for the apparent negative correlation of directionality to binder content is not immediately apparent but may be speculated upon. It is proposed that an increase in the amount of binder will have an associated decrease in the amount of aggregate per unit volume of the wet mixture. This is different from what has been speculated elsewhere where it has been assumed the amount of aggregate would stay constant with the binder simply occupying the natural voids between particles (Hirst, 2013). However, if an increased binder to aggregate ratio is presumed to lower the volumetric proportion of aggregates in an un-compacted mix, then there will be greater spacing of the particles. This would reduce direct particle connectivity and may lessen the rotation applied to particles in compaction. Irrespective of reasoning, this observation is significant as it

implies that the level of directionality within the internal structure is altered by this variable. It can also be speculated that a greater binder content may increase the overall viscosity of the mixture and again act as a mechanism to oppose particle rotation.

The binder to aggregate ratio from Figure 4.25, Figure 4.28, Figure 4.30 and Figure 4.31 can be seen to impact on the assessed properties of the material in both directions. In general terms the findings are in line with what was found in the literature review: an increase in mechanical strength and thermal conductivity with increased binder content. This may, as has been presumed previously by others, be attributed here to an increase in the proportion of one element altering the properties of the composite towards the properties of that constituent. In this instance the cured binder paste is known to have a higher mechanical strength than the composite material and higher thermal conductivity which might explain this assessment.

What is different to preceding work is the ability within this study to consider the degree of impact in each of the two directions of interest, parallel and perpendicular to casting compaction. Figure 4.35 plots the assessed physical properties against binder aggregate ratio in the parallel to compaction direction while Figure 4.36 plots the perpendicular direction and enables this comparison to be made.

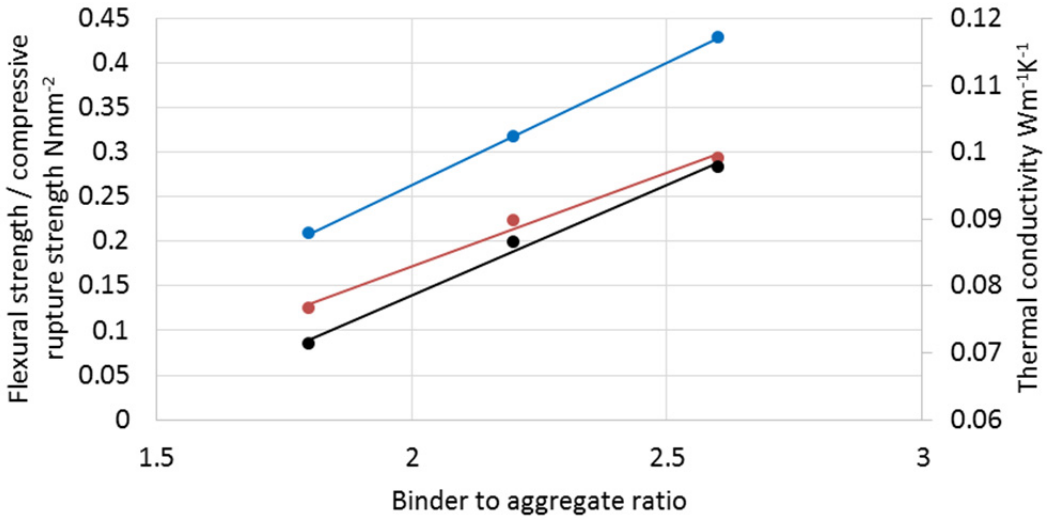

Figure 4.35: Flexural strength (red), compressive rupture strength (blue) and thermal conductivity (black) Vs binder to aggregate ratio from parallel loading of specimens.

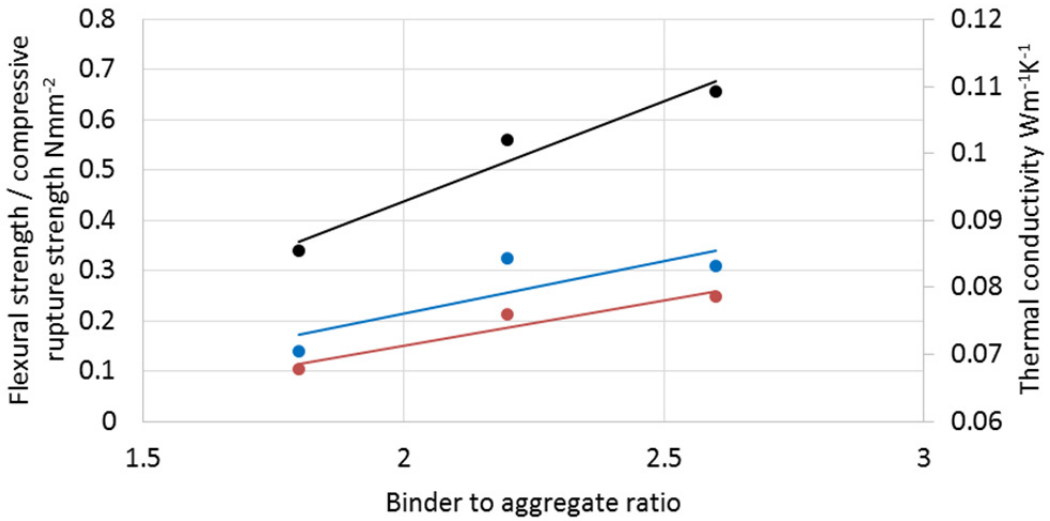

Figure 4.36: Flexural strength (red), compressive rupture strength (blue) and thermal conductivity (black) Vs binder to aggregate ratio from perpendicular loading of specimens.

From Figure 4.35 it can be seen that binder to aggregate ratio within the range discussed here may be considered to have a linear relationship to parallel flexural strength, compressive rupture strength and thermal conductivity that may be attributed to the reasons already laid out. Figure 4.36 indicates again a strong linear relationship between the binder to aggregate ratio and thermal conductivity in a perpendicular direction but less clear trends when it comes to the mechanical properties. In terms of thermal conductivity it is noticed that the thermal conductivity is consistently higher in the perpendicular to compaction direction but that the gradient of the plot in the parallel direction is also higher. This implies that the impact of binder to aggregate ratio on the thermal conductivity is greater in the parallel direction and directly supports the theory that this variable has a directionally dependent impact.

The consistently higher thermal conductivities in the perpendicular to compaction direction may be directly attributed to the internal structure of the material. It is shown in Figure 4.32 that all variations of material exhibit an isotropic internal structure whereby the particles tend towards planes that are horizontal to compaction force. Thermal loading in the direction of this compaction is therefore through these planes while perpendicular loading as is across them. Across the planes, the binder coated particle may offer more direct thermal paths, accounting for this observation.

The greater impact of the binder to aggregate ratio on the parallel loading is considered to likely stem from the increase in particle directionality with lowering binder contents. It is proposed that the observed correlation between binder to aggregate ratio and degree of orientation, $(f_0 - f_{90})$ in Figure 4.34, implies that, as the binder to aggregate ratio

increases, the material will move towards a more isotropic form; it may be theorised that an isotropic state of hemp-lime exists at a high enough binder to aggregate ratio where the particles are independent during compaction and thus may not orientate. It would therefore be logical to see a convergence of the parallel and perpendicular thermal conductivities with increasing binder content which is evidenced in the steeper gradient observed. It may be surmised that it is the impact this variable therefore has on the level of particle orientation that introduces a directional, as opposed to global, impact on thermal conductivity.

In terms of mechanical properties a slightly different result is found. Firstly it is noticeable that, using the definitions of flexural and compressive rupture strength adopted by this study, there is generally a smaller difference between the parallel and perpendicular to compaction compressive performance than might be expected based on the limited previous work and the striking visual differences in failure mode, Figure 4.29. This is considered to be a result of the difference between the compressive rupture strength and compressive strength either at a set strain or peak load reported in other studies. This was not the case in flexural tests where the similar results can be considered to be a result of the material conveying load in a broadly similar way in both orientations of loading. This is supported by the consistency of failure modes, Figure 4.26 and stress strain plots, Figure 4.24.

The difference in failure mode and form of the stress strain relationship between the two directions of compressive loading is in line with results presented elsewhere: a stiffer and more brittle behaviour in perpendicular loading (Youssef et al., 2015, Amziane et al., 2015). This may be attributed directly to the anisotropic arrangement of particles shown in Figure 4.32 where perpendicular loading can be considered across the planes of particles while parallel loading through them. Perpendicular loading may resultantly be considered to have considerably more particles with the major axis aligned in the loading direction acting as a stiffer load path. The failure of these particles is likely to therefore be a rotation out of this alignment as is evidenced in Figure 4.29. For parallel to compaction loading, through the planes of particles, loading is likely to be transferred across the less stiff secondary and tertiary axes of the particles and failure linked to a compression of the particles and horizontal displacement. Again this is supported by Figure 4.29, which indicates loading in this direction causes a bulging of the material. The stress strain plots can be considered to directly reflect this observed difference in behaviour, the alignment and rotational failure of particles in the perpendicular loading case leading to a greater stiffness and more brittle failure mode while the perpendicular loading case across particle planes producing a lower stiffness but gradual yielding failure.

While the impact of the binder to aggregate ratio presents a positive correlation to both flexural and compressive rupture strength in both directions, it is noticed that when lines of best fit are applied to the plots, Figure 4.35 and Figure 4.36, a steeper gradient and thus more significant impact is seemingly in the parallel loading condition in both cases. In this case a diverging behaviour with decreasing orientation is therefore observed, seemingly going against the previous assessment of thermal directional behaviour converging as the material becomes more isotropic as was seen in thermal conductivity.

The reason for the observed discrepancy is believed to be a more complex relationship between binder content and perpendicular flexural and compressive resistance than simply the composite tending towards the properties of the increasing constituent. From Figure 4.36 there is a suggestion that the capacity of the material in perpendicular loading begins to plateau at higher binder contents. This sways the linear trend lines that are fitted which might otherwise have exhibited a higher gradient and thus the expected convergence to the parallel behaviour. The assumed reason for this is the mechanical capacity in perpendicular loading being governed not by the volume of binder but rather the surface contact between aggregates and binder. If the major axis of the aggregate particle is assumed to be stiffer then when this is aligned to loading, as it is in perpendicular loading, the particles and binder are likely to act in composite action with the binder, the boundary determining the strength. Conversely in parallel loading where the less stiff particle axes are in line with loading, the stiffer binder skeleton may be the only constituent to convey the load and so performance will depend purely on the binder content. This implies a difference in basic mechanical behaviour in the two directions that could account for the observed plateauing in capacity.

4.3.4.3 The directional impact of aggregate grade

The impact of the particle size distribution on the material properties was found to be contradictory within previous studies. A key reason for undertaking this work was to provide additional insight to this aspect and uniquely assess if any impacts are again global or directional.

From Table 4.8 and Figure 4.32 it may be observed that, as with the ratio of binder to aggregate, the grade of aggregate used has an impact on the reported level of directionality within the material. When the mean particle length is plotted against the value of $(f_0 - f_{90})$, Figure 4.37, a clear trend can be seen although the same correlation is seen to aspect ratio which alters with length. It is considered more likely that it is the aspect ratio of the particles that accounts for the increase in anisotropy for the logical reason that

more elongated particles would be more susceptible to rotation during compaction; additional assessment is however required to verify this assessment.

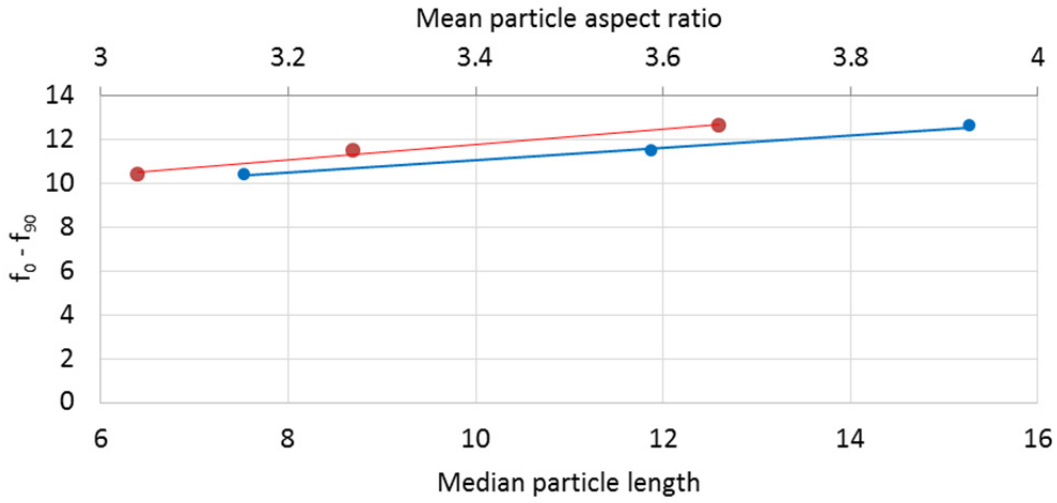

Figure 4.37: $(f_0 - f_{90})$ Vs median particle length (blue) and mean particle aspect ratio (red) based on two dimensional image analysis.

From Figure 4.25, Figure 4.28, Figure 4.30 and Figure 4.31 it is apparent that there is no correlation found between the particle median length /mean aspect ratio, and the thermal conductivity or mechanical resistance of the composite. This observation is consistent across both directions of loading in all cases and may broadly be seen to be in support of the contradictory set of preceding studies where both positive and negative correlations have been observed. In light of this it is suggested that while the length and aspect ratio of the particles used, and so in general terms the grade of particle used, have a measurable impact on the internal structure, which will have some associated impact on behaviour, other aspects of the particle size distribution must also contribute and indeed dominate.

In consideration of the particle size distribution data presented in Figure 4.3 and Table 4.1, and the results found in this study where the medium grades of aggregate seem to perform consistently differently to the fine and coarse grades, it is proposed that the spread of particle sizes is likely to have some bearing on the composite properties. The interquartile range as a percentage of the median for each grade of aggregates is plotted against thermal conductivity, compressive rupture strength and flexural strength in Figure 4.38 and Figure 4.39.

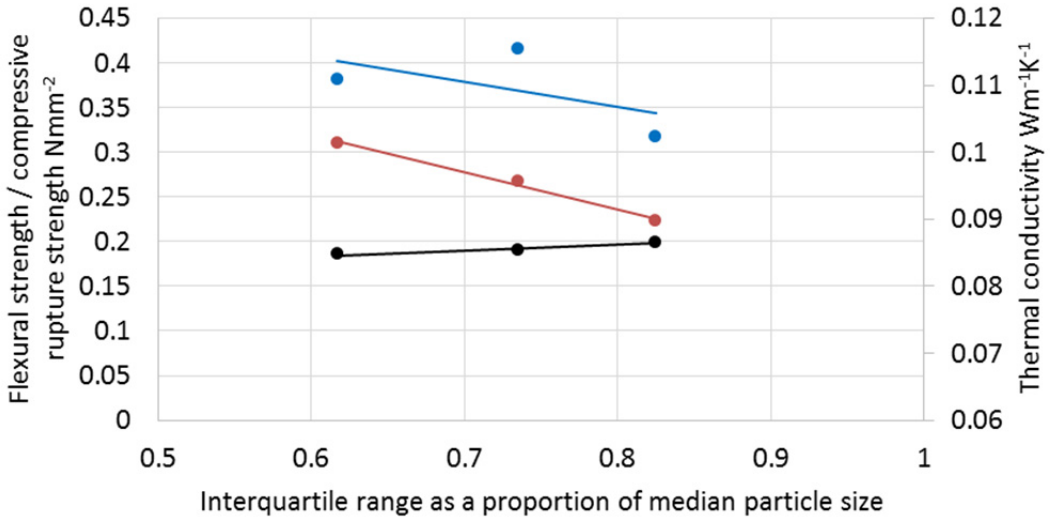

Figure 4.38: Flexural strength (red), compressive rupture strength (blue) and thermal conductivity (black) Vs proportional particle interquartile range from parallel loading of specimens.

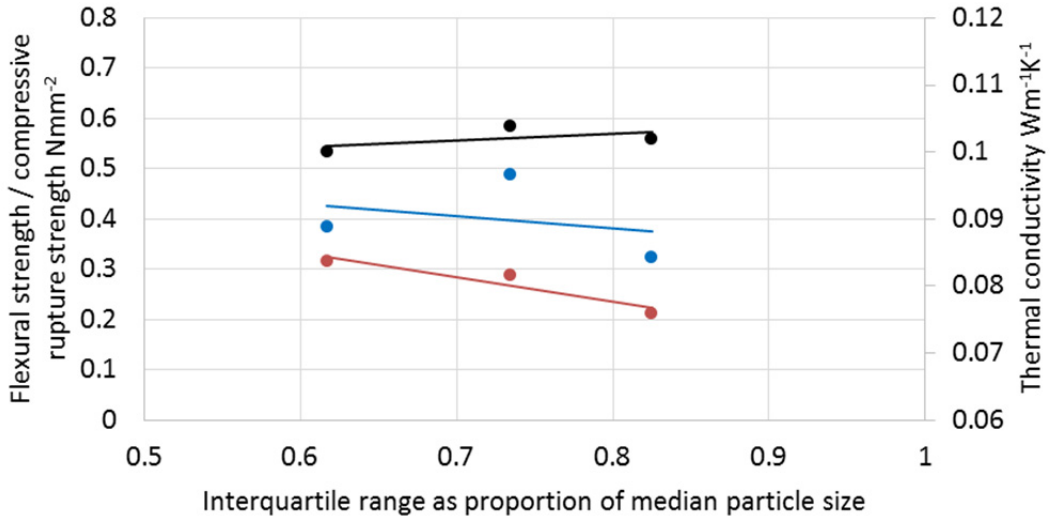

Figure 4.39: Flexural strength (red), compressive rupture strength (blue) and thermal conductivity (black) Vs proportional particle interquartile range from perpendicular loading of specimens.

From Figure 4.38 and Figure 4.39 it can be seen that there is some correlation between the spread of the particle size distribution of aggregates and the mechanical and thermal properties. The level of correlation seems to be better in both directions for the thermal conductivity and the flexural capacity but weaker for compressive rupture strength. As has been mentioned previously, the grade of aggregate and resulting length and aspect ratio of particles can be seen to impact upon the internal structure and will logically have an impact on the thermal and mechanical properties despite there being little direct evidence.

It is therefore logical in light of Figure 4.38 and Figure 4.39 to suggest that all these properties are impacted by the spread, size and aspect ratio of the particles in combination producing a complex relation between particle size distribution and physical properties.

A possible explanation for spread of particle distribution impacting thermal conductivity is a greater spread of particles creating a greater degree of particle tessellation and more continuous thermal paths through the material. What is therefore surprising is then the negative correlation to the mechanical properties where, by the same logic, a similar positive correlation would be assumed. A possible reasoning for this is that while the thermal paths through the material may be improved by a range of particle sizes, the loading paths through a material, which rely on direct contact, are not. A proposal that could be put forward is that a greater spread of particles may therefore produce a higher number of "floating" particles that do not contribute to the load path but may still contribute to the thermal paths.

It is clear currently from both the results here and those presented previously, and discussed in the literature review, that the impact of particle size distribution is complex and still not well understood. It is apparent that certain aspects of the particle size distribution do impact the orientation but that other aspects may influence the structure or have a direct impact on the properties in ways not yet realised. This topic therefore offers great potential for further work that may be of use to suppliers of the materials.

4.3.5 Conclusion

In this section the impacts of the two most easily altered constituent variables were assessed in terms of thermal conductivity, compressive strength and flexural strength. Unlike previous work, all tests were conducted in two directions to originally ascertain if the impacts were global or directionally dependent. To support this and aid interpretation of the results, a novel method for the assessment of the degree of orientation within the internal structure of the materials, developed for this project, was also implemented.

The results found that the behaviour of the bio-aggregate composite, hemp-lime, was anisotropic in terms of thermal conductivity, compressive rupture strength and flexural strength. Differing failure modes and differing responses to compressive loading were also observed in the two directions. This can be directly attributed to the observation of an anisotropic internal structure present in the material irrespective of constituents. This structure may be described by a tendency of the elongated particles to sway towards

planes perpendicular to compaction applied in casting and may be considered a result of both the elongated particles and the formation process used.

Both the ratio of binder to aggregates and the particle size distribution of the aggregates were observed to alter the degree of orientation found. The implications of this are that these variables should have a directionally dependent impact on properties rather than a global impact and indeed this was observed to be the case. It is speculated that the internal structure of the material is further influenced by the particle size distribution in ways that have not been assessed in this study.

The thermal conductivity was found to increase with increasing binder content at a higher rate in the parallel direction, attributed to an associated reduction in directionality. There is a suggestion that a similar trend may exist in the mechanical properties however an interesting plateau of strengths in perpendicular loading seems to occur between an aggregate to binder ratio of 1:2.2 and 1:2.6 meaning this could not be verified. This is considered a result of a more complex composite action in this direction of loading that is limited by aggregate-binder contact area rather than binder volume. The density of the material was also found to increase with increasing binder content as would be expected.

Both the mean particle length and particle aspect ratio were found to correlate to the degree of orientation with the latter considered to be the driving factor. Despite this, no correlation was observed between the aspect ratio and the physical properties within the range considered although a logical reasoning would suggest that at an aspect ratio of one, the parallel and perpendicular behaviours would converge. Some correlation was observed between the range of particle sizes and some physical properties although the explanation of this remains unclear; it is uncertain why seemingly contrasting positive and negative correlations were found for mechanical properties and thermal conductivity respectively. It is therefore proposed that a complex interaction of several aspects of the particle size distribution probably combine to determine the directional physical properties through both altering the degree of directionality as well as other aspect of the material structure. The density of the material was found to increase with smaller and less elongated particles as may be expected.

4.4 Experimental study into the directional impact of implementation

4.4.1 Introduction

This section details the experimental outline and results obtained from a study into the impact of implementation on the behaviour of bio-aggregate composites. As has been previously mentioned, the implementation variables considered within this study are the choice of projection forming or casting, the layer sizing, and level of compaction applied. The physical behaviours assessed were the flexural behaviour, compressive behaviour and thermal conductivity using the methods previously detailed in Chapter 4.2. In addition to this, results are also presented from two dimensional image analysis of the material in two directions using the method detailed in Chapter 3. A proportion of the results from this study have been previously presented as a journal paper entitled "The influence of the casting process on the internal structure and physical properties of hemp-lime" (Williams et al., 2016a) and as a conference paper entitled "Projection formed and precast hemp-lime: better by design" (Williams et al., 2017).

4.4.2 Experimental outline

4.4.2.1 Assessed variables

Two methods of implementation were considered: casting, and projection. Within the cast material, three variations of layer size and compaction were considered. In order to limit the total number of specimens produced, not every one of the nine possible permutation of the variable combinations within the cast material were assessed but rather each variable was considered independently with the specimens of median value being applicable to both. The full range of possible and undertaken permutations of material is displayed diagrammatically in Figure 4.40**.** As a result six variations of material were considered in this study. In total 40 specimens of cast hemp-lime were produced: 30 prismatic, 150mm X 150mm by 400mm, and 10 panel, 50mm X 400mm X 400mm. Two large specimens of projection formed material 800mm X 800mm X 200mm were also produced that were subsequently each sectioned into three prismatic and one panel specimens of the dimensions stated above.

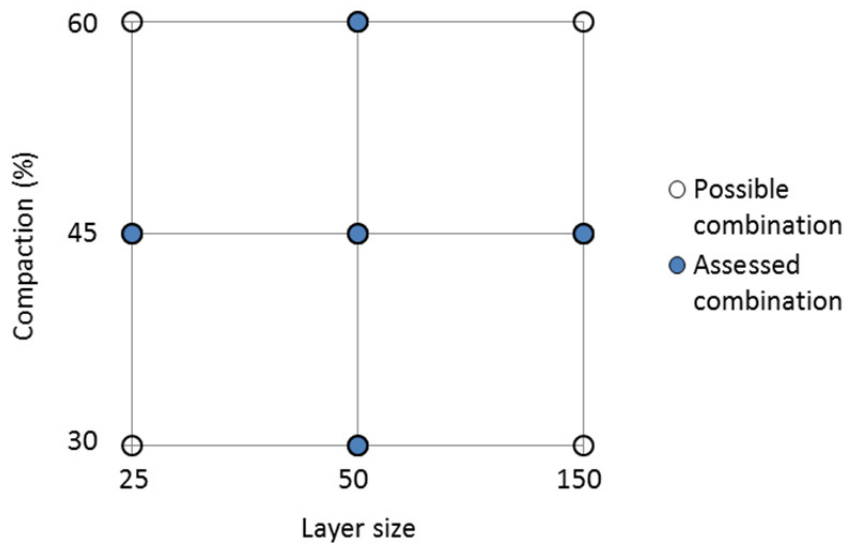

Figure 4.40: Diagrammatic view of the full range of implementation variations possible and the variations considered for cast material.

The selection of the values of layer thickness to be used was made based on the values found in various studies in the review of the literature as well as the layer thicknesses quoted as used in industry (Bevan et al., 2008, Stanwix and Sparrow, 2014). The layer sizes selected were also in part determined by the size of the specimen and the requirement to have a whole number of layers within each specimen wherever possible. Layer sizes of 25mm, 50mm and 150mm were used in this study with 25mm being typical of the smallest used in previous studies, 50mm typical of the most common layer size used in previous studies and 150mm being as close as possible to the standard industry applied layer sizes of around 200mm.

The range of compactions used in this study was 30%, 45% and 60% increase in density above a loose state material. This definition of compaction was used over a standardised compaction regime or static compaction pressure due to its improved repeatability in the former case and higher applicability to industry in the latter case. The un-compacted density of each mix of material was found using the standardised method already described in Chapter 4.3 repeated five times and averaged, the results of which are presented in Table 4.9. The values of compaction used were selected based on several factors. The highest level of compaction is reflective of the maximum compaction obtainable using manual tamping of the material and so is the effective limit of most current industry practice. The middle level of compaction was determined to be reflective of the level of compaction routinely used in industry based on the values presented in manufacturers' (Tradical®, 2015) and practitioners' (Stanwix and Sparrow, 2014) literature of wet density for similar materials. The lowest level of compaction was

determined by the minimum perceived level still sufficient to provide a material of sufficient strength to conduct the experimental program based on preliminary work and the study of Hirst (Hirst, 2013).

The six variations of material that were considered in this study are summarised in Table 4.9 (the nomenclature used to refer to the mixes being of the form: "formation method" "layer thickness" "compaction level" for cast material and projection formed material being referred to simply as "projected").

Table 4.9: Mixtures of hemp-lime used in the study of the directional impact of implementation.

Mixture Ref	Formation method	Layer thickness (mm)	Compaction level (% density increase)	Uncompact wet density (kgm^{-3})	Target wet density (kgm^{-3})
Cast 150 45	Cast	150	45	433	628
Cast 50 30	Cast	50	30	433	563
Cast 50 45	Cast	50	45	433	628
Cast 50 60	Cast	50	60	433	693
Cast 25 45	Cast	25	45	433	628
Projected	Projection	N/A	45 (targeted)	433 (targeted)	628 (targeted)

4.4.2.2 Controlled variables

All the cast specimens were produced using the basic methodology for cast material production detailed in chapter 4.2 and cured following the regime outlined within the same chapter relevant to the tests conducted. The projection formed specimens were all produced using the methodology detailed in Chapter 4.2 for projection forming. The constituent variables, binder content and bio-aggregate that were the focus of Chapter 4.3, were controlled within this study as far as possible.

The bio aggregate used in this study was the one referred to as medium, the characteristics of which are presented in Chapter 4.1. This was selected as it represents the median grade in terms of particle sizes and aspect ratio used in the preceding section and therefore ensures that the two sets of results are concurrent.

The binder to aggregate ratio used in this study was the median used in the preceding section: 2.2:1 by mass. The selection of this value, as with the bio-aggregates used, ensures the studies are consistent as a single data set but is also reflective of the most common

ratios currently proposed by industry and manufacturers for walling applications (Bevan et al., 2008, Stanwix and Sparrow, 2014, Tradical®, 2015). As the binder to aggregate ratio is constant within this study, the water to binder ratio and the water to aggregate ratio are also controlled. The percentage mass breakdown of constituents used throughout this study was 16% aggregate, 36% binder and 48% water obtained by the method presented in Chapter 4.2. As a result of using the same aggregate and binder ratio as one of the mixtures considered in the last study, there is an overlap between the "medium 2.2" mixture in the previously presented results and the "cast 50 45" mixture used here.

In order to compare the basic processes of projection forming and casting, specimens were produced to be as close as possible to the median cast material from both this and the preceding study; the mix design used being: the medium grade of hemp aggregate, a constituent ratio by mass of 16% aggregate, 36% binder and 48% water and a compaction level of 45%. This was achieved as far as possible using the procedures outlined in Chapter 4.2 and the success of this approach will be commented on in the results and discussion element of this section. It is not practical to control or define the layer size of sprayed material and so it is considered an intrinsic part of the process.

An additional variable that is inherent to the projection method adopted in the study is the location of the specimens sectioned out of the larger originals. The approach adopted in this instance was to remove the sections in the same locations from each specimen in the pattern given in Figure 4.41. The pattern chosen was selected to be reflective of the whole specimen as far as possible and to maintain a constant effective projection angle across the specimens and as close to 90° as possible.

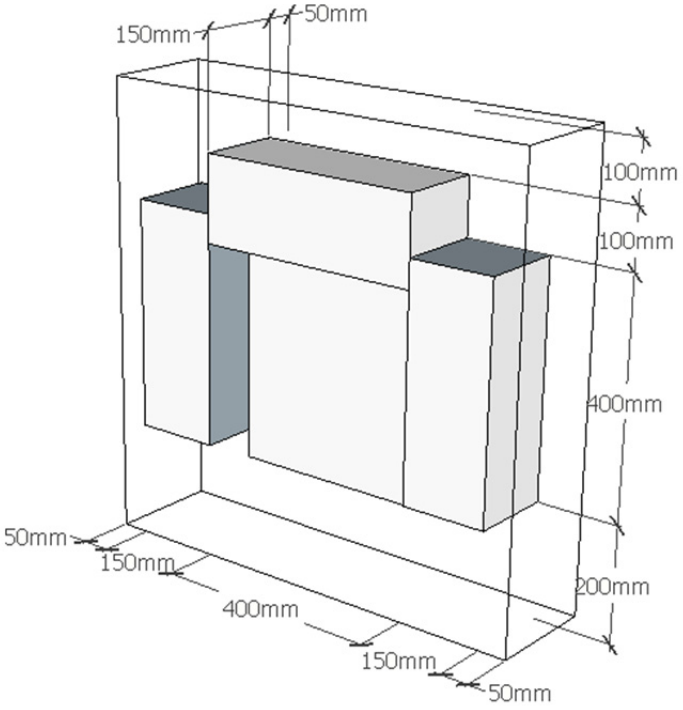

Figure 4.41: Diagram of specimen removal location within the larger projection formed specimens.

4.4.3 Results

4.4.3.1 Flexural behaviour

The measured physical dimensions and mass of each of the specimens are given in Table 4.10 as well as the calculated values of 28 day density; the moisture content determined subsequently to testing for each specimen is also given. In each case the mean value and uncertainty for each material variation are presented.

The stress / strain plots produced using the methodology in Chapter 4.2 for all specimens tested within this part of the study are presented in Figure 4.42. From the results presented in Figure 4.42, the failure stress in each specimen can be identified and the mean value and variance found - Figure 4.43.

Table 4.10: Physical parameters of the flexural specimens produced for the study of the directional impact of implementation.

Mixture Ref	Specimen length (mm)	Specimen width (mm)	Specimen depth (mm)	Specimen mass, 28 days (g)	Specimen density, 28 days (kgm^{-3})	Specimen moisture content (%)
Cast 150 45	397.7 ± 0.7	149.4 ± 0.7	149.1 ± 1.8	3718 ± 94	420 ± 12	18.0 ± 1.8
Cast 50 30	396.6 ± 1.3	147.4 ± 1.5	148.1 ± 1.3	3202 ± 70	370 ± 10	14.5 ± 4.8
Cast 50 45	398.2 ± 1.0	149.2 ± 2.7	149.3 ± 1.7	3640 ± 57	411 ± 12	16.6 ± 1.7
Cast 50 60	397.4 ± 1.7	149.3 ± 1.0	149.8 ± 1.7	4058 ± 81	456 ± 15	17.9 ± 1.9
Cast 25 45	397.5 ± 0.8	148.4 ± 1.3	149.6 ± 1.2	3635 ± 42	412 ± 5	16.2 ± 1.3
Projected	400.2 ± 1.8	149. ± 1.0	149.3 ± 0.9	4353 ± 197	488 ± 22	30.6 ± 1.6

Photograph sequences for the first tested specimen of each variation, used to help ascertain the failure mode and interpret the likely internal flow of forces within the material, are presented in the appendices. The image sequences for parallel and perpendicular loading for the median material tested, “cast 50 45”, are presented in Figure 4.26 and the equivalent of the projection formed material is presented in Figure 4.44.

Table 4.10 shows that, as with the specimens presented in the previous section considering constituents, the dimensional consistency of the specimens is generally very good. The small dimensional variations observed can be mainly attributed to slight variations in the moulds and are of negligible scale; the seeming tendency for slight under sizing of specimens may be attributed to a slight material shrinkage during drying. The density of the three mixtures made with the same compaction and differing layer sizes show a very consistent density as should be expected; the slightly higher density of the Cast 150 45 mix is considered to be a result of a slightly higher moisture content at 28 days attributed to variations of curing conditions at differing times and locations within the room. The three mixtures with differing compaction levels show the same variation in density between the levels as was designed and exhibit mostly similar moisture contents. The projection formed material is observed to have a higher 28 day density than any other of the materials. This can be attributed in part to the significantly higher moisture content

considered to be a result of the difference in curing regime as opposed to the method of production. This however is unlikely to be the sole reason, with the dry density of the projection formed material calculated at 375 kgm^{-3}, significantly higher than the targeted equivalent "cast 50 45" material at 354 $kgmm^{-3}$.

From Figure 4.42 it is apparent that the same general difference between parallel and perpendicular to casting compaction can be noted as was observed in the study of constituents: broadly a similar parallel and perpendicular plot forms indicative of a sudden and moderately brittle failure of the material at similar stress in both orientations. In most cases a slightly steeper initial ramp of the plot in perpendicular loading is also observed. The three plots representing changes in layer sizes (top left, middle left and bottom left of fig 4.42) in general can be considered mostly similar in terms of form, indicating similar apparent material stiffness, failure mode, and peak strength. The three plots representing changes in compaction (top right, middle left and middle right of fig 4.42) indicate a very clear trend of increasing flexural strength with compaction in both orientations as well as increasing stiffness. The projection formed material is seen from Figure 4.42 to have a considerably more sporadic behaviour: in two perpendicular cases a standard clear failure peak around 5% strain is observed, comparable to that of cast material, but in all other tests the material is seen to have a prolonged curve with an apparent slow degradation of stiffness.

Figure 4.43 shows that there is no apparent difference in flexural strength between parallel and perpendicular loading irrespective of implementation. The layer size can be seen to have no impact between values of 150mm and 50mm however it is noticed that a layer size of 25mm provides an increase in both directions outside of the natural variance. Figure 4.43 also shows a strong trend between both parallel and perpendicular flexural strength and compaction as was anticipated. Despite the much higher values of strain at which peak loads were recorded, the projection formed material is observed to have comparable flexural strength to the median cast material but with a higher variation, it also seems to exhibit the greatest difference between parallel and perpendicular behaviour although this is within the natural variation observed.

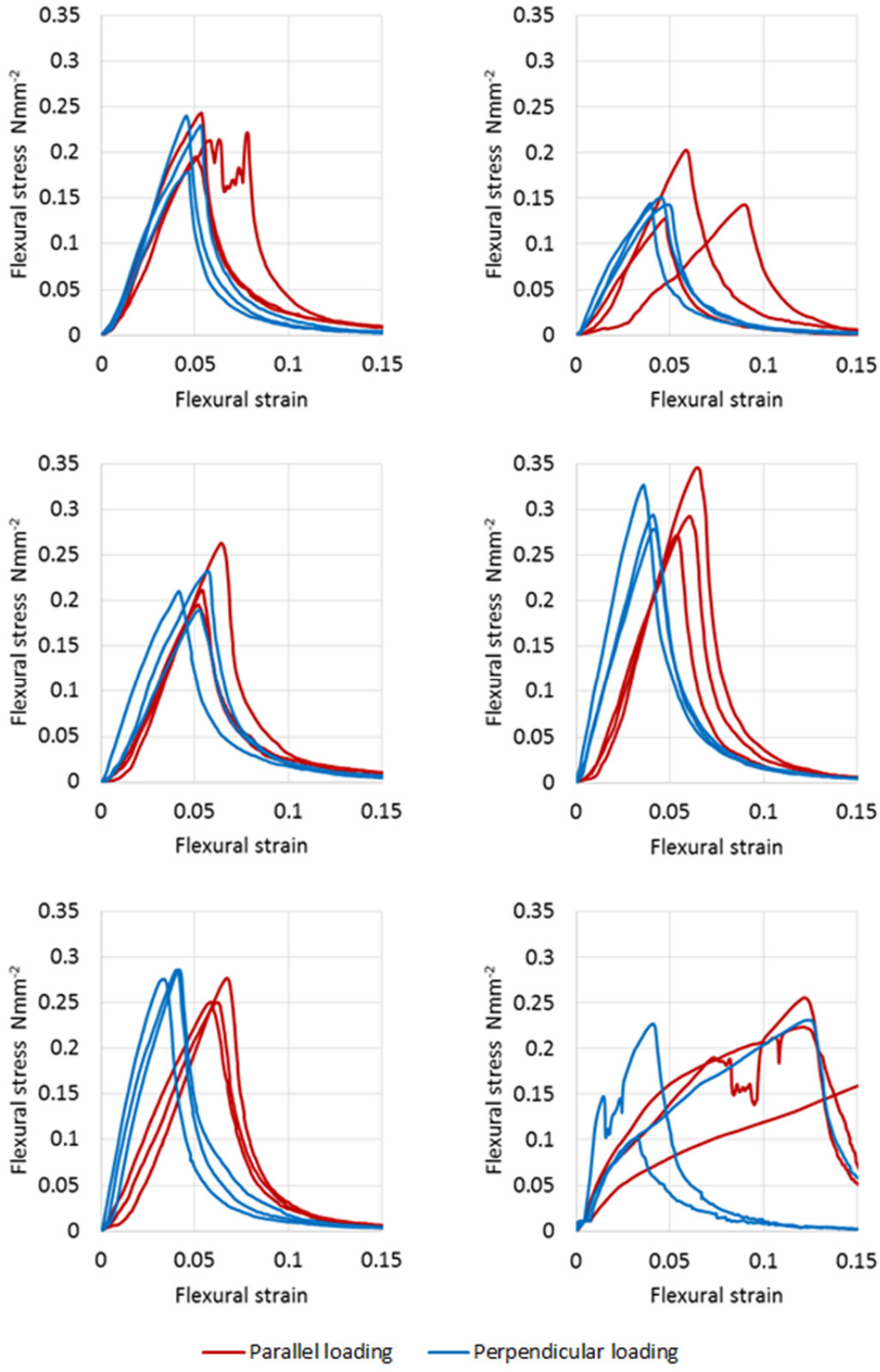

Figure 4.42: The flexural stress/strain plots for cast 150 45 (top left,) cast 50 30 (top right), cast 50 45 (middle leftt), cast 50 60 (middle right), cast 25 45 (bottom left), and projected (bottom right) mixtures.

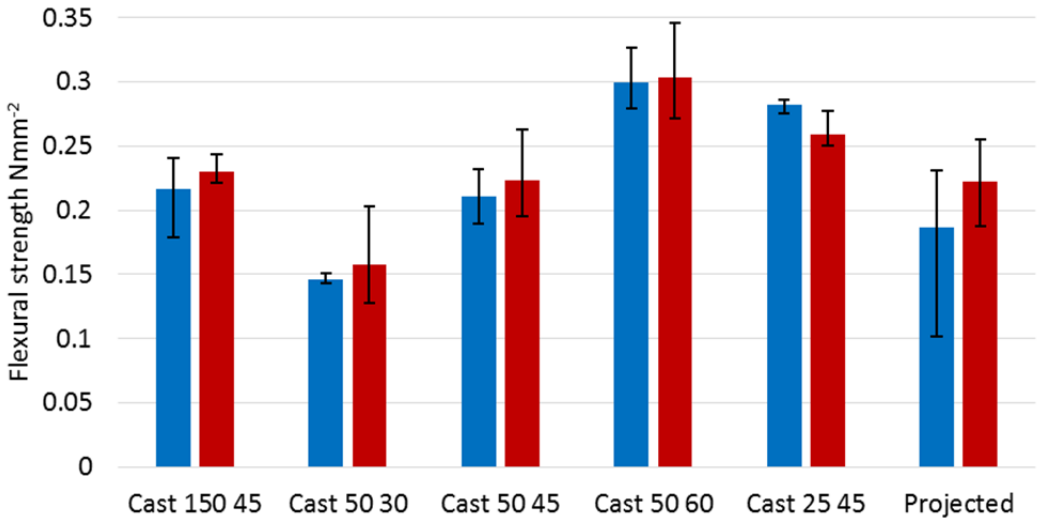

Figure 4.43: The flexural strength of parallel loaded (red) and perpendicular loaded (blue) hemp-lime of differing constituents.

The image sequence Figure 4.44 for projection formed material, in comparison to the image sequence presented in Figure 4.26 for the "cast 50 45" mixture, indicates two clear differences between the material. Firstly it is noted that there is a degree of localised compression at supports and under the loading pin in the projection formed material that was not observed in any cast material and is a likely contributor to the delayed failure of the material at often higher strains. Secondly it is also seen in the perpendicular loading sequence that the line of failure does not originate from the centre of the material and propagate vertically, but rather originates near the support and propagates at around 45°. This specific form of failure was not observed in any of the cast material considered but was seen in four out of six projection formed specimens.

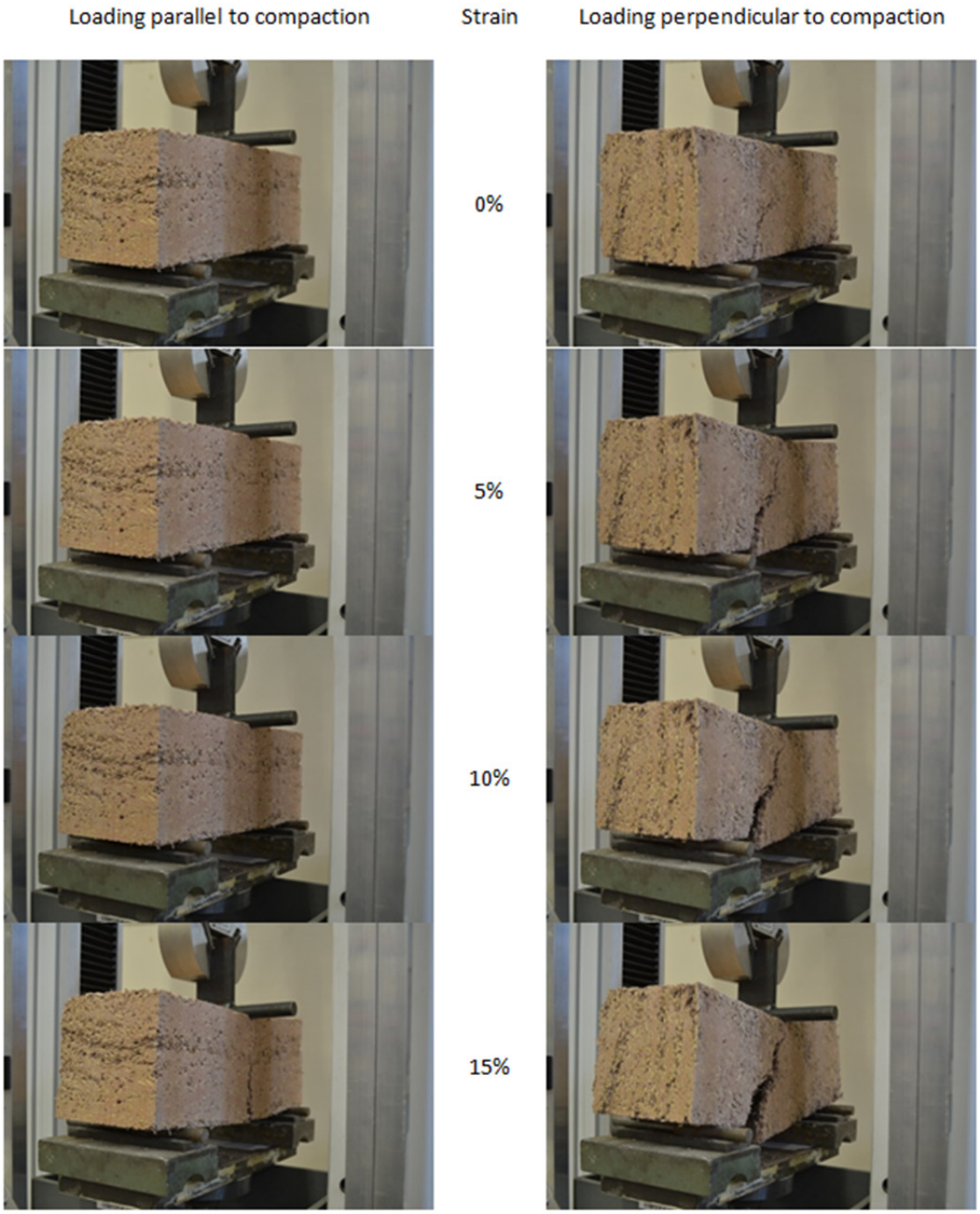

Figure 4.44: Loading image sequenced for projected mixture hemp-lime in flexure.

4.4.3.2 Compressive behaviour

The measured physical dimensions and mass of each of the specimens are given in

Table 4.11 as well as the values of 28 day density; the moisture content determined subsequently to testing for each specimen is also given. In each case the mean value and uncertainty for each material variation are presented.

The stress / strain plots for all specimens tested within this part of the study produced using the methodology in Chapter 4.2 are presented in Figure 4.45. From the results presented in Figure 4.45, using the method detailed within Chapter 4.2, the compressive rupture stress in each specimen can be found and the mean value and uncertainty calculated, Figure 4.46.

Table 4.11: Physical parameters of the compressive specimens produced for the study of the directional impact of implementation.

Mixture Ref	Specimen height (mm)	Specimen width (mm)	Specimen depth (mm)	Specimen mass, 28 days (g)	Specimen density, 28 days (kgm^{-3})	Specimen moisture content (%)
Cast 150 45	149.9 ± 1.2	149.5 ± 0.8	149.1 ± 1.7	1388 ± 22	416 ± 11	18.0 ± 1.8
Cast 50 30	148.6 ± 2.0	148.2 ± 2.2	148.3 ± 2.3	1190 ± 52	364 ± 19	14.5 ± 4.8
Cast 50 45	149.4 ± 1.0	150.0 ± 0.5	150.0 ± 1.7	1363 ± 49	405 ± 14	16.6 ± 1.7
Cast 50 60	149.3 ± 1.0	149.2 ± 1.2	149.8 ± 1.5	1521 ± 58	456 ± 19	17.9 ± 1.9
Cast 25 45	149.8 ± 0.7	148.7 ± 2.2	148.8 ± 1.7	1354 ± 40	409 ± 10	16.2 ± 1.3
Projected	149.6 ± 1.0	149.3 ± 0.9	150.1 ± 1.4	1644 ± 30	490 ± 10	30.6 ± 1.6

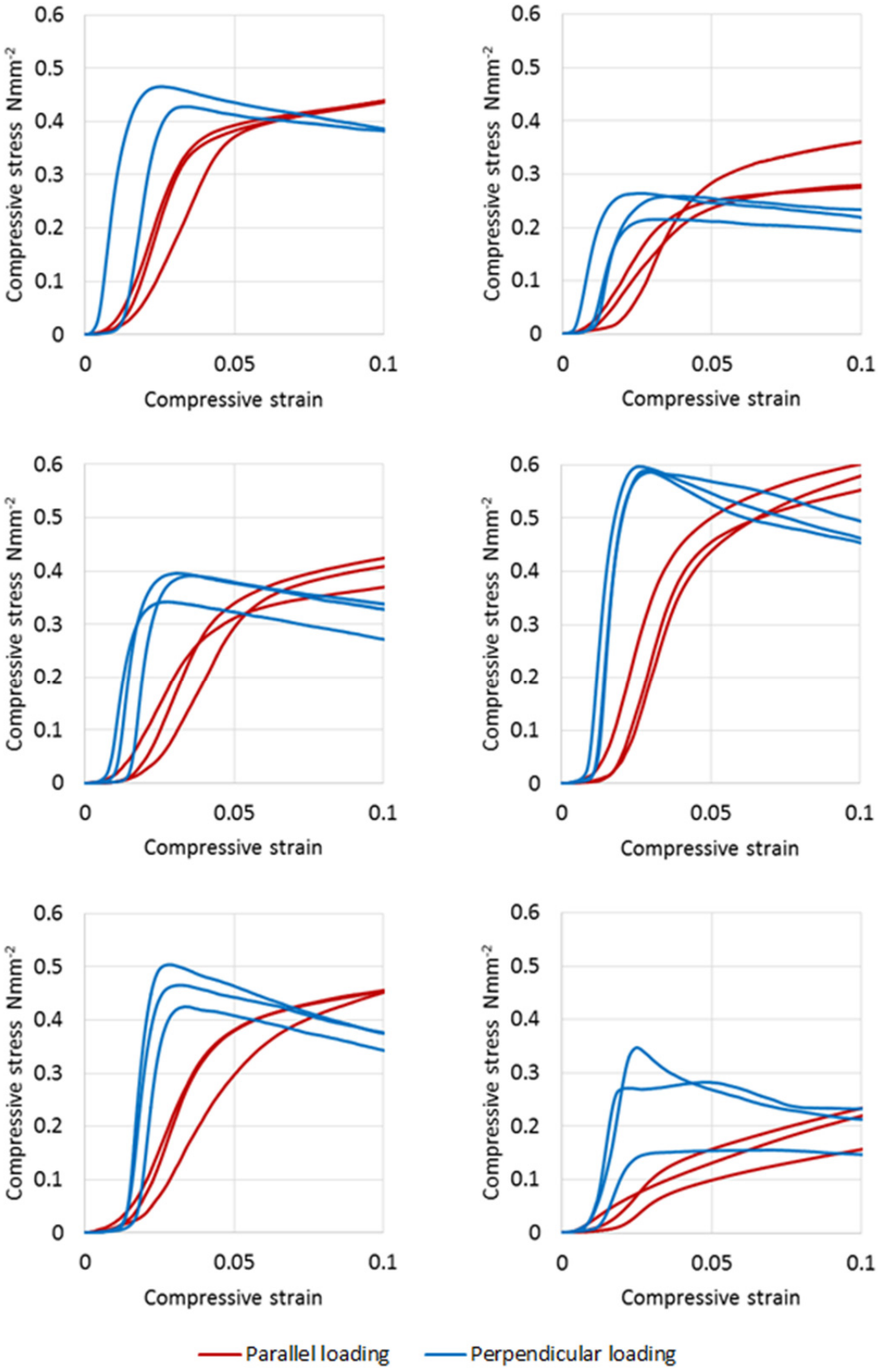

Figure 4.45: The compressive stress/strain plots for cast 150 45 (top left,) cast 50 30 (top right), cast 50 45 (middle lefttt), cast 50 60 (middle right), cast 25 45 (bottom left), and projected (bottom right) mixtures.

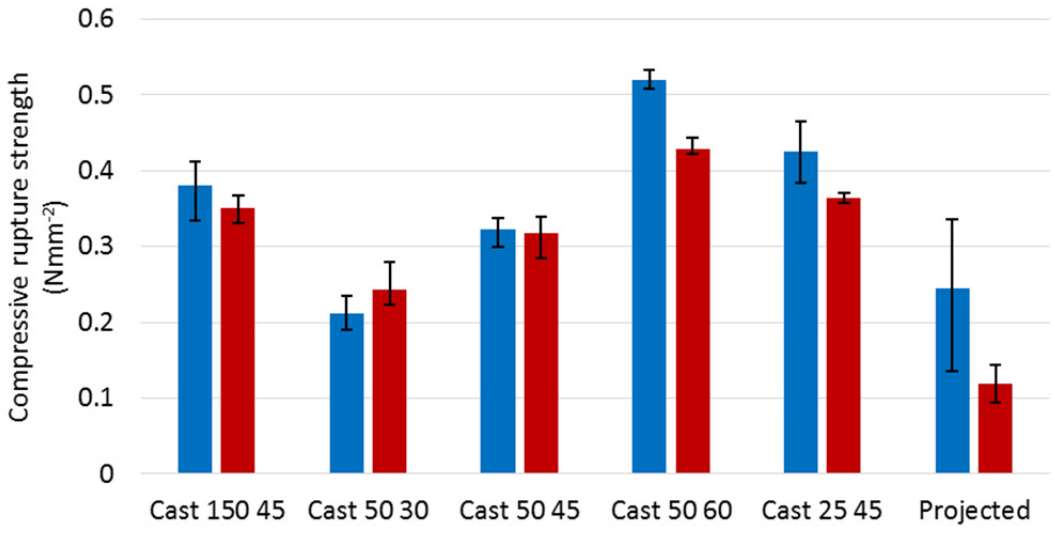

Figure 4.46: The compressive rupture strength of parallel loaded (red) and perpendicular loaded (blue) hemp-lime of differing implementation.

Photograph sequences for the first tested specimen of each variation, used to help ascertain the failure mode and to interpret the likely internal flow of forces within the material, are presented in the appendices. The image sequences for parallel and perpendicular loading for the median material tested, "cast 50 45", are presented in Figure 4.26 of the previous section and the equivalent of the projection formed material is presented in Figure 4.47.

From Table 4.11 a similar picture is observed to that in Table 4.10 as would be expected. Again the main aspects of note are the good dimensional and density consistency of the cast material and the higher than expected density of the projected material.

The results presented in Figure 4.45 reinforce the results of the compressive tests reported in Chapter 4.3 with regards to the difference in behaviour under parallel and perpendicular loading. It may be suggested therefore that these differences occur irrespective of both the constituent and implementation variables of hemp-lime. For altering layer sizes (top left, middle left and bottom left of Figure 4.45) it can be seen that this aspect has a negligible impact on the behaviour of the material under compression whereas it is equally clear that the compaction (top right, middle left and middle right of Figure 4.45) has a significant impact. The impact of increasing compaction from 30% to 60% is observed to produce an increase in both the apparent stiffness of the material and rupture capacity in both loading orientations. The projection formed material, bottom right of Figure 4.45, is found to show greater variation in behaviour than the cast material in compression as was also found in flexure. In parallel loading of the projection formed

material, the change from pre-rupture to post-rupture clearly seen in cast material is much more subtle with one specimen exhibiting a near linear low stiffness behaviour throughout loading.

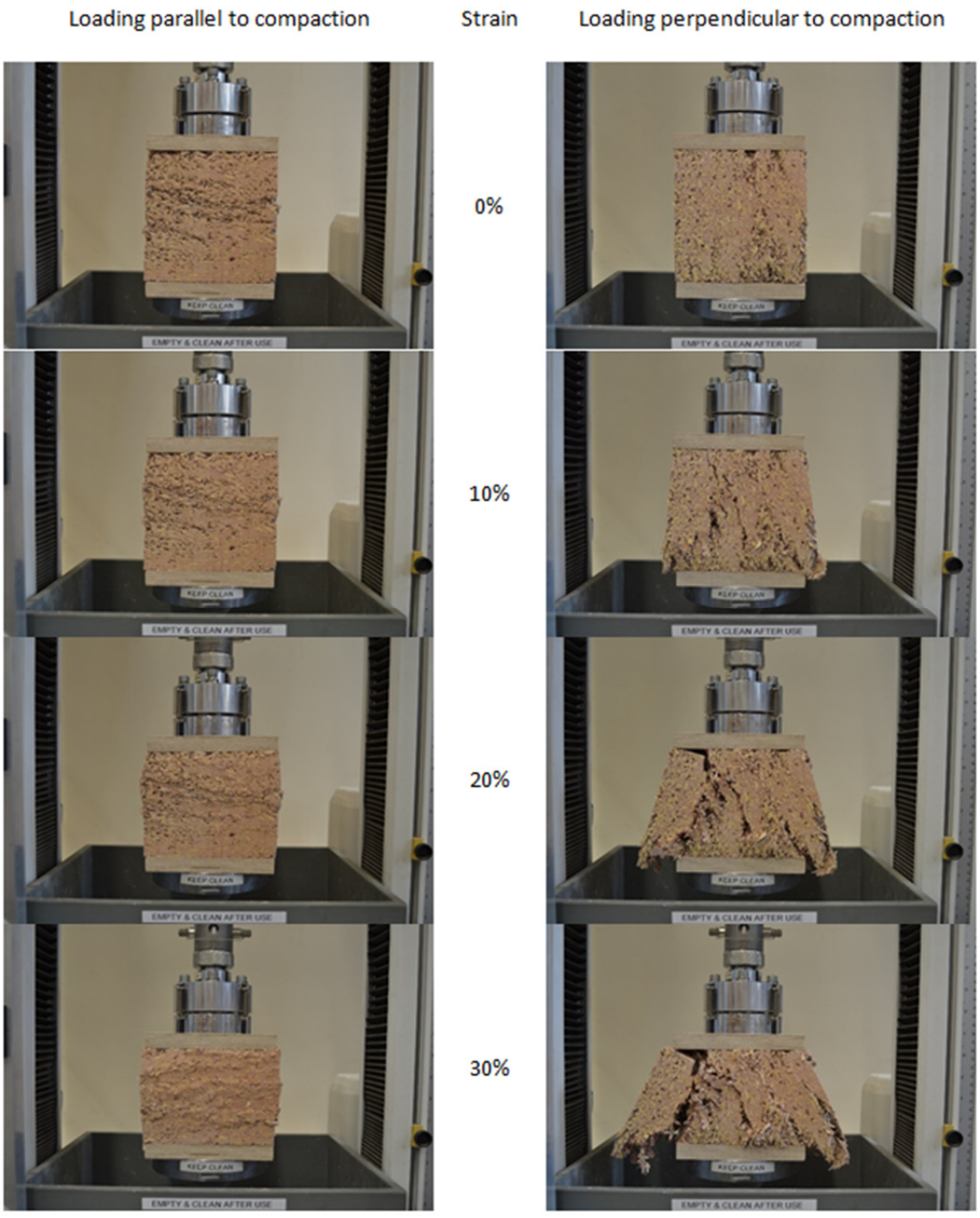

Figure 4.47: Loading image sequenced for projected mixture hemp-lime in compresison.

Figure 4.46 presents the results of compressive rupture stress as defined in Chapter 4.2. The results confirm the apparent lack of correlation between layer size and compressive rupture strength suggested by Figure 4.45 and the strong correlation to compaction. It is

further apparent that the compaction influences the perpendicular behaviour more so than the parallel behaviour with a significantly higher increase observed in perpendicular compressive rupture stress when compaction increases from 45% to 60%. The compressive rupture stress of the projection formed material is seen to vary considerably and is generally low compared to the cast materials in this study. The projection formed material is also seen to have the largest difference between parallel and perpendicular behaviour.

The image sequence, Figure 4.47, for projection formed material, in comparison to the image sequence presented in Figure 4.29 for the ”cast 50 45” mixture, shows certain similarities in the way the cast and projection formed materials behave in compression. In both cases the material exhibits the same distinct mechanisms of failure in the two loading directions typified by a densification of material in parallel loading and sideway bursting of material in perpendicular loading. These two behaviours were something seen across all materials studied irrespective of implementation. The main differences between the cast and projection formed materials seem to occur in the parallel loading scenario where less horizontal linear displacement is noted in the projection formed material and rather localised “ripples” appear on the surface. It is considered that this may imply that the projection formed material is not failing uniformly but rather in specific layers within the material.

4.4.3.3 Thermal conductivity

The measured physical dimensions, stable density and dry density of each of the specimens are given in Table 4.12; the stable moisture content is also given. Both the dry thermal conductivity and stable thermal conductivity for each material variation are presented in Figure 4.48 and Figure 4.49 respectively. In all cases, stable refers to the specimen being of stable mass for a period of 24 hours within a 20°C and 50% relative humidity environment as was defined in Chapter 4.2.

From Table 4.12 it is observed, as has been previously noted for the flexural and compressive specimens, that the dry and stable density follows what would be expected from the wet densities. It may also be seen that compared to the 28 day densities for the similar flexural and compressive specimens, the stable density is consistently lower indicating stability has not been reached at 28 days; the lower moisture contents in this stable state tally with this observation. In general the stable moisture content is found to be relatively consistent across all materials.

Table 4.12: Physical parameters of the thermal specimens produced for the study of the directional impact of implementation.

Mixture Ref	Specimen length (mm)	Specimen width (mm)	Specimen thickness (mm)	Specimen density, dry (kgm^{-3})	Specimen density, stable (kgm^{-3})	Specimen stable moisture content (%)
Cast 150 45	399.5 ±1.1	398.4 ±0.4	49.3 ±0.6	345 ± 0	381 ± 0	9.6 ± 0.0
Cast 50 30	399.3 ±1.8	399.7 ±1.5	50.1 ±0.5	311 ± 3	330 ± 4	5.9 ± 0.0
Cast 50 45	400.4 ±2.2	398.0 ±1.2	50.1 ±0.5	345 ± 2	366 ± 1	5.9 ± 0.2
Cast 50 60	399.9 ±1.4	398.6 ±1.7	50.1 ±1.0	374 ± 2	397 ± 2	6.1 ± 0.1
Cast 25 45	400.3 ±1.1	398.2 ±1.1	49.3 ±0.9	345 ± 2	367 ±2	6.4 ± 0.1
Projected	398.7 ±0.7	398.5 ±1.0	50.9 ±0.2	355 ±1	389 ±1	9.5 ±0.1

Figure 4.48 and Figure 4.49 present the dry and stable thermal conductivity of the hemp-lime specimens. As has been previously noted the main difference between the two plots is a global decrease in thermal conductivity after drying associated with removal of moisture. It is also seen that the parallel to casting compaction thermal conductivity is consistently lower as has been previously seen although this difference varies with the differing implementation variables. The layer size seems to have no discernible impact on the results although, due to the specimen thickness being smaller than the layer thickness, the parallel cast 150 45 mixture was not tested and so the data set is not complete. Compaction, when increased, is seen to produce an increasing thermal conductivity in both directions with an apparently greater influence in the perpendicular direction. The projection formed material is found to have both the lowest dry parallel thermal conductivity as well as the biggest difference between the parallel and perpendicular results.

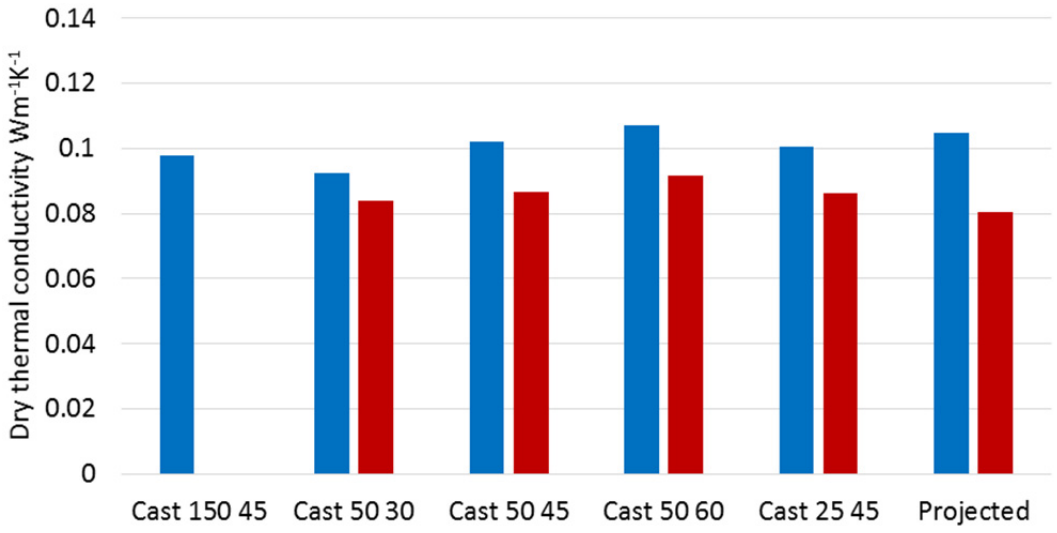

Figure 4.48: The dry thermal conductivity of parallel loaded (red) and perpendicular loaded (blue) hemp-lime of differing implementation.

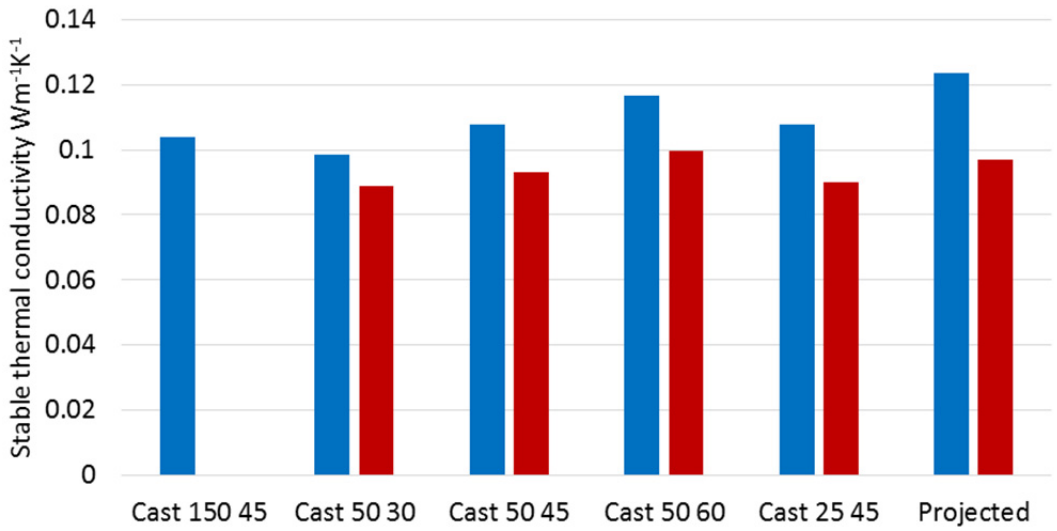

Figure 4.49: The stable thermal conductivity of parallel loaded (red) and perpendicular loaded (blue) hemp-lime of differing implementation.

4.4.3.4 Two dimensional image analysis

Figure 4.50 presents the frequency distribution of particle orientation for each of the variations of material. In each case the distributions are presented from the two dimensional images taken parallel to the direction of compaction and images taken perpendicular to the direction of compaction. Each distribution represents the total population of particles observed from six cross sections taken from each of the three specimens; totalling 18 images. All the images were produced, processed and analysed using the methodology developed in the pilot study and outlined in Chapter 3. In all plots a

fitted Hankinson form equation is also shown where the equation has been fitted via a least squares fitting approach.

The derived parameters of the fitted Hankinson equation: f_0, f_{90} and n, for each of the material variations in the perpendicular viewing direction are presented in Table 4.13 in order to provide additional information about the distributions in this direction. Alongside this, the calculated value of $(f_0 - f_{90})$ and the sum of the least squares values that were determined in fitting are also given.

Table 4.13: Summary of particle orientation frequency distributions from hemp-lime of differing production methods.

Mixture Ref	f_0	f_{90}	n	f_0 - f_{90}	Sum of least squares
Cast 150 45	17.26	6.90	2.08	10.35	0.476
Cast 50 30	16.81	7.08	2.08	9.73	0.503
Cast 50 45	17.98	6.50	2.13	11.48	0.121
Cast 50 60	17.64	7.21	1.93	10.42	0.570
Cast 25 45	17.91	6.81	2.03	11.09	0.103
Projected	19.20	5.50	2.36	13.70	0.595

From Figure 4.50 a swayed distribution, when imaging in a perpendicular direction, is observed across all material indicating the tending of particles into planes that are perpendicular to the compacting force occurs irrespective of implementation. When imaging parallel to compaction, the distribution is observed to be flatter with slight increases towards 0° and 90° that may be associated with particle alignment to the edges of the moulds. The projection formed material exhibits a very strong anisotropy when imaged perpendicular to compaction but also exhibits a sway in the parallel direction of lesser but significant magnitude. This observation is believed to be as a result of the angle of assumed compaction not being 90° but rather varying as the lance is directed at differing parts of the mould. If the production of these specimens is considered to reflect normal industry practice then projection forming may be considered to have a more varied compaction direction than casting with an associated increased variability of the material's structural alignment.

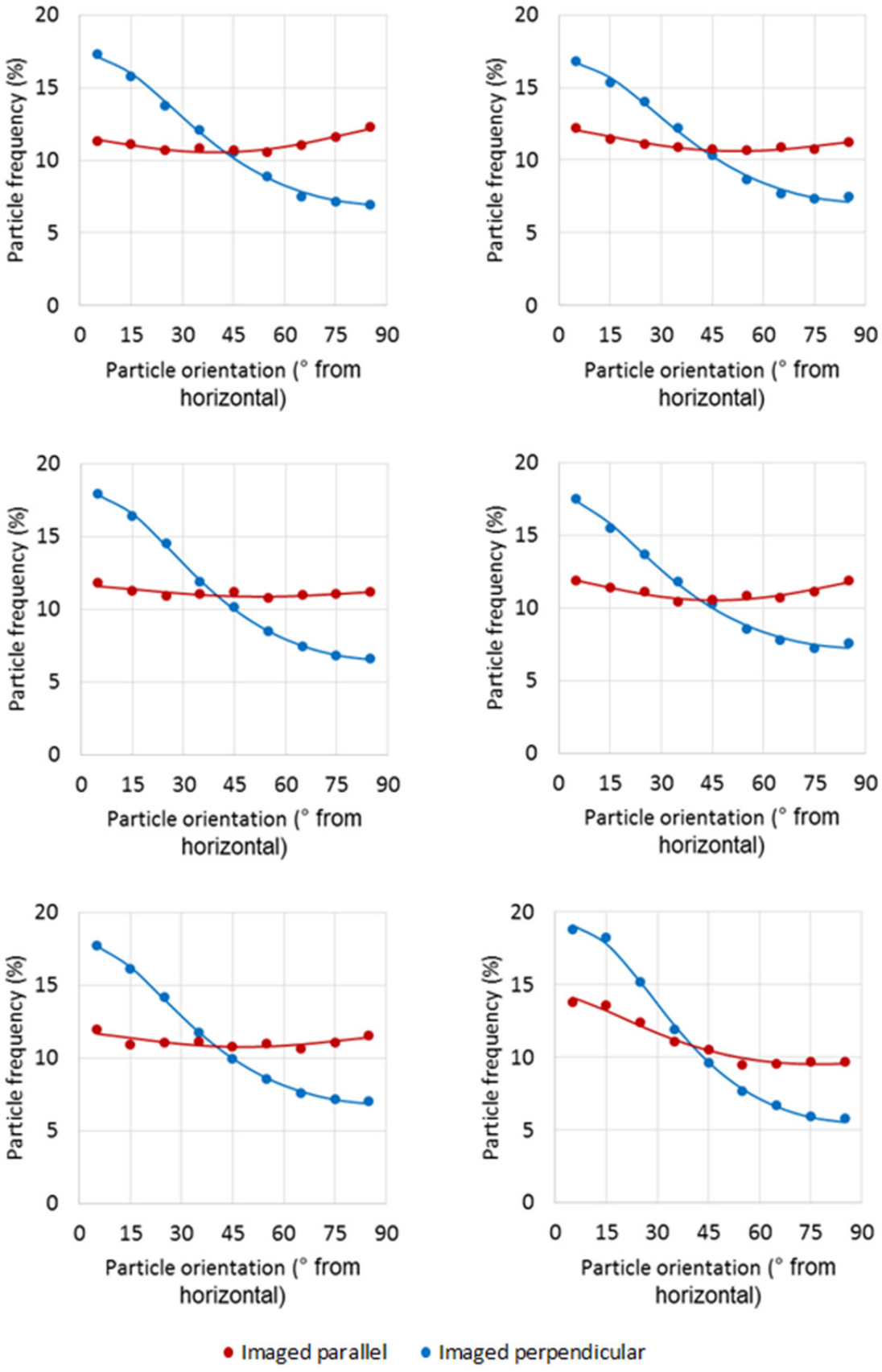

Figure 4.50: The particle orientation frequency distrubution for cast 150 45 (top left,) cast 50 30 (top right), cast 50 45 (middle lefft), cast 50 60 (middle right), cast 25 45 (bottom left), and projected (bottom right) mixtures.

Comparing the perpendicular plots of the differing implementations it is observed that projection forming produces the greatest value of $(f_0 - f_{90})$ and thus the highest level of orientation. It is also observed that the value of n in this case is different to the cast material indicating a differing plot shape, believed to be a result of the varied angle of projection mentioned previously. For cast material, the form of the graphs is moderately consistent and the Hankinson's equation form in all cases gives a good fit to the data, Table 4.13. There is no obvious correlation between layer sizing and $(f_0 - f_{90})$ indicating this variable has limited or no impact on the degree of orientation within the range considered. For material of differing compaction a very significant increase in $(f_0 - f_{90})$ was found from 30% to 45% however this was not seen to continue to 60% where the value falls. This result is believed to be an anomaly produced as a result of the method used and will be addressed fully in the discussion.

4.4.4 Discussion

4.4.4.1 Density profiles

Using the data from the compressive and thermal specimens, the density and moisture content of the differing material variations considered within this part study may be plotted against one another, Figure 4.51.

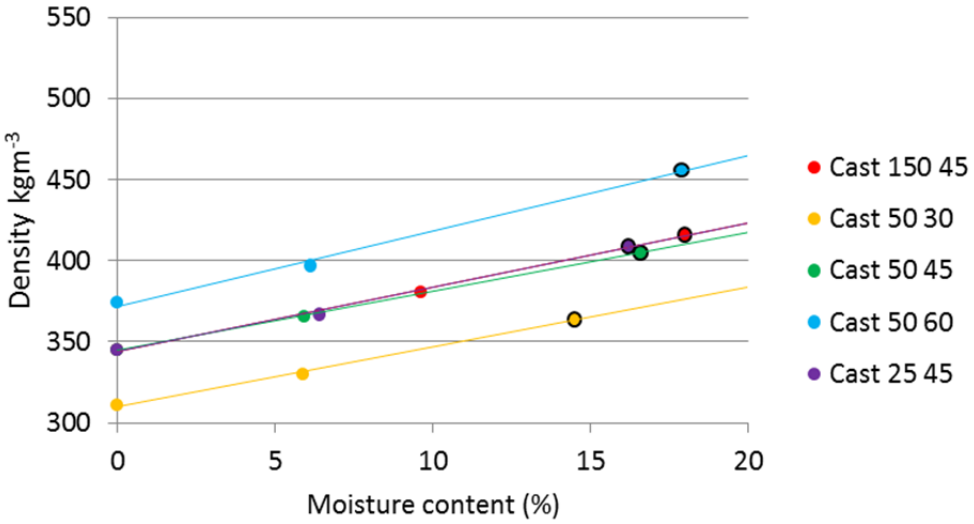

Figure 4.51: The moisture content/density plots for thermal and mechanical (black ringed) specimens of hemp-lime of differing implementations.

From Figure 4.51 the standard trend of density increasing with moisture content is seen in all mixtures. The density profiles have a strong linear fit indicating a high degree of

consistency between the thermal and prismatic specimens was achieved in this stage of work. Layer size, which should not have affected density, is indeed seen to have very minimal impact, again suggesting good consistency between batches of specimens produced. The compaction is observed to have the expected uniform increase of density between the three compaction levels. Furthermore this increase is in line with that set out in the experimental design and so again may be considered to have been applied correctly in the production of the specimens.

From

Table 4.11 and Table 4.12 it can be identified that the density of the projection formed specimens is quite high compared to what was targeted, Table 4.9. In the mechanical specimens this high density is partially a result of moisture content although it is also apparent that this is not the only factor. The high density may be attributed to either one or both of two aspects that were difficult to control in the process: the compaction applied and the ratio of binder to hemp. In order to ascertain to what extent each of these aspects were attributable, the images used for the image analysis of particle orientation were also used to estimate the actual volumetric binder to aggregate ratio. This was simply achieved through selecting a threshold to identify each of these constituents and then measuring the proportions of the image respectively. From this the estimated ratio of constituents by mass and apparent level of compaction applied may be retrospectively found, Table 4.14.

Table 4.14: The retrospectively calculated mixture characteristics of the projection formed material based on image analysis.

Mixture Ref	Estimated binder to aggregate ratio	Estimated compaction level (%)	Estimated uncompact wet density (kgm^{-3})	Estimated compacted wet density (kgm^{-3})
Projected	2.4	56	453	707

It can be seen from Table 4.14 that the projection formed material is estimated to have both a higher binder to aggregate ratio than was targeted and higher compaction. This is to the extent that it is closer in this aspect to the most compact cast material, ”cast 50 60” mix, than the median cast material targeted. Both the compaction and the binder to aggregate ratio, assessed in Chapter 4.3, were found to positively correlate to the mechanical properties and thermal conductivity. To fairly assess the impact of the projection process on these properties therefore it is prudent to consider the results compared to the “cast 50 60” mix and the “medium 2.6” mix from the previous chapter as

well as the “cast 50 45” mix that the projection formed material was designed to compare to.

4.4.4.2 The directional impact of compaction

The impact of compaction on both the physical and thermal characteristics of hemp-lime and other bio-aggregate composites has been studied extensively as was discovered in the literature review and has been identified as an area of high interest due to the extent of performance gains demonstrated. Despite this, a directionally sensitive study has not previously been undertaken and so is of specific value to the field.

A logical assumption about increasing compaction would be an increasing tendency of the particles to orientate. This follows from the understanding that the compaction in the production is what drives the elongated particle to rotate towards perpendicular planes and has been qualitatively observed elsewhere (Nguyen et al., 2010). The directly measured results from this study at first seem to call into question this proposal, Figure 4.52. The trend presented in Figure 4.52 appears to be only slightly positive and with a comparably low degree of fit to a linear relation compared to the very strong correlations presented by binder to aggregate ratio, Figure 4.34 and Figure 4.37. This is ill fitting with the logical argument presented for a strong positive correlation and therefore it is considered likely this result is unrepresentative.

The value of $(f_0 - f_{90})$ for the 60% compacted material, identified in Figure 4.52, is considered the likely reason for the discrepancy between the expected result and the observed result. It is believed that this lower than expected value may have occurred as a result of a limitation within the methodology applied. As the particles are compacted, it follows that the separation between adjoining particles decreases and thus a higher proportion are likely to be connected. Despite the efforts made within the method to segregate particles, it is considered likely that at this higher level of compaction the number of particle groups touching and misidentified as a single particle will be higher. If this misidentification is significant this will have a damping impact on the results and may be assumed to have occurred in this case. This explanation is justified by the lower number of particles identified in the analysis of the 60% compacted material, 33839, than in the 45% compacted material, 35475, despite compaction logically increasing the number of particles per unit volume. The value of $(f_0 - f_{90})$ found from the 60% compacted material is therefore considered to be an anomaly and if ignored, then a more positive correlation between the compaction and $(f_0 - f_{90})$ is found, Figure 4.52, considered to be more representative of the reality.

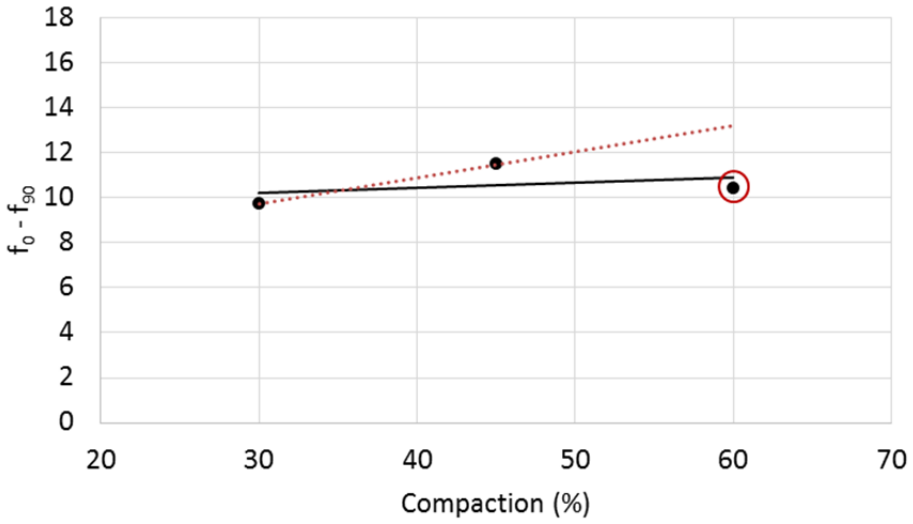

Figure 4.52: $(f_0 - f_{90})$ Vs compaction based on two dimensional image analysis. Solid line of best fit applied to full data set, dashed line of best fit applied to the data set without the believed anomalous point, ringed.

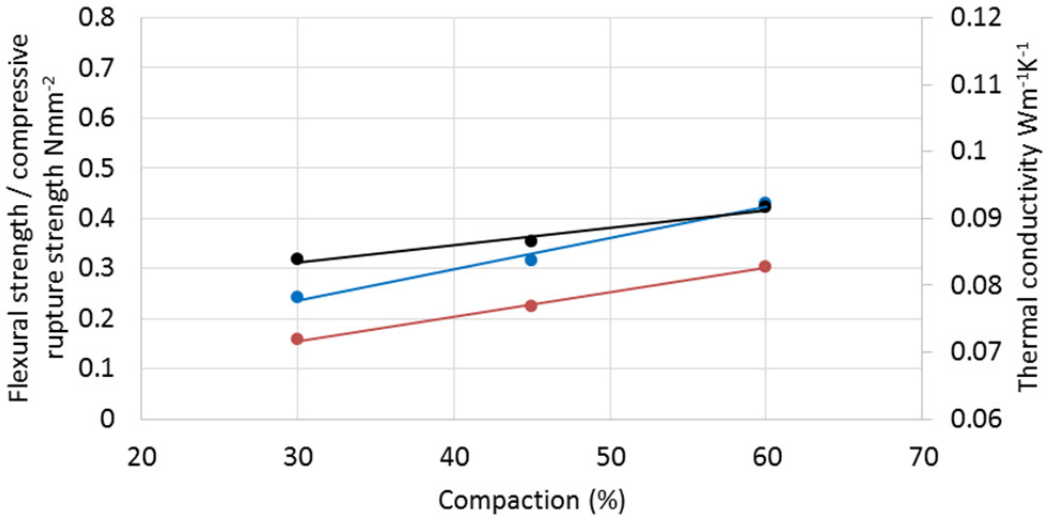

Figure 4.53: Flexural strength (red), compressive rupture strength (blue) and thermal conductivity (black) Vs compaction from parallel loading of specimens.

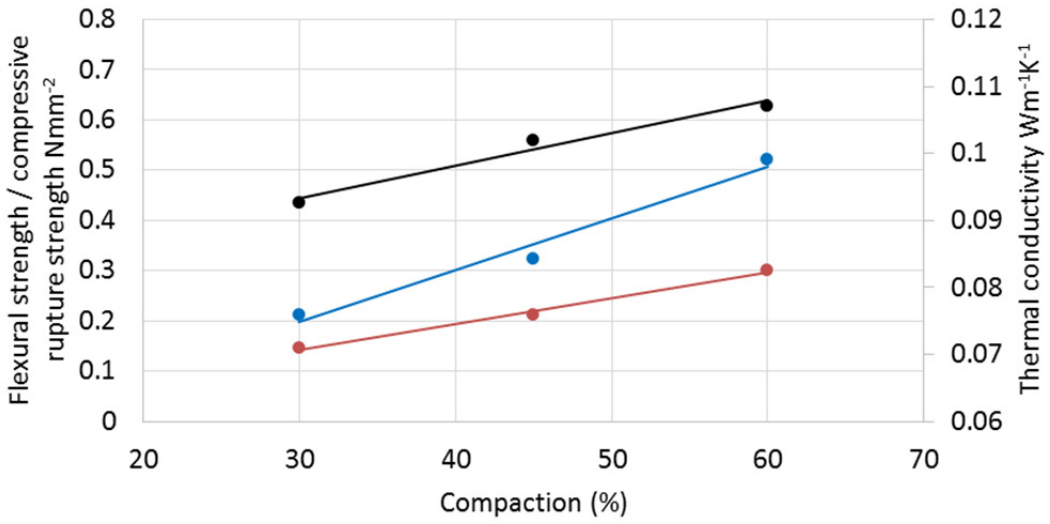

Figure 4.54: Flexural strength (red), compressive rupture strength (blue) and thermal conductivity (black) Vs compaction from perpendicular loading of specimens.

The impact of compaction on the thermal conductivity, compressive rupture strength and flexural strength parallel and perpendicular to compaction can be seen in Figure 4.53 and Figure 4.54 respectively.

In both directions the thermal conductivity is seen to have a strong positive correlation with compaction that follows logically from decreasing material porosity. The perpendicular thermal conductivity is found to be higher than the parallel thermal conductivity and also more sensitive to compaction. This may be attributed to an increasing level of orientation with compaction, widening the discrepancy in behaviour and further supporting the previously made statements regarding Figure 4.52 and an outlying value. It may be speculated from the results that a theoretical intercept of parallel and perpendicular thermal conductivity exists at a point of negative compaction symbolic of a state where material arranges in an isotropic random structure not physically realisable due to self-weight.

Compaction is observed to have a near uniform impact on the flexural strength as has been seen in variations of constituents. The increase in flexural strength with compaction may be attributed to the increase of load carrying structure per unit volume with increasing compaction. A seemingly global as opposed to directionally dependent impact of compaction, as well as all assessed variables within this project, suggests that flexural strength is less sensitive to the direction of testing.

The compressive rupture strength is observed to not only vary considerably with compaction but also to be directionally sensitive to this variable: the perpendicular resistance is observed to increase considerably more with compaction that the parallel

resistance. At least part of this is expected to come from the associated increase in orientation with increasing compaction; the opposite higher sensitivity of parallel loading was noted for increasing binder to aggregate ratio where an inverse relation was seen to $(f_0 - f_{90})$ making this result concurrent in this respect. It can also be seen from Figure 4.53 and Figure 4.54 that an intercept of the parallel and perpendicular compressive rupture stress exists within the compaction range studied at around 40% compaction. Despite this moment of isotropic loading capacity, the material is known to not be isotropic in structure at this stage. This point therefore indicates a moment where the two differing loading structures have similar capacity but not form.

4.4.4.3 The directional impact of layer size

The impact of layer sizes has not been previously studied but through interpretation of some preceding literature it was hypothesised that smaller layer sizes may produce a more even compaction state across the material. This was anticipated to have a possibly beneficial impact on the mechanical properties although there was no specific pre-existing data to corroborate this.

There was no apparent correlation observable between the degree of orientation, $(f_0 - f_{90})$, and the layer size used, Table 4.13. This is in keeping with the hypothesis that layer sizes may alter distribution of density as opposed to global density; the consistent overall density thus preserving the orientation distribution of the material. A confirmation of this may be provided by a regional assessment of directionality in future work.

In consideration of the mechanical and thermal properties it can be seen from Figure 4.54 and Figure 4.55 that there is a subtle suggestion that both the parallel and perpendicular compressive rupture strength and flexural strength decrease with increasing layer size as hypothesised. The trend however, if there at all, may be considered very slight and within the natural variation of material. Consequently it may be stated that within the range of 25mm to 150mm, the layer size has no bearing on mechanical properties. Similarly with the thermal conductivity any trends observed are very slight and may be considered a result of natural variance in the limited number of data points collected. Layer size within this range may therefore also be considered to have negligible impact on the thermal conductivity of hemp-lime. Both these results tally with the assessment of the internal structure that found no significant topographical difference in the material's physical distribution. While further studies would be required to extend this observation into some larger layer sizes, it may be concluded that material produced with layer sizes in the range of 150mm to 25mm can be considered as equivalent.

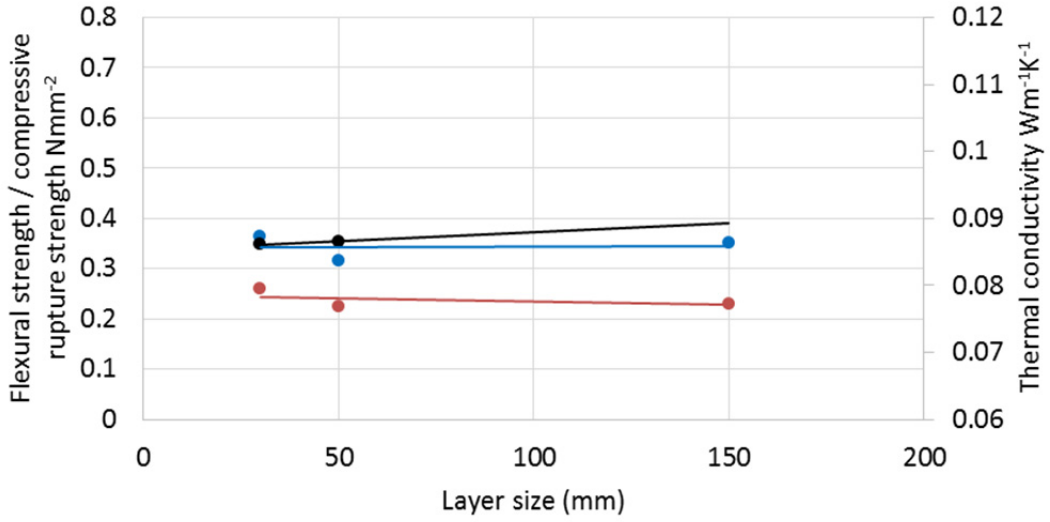

Figure 4.55: Flexural strength, compressive rupture strength and thermal conductivity Vs layer size from parallel loading of specimens.

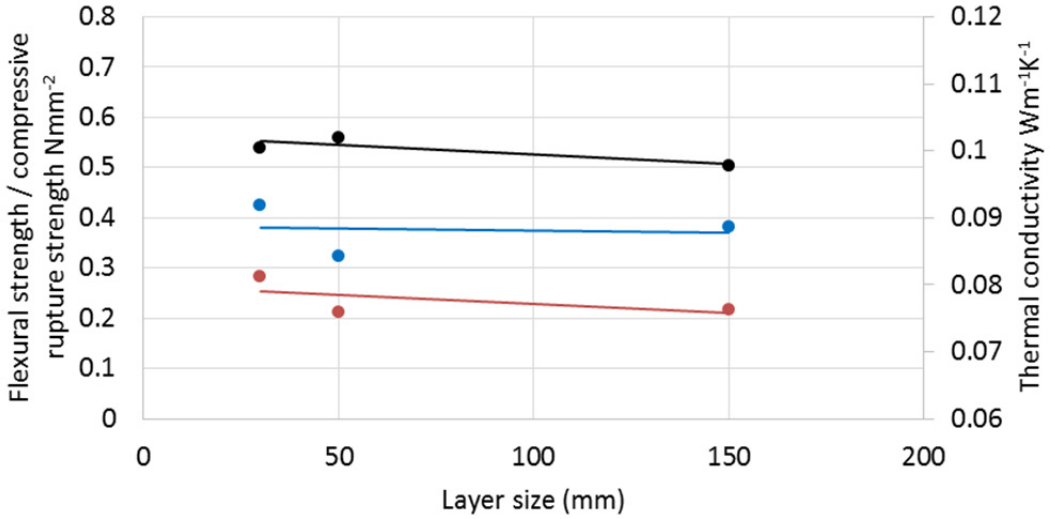

Figure 4.56: Flexural strength, compressive rupture strength and thermal conductivity Vs layer size from perpendicular loading of specimens.

4.4.4.4 The directional impact of production method

The projection formed material was found to have the highest value of $(f_0 - f_{90})$ when imaged in the perpendicular to compaction direction. This is indicative of the process inherently producing higher degrees of orientation as a result of the way material is built up. It is not certain what aspect of the method may provide this although it may be theorised that projection forming builds up material almost particle by particle producing this extreme orientation. The equivalent in cast material would be to individually place particles, reducing the layer size to its lowest effective value. As there was no observed

trend between particle orientation and layer size noted within the range considered here, further study into very small layer sizes could be of interest to future development. It was also observed for projection formed material that parallel imaging also shows a sway in particle orientation. This is attributed to the projection angle being not true to 90° and varying slightly during production, providing a more varied structure to the material.

The high level of orientation observed in the projection formed material is unquestionably the reason for the high level of contrast between parallel and perpendicular thermal conductivity in the material. It has generally been seen through all cast material that the parallel and perpendicular thermal conductivity diverge with increasing $(f_0 - f_{90})$ and so it is logical that this process should produce the largest difference. Similarly to the thermal conductivity, some of the largest discrepancies between parallel and perpendicular mechanical parameters were also seen in the projection formed material and are similarly attributed.

A generally higher level of variance was seen in the mechanical results from similar projection specimens. This may in part be a result of the differing locations the specimens were taken from the original larger specimen, Figure 4.41, and the aforementioned variation in projection direction producing localised variations in the material's preferential plane. It is also however suggestive of a higher degree of variation within material distribution creating areas of localised weakness. This idea is supported by visual inspections of the specimens where there is a noticeable inconsistency in the form of banding, Figure 4.57.

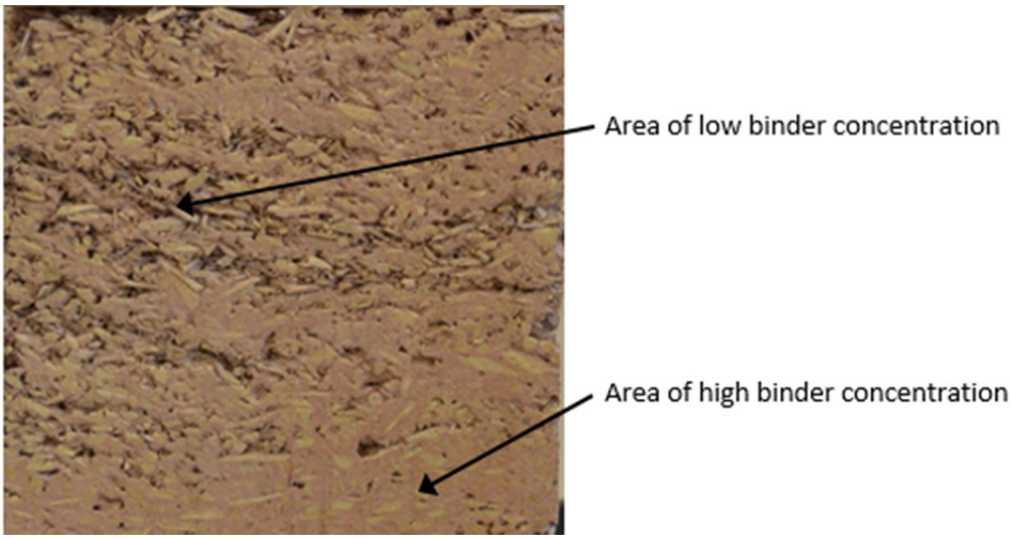

Figure 4.57: The areas of low and high binder concentration observed in the projection formed mixture.

The apparent inconsistency of the material distribution and "banding" pattern, Figure 4.57, is believed to be a result of the specific machinery and process used to produce the specimens for this project. The process employed used an auger fed air stream to convey the bio-aggregate to the lance. It was noticed during production that this produced an intermittent delivery of the aggregates while the binder slurry was provided continuously. This may cause the banding that is visually noticeable, being areas of lesser and greater binder concentration. In turn such areas of lower binder concentration could lead to the localised weaknesses in the material believed to produce the more sporadic and generally low mechanical performance than may be expected based on the estimated binder to aggregate ratio and compaction for the material as a whole, Table 4.14. In other studies it has not been identified that projection formed material may exhibit this and indeed it is often quoted as having comparable mechanical performance to cast material although it is known that several differing designs of projection forming machine are available and would possibly account for this.

In the flexural test it was observed that the projection formed material had a tendency to fail in a unique way that was not observed in any cast material and is suggestive of shearing failure. It is not clear why this is the case but it is theorised that this is a result of the variation in projection angle and the preferred plane of the material: a projection angle significantly lower than 90° could provide preferential planes close to the shearing planes observed. It is evident that the process of projection forming has a significant and wide ranging bearing on the internal structure of the material that seems to be less controlled than for cast material and that this may prove to be an issue in ensuring the quality control needed for market confidence.

4.4.5 Conclusion

In this part of the study the impact of the two production processes, casting and projection forming, as well as several casting implementation variables, was assessed on the thermal conductivity, compressive strength and flexural strength of hemp-lime. Unlike previous work, all tests were conducted in two directions to ascertain if the impacts were global or directionally dependent. To support this and aid interpretation of the results, a novel method for the assessment of the degree of orientation within the internal structure of the materials, developed for this project, was also implemented.

The results indicate that the anisotropy in internal structure and resultant material behaviour noted in the preceding section are present regardless of both the implementation method and the casting variables of layer sizes and compaction. It is

considered that the same mechanism by which particles tend towards a perpendicular alignment to imposed compacting force during production acts in both cases.

The degree of orientation in projection formed material was found to be higher than that of cast material and is believed to be a direct result of the process rather than other factors; a higher anisotropy in thermal conductivity was consequently noticed. It was also observed that the alignment of the particle planes is more variable using this method on account of an altering direction of compaction inherent to not projecting at a constant 90° angle to the substrate. The homogeneity of projection formed materials seen in this study was considered low with variations in the local distribution of binder observed in the material. This, along with the varying compaction direction, was attributed to the more varied mechanical performance which was lower than would be expected for similarly compacted material of similar binder to aggregate ratio as well as alternative failure modes from cast material. Both the compaction and binder to aggregate ratio of the specimens produced were higher than planned, indicating the difficulty of specifying material within this process.

The layer sizes used in casting material were generally seen to have very little or no impact on either the internal structure or the physical properties within the range considered, however it is believed that this should not be extrapolated outside of this range reliably. Within the context of industry, it has been established that casting in layers of up to 150mm in thickness will produce material that is representative of the majority of data in the literature.

Compaction was observed to positively correlate to both the mechanical strength and thermal conductivity of hemp-lime in both orientations considered. In this respect the result is both in line with previous findings and with what a logical assessment would predict. The impact of compaction was not seen to be global across the testing direction but rather directionally dependent. In terms of thermal conductivity and compressive rupture strength, the perpendicular values were seen to increase considerably more with compaction than the parallel values although a uniform rise was seen in directional flexural strength. The logical assessment made is that the increasing compaction will also increase the degree of anisotropy of the internal structure, the alignment of the particles being a direct result of compaction. The anticipated increase in directionality of the internal structure was not conclusively observed in the two dimensional image analyses but this was considered to be a result of a limitation of the method.

5 Modelling the properties of bio-aggregate composites with respect to orientation

5.1 Introduction

The structure of hemp-lime is known to be a combination of aggregates and binder both of which have nano-scale porosity, combined imperfectly to produce macro scale porosity between the particles. Furthermore it is known that the aggregates themselves are anisotropic in both internal structure and shape and it has been shown in this work that they arrange with a certain degree of alignment brought about during the production process. The degree of macro scale orientation was assessed and found to alter with several inherent variable characteristics of the materials. It follows that to effectively model behaviour both the multi scale structure and topology of the macro scale structure must be accounted for.

In some of the most recent work in modelling the thermal behaviour of hemp-lime, a multi scale approach has been adopted (Nguyen-Sy et al., 2017). The approach taken, as was discussed in the review of the literature, was to consider hemp-lime as "a mixture of binding matrix containing hemp particles and macro pore inclusions" where both the hemp and binder matrix are modelled at a smaller scale that represents their respective porosities and structure. This basic model presented is for randomly orientated hemp particles but is also later expanded to present a parallel and perpendicular thermal conductivity assuming perfect alignment as a result of compaction. While this model fits well the limited amount of experimental data for parallel and perpendicular thermal conductivity presented elsewhere (Nguyen et al., 2010), it is apparent from the results collected in this study that an assumption of full particle alignment is not appropriate and that this model may fail to adapt to the large range of material variables. Irrespective of this, the model's multi-scale, nested approach is considered to be very appropriate and a similar multi scale approach has been adopted in this work. This approach has not knowingly been applied to the mechanical properties previously.

On the basis of micromechanical models interpreting the quantities, properties and arrangement of constituents it follows that a general form accounting for quantity and arrangement may be used for the estimation of several properties. In this chapter, models describing the composite components at constituent scale are proposed based on

experimental data. A general form for a macro scale model is then put forward with specific adaptations for thermal conductivity and mechanical properties. The model in each case is fitted to the experimental data set gathered to assess its effectiveness.

5.2 A general model of structural form

The structural form of bio-aggregate composites may be split into two scales, the scale of the constituents and the larger scale of the composites, the macro scale. At the macro scale, three phases may be considered: aggregate particles, binder paste and air. These are then considered individually at the smaller constituent scale to account for the multi scale structure of the material. At the constituent scale, the binder, in the case of lime, may be considered a multi-phase material of solid hardened binder paste and voids containing air and/or water. The particles may similarly be considered in the case of hemp to be a multi-phase material comprising a solid phase and voids. Air may be considered a single phase of known properties. The volumetric proportions and the layout of the phases at both scales will now be discussed.

5.2.1 Constituent scale

The volumetric proportions and the layout of phases within hemp and lime as constituents will be discussed in turn. The other constituent at the macro scale, air, is a continuous medium where the properties are known. The properties of air assumed in this study are given in Table 5.1 for air at 20°C.

5.2.1.1 Hemp particles

In a most accurate representation, a particle of hemp may be considered to have the rough form of a rectangular prism with three defined axes relating to the major axes of the plant stem. The particle could therefore be considered to have three sets of properties pertaining to loading across each axis and therefore at a macro scale the orientation of all three axes must be considered. As particle size data and two dimensional digital imaging data of the macro structure do not provide information about the particle within a three dimensional context, assumptions would be required regarding the tertiary axis of the particles based on no experimental evidence. A better approach is therefore to simplify the particle to a square prism with bi-axial properties and geometry where both the shape and orientation can be defined by the data collected. This simplification is justified based on

observations that the particles have a highly defined major axis structure and more similar structure in the secondary and tertiary axis from microscopy (Hustache and Arnaud, 2008, Picandet, 2013).

If hemp particles are considered as three phase materials: air, water and a solid phase, the volumetric proportions of the phases may therefore be described by the measurable properties of porosity and moisture content. The properties of air and water are well known and while the properties of the solid phase are difficult to measure, as the properties of this phase are the only unknowns, it is possible to deduce them from reverse working behavioural models at this scale as has been done elsewhere (Nguyen et al., 2016). The topology of the structure can be studied via microscopy and computer tomography imaging and so representative descriptions of structure and appropriate model forms may be proposed. Probably the most appropriate of these models was presented in recent work (Nguyen-Sy et al., 2017) where the particles are described as a solid phase with transversely isotropic inclusions of "needle like" form of aspect ratio tending toward infinity. This gives a bi-directional structure and properties and when applied to dry thermal conductivity gives bi-directional thermal conductivity as in terms of particle porosity, Equations 5.1 and 5.2 presented by (Nguyen-Sy et al., 2017).

$$\lambda_{p1} = \varphi_p \lambda_a + (1 - \varphi_p)\lambda_h \tag{5.1}$$

$$\lambda_{p2} = \left(\frac{\varphi_p}{\lambda_a + \lambda_h} + \frac{1 - \varphi_p}{2\lambda_h}\right)^{-1} - \lambda_h \tag{5.2}$$

The thermal conductivity model given by Equations 5.1 and 5.2 was used successfully to model both thermal conductivity of bulk aggregates and hemp-lime composites and indicates that simplifying hemp particles to a biaxial element is sufficient within this context. This form of multi-phase model is considered the most appropriate for the thermal conductivity of hemp-particles within the context of modelling hemp-lime and so has been adopted here. A similar approach may be applied to model the particles' stiffness using the Eshelby's solution for elastic bodies within an elastic medium that the above is derived from although this has not been applied in previous work.

As there are limited data available regarding the mechanical performance of individual particles, and bulk properties are a complex combination of particle cohesion and properties, the inclusion model used for thermal conductivity is relatively impractical to apply and indeed will not directly provide the ultimate strength of the particles but rather stiffness. In the context of bio-aggregate composites, the actual contribution of the aggregates mechanically is likely to not be a result of their inherent strength and stiffness

but rather a result of their cohesion. One of the few studies to previously model the compressive strength of bio-aggregate composites appropriately accounted for cohesion by considering an effective pre-stress applied in the compaction of the composite (Tronet et al., 2016). If this is considered to be the case then there is no requirement to model the individual properties of a particle as their strength is irrelevant to the aggregate's contribution and may be taken as zero. As the binder and arrangement of the particles will determine cohesion then it is the macro scale that will account for the aggregate's contribution.

The required inputs to model the thermal and mechanical properties of hemp particles may be distilled to the thermal conductivity of the three phases (solids, air and water) and their volumetric proportions. The assumed structure and thus most appropriate model used for thermal conductivity is that given by Equations 5.1 and 5.2, while the mechanical properties of the particles may simply be taken as zero on the assumption their contribution will be independent of the physical strength of the particles. The porosity of dry hemp particles used in this study has been taken as 0.0767 as presented previously by others (Jia et al., 2017), the thermal conductivity and density of the solid phase of hemp have been taken as the values given in (Picandet, 2013) and (Glé et al., 2012) as 1215kgm^{-3} and 0.576Wm^{-1}K^{-1} respectively. The resulting properties of hemp particles as modelled are given in Table 5.1.

5.2.1.2 Binder paste

The binder paste, much like the hemp particles, can be modelled as a continuous medium with inclusions. In this case a simple spherical inclusion model can be considered appropriate to represent the structure and the same thermal models as used for hemp particles but with an inclusion aspect ratio of 1. This would be an appropriate method to model the stiffness also, however further steps would be required to model strength. To model the thermal and mechanical properties in this way would require the measurement of the porosity of the binder and the intrinsic properties of the solid phase.

In the context of creating something of use to industry, a primary driver of this thesis, a micromechanical model of binder paste may be an over complication. Unlike hemp particles, it is very simple in practical terms to measure the thermal conductivity and mechanical properties of pure binder paste as was done in the material's classification within this study, Chapter 4.1. As both the porosity and physical characteristics of binder paste are known to be a result of the water to binder ratio, for a given binder a more

simplistic and relevant approach in the context of this study is to model the properties as an empirical function of water to binder ratio based on experimental data.

An appropriate form for a universal model of behaviour of binder paste is proposed as a power law. This has been used previously to model similar properties of hemp-lime (Elfordy et al., 2008) and ceramics (Wagh et al., 1993, Wagh, 1993) with a good degree of fit. Using the data gathered in the characterisation of the binder conducted in this study and presented in Chapter 4.1, the density, thermal conductivity, compressive and flexure strength of the binder paste are found to be represented by Equations 5.3, 5.4, 5.5 and 5.6:

$$\rho_b = 1290(a_b)^{-0.26} \quad 5.3$$

$$\lambda_b = 0.20(a_b)^{-1.00} \quad 5.4$$

$$\sigma_b^C = 2.61(a_b)^{-2.40} \quad 5.5$$

$$\sigma_b^F = 2.31 - 0.68(a_b)^{1.95} \quad 5.6$$

From this and the estimated in situ water to binder ratio of 0.5 (Chapter 4.2), the properties of the binder paste modelled by Equations 5.3, 5.4, 5.5 and 5.6 can be found for this study, Table 5.1.

5.2.1.3 Summary of constituent properties

From the various constituent scale models, the properties of the phases at the macro scale model can be found as follows, Table 5.1.

Table 5.1: Properties of macro scale phases as given by the constituent scale models.

Constituent	Phases	Density (kgm^{-3})	Thermal conductivity ($Wm^{-1}K^{-1}$)	Compressive strength (Nmm^{-2})	Flexural strength (Nmm^{-2})
Air	Air	1.21 (The Engineering Toolbox, 2017)	0.0257 (The Engineering Toolbox, 2017)	N/A	N/A
Hemp particle primary axis	Solid/Air	283	0.154	0	0
Hemp particle secondary axis	Solid/Air	283	0.101	0	0
Binder paste	Solid/Air	1536	0.412	14.0	2.02

5.2.2 Composite scale

At the composite scale a multi-phase model that accounts for the quantity and arrangement of the constituents should be considered. In the case of hemp-lime and other bio-aggregate composites, the constituents at a composite scale are the binder paste, air in the form of inter-particle voids and the aggregate. It may also be suggested, as indicated previously, that as the aggregate is considered as a bi-axial element, this constituent may in fact be represented better by two constituents: particles that have a major axis tending to the orientation of interest and particles that are tending away from it. When the properties of the constituents are known, what must be established is the volumetric ratio and a description of the arrangement at the macro scale.

5.2.2.1 Volumetric proportions

The volume ratio of the constituent parts at the macro scale will dependent on the mix constituents as well as the production process; higher compaction will naturally lead to a lower inter-particle porosity for example. If the density of the material and the individual constituents are known then this ratio may be found from the known binder to aggregate ratio used in the mix and therefore a relationship between the design variables and the density of the material is required. From the results gathered in Chapter 4.3 it may be seen that, within the range of binder to aggregate ratios and particle aspect ratios, a linear relationship may be assumed between both of these variables and the un-compacted

density when considered in isolation. If it is assumed that they are independent then the un-compacted density of the material can be written as a function of both, Equation 5.7.

$$\rho_c^{uncompact} = a\left(\frac{m_b}{m_p}\right) + b\phi_p + c \qquad 5.7$$

Where a and b are the gradients of the best fitting linear relations to the variables considered in isolation and c is a constant derived by fitting to the full data set; found as 79, -75 and 504 respectively for this combination of binder and aggregate. From this, where C is the compaction as a ratio of compacted to uncompacted density, the wet density of the compacted mixture may be expressed for this combination, Equation 5.8.

$$\rho_c^{wet} = C\left(79\left(\frac{m_b}{m_p}\right) - 75\phi_p + 504\right) \qquad 5.8$$

Finally the dry density of the composite may be found assuming a complete removal of the water except for that chemically bound in hydration with the binder. This then allows for the dry density of hemp-lime to be described in terms of the mass constituents, the compaction, the particle aspect ratio and the binder hydration level, which when fitted to the binder and aggregate used in this study gives Equation 5.9.

$$\rho_c = C\left(79\left(\frac{m_b}{m_p}\right) - 75\phi_p + 504\right)\left(1 - (m_w - km_b)\right) \qquad 5.9$$

The modelled and the measured dry densities of the differing variants of composites within this study are given in Table 5.2. In general it can be seen that this approach gives a good correlation to the measured results and so may be confidently used to predict the dry density of material within the window of variable values used in this study. The biggest errors were found to come in the highest density material where the model over predicts the values. This is a likely result of the assumption of independent linear relations that may be proven inappropriate beyond the range of values considered in this study, although remain reasonably accurate within this window.

The dry density in combination with the known mass proportions of the constituents and their respective densities at this scale can then be combined to ascertain the volumetric proportions of air (inter particle), aggregate and binder paste from the known densities of these constituents, Table 5.1, and the binder to aggregate ratio, $\left(\frac{m_b}{m_p}\right)$. This is achieved by

first finding the average density of the solid phase of the material, particles and binder, from the known mass proportions and then using this to inversely derive the inter particle porosity and then the volumetric proportions of the constituents, Equations 5.10, 5.11, 5.12, 5.13 and 5.14. Where volumetric proportions are used, the volume of the composite, v_c, may be taken as 1:

$$\rho_s = \frac{m_b + m_p}{\frac{m_b}{\rho_b} + \frac{m_p}{\rho_p}} = \frac{\left(\frac{m_b}{m_p}\right) + 1}{\left(\left(\frac{m_b}{m_p}\right) \times \frac{1}{\rho_b}\right) + \frac{1}{\rho_p}} \quad 5.10$$

$$\rho_c = \frac{m_a + m_s}{v_c} = v_a\rho_a + v_s\rho_s \quad 5.11$$

$$v_a = \frac{\rho_c - \rho_s}{\rho_a - \rho_s} \quad 5.12$$

$$v_b = \frac{\left(\frac{m_b}{m_p}\right) \times \frac{\rho_p}{\rho_b} \times (1 - v_a)}{1 + \left(\left(\frac{m_b}{m_p}\right) \times \frac{\rho_p}{\rho_b}\right)} \quad 5.13$$

$$v_p = \frac{1 - v_a}{1 + \left(\left(\frac{m_b}{m_p}\right) \times \frac{\rho_p}{\rho_b}\right)} \quad 5.14$$

Equations 5.10, 5.11, 5.12, 5.13 and 5.14 resultantly allows for the estimation of the volumetric proportion of aggregate, binder paste and air at the composite scale based on the constituent densities and the following known design parameters: mass ratios of the constituents, particle aspect ratio, binder hydration, and casting compaction. For the materials considered within this study, using the constituent densities in Table 5.1, application of this method gives estimated volumetric proportions as given in Table 5.3.

Table 5.2: Modelled and measured dry density of various hemp-lime variations.

Mix	Proportional mass content			ϕ_p	C	Modelled dry density (kgm^{-3})	Actual dry density (kgm^{-3})	Difference (%)
	Binder	Aggregate	Water					
Fine 2.2	0.355	0.161	0.484	3.04	1.45	360	363	0.90
Medium 1.8	0.321	0.179	0.500	3.27	1.45	309	312	0.85
Medium 2.2 / cast 50 45	0.355	0.161	0.484	3.27	1.45	346	345	-0.27
Medium 2.6	0.382	0.147	0.471	3.27	1.45	382	374	-2.14
Coarse 2.2	0.355	0.161	0.484	3.66	1.45	323	326	1.06
Cast 150 45	0.355	0.161	0.484	3.27	1.45	346	345	-0.27
Cast 50 30	0.355	0.161	0.484	3.27	1.30	310	311	0.28
Cast 50 60	0.355	0.161	0.484	3.27	1.60	382	374	-2.06
Cast 25 45	0.355	0.161	0.484	3.27	1.45	346	345	-0.27

Table 5.3: Estimated volumetic proportions of binder, particle and air at the composite scale.

Mix	ρ_c (kgm^{-3})	$\frac{m_b}{m_p}$	ρ_s (kgm^{-3})	v_a (inter particle)	v_b	v_p
Fine 2.2	360	2.2	932	0.612	0.162	0.226
Medium 1.8	309	1.8	883	0.647	0.130	0.222
Medium 2.2/ cast 50 45	346	2.2	932	0.630	0.154	0.215
Medium 2.6	382	2.6	975	0.617	0.176	0.207
Coarse 2.2	323	2.2	932	0.652	0.145	0.203
Cast 150 45	346	2.2	932	0.631	0.154	0.215
Cast 50 30	310	2.2	932	0.667	0.139	0.194
Cast 50 60	382	2.2	932	0.599	0.167	0.233
Cast 25 45	346	2.2	932	0.631	0.154	0.215

From Table 5.2 and Table 5.3 it can be identified that the volumetric proportions of all three constituents at the composite scale are dependent on the mix ratio, the compaction and the aspect ratio of the aggregate solely and therefore all aspects are easily specifiable and controllable. In general the results may be considered comparable to the other results

presented in the literature elsewhere for the inter particle porosity of hemp-lime giving good confidence in the method applied (Collet et al., 2008, Pierre et al., 2014).

As mentioned previously it is thought appropriate to consider the aggregates not as a single constituent but rather as two separate constituents due to assumed biaxial properties. The volumetric proportion of particles that have their primary and secondary axis tending to the direction of interest must be expressed as a fraction of the total particle volume. There are two axes of interest within hemp-lime: parallel and perpendicular to compaction with the relative distribution of particle orientations between these two experimentally quantified in this work as the parameter $(f_0 - f_{90})$. It therefore follows that the volumes of particles with their primary (subscript 1) and secondary (subscript 2) axis tending towards a specific direction of interest may be described via functions of this parameter, Equations 5.15 and 5.16.

$$v_{p2} = v_p \times F(f_0 - f_{90}) \quad 5.15$$

$$v_{p1} = v_p\big(1 - F(f_0 - f_{90})\big) \quad 5.16$$

The degree of orientation, $(f_0 - f_{90})$, so far has been measured and so is not an intrinsic design parameter of specifying the material although it is known through the experimental phase to be a function of the variables of particle aspect ratio, binder to aggregate ratio and compaction. If it is assumed that $(f_0 - f_{90})$ follows a linear relation to these variables and that they are independent, as was done with un-compacted density, then using the same approach an empirical estimation of $(f_0 - f_{90})$ is found for the aggregates and binder used in this study from Equation 5.17.

$$f_0 - f_{90} = 3.50\phi + 11.7C - 3.85\left(\frac{m_b}{m_p}\right) - 8.46 \quad 5.17$$

The predicted and measured values of $(f_0 - f_{90})$ may be compared to test the validity of this equation, Table 5.4. From Table 5.4 it can be seen that this approach of assuming linear and independent relations gives reasonable correlation to the experimental data. Where the biggest deviation has occurred, “cast 50 60” mix of material, this is believed to be a result of the experimental method underestimating the value in this case due to a limitation of the method when used with highly compacted material as was discussed in Chapter 4.4. In general the relationship proposed is considered to be of sufficient accuracy to predict the value of $(f_0 - f_{90})$ for hemp-lime within the range of materials considered in this study.

Table 5.4: Modelled and measured values of $(f_0 - f_{90})$ of various hemp-lime variations.

Mix	$\frac{m_b}{m_p}$	ϕ_p	C	Modelled $(f_0 - f_{90})$	Actual $(f_0 - f_{90})$	Difference (%)
Fine 2.2	2.2	3.04	1.45	10.68	10.42	2.5
Medium 1.8	1.8	3.27	1.45	13.02	13.4	-3.8
Medium 2.2/ cast 50 45	2.2	3.27	1.45	11.48	11.48	0.00
Medium 2.6	2.6	3.27	1.45	9.94	10.32	-3.8
Coarse 2.2	2.2	3.66	1.45	12.85	12.63	2.1
Cast 150 45	2.2	3.27	1.45	11.48	10.35	11.3
Cast 50 30	2.2	3.27	1.30	9.73	9.73	0.00
Cast 50 60	2.2	3.27	1.60	13.24	10.42	28.2
Cast 25 45	2.2	3.27	1.45	11.48	11.09	3.9

From Equations 5.15 and 5.16, if it is assumed that, when the degree of material orientation, $(f_0 - f_{90})$, tends towards zero, a random distribution of particles occurs, then it would be expected that one third of the population would have their major axis tending towards each of the three material axes. It therefore follows that two thirds of the particles will have a secondary axis tending to that direction assuming a biaxial element and thus in the axis of applied compression. If a function of $(f_0 - f_{90})$ is defined to give the proportion of particles with their secondary axis tending towards the direction of compaction then Equation 5.18 defines a limiting case.

$$f_0 - f_{90} \rightarrow 0$$
$$F(f_0 - f_{90}) \rightarrow \frac{2}{3} \qquad 5.18$$

If a new function, F_b, is introduced that gives the proportion of particles observed between the orientations of 0° and 45° in the perpendicular images and it is assumed that these values represent the true orientation of the particles then $F_b(f_0 - f_{90})$ will tend to ½ when $(f_0 - f_{90})$ tends to zero. Equations 5.15 and 5.16, may be rewritten for the axis parallel to applied compaction so as to satisfy Equation 5.18 to give Equations 5.19 and 5.20.

$$v_{p2}^{||} = v_p \left(F_b(f_0 - f_{90}) \frac{2}{3} + \frac{1}{3} \right) \qquad 5.19$$

$$v_{p1}^{||} = v_p\left(\frac{2}{3} - F_b(f_0 - f_{90})\frac{2}{3}\right) \quad 5.20$$

If an axis perpendicular to applied compaction is considered then it may be assumed that a random distribution of particles in perpendicular planes will exist and thus it can be expected that half of the particles with their primary axis not tending to the axis of compaction, will tend towards each of the other axes of the material. Equations 5.21 and 5.22 may therefore be deduced for an axis perpendicular to compaction.

$$v_{p1}^{\perp} = v_p\left(F_b(f_0 - f_{90})\frac{1}{3} + \frac{1}{6}\right) \quad 5.21$$

$$v_{p2}^{\perp} = v_p\left(\frac{5}{6} - F_b(f_0 - f_{90})\frac{1}{3}\right) \quad 5.22$$

A true form of $F_b$would be the bounded integral of the Hankinson equation used to fit to particle orientation and give the values of $(f_0 - f_{90})$. Given the nature of the Hankinson form, when the values of n are not whole numbers, the integral of this equation is not easily found and would vary with n, removing a universal solution. It is therefore proposed that the distribution might be effectively simplified to a linear one, defined as the straight line that passes through the values of f_0 and f_{90} respectively. As a perfectly even frequency distribution in 10° groupings would give values of 11.1°, then the points f_0 and f_{90} may be written in terms of $(f_0 - f_{90})$, Equations 5.23 and 5.24.

$$f_0 = 11.1 + \frac{(f_0 - f_{90})}{2} \quad 5.23$$

$$f_{90} = 11.1 - \frac{(f_0 - f_{90})}{2} \quad 5.24$$

The definite integral of the straight line passing through these points bounded by 0° and 45° and corrected for the 10° groupings may then be calculated, Equation 5.25.

$$F_b(f_0 - f_{90}) = 45^2\left(\frac{(f_0 - f_{90})}{4}\right) + 45\left(11.1 + \frac{(f_0 - f_{90})}{2}\right) \quad 5.25$$

Together Equations 5.19, 5.20, 5.21, 5.22 and 5.25 enable the calculation of proportional particle orientation towards a given axis for the experimentally measured values. This in turn can be estimated from the empirical relations to parameters of particle aspect ratio, compaction level and binder to hemp ratio. As the overall volumetric proportion of air,

binder, aggregate may be also found from known parameters of the material, the volumetric proportions of all constituents at the macro scale may therefore be estimated from three known design parameters and the properties of the constituents.

5.2.2.2 Constituent arrangement

As there are four phases at the macro scale, accurately describing the structure without rapidly increasing the complexity becomes a challenge. From the images collected and analysed throughout this study, such as in Figure 5.1, a good basic description of the macro structure might be: elongated particles coated in binder, imperfectly arranged to leave inter-particle porosity but tending towards a similar orientation. It is apparent therefore that, even if the inclusions are elongated, a simple inclusion model will struggle to describe this complex structure even if several scales are considered.

Figure 5.1: The complex macro scale topology of hemp-lime.

A way to simplify this is to consider that the properties of a composite material must lie between two boundaries that represent the constituents arranged perfectly in series and perfectly in parallel, Figure 5.2. From this it was suggested by Krischer that the composite thermal conductivity may be found as a weighted harmonic mean of these boundaries where the weighting factor, referred to herein as shape factor and denoted by s, is representative of the material's structure (Krischer and Kast, 1978). This approach could be broadened to suggest that any property may be represented by an appropriate weighted mean of these idealised arrangements.

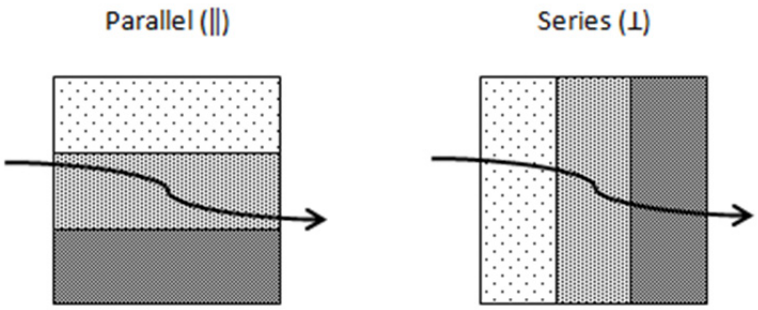

Figure 5.2: Series and parallel arrangements of materials with respects to loading direction (indicated by arrow).

As was found in the review of the literature, this approach has already been applied to hemp lime with some success for modelling the thermal conductivity (Pierre et al., 2014). In this instance the approach was applied to a single scale model and relied on acquiring the volumetric proportions through experimental fitting. This earlier work gives a good precedent for the approach but can be improved upon by applying it purely to the composite scale where the volumes are known and the shape factor may be empirically linked to the known variations in material composition and manufacture.

Based on the description of the structure proposed above, one might consider what aspects of the mix design and production will logically impact on the layout of the macro structure and thus should influence the shape factor. If the square prismatic form of particles is assumed to hold and the binder is assumed to be evenly distributed over the surface during the mixing, then the shape of the binder coated particles will be a function of the particle aspect ratio and the amount of binder. If these units are then considered to form an imperfect arrangement but with a degree of sway in orientation, the overall structure will be dependent on the orientation distribution and the degree and nature of connectivity; a function of compaction and particle size spread. From this description it may therefore be proposed that the shape factor, s, can be written as a function of five prescribed or measurable aspects (mean particle aspect ratio: ϕ_p, mass of binder: m_b, proportion of particles aligned in the primary axis: $\frac{v_{p1}}{v_p}$, the interquartile range of particle sizes: IQR_p and the compaction: C), Equation 5.26.

$$s = F\left(\phi_p, m_b, \frac{v_{p1}}{v_p}, IQR_p, C\right) \qquad 5.26$$

The specific form of the shape functions that describe the material relevant to a certain property will depend on the nature of that property and the direction of loading and so it

can be expected that a differing function will be required for each property and each direction of loading however with similar trends between them.

5.2.3 Multi scale model

By combining the constituent models and the macro scale models it is proposed that the thermal conductivity and mechanical strength of hemp-lime should be describable for any variation of material. It is further suggested that, as the basic model form is generic, then it is likely to also be applicable to other bio-aggregate composites that can be described in the same structural terms and phases. In general the properties of a bio-aggregate composite may then be found from Equation 5.27.

$$F_c\left(s, v_m^{1,2,3\dots}, F_1\left(v_1^{a,b,c\dots}, x_1^{a,b,c\dots}\right), F_2\left(v_2^{a,b,c\dots}, x_2^{a,b,c\dots}\right), F_3\left(v_3^{a,b,c\dots}, x_3^{a,b,c\dots}\right)\dots\right) \quad 5.27$$

Where:

- F_c is the function at the macro, composite, scale and is a form of weighted mean between limiting series and parallel arrangements
- s is the shape function at the macro scale
- v_m is the volume proportions of the phases at a macro scale
- F_i is the functions at the constituent scale for the macro scale phase
- v_i is the volume of the phase at a constituent scale
- x_i is the property of the phase at a constituent scale.

5.3 Bi-directional thermal conductivity model

5.3.1 Theoretical model

If the general model, Equation 5.27, is applied to the thermal conductivity of hemp lime then the most appropriate macro scale function is the standard Krischer model (Krischer and Kast, 1978). In this the thermal conductivity of a composite is given by the weighted harmonic mean of idealised series ($\perp$) and parallel ($\parallel$) arrangements of the constituents. For hemp lime, orientated parallel ($\parallel$) and perpendicular ($\perp$) to the direction of compaction then the thermal conductivity can be given by Equations 5.28 and 5.29 where Equations 5.30 and 5.31 describe the idealised series ($\lambda_\perp$) and parallel ($\lambda_{||}$) arrangements respectively.

$$\lambda_c^{||} = \frac{1}{\frac{s_\lambda^{||}}{\lambda_\perp^{||}} + \frac{1 - s_\lambda^{||}}{\lambda_{||}^{||}}} \quad 5.28$$

$$\lambda_c^{\perp} = \frac{1}{\frac{s_\lambda^{\perp}}{\lambda_\perp^{\perp}} + \frac{1 - s_\lambda^{\perp}}{\lambda_{||}^{\perp}}} \quad 5.29$$

$$\lambda_\perp = \frac{1}{\frac{v_{p1}}{\lambda_{p1}} + \frac{v_{p2}}{\lambda_{p2}} + \frac{v_b}{\lambda_b} + \frac{v_a}{\lambda_a}} \quad 5.30$$

$$\lambda_{||} = v_{p1}\lambda_{p1} + v_{p2}\lambda_{p2} + v_b\lambda_b + v_a\lambda_a \quad 5.31$$

The constituent volumes are given by Equations 5.12, 5.13, 5.19, 5.20, 5.21 and 5.22, and the constituent properties those listed in Table 5.1.

Table 5.1.

5.3.2 Fitting to experimental data

5.3.2.1 Constituent scale

The thermal conductivity and density of air is known and given in Table 5.1.

Table 5.1. The thermal conductivity of the binder paste may be found from Equation 5.4 and the density from Equation 5.3 and are given for the estimated in-situ water to binder ratio used in this study, 0.5, in Table 5.1.

Table 5.1. The thermal conductivity of hemp particle in the primary and secondary axes are given by Equations 5.1 and 5.2 for the known porosity of the hemp aggregate used and using the thermal conductivity of the solid phase presented elsewhere in the literature.

5.3.2.2 Macro scale

Equations 5.28 and 5.29 can be fitted to the experimental data by finding the idealised sets of shape factors for parallel and perpendicular loading with respect to compaction, $s_{||}$ and $s_\perp$. As an individual value for $s_{||}$ and $s_\perp$ are assumed for each variation of material, a perfect fit to the data can be obtained. The set of shape factors was found by applying a least squares fitting approach to the experimental data and resulted in the set of values given in Table 5.5.

Two shape functions were then determined separately for the parallel and perpendicular cases by considering each of the variables in Equation 5.26 in turn with respect to the idealised set of values. The form of the relationship between each of these variables was thus gauged assuming independence and then a combined equation formed. This equation was then fitted to the idealised shape factors in each direction to give an empirically derived shape function for thermal conductivity of hemp-lime in each of the two material directions, Equations 5.32 and 5.33.

$$s_{\lambda}^{\perp} = -53.17\left(\frac{v_{p1}}{v_p}\right) - 11.69m_b + 2.39C + 0.63\phi_p + 18.77 \qquad 5.32$$

$$s_{\lambda}^{\parallel} = 26.86\left(\frac{v_{p1}}{v_p}\right) - 13.18m_b + 2.56C + 0.60\phi_p - 7.41 \qquad 5.33$$

By applying Equations 5.32 and 5.33 to the range of materials considered in the experimental study, a set of modelled bi-directional thermal conductivities are obtained and may be compared to the measured results, Table 5.5 and Figure 5.3.

From Table 5.5 and Figure 5.3 it can be seen that the multi-scale weighted series and parallel model is able to fit the experimental data with a good degree of accuracy both in loading parallel (R^2 = 0.98) and perpendicular (R^2 = 0.96) to compaction. The parallel loading is observed to give a better fit between the experimental and modelled results with all the major trends in the data well represented. In the perpendicular direction, again a reasonable fit is seen although not quite as good as the parallel direction. A possible reason for this is the larger spread of values found with differing layer sizes in this direction which has not been assumed to impact the macro scale structure.

Table 5.5: Shape factors,bi-directional measured thermal conductivity and bi-directional modeled thermal conductivity forvariations of hemp-lime.

Mix	Idealised shape factors		Modelled shape factors		Measured thermal conductivity ($Wm^{-1}K^{-1}$)		Modelled thermal conductivity ($Wm^{-1}K^{-1}$)	
	$s_\lambda^{\parallel}$	$s_\lambda^{\perp}$	$s_\lambda^{\parallel}$	$s_\lambda^{\perp}$	$\lambda_c^{\parallel}$	$\lambda_c^{\perp}$	$\lambda_c^{\parallel}$	$\lambda_c^{\perp}$
Fine 2.2	0.275	0.128	0.259	0.143	0.085	0.104	0.087	0.102
Medium 1.8	0.366	0.212	0.366	0.211	0.071	0.085	0.071	0.085
Medium 2.2/ Cast 50 45	0.234	0.118	0.236	0.128	0.087	0.102	0.086	0.101
Medium 2.6	0.182	0.112	0.183	0.112	0.098	0.109	0.098	0.109
Coarse 2.2	0.206	0.093	0.197	0.102	0.085	0.100	0.086	0.099
Cast 150 45	N/A	0.149	N/A	0.128	N/A	0.098	N/A	0.101
Cast 50 30	0.194	0.127	0.206	0.120	0.084	0.093	0.083	0.094
Cast 50 60	0.254	0.142	0.266	0.136	0.092	0.107	0.090	0.108
Cast 25 45	0.239	0.129	0.236	0.128	0.086	0.101	0.086	0.101

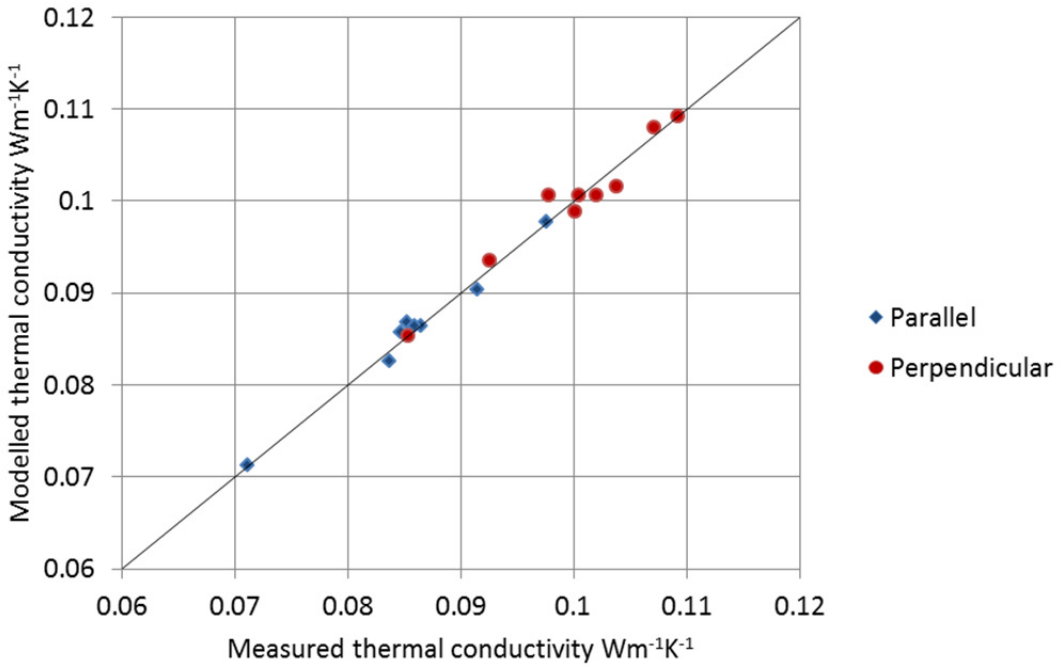

Figure 5.3: Measured vs modelled parallel and perpendicular to compaction thermal conductivity of hemp lime produced to a range of constituent and production variations.

5.3.3 Discussion

From Equations 5.32 and 5.33 it can be seen that linear relationships were found as sufficient to describe the shape factor in the case of all variables considered although, as this is based on a limited data set, it is not apparent if this will be appropriate beyond the limits of the ranges considered in this study. In both the parallel and perpendicular loading cases, a shape function of the same form was obtained as might be expected, given variables are likely to have a similar impact in both directions of loading but to differing degrees, reflecting the observations from the experimental studies. Despite the shape factor being put forward as a function of five possible variables, Equation 5.26, the inter quartile range of the particle sizes was not found to correlate to the shape factor in any definable way indicating that this has a negligible impact on the macro scale structure in terms of thermal conductivity which is again broadly consistent with experimental results.

The degree of particle orientation appears to have the largest impact on the shape factor which accounts for the major difference between the materials in the two directions. The degree of particle orientation is found to have a positive impact in the parallel loading direction and a negative impact in the perpendicular direction, tending the model to the parallel arrangement. It was anticipated that a negative impact should have been found in both directions, as an increase of particles tending to have their longer major axis in the direction of interest should logically tend the material to a parallel arrangement in that direction. This result therefore indicates the more complex relationship the shape factor has with the material and how other aspects such as compaction and binder content might dominate this aspect despite the seemingly lower weighting; the fluctuations in the values and thus impact on the shape factor being of greater importance.

Both an increase in compaction and aspect ratio of the particles were found to have a positive correlation to the shape factor indicating they preferentially direct the arrangement to a series one while the binder content seems to preferentially direct the behaviour to a parallel arrangement. The physical basis of these trends might be speculated to be that compaction and particle aspect decrease the continuity of the inter particle air voids and thus shift the behaviour towards a series model whilst binder content, as the most thermally conductive component, will tend the behaviour towards parallel with increased continuity. In both cases these assessments are speculative only and it is considered likely that the assumption of these variables being independent is an oversimplification that hides a more complex actual behaviour.

In general, from Figure 5.3, a high level of fit can be found with the experimental data from the modelled values in both directions when the empirically derived shape factors are used; R^2 values of 0.98, and 0.96 were obtained for parallel and perpendicular loading respectively. This is indicative of the power of this form of multi scale model and the use of a shape factor to account for macro structure, especially as the range of material variations examined compared to preceding studies is comparatively large. The biggest discrepancy can be found in the perpendicular results which is believed to come from variations with layer size, a variable currently not included within the function of shape factor.

Currently the model presented accounts only for dry thermal conductivity however could easily be extended to account for a range of moisture contents through an adaptation of the constituent models for hemp particle and binder paste. Similarly, while the model is specifically fitted to hemp-lime in this instance and only a restricted range of variations defined by the experimental data set, it is reasonable to assume that it could also be applied to a wider range of material. It is apparent from Equations 5.30 and 5.31 that the model intrinsically accounts for the extreme cases of volumetric proportions – 100% aggregate and 100% binder - and so could in theory model any variation of hemp lime provided an appropriate form of the shape function is defined. Furthermore other bio-aggregate composites (such as those using alternative aggregates: rape shiv, sunflower stem etc. and alternative binders such as starch) could be modelled via the insertion of appropriate constituent scale models and redefining of the empirical relations appropriately. In this sense the basic form of the model may be considered reasonably universal to many bio-aggregate composites when sufficient data sets are available for fitting.

5.3.4 Conclusion

The model proposed is able to predict the parallel and thermal conductivity of hemp-lime based on a selection of variables that are easily obtained or specified at a practitioner level. In this respect the model may be considered unique in its application potential. The inputs required may be summarised as follows:

- The mass ratios of the constituents used
- The mean aspect ratio of the aggregate
- The compaction level
- The properties of the constituents:
    - Thermal conductivity of the solid phase of hemp

- Porosity of hemp
- Density of the solid phase of hemp
- Water to binder ratio of the paste

If values relating to the properties of the constituents are assumed to be constant then this allows for the bi-directional dry thermal conductivity to be found based on three known design parameters and so could be of considerable use as a design tool or in industrial product development.

In general the closeness of fit of the experimental with the modelled data was very good using the empirically derived function for shape factor. The limitations of the model are considered to be a limited physical basis for the empirical relationship to the shape factor and the assumption of interdependence of the variables. Despite this, the accuracy of the model across the wide range of materials considered in this study is good and the model could be easily developed to be more physically representative and remove these assumptions; refinements to the shape functions are the obvious area of development.

5.4 Bi-directional compressive capacity model

5.4.1 Theoretical model

If the general model, Equation 5.27, is applied to the compressive rupture strength of hemp lime then the most appropriate macro scale function is a rule of mixtures as used consistently for the modelling of other composites' mechanical properties (Askeland and Phulé, 2006). In this model the mechanical property of a composite is given by the weighted arithmetic mean of the constituents based on their cross section in the relevant direction. As the binder is the sole structural component in this model then the compressive strength can be given as a weighted mean between an optimised and minimised arrangement of binder in terms of cross section described by the shape factor. The maximum continuous cross section of binder possible would be for the case of a parallel arrangement of materials, Figure 5.2, while the minimal continuous cross section would be the case of a series arrangement and equal to zero. The equations describing the compressive strength of the composite can therefore again be expressed as a weighted mean of a series and parallel arrangement however using an arithmetic mean in this case: Equations 5.34 and 5.35.

$$\sigma_{Cc}^{||} = s_C^{||}\sigma_{C\perp}^{||} + \left(1 - s_C^{||}\right)\sigma_{C||}^{||} \qquad 5.34$$

$$\sigma_{Cc}^{\perp} = s_C^{\perp}\sigma_{C\perp}^{\perp} + (1 - s_C^{\perp})\sigma_{C||}^{\perp} \quad 5.35$$

The bounding series ($\sigma_{C\perp}$) and parallel ($\sigma_{C||}$) idealised cases can be described by Equations 5.36 and 5.37 using the standard forms.

$$\sigma_{C\perp} = \frac{1}{\frac{v_{p1}}{\sigma_{Cp1}} + \frac{v_{p2}}{\sigma_{Cp2}} + \frac{v_b}{\sigma_{Cb}} + \frac{v_a}{\sigma_{Ca}}} \quad 5.36$$

$$\sigma_{C||} = v_{p1}\sigma_{Cp1} + v_{p2}\sigma_{Cp2} + v_b\sigma_{Cb} + v_a\sigma_{Ca} \quad 5.37$$

In this study where the compressive strength of air and aggregate particles are considered to be zero this can be simplified to Equations 5.38 and 5.39.

$$\sigma_{C\perp} = 0 \quad 5.38$$

$$\sigma_{C||} = v_b\sigma_{Cb} \quad 5.39$$

The constituent volumes are given by Equations 5.12, 5.13, 5.19, 5.20, 5.21 and 5.22, and the constituent properties those listed in Table 5.1.

Table 5.1.

5.4.2 Fitting to experimental data

5.4.2.1 Constituent scale

The compressive strength and density of the binder is found from Equations 5.3 and 5.5 and are given for the estimated in-situ water to binder ratio used in this study, 0.5, in Table 5.1.

Table 5.1. The density of air is known and its compressive strength can be taken as zero. The compressive strength of the aggregates themselves is considered to be zero as it is considered that all resistance of this material in bulk comes from cohesion that in the context of a composite is assumed to be determined by the presence of the binder. The density of the particles is given in Table 5.1.

Table 5.1.

5.4.2.2 Macro scale

An individual value of shape factor may be fitted to each material and in the parallel and perpendicular direction respectively, accounting for the differing structure in all cases. This then allows for a perfect fit to the experimental data via finding the optimum set of values of shape factor that are given in Table 5.6. Based on the experimental data it was apparent that the compressive behaviour of hemp-lime was governed by differing mechanisms in the parallel and perpendicular directions. It is appropriate therefore to consider separate shape functions in these directions to account for this although in both cases the shape factor can be considered a function of the same intrinsic variables that are given in Equation 5.26.

Shape functions were determined separately for parallel, $s_C^{||}$, and perpendicular, $s_C^{\perp}$, loading by considering each of the variables in Equation 5.26 in turn with respect to the idealised set of values. The form of the relationship between each of these variables was thus gauged and then a combined equation formed assuming independence of the variables. Constants were determined via a least square approach to fit the modelled and shape factors to the idealised ones in each direction to give an empirically derived shape function. In parallel loading the best fit was found with Equation 5.40.

$$s_C^{||} = 3.12\left(\frac{v_{p2}^{||}}{v_p}\right) - 2.10m_b + 0.09C + 0.01\left(IQR_p\right) + 0.57 \qquad 5.40$$

In the perpendicular direction, taking the same approach was not able to initially provide a good fit to the idealised shape factors. While clear correlations were found to most variables, no clear correlation was found to the volumetric proportion of binder despite it having a significant impact, preventing reliable fitting. What was instead observed was a very large impact of this variable when the binder to aggregate ratio was increased from 1.8 to 2.2 but then no additional impact beyond this. The observation made in the experimental work concerning the impact of the aggregate to binder ratio on perpendicular compressive rupture strength was also found to be of inconsistent nature: an increase from 1:1.8 to 1:2.2 was seen to improve rupture strength while a further increase to 1:2.6 was not. The explanation proposed was of the effective surface area of the particles providing restraint to the binder paste becoming saturated and capping the strength at a certain binder concentration. To overcome this in the model a simple solution is to cap the value of the binder volume that can be used in order to represent this apparent physical limit. When applied, this allowed for a significantly better fit between the idealised values of the shape factor and the empirically derivable values. The function

in this case was resultantly found as Equation 5.41 where the modified value of the binder mass, m_{b*}, is given by Equation 5.42.

$$s_C^{\perp} = -5.74\left(\frac{v_{p1}^{\perp}}{v_p}\right) - 3.67m_{b*} - 0.11C + 0.02\left(IQR_p\right) + 4.30 \quad 5.41$$

$$m_{b*} = min(m_b, 0.3548) \quad 5.42$$

The empirically estimated values of the shape factor found using Equations 5.40 and 5.41 as well as the resulting modelled values of compressive rupture strength found using Equations 5.34 and 5.35 are given in Table 5.6. The modelled and measured values of compressive rupture strength are also plotted against each other in Figure 5.4.

Table 5.6: Shape factors,bi-directional measured compresive rupture strength and bi-directional modeled compresive rupture strenght for variations of hemp-lime.

Mix	Idealised shape factors		Modelled shape factors		Measured compressive rupture strength (Nmm^{-2})		Modelled compressive rupture strength (Nmm^{-2})	
	$s_C^{\parallel}$	$s_C^{\perp}$	$s_C^{\parallel}$	$s_C^{\perp}$	$\sigma_{Cc}^{\parallel}$	$\sigma_{Cc}^{\perp}$	$\sigma_{Cc}^{\parallel}$	$\sigma_{Cc}^{\perp}$
Fine 2.2	0.815	0.783	0.815	0.784	0.416	0.488	0.416	0.487
Medium 1.8	0.884	0.924	0.880	0.924	0.209	0.138	0.217	0.138
Medium 2.2/ cast 50 45	0.854	0.851	0.846	0.834	0.317	0.323	0.333	0.359
Medium 2.6	0.829	0.877	0.824	0.867	0.428	0.308	0.442	0.333
Coarse 2.2	0.811	0.809	0.809	0.799	0.382	0.385	0.384	0.406
Cast 150 45	0.838	0.824	0.846	0.834	0.350	0.380	0.333	0.359
Cast 50 30	0.875	0.891	0.873	0.889	0.242	0.211	0.246	0.215
Cast 50 60	0.820	0.782	0.818	0.779	0.429	0.520	0.433	0.526
Cast 25 45	0.832	0.804	0.846	0.834	0.364	0.425	0.333	0.359

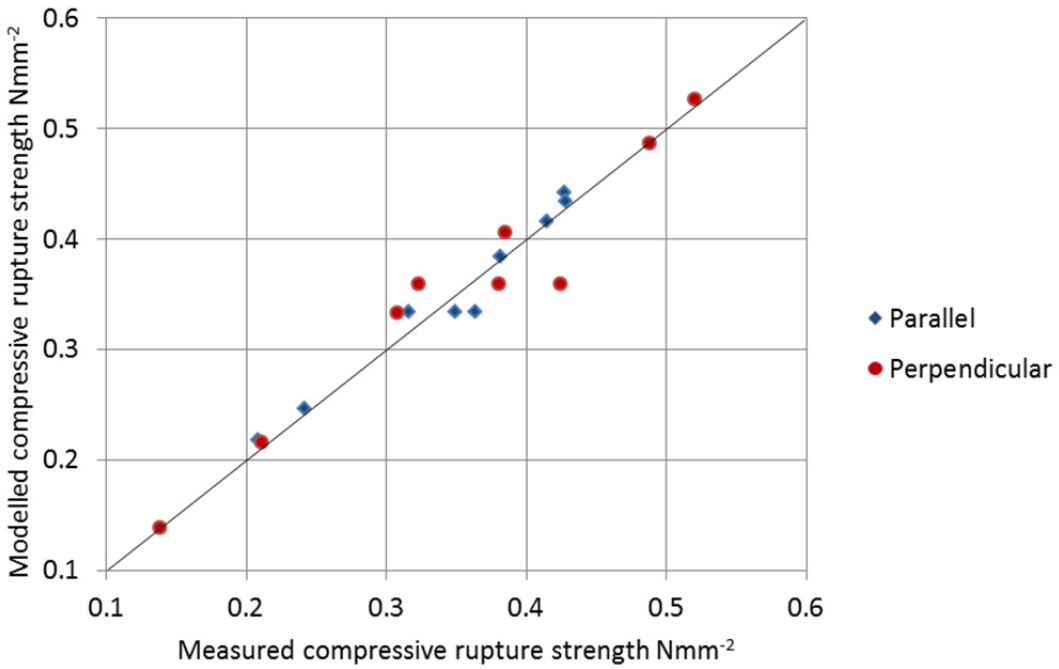

Figure 5.4: Measured Vs modelled parallel and perpendicular to compaction compressive rupture strength of hemp lime produced to a range of constituent and production variations.

From Table 5.6 and Figure 5.4 it can be seen that in general the model using empirically estimated values of the shape factor is able to give reasonable correlation to the experimentally gathered data; R^2 values of 0.96 and 0.94 for parallel and perpendicular loading respectively. The model is more accurate in the parallel to compaction direction of loading although in both directions the predicted values are within or close to the range of experimental values gathered for similar specimens. As was the case in thermal conductivity, the biggest discrepancy is observed in the layer sizing where variation in the experimental results are not accounted for by the model which assumes that layer size has no impact on the internal structure.

5.4.3 Discussion

From Equations 5.40 and 5.41 it can be seen that the particle aspect ratio was not found to have an impact on the shape factor, indicating that this does not affect the fundamental arrangement of the compressive load path beyond altering the degree of orientation, $\left(\frac{v_{p1}^{\perp}}{v_p}\right)$. This was not the case in the thermal conductivity functions and is reflective of the experimental results which concluded that both the spread of particle size and the aspect ratio of the particles affect differing properties in differing ways.

The proportion of particles with their primary axis aligned to the direction of loading is observed here, as was found in the thermal conductivity, to have a positive impact on the shape factor in the parallel direction and a negative impact in the perpendicular direction. Similar reasons of a low fluctuation in the values of this variable and a dominance of other factors can again be cited as reasons for this although it is not as was hypothesised and further investigation is warranted.

Mass of binder has a bi-directionally negative impact on the shape factor, tending the compressive rupture strength of the composite towards that of the parallel model. As the binder is considered to be the only structural element and the increased proportion will increase the effective cross sectional area, this observation is logical. It is also considered that an increase in binder will increase cohesion of the particles and thus the composite strength. The range of particle sizes tending towards a series arrangement can be attributed to the assumed increase of "floating" particles caused by the wider range of particle sizes as was discussed in the relevant experimental chapter. Compaction was found to have a positive impact in the parallel direction of loading and negative in the perpendicular direction, tending the behaviour to that of series and parallel respectively. Increased compaction would be expected to increase the stratification of all elements towards perpendicular planes. As such stratification would pose an increased tendency towards series and parallel arrangement in opposing directions, this directional as opposed to global impact of compaction on the shape factor is reasonable.

Figure 5.4 shows that a good degree of fit between the experimental and modelled values of bi-directional compressive rupture strength can be achieved using this model with an empirically derived shape function. Given the level of variation that was observed in similar specimens the model can be considered very reliable at predicting the approximate compressive rupture strength within the window of material variations used in this work. The weakest assumptions made in the model are considered to be the assumed interdependence of the variables determining the shape function and the assumption that the binder is the only structural component. Both of these aspects may be addressed by refining the model both in terms of the form of the shape functions used and by the inclusion of a constituent scale model for the compressive resistance of the particles.

While the model is specifically fitted to hemp-lime in this instance, it is reasonable to assume that it could also be applied to other bio-aggregate composites (such as those using alternative aggregates: rape shiv, sunflower stem etc. and alternative binders such as starch) via the insertion of appropriate composite scale models and the redefining of

the empirical relations. It is also apparent from Equations 5.38 and 5.39 that while the model is only fitted to the limits of the available data set, it is able to inherently account for the limiting condition of 100% binder. The other extreme volumetric case of 100% aggregate would produce a result of zero compressive rupture strength and so the model is considered likely to have a lower limit of binder volume. Despite this it is certain that the model is theoretically applicable to a wider range of variations that the current data set so long as the shape function can be appropriately defined. In this sense the basic form of the model may be considered reasonably universal to many bio-aggregate composites and additional experimental work to generate the required data sets to validate this would be another way to develop this.

5.4.4 Conclusion

The final model proposed is able to predict the parallel and perpendicular compressive rupture strength of hemp-lime to a good degree of closeness to experimental results, based on a selection of variables that are easily obtained or specified at a practitioner level. In this respect the model may be considered unique in its industrial application potential; if compressive strength of the binder paste is known then the bi-directional compressive rupture strength can be predicted based on five measured or specifiable parameters.

The inputs required may be summarised as follows:

- The mass ratios of the constituents used
- The mean aspect ratio of the aggregate
- The interquartile range of the aggregate particles
- The compaction level
- The water to binder ratio of the paste

In general the closeness of fit of the experimental to the modelled data was good (R^2 values of 0.96 and 0.94 for parallel and perpendicular loading respectively) using empirically calculated values of the shape factor. The main trends seen in the experimental data are all well accounted for by the model and results predicted with sufficient accuracy to be within the error of the experimental data and natural variation of the material. Further refinements to the form of the shape function, to account for interdependence of variables and give more physical meaning, are considered the best way to refine the model.

Currently the model assumes no contribution of the particles' natural cohesion or resistance beyond altering the shape factor. For material where higher levels of compaction are applied during forming it is considered likely that this assumption may not hold, as the loose particles were found to exhibit strain hardening when tested in confined compaction. At high levels of production compaction it may therefore be assumed that the particles become effectively pre-stressed to the point of exhibiting a significant stiffness and contribution to the material. It is proposed that the model's multi scale approach may allow for the easy inclusion of this through developing an appropriate constituent model for the particles, based on their degree of effective pre-stress as has been considered by others (Tronet et al., 2016).

5.5 Bi-directional flexural capacity model

5.5.1 Theoretical model

If the general model, Equation 5.27, is applied to the flexural strength of hemp lime then the most appropriate macro scale function is a rule of mixtures as was used in the compressive rupture strength for the reasons as previously stated. Again it is assumed that the binder is the sole structural component and that the strength is thus determined by the effective cross sectional area of this element. The effective boundaries of maximal and minimal effective cross sectional area may again be assumed as a series and parallel arrangement. In applying this, the flexural strength of hemp-lime loaded parallel and perpendicular to the direction of compaction, can then be given by Equations 5.43 and 5.44 were the bounding series and parallel arrangements, $\sigma_{F\perp}$ and $\sigma_{F\perp}$ respectively, are given by Equations 5.45 and 5.46.

$$\sigma_{Fc}^{||} = \left(1 - s_F^{||}\right)\sigma_{F||}^{||} + s_F^{||}\sigma_{F\perp}^{||} \tag{5.43}$$

$$\sigma_{Fc}^{\perp} = \left(1 - s_F^{\perp}\right)\sigma_{F||}^{\perp} + s_F^{\perp}\sigma_{F\perp}^{\perp} \tag{5.44}$$

$$\sigma_{F\perp} = \frac{1}{\frac{v_{p1}}{\sigma_{Fp1}} + \frac{v_{p2}}{\sigma_{Fp2}} + \frac{v_b}{\sigma_{Fb}} + \frac{v_a}{\sigma_{Fa}}} \tag{5.45}$$

$$\sigma_{F||} = v_{p1}\sigma_{Fp1} + v_{p2}\sigma_{Fp2} + v_b\sigma_{Fb} + v_a\sigma_{Fa} \tag{5.46}$$

Where the flexural strength of air and aggregate particles are considered to be zero, Equations 5.45 and 5.46 can be simplified to Equations 5.47 and 5.48.

$$\sigma_{F\perp} = 0 \quad (5.47)$$

$$\sigma_{F||} = v_b \sigma_{Fb} \quad (5.48)$$

The constituent volumes are given by Equations 5.12, 5.13, 5.19, 5.20, 5.21 and 5.22, and the constituent properties those listed in Table 5.1.

Table 5.1.

5.5.2 Fitting to experimental data and discussion

5.5.2.1 Constituent scale

The flexural strength and density of the binder is found from Equations 5.3 and 5.5 and are given for the estimated in-situ water to binder ratio used in this study, 0.5, in Table 5.1.

Table 5.1. The density of air is known and its flexural strength can be taken as zero. The flexural strength of the aggregates themselves is considered to be zero as it is considered that all resistance of this material in bulk comes from cohesion that in the context of a composite is determined by the presence of the binder. The density of the particles is taken as that in Table 5.1.

Table 5.1.

5.5.2.2 Macro scale

A separate shape factor may be fitted to each material and in the parallel and perpendicular loading respectively to account for the differing structure in all cases. This then allows for a perfect fit to the experimental data via finding the optimum set of shape factors that are given in Table 5.7. As with the compressive behaviour, based on the experimental data it is apparent that the flexural behaviour of hemp-lime exhibits differing mechanisms under parallel and perpendicular loading. Separate shape functions in these two directions can therefore be considered to account for this although in both cases it will be a function of the same intrinsic variables that are given in Equation 5.26.

Taking the optimised set of values for shape factor and plotting these in turn against the variables in Equation 5.26, it was established that linear relationships could effectively describe the impact of these variables in both directions of loading. If it is assumed that these variables are independent then a combined function can be found by combining the

linear functions and fitting to the data. In this instance the best functions for shape factor were found for parallel and perpendicular loading as Equations 5.49 and 5.50 respectively.

$$s_F^{||} = -31.18\left(\frac{v_{p2}^{||}}{v_p}\right) - 17.30m_b + 1.68C + 0.07\left(IQR_p\right) + 26.80 \qquad 5.49$$

$$s_F^{\perp} = -73.26\left(\frac{v_{p2}^{||}}{v_p}\right) - 18.93m_{b*} + 2.05C + 0.10\left(IQR_p\right) + 30.66 \qquad 5.50$$

The empirically derived shape factors for parallel and perpendicular flexural loading, as well as the measured flexural strength and model flexural strength given by Equations 5.43 and 5.44, are presented in Table 5.7. The degree of fit between the experimental data and modelled values is visualised in Figure 5.5.

From Table 5.7 and Figure 5.5 it can be seen that in general using empirically estimated values of the shape factor, it is possible to model the parallel behaviour to a reasonable level of accuracy, $R^2 = 0.96$, but it is less effective at modelling the perpendicular behaviour, $R^2 = 0.84$ and with some values over or under estimated by nearly 50%. In part this may be attributed to the relatively wide spread within the flexural results that indicate a reasonably high natural variation. It is however also clear that the model is flawed: for one mixture, “coarse 2.2”, negative values of shape factor are proposed indicating that the actual flexural strength lies outside the assumed bounding conditions of a series and parallel arrangement. The biggest discrepancy is again observed in the layer sizing in both parallel and perpendicular loading. Layer size is not assumed to impact shape factor within the model and so this result might be expected. As there was no clear positive or negative actual correlation between layer size and flexural strength, it remains unclear if this is as a result of natural variation or a subtle impact that is not yet understood.

Table 5.7: Shape factors,bi-directional measured flexural strength and bi-directional modeled flexural strenght forvariations of hemp-lime.

Mix	Idealised shape factors		Modelled shape factors		Measured flexural strength (Nmm^{-2})		Modelled flexural strength (Nmm^{-2})	
	$s_F^{\parallel}$	$s_F^{\perp}$	$s_F^{\parallel}$	$s_F^{\perp}$	$\sigma_{Fc}^{\parallel}$	$\sigma_{Fc}^{\perp}$	$\sigma_{Fc}^{\parallel}$	$\sigma_{Fc}^{\perp}$
Fine 2.2	0.176	0.109	0.176	0.111	0.268	0.289	0.267	0.289
Medium 1.8	0.522	0.610	0.488	0.519	0.125	0.102	0.134	0.126
Medium 2.2/ cast 50 45	0.284	0.325	0.270	0.310	0.224	0.211	0.228	0.215
Medium 2.6	0.192	0.319	0.152	0.210	0.292	0.247	0.307	0.286
Coarse 2.2	-0.069	-0.084	-0.0746	-0.103	0.311	0.315	0.313	0.321
Cast 150 45	0.262	0.307	0.270	0.310	0.230	0.216	0.228	0.215
Cast 50 30	0.436	0.477	0.428	0.484	0.158	0.146	0.160	0.144
Cast 50 60	0.119	0.129	0.112	0.136	0.303	0.300	0.306	0.298
Cast 25 45	0.169	0.094	0.270	0.310	0.259	0.283	0.228	0.215

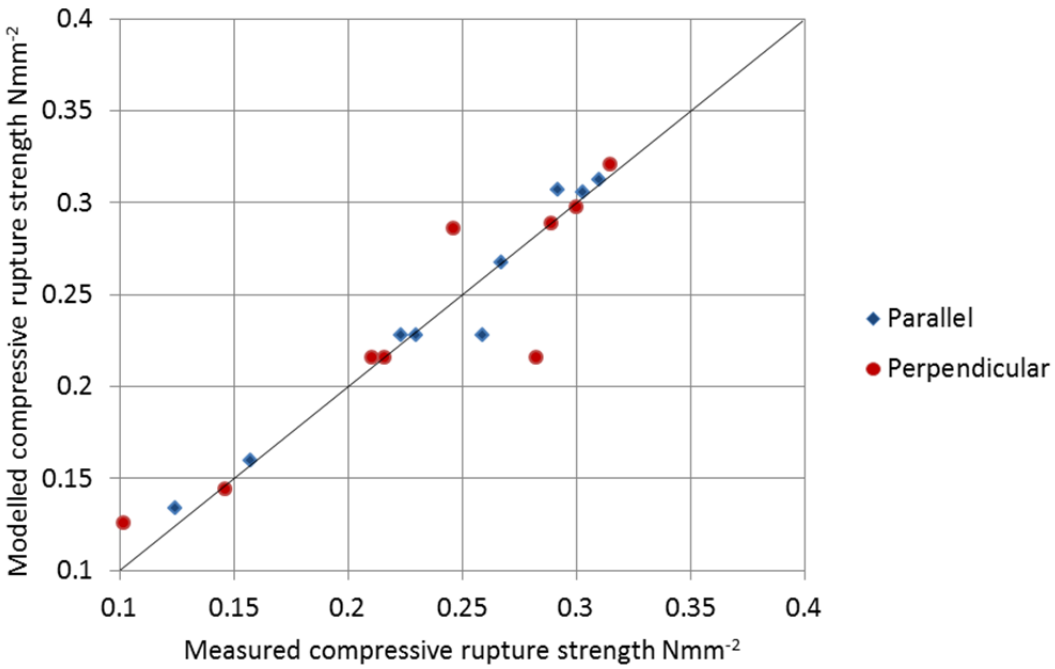

Figure 5.5: Measured Vs modelled parallel and perpendicular to compaction flexural strength of hemp lime produced to a range of constituent and production variations.

5.5.3 Discussion

From Equations 5.49 and 5.50 it is noted that the same variables that determined shape factor for compressive rupture strength were found to determine the shape factor for flexural strength. This is logical as many of the reasons cited for variables impacting or not impacting compressive rupture strength will be applicable here. What is possibly surprising is the omission of the particle aspect ratio which might be expected to have a large impact on the structure determining flexural strength due to increased particle overlap. No such observation was made however which may be a result of the particle aspect ratio being a controlling factor in the particle orientation distribution and thus already accounted for.

The negative impact of the degree of particle alignment and the negative impact of the binder content means both sway the materials behaviour towards a parallel arrangement. In both cases this would seem a reasonable result as an increased alignment of the major particle axis and increased binder mass should both increase the cross sectional area of binder available to transfer load. A positive impact on the shape factor was found in both directions for the spread of particle sizes and the compaction indicating these aspects tend the structure towards that of a series arrangement. It is not apparent why this is the case for compaction, however the particle size spread may be considered to have a physical basis in the concept of “floating particles” previously discussed.

Figure 5.5 shows that a reasonable degree of fit between the experimental and modelled values of bi-directional flexural strength can be achieved using this model with an empirically derived shape function. Given the high variation that was observed in similar specimens the model can be considered reasonable for approximating this parameter within the range of data it has been fitted to. The weakest assumptions made in the model are the same as those for the compressive rupture strength model: the assumed interdependence of the variables determining the shape function and the assumption that the binder is the only structural component. In this case where a negative value of shape factor is obtained in fitting the data, indicating the measured value lies outside the assumed limiting values, the assumptions must be particularly questioned. It is considered in respect of this that the model dose not account for the physical reality in assuming full load transfer in the binder and that the actual behaviour must therefore be thought of as that of composite action. While the binder in this scenario will still be the failing aspect, the assumption that the binder is loaded in flexure is unfounded and the reality might more likely to be a shear loading through adjoining particles to give composite behaviour.

While the model is specifically fitted to hemp-lime in this instance, it is reasonable to assume that it could also be applied to other bio-aggregate composites via the insertion of appropriate composite scale models and the redefining of the empirical relations. Similarly, for the same reasons as stated for the compressive rupture strength, it is apparent that the model is theoretically applicable to a wider range of hemp-lime variations that encompassed in the current data set as long as a definition of the shape function can be found. In this sense the basic form of the model may be considered reasonably universal to many bio-aggregate composites and additional experimental work to generate the required data sets to validate this would be another way to develop this.

5.5.4 Conclusion

The final model proposed was able to predict the parallel and perpendicular flexure strength of hemp-lime to a reasonable degree of accuracy based on a selection of variables that are easily obtained or specified at a practitioner level. The inputs required may be summarised as follows:

- The mass ratios of the constituents used
- The mean aspect ratio of the aggregate
- The interquartile range of the aggregate particles
- The compaction level
- The water to binder ratio of the paste

If flexural strength of the binder paste is known then this allows for the bi-directional flexural strength to be found based on four known measured or specifiable parameters making it uniquely useful to industry.

In general the closeness of fit of the experimental with modelled data was reasonable using empirically calculated values of the shape factor. The main trends seen in the experimental data are all accounted for and results are predicted with sufficient accuracy to be within the error of the experimental data and natural variation of the material.

Currently the model assumes loading solely in the binder skeleton in flexure. This produced for one result a negative shape factor and indicates this assumption was not correct. A better assumption may be that the material acts in composite behaviour and that binder conveys load between particles in shear. A refinement of the model to account for this could simply be altering the constituent scale model of the binder strength to assume shear loading as opposed to flexure. The model also shares the other limitation previously discussed for the thermal conductivity and compressive rupture strength

models, in terms of assuming independence of variables and having limited physical basis for the shape function.

5.6 Modelling Conclusions

In this chapter a universal form of bi-directional behavioural model was proposed that utilised a multi scaled approach and a shape function to describe the complex and orientated structure of the material at the macro scale. This form was then applied to the thermal conductivity, compressive rupture strength and flexural strength of hemp-lime where specific adaptations were applied and empirical relationships for the shape function determined via fitting to the data set collected in the experimental part of this project.

Once optimised, the models were able to fit the experimental results to a very good degree of accuracy within the wide range of constituent and production variables considered within this study. Both parallel and perpendicular behaviour was modelled via a consideration of the degree of orientation within the axes of interest. The model form is considered unique in terms of its use of specifiable variables as inputs and its applicability across a large variety of material variants making it a potentially valuable tool for industry.

Where the model requires development is in some of the underlying assumptions that were made. The primary assumption that must be questioned is the independence of the variables in determining several key material descriptors such as density, degree of orientation and shape factor. This was as a result of the data set collected not assessing the combined impact of variables due to the increased scope this would have added to the project. Additional experimental work to expand the data set could be undertaken to refine these relationships and remove this assumption.

A further assumption made in the modelling of mechanical properties was the consideration of the binder being the sole structural element. This may be considered an invalid assumption in light of the negative shape factor obtained in one set of flexural results. The mechanical modelling of these materials is still a very new field and their behaviour considered to be not well understood in terms of loading paths and mechanisms. Refinements to the model proposed here to account for the contribution of the aggregates or the shear resistance of the binder may prove appropriate as greater understanding of the mechanical properties develops.

The final limitation of the model is the scope of the data set that it is fitted to, which determines the reliable window of behavioural prediction. In general the window of material variables considered here is quite broad and reflective of those used in industry, however as the material and process develops this window may prove to be too small. Expanding the data set to an increased range of variable values and appropriate refinement of empirical relationships could be easily applied to the basic model form to account for this once data are available.

Despite some limitations and concerns over assumptions, the model form and individual models proposed are able to predict three, bi-directional, properties of hemp-lime based only on highly accessible information to a designer or manufacturer. In the context of the large natural variability in the material that can't be accounted for, the model is considered to be a valid and very useful tool to guide design, and steer development of industry. The model is the first to directly link the production of a bio-aggregate composite to the degree of orientation within it and the directional impact on the properties, and so is arguably the first model to directly account for the varying degree of orientation within the material and the directionally dependent impact of variables. In consideration of these points, the objective of the modelling phase of work can be considered to have been met although there is still considerable scope to develop this area of understanding.

6 Conclusions

6.1 Introduction

This chapter presents the main conclusions drawn from this investigation within the context of the project aim and objectives.

Project aim:

To develop an understanding of bio-aggregate composites sufficient for performance criteria led specification of products.

Project objectives:

1. ***Establish a method of classifying and numerically analysing the degree of orientation within the internal structure of bio-aggregate concretes.***
2. ***Link the variables associated to production method to the internal structure and key physical properties of bio-aggregate composites.***
3. ***Link the constituent variables to the internal structure and key physical properties of bio-aggregate composites.***
4. ***Model key physical properties of bio-aggregate composites in a directional context based on the internal structure and main design variables.***

The conclusion is presented in three sections covering the methods applied, experimental results and theoretical modelling that combine to produce this thesis and specifically address the separate objectives. Finally, recommendations both for industry and for additional work are briefly put forward based on the outcomes.

6.2 Methods

Most experimental processes used in this project were previously established and were applied here as closely as could reasonably be achieved so as to facilitate comparability between this and other studies. However, where no method was pre-existing or there were perceived flaws with previous approaches, new or alternative approaches have been used.

Innovations have been developed not only with respect to established procedures, but in addition an entirely new methodology has been established to better understand performance characteristics.

6.2.1 Innovations to established procedures

The two key proposed enhancements to otherwise established procedures were in the production of specimens and the analysis of compressive cube tests:

- A theoretical basis for the determination of water content to be used in lime based bio-aggregate composites was proposed to isolate the variable of in-situ water to binder ratio. In-situ water to binder ratio has not been effectively isolated in preceding work and could be a useful basis for on-site specification of differing mixes where previously rules of thumb have been applied.
- A material compressive characteristic, compressive rupture stress, was defined representing a change in behaviour from composite to cohesive that enables comparison of cube tests conducted parallel and perpendicular to compaction. Compressive rupture stress was applied successfully as a metric to allow comparison between parallel and perpendicular loading and is considered an improvement on reporting a stress and a set value of strain as has been done previously.

6.2.2 Development of new methodology

No pre-existing method for the direct assessment and comparison of the degree of orientation present in the particle arrangement of bio-aggregate composites of any form was found to exist. A method was proposed based on available precedents in other materials using two dimensional image analyses. The method was developed via a pilot-study that considered several approaches of which the key finding were:

- Two dimensional image analysis provides sufficient data to compare material and infer but not directly asses 3D topology. It requires a larger number of destructive tests to provide a reasonable sample size compared to a single, non-destructive, computer tomography scan.
- The method is sufficient for identifying trends in materials when used in the window of variables considered in this study but is considered to have limitations when used with more compact materials.

- The low cost of the method was seen as the biggest advantage over computer tomography scanning in this project.
- Consistency of the method application is critical due to the sensitivity of the results to the image processing.

The establishment of this novel method fulfilled the first objective of this project and facilitated the experimental program subsequently undertaken. The added benefits of CT scanning were also demonstrated and may be studied further.

6.3 Experimental conclusions

The experimental phases of work set out to address the second and third objectives: to link the production and constituent variables of hemp-lime respectively to the internal structure and key physical properties. The experimental phase was unique in its consideration of bi-directional properties and implementation of the image analysis method for assessing internal orientation. Both implementation and constituent variables within hemp-lime were considered and it was shown that in most cases these have a directionally dependent impact on the material's properties.

6.3.1 Constituent variables

The constituent variables assessed were the particle size distribution and the binder content. The key findings to result from this investigation were:

- A negative correlation between binder content and degree of particle orientation resulting in directionally dependent impacts on thermal conductivity and mechanical performance.
- A complex relationship between the aggregate particle size distribution and both orientation and physical properties that is dependent both on the spread of particle sizes, dominant in mechanical behaviour, and the aspect ratio of particles, dominant in thermal behaviour and particle orientation.

Both of these findings are original in the field and enhance understanding of how constituent variables impact the physical properties of bio-aggregate composites through the internal structure. The outcomes of this experimental work, both in terms of the data set produced and analysis, directly meet the requirements of the second project objective.

6.3.2 Production variables

The production variables assessed were the implementation method: casting or projection forming, the level of compaction and the size of layers. The key findings to result from this investigation were:

- A higher level of particle orientation was found in projection formed material compared to equivalent cast material. The observation is considered to be a direct result of the process and produced an increase in anisotropy in the material's mechanical and thermal properties.
- A higher variation in the mechanical performance of projection formed material compared to equivalent cast material attributed to a possible issue with the particular projection method used in the study: an auger fed air stream delivery of aggregates.
- A positive correlation between compaction and degree of particle orientation in cast material that results in a directionally dependent impact on the compressive rupture strength, flexural strength and thermal conductivity.
- No discernible impact of casting layer size in the range of 25mm to 150mm layers was seen on either the degree of particle orientation or on the material's physical properties.

All of these findings are original to this study and enhance understanding of the development of the properties of bio-aggregate composites. The outcomes of this experimental work, both in terms of the data set produced and analysis, directly meet the requirements of the third project objective.

The experimental parts of this project can be considered highly successful in meeting the specific objectives targeted. A greatly improved understanding of how the internal structure of bio-aggregate composites are determined and how this impacts the directional behaviour has been achieved and a significant data set has been produced that considers the wide range of variables that are relevant to industry.

6.4 Modelling bio-aggregate composite behaviour with respect to an orientated internal structure

The concluding part of the work conducted in this project was to apply the insight gained from the experimental phase to modelling the behaviour of the materials in a

way that accounts for the observations of an orientated internal structure. A universal multi scale micromechanical system was proposed based on modelling the behaviour of the individual constituents and combining these into a macro scale model that accounts for their volumetric proportions and arrangement. The models used at the constituent scale were varied with application and constituent while at the macro scale an appropriate form of weighted mean between parallel and series arrangements of the constituents, assumed to be the limiting cases, was applied. The weighting or shape factor used was empirically derived and uniquely accounted for the degree of orientation and wider arrangement of the constituents in the orientation of interest.

The key findings to result from applying the model to the experimental data were:

- Multi-scale, empirically weighted models are able to predict thermal and mechanical experimental results to a high degree of accuracy sufficient to be within the material's perceived natural variation. Within the range of the material considered in this study, the model may therefore be considered a useful tool to guide performance-based design and to develop products.
- The assumption of variables having an independent impact on the material structure is seen as a current aspect that could be improved via the development of the empirical relationships based on an increased data set.
- The assumption that the binder is the sole structural component when considering the compressive rupture strength and flexural strength is considered to be only a first approximation and the model requires modification to account for other more subtle structural components.
- The universal modelling approach can be considered applicable to other bio-aggregate composites and to be easily expanded to account for other variables with an increased data set making possible application wide ranging.

The models proposed can be considered unique in their possible application by predicting behaviour based on parameters that may be specified and properties that may be measured. The range of material variations accounted for is also large, further increasing applicability. The developed models should directly enable both criteria led specification of hemp-lime and optimisation.

While similarities between the models proposed here and elsewhere exist, the exact form is original to this study and allows for possible criteria led design of hemp-lime composites within the range of the current fitted data set. This goes some considerable way to meeting the fourth objective and the overall project aim. Arguably In order to fully satisfy the project aim the model and underlying theory would need to be proven

for additional bio-aggregate composites and ideally a wider range of variables which could become the focus of future work. Within the context of current industry use however that almost exclusively uses hemp aggregate and lime binders within the range of formulations and processes considered in this thesis, the aim of the project can be considered satisfactorily met.

6.5 Recommendations for further work

The outcomes from this project have highlighted several areas that could benefit from additional investigation and several previously unconsidered avenues for further work that have the potential to be fruitful have been uncovered:

- Further investigation into the compatibility of lime as a bio-aggregate binder and the development of more reliable alternatives.
- An experimental study of what impacts the in-situ water to binder ratio when a water activated binder is used with a porous bio-aggregate.
- Refinement of the proposed method of assessing the degree of particle orientation within bio-aggregate composites or proposal of a superior method to ensure validity of results across a wide range of materials and particularly those formed with high degrees of compaction.
- An experimental investigation of the impact of production and constituent variables where independence is not assumed.
- A full assessment of the way different aspects of particle size distribution impact structure and behaviour of bio-aggregate composite materials and a development towards an optimised grading of particles for differing applications.
- Development of the model form proposed in this work or the proposal of a superior model to remove the assumptions of independence of variables and the binder as the sole structural contributor.
- Integration of behavioural models of bio-aggregate composites into an optimisation processes to aid the development of enhanced products and processes.

6.6 Recommendations for industry

The project has identified several key findings that should directly impact industry and produced several outputs that could also have direct benefit:

- The structure and behaviour of hemp-lime have conclusively been shown to be anisotropic; many variables have also been shown to have a directionally dependent impact on the behaviour. To therefore appraise a specific bio-aggregate composite system, tests should be conducted in two directions and data presented appropriately by manufacturers of systems and units.
- The bi-directional properties offer significant performance differences that could be exploited by manufacturers of precast units: the parallel to compaction thermal conductivity can be almost 20% lower while changing the orientation of the block in a wall could have almost negligible difference on compressive and flexural strength.
- Projection forming using an auger fed airstream may result in inconsistent material and reduce performance compared to that predicted.
- The data sets provided for cast material could be used as a direct guide for specification of material to set criteria and be used to inform product development.
- The models proposed could be used as design tools to predict performance in a criteria led specification scenario and as an optimisation tool in the design of products.

7 References

AÏT OUMEZIANE, Y., MOISSETTE, S., BART, M., COLLET, F., PRETOT, S., et al. 2017. Influence of hysteresis on the transient hygrothermal response of a hemp concrete wall. *Journal of Building Performance Simulation,* 10**,** 256-271.

AKKAYA, Y., SHAH, S. & ANKENMAN, B. 2001. Effect of Fiber Dispersion on Multiple Cracking of Cement Composites. *Journal of Engineering Mechanics,* 127**,** 311-316.

AL-AJLAN, S. A. 2006. Measurements of thermal properties of insulation materials by using transient plane source technique. *Applied Thermal Engineering,* 26**,** 2184-2191.

ALCORN, A. & DONN, M. 2010. Life cycle potential of strawbale and timber for carbon sequestration in house construction. *2nd International Conference on Sustainable Construction Materials and Technologies, Ancona, Italy.*

ALLIN, S. 2005. *Building with hemp,* Kenmare, Kerry, SeedPress.

AMZIANE, S., COLLET, F., LAWRENCE, M., MAGNIONT, C., PICANDET, V., et al. 2017a. Recommendation of the RILEM TC 236-BBM: characterisation testing of hemp shiv to determine the initial water content, water absorption, dry density, particle size distribution and thermal conductivity. *Materials and Structures,* 50**,** 167.

AMZIANE, S., NOZAHIC, V. & SONEBI, M. 2015. Design of mechanically enhanced concrete using hemp shiv. *First international conference on bio-based building materials* Clermont-Ferrand, France.

AMZIANE, S., NOZAHIC, V. & SONEBI, M. 2017b. Water absorption of plant aggregate. *In:* AMZIANE, S. & COLLET, F. (eds.) *Bio-aggregates Based Building Materials : State-of-the-Art Report of the RILEM Technical Committee 236-BBM.* Dordrecht: Springer Netherlands.

ARNAUD, L. 2000. Mechanical and thermal properties of hemp mortars and wools: experimental and theoretical approaches. *Bioresource Hemp 2000 & other fibre crops.* Wolfsburg: Nova Instatute, Hurth Germany.

ARNAUD, L., AMZIANE, S., NOZAHIC, V. & GOURLAY, E. 2013a. Mechanical Behaviour. *Bio-aggregate-based Building Materials.* John Wiley & Sons.

ARNAUD, L. & GOURLAY, E. 2012. Experimental study of parameters influencing mechanical properties of hemp concretes. *Construction and Building Materials,* 28**,** 50-56.

ARNAUD, L., SAMRI, D. & GOURLAY, É. 2013b. Hygrothermal Behaviour of Hempcrete. *Bio-aggregate-based Building Materials.* John Wiley & Sons.

ASKELAND, D. R. & PHULÉ, P. P. 2006. *The science and engineering of materials,* Toronto, Thomson.

BADEL, E., DELISEE, C. & LUX, J. 2008. 3D structural characterisation, deformation measurements and assessment of low-density wood fibreboard under compression: The use of X-ray microtomography. *Composites Science and Technology,* 68**,** 1654-1663.

BAGHAEI, B., SKRIFVARS, M., SALEHI, M., BASHIR, T., RISSANEN, M., et al. 2014. Novel aligned hemp fibre reinforcement for structural biocomposites: Porosity, water absorption, mechanical performances and viscoelastic behaviour. *Composites Part A: Applied Science and Manufacturing,* 61**,** 1-12.

BALČIŪNAS, G., VĖJELIS, S., VAITKUS, S. & KAIRYTĖ, A. 2013. Physical Properties and Structure of Composite Made by Using Hemp Hurds and Different Binding Materials. *Procedia Engineering,* 57**,** 159-166.

BENFRATELLO, S., CAPITANO, C., PERI, G., RIZZO, G., SCACCIANOCE, G., et al. 2013. Thermal and structural properties of a hemp–lime biocomposite. *Construction and Building Materials,* 48**,** 745-754.

BENITHA SANDRINE, U., ISABELLE, V., TON HOANG, M. & CHADI, M. 2015. Influence of chemical modification on hemp–starch concrete. *Construction and Building Materials,* 81**,** 208-215.

BESSA, I., CASTELO BRANCO, V. & SOARES, J. 2012. Evaluation of different digital image processing software for aggregates and hot mix asphalt characterizations. *Construction and Building Materials,* 37**,** 370-378.

BEVAN, R., WOOLLEY, T., PRITCHETT, I., CARPENTER, R., WALKER, P., et al. 2008. *Hemp Lime Construction: a guide to building with hemp lime composites*, BRE Press.

BOUYER, T. 2008. De la qualité de matériau béton-chanvre: Rapport destage. ENGREF.

BRITISH STANDARDS 1999. *BS EN 1015-11:1999 - Methods of test for mortar for masonry Part 11: determination of flexural and compressive strength of hardened mortar*.

BRITISH STANDARDS 2005. *BS EN 196-1:2005 - Methods of testing cement. Determination of strength*.

BRITISH STANDARDS 2007. *BSEN 12667:2001 - Thermal performance of building materials and products–Determination of thermal resistance by means of guarded hot plate and heat flow meter methods Products of high and medium thermal resistance*.

BRITISH STANDARDS 2009. BS EN 12390-3:2009 - Testing hardened concrete. Compressive strength of test specimens.

BRITISH STANDARDS 2012. *BS EN 933-1:2012 - Tests for geometrical properties of aggregates. Part 1: determination of particle size distribution. Sieving method*.

BRITISH STANDARDS 2013a. *BS EN 826:2013 - Thermal insulating products for building applications. Determination of compression behaviour*.

BRITISH STANDARDS 2013b. *BS EN 12085:2013 - Thermal insulating products for building applications. Determination of linear dimensions of test specimens*.

BRZYSKI, P., BARNAT-HUNEK, D., SUCHORAB, Z. & ŁAGÓD, G. 2017. Composite Materials Based on Hemp and Flax for Low-Energy Buildings. *Materials,* 10**,** 510.

BUSBRIDGE, R. & RHYDWEN, R. 2010. An investigation of the thermal properties of hemp and clay monolithic walls. *The School of Computing and Technology 5th Annual Conference.* University of East London.

BÜTSCHI, P.-Y., DESCHENAUX, C., MIAO, B. & SRIVASTAVA, N. 2004. *Utilisation du chanvre pour la préfabrication d'éléments de construction*, Département de génie civil, Faculté d'ingénierie, Université de Moncton.

CENTRE SCIENTIFIQUE ET TECHNIQUE DU BÂTIMENT 2011. Analyse des caracteristiques des systemes constructifs non industrialises. .

CEREZO, V. 2005. *Propriétés mécaniques, thermiques et acoustiques d'un matériau à base de particules végétales : approche expérimentale et modélisation théorique* PhD, L'Institut National des Sciences Appliquées de Lyon.

CEYTE, I. 2008. Béton de chanvre, définition des caractéristiques mécaniques de la chènevotte *Travail de Fin d'Études, ENTPE,* 155**,** 2008.

CHABANNES, M., BÉNÉZET, J.-C., CLERC, L. & GARCIA-DIAZ, E. 2014. Use of raw rice husk as natural aggregate in a lightweight insulating concrete: An innovative application. *Construction and Building Materials,* 70**,** 428-438.

CHABANNES, M., GARCIA-DIAZ, E., CLERC, L. & BÉNÉZET, J.-C. 2015a. Studying the hardening and mechanical performances of rice husk and hemp-based building materials cured under natural and accelerated carbonation. *Construction and Building Materials,* 94**,** 105-115.

CHABANNES, M., NOZAHIC, V. & AMZIANE, S. 2015b. Design and multi-physical properties of a new insulating concrete using sunflower stem aggregates and eco-friendly binders. *Materials and Structures,* 48**,** 1815-1829.

CHABRIAC, P. A., GOURDON, E., GLE, P., FABBRI, A. & LENORMAND, H. 2016. Agricultural by-products for building insulation: Acoustical characterization and modeling to predict micro-structural parameters. *Construction and Building Materials,* 112**,** 158-167.

CIGASOVA, J., STEVULOVA, N. & JUNAK, J. 2013. Properties monitoring of fibrous composites based on hemp hurds with different mean particle size. *Pollack Periodica,* 8**,** 41-46.

COENEN, A. R., KUTAY, M. E., SEFIDMAZGI, N. R. & BAHIA, H. U. 2012. Aggregate structure characterisation of asphalt mixtures using two-dimensional image analysis. *Road Materials and Pavement Design,* 13**,** 433-454.

COLLET, F. 2004. *Caractérisation hydrique et thermique de matériaux de génie civil à faibles impacts environnementaux (Characterization of water and heat engineering materials with low environmental impacts).* PhD, INSA de Rennes.

COLLET, F. 2017. Hygric and Thermal Properties of Bio-aggregate Based Building Materials. *In:* AMZIANE, S. & COLLET, F. (eds.) *Bio-aggregates Based Building Materials : State-of-the-Art Report of the RILEM Technical Committee 236-BBM.* Dordrecht: Springer Netherlands.

COLLET, F., BART, M., SERRES, L. & MIRIEL, J. 2008. Porous structure and water vapour sorption of hemp-based materials. *Construction and Building Materials,* 22**,** 1271-1280.

COLLET, F. & PRETOT, S. 2014. Experimental highlight of hygrothermal phenomena in hemp concrete wall. *Building and Environment,* 82**,** 459-466.

COLLET, F. & PRÉTOT, S. 2014. Thermal conductivity of hemp concretes: Variation with formulation, density and water content. *Construction and Building Materials,* 65**,** 612-619.

CONSTRUIRE EN CHANVRE 2009. Règles professionnelles d'exécution d'ouvrages en Béton de Chanvre. SEBTP.

COQUARD, R., COMENT, E., FLASQUIN, G. & BAILLIS, D. 2013. Analysis of the hot-disk technique applied to low-density insulating materials. *International Journal of Thermal Sciences,* 65**,** 242-253.

COURGEY, S. 1993. La construction de murs à base de fibres de chanvre.

DE BRUIJN, P. 2008. *Hemp conctretes: Mechanical properties using both shivs and fibres.* Sveriges Lantbruksuniversitet.

DE BRUIJN, P., JEPPSSON, K.-H., SANDIN, K. & NILSSON, C. 2009. Mechanical properties of lime–hemp concrete containing shives and fibres. *Biosystems Engineering,* 103**,** 474-479.

DE BRUIJN, P. & JOHANSSON, P. 2013. Moisture fixation and thermal properties of lime–hemp concrete. *Construction and Building Materials,* 47**,** 1235-1242.

DECORTE, T. 2011. Fibre hemp and marihuana: assessing the differences between distinct varieties. *Working Paper Series on Policing.* International police executive symposium.

DEPARTMENT FOR BUSINESS INNOVATION AND SKILLS 2010. Low Carbon Construction - Final Report. Crown.

DINH, T., MAGNIONT, C., COUTAND, M. & ESCADEILLAS, G. 2015. Hemp concrete using innovative pozzolanic binder. *First international conference on bio-based building materials.* Clermont-Ferrand, France.

DIQUÉLOU, Y., GOURLAY, E., ARNAUD, L. & KUREK, B. 2015. Impact of hemp shiv on cement setting and hardening: Influence of the extracted components from the aggregates and study of the interfaces with the inorganic matrix. *Cement and Concrete Composites,* 55**,** 112-121.

DRAŽIĆ, S., SLADOJE, N. & LINDBLAD, J. 2016. Estimation of Feret's diameter from pixel coverage representation of a shape. *Pattern Recognition Letters,* 80**,** 37-45.

DUFFY, E., LAWRENCE, M. & WALKER, P. 2014. Hemp-Lime: Highlighting room for improvement. *International Congress on Materials and Structural Stability.* Rabat.

ELFORDY, S., LUCAS, F., TANCRET, F., SCUDELLER, Y. & GOUDET, L. 2008. Mechanical and thermal properties of lime and hemp concrete ("hempcrete") manufactured by a projection process. *Construction and Building Materials,* 22**,** 2116-2123.

ESCADEILLAS, G., MAGNIONT, C., AMZIANE, S. & NOZAHIC, V. 2013. Binders. *Bio-aggregate-based Building Materials.* John Wiley & Sons, Inc.

EVRARD, A. 2003. Beton de chanvre: Synthèse de propriétés physiques. Association Construire en Chanvre.

EVRARD, A. 2006. Sorption behaviour of Lime-Hemp Concrete and its relation to indoor comfort and energy demand. *Proceedings of the 23rd Conference on Passive and Low Energy Architecture, Geneva, Switzerland.*

EVRARD, A. 2008. *Transient hygrothermal behaviour of lime-hemp materials.* PhD, Universite catholique de louvain.

EVRARD, A. & DE HERDE, A. 2010. Hygrothermal performance of lime-hemp wall assemblies. *Journal of Building Physics,* 34**,** 5-25.

FAN, M. Z., DINWOODIE, J. M., BONFIELD, P. W. & BREESE, M. C. 2004. Dimensional instability of cement bonded particleboard: Modelling CBPB as a composite of two materials. *Wood Science and Technology,* 37**,** 373-383.

FANG, L., CLAUSEN, G. & FANGER, P. O. 1998. Impact of temperature and humidity on the perception of indoor air quality. *Indoor air,* 8**,** 80-90.

FEI VISUALIZATION SCIENCES GROUP 2007. Avizo Fire 8.

FEI VISUALIZATION SCIENCES GROUP 2014. Avizo 8, Avizo User's Guide, English. Konrad-Zuse-Zentrum fu¨r Informationstechnik, Berlin, Germanry.

FERREIRA, T. & RASB, W. 2012. ImageJ user guide. ImageJ/Fiji, 1.

FIELD, C. B., BARROS, V. R., MACH, K. J., MASTRANDREA, M. D., AALST, M. V., et al. 2014. Technical Summary. *In:* FIELD, C. B., BARROS, V. R., DOKKEN, D. J., MACH, K. J., MASTRANDREA, M. D., et al. (eds.) *Climate Change 2014: Impacts, Adaptation, and Vulnerability. Part A: Global and Sectoral Aspects. Contribution of Working Group II to the Fifth Assessment Report of the Intergovernmental Panel on Climate Change.* Cambridge, United Kingdom and New York, NY, USA: Cambridge University Press.

FLIEGENER, S., LUKE, M. & GUMBSCH, P. 2014. 3D microstructure modeling of long fiber reinforced thermoplastics. *Composites Science and Technology,* 104**,** 136-145.

FRANZONI, E. 2011. Materials Selection for Green Buildings: which Tools for Engineers and Architects? *Procedia Engineering,* 21**,** 883-890.

GARCIA-JALDON, C. 1995. *Caracterisation et morphologique et chimique du chanvre (Cannabis sativa). Pretraitement a la vapeur et valorisation (Morphological and chemical characterization of hemp (Cannabis sativa) . Development of steaming pretreatment).* PhD.

GLÉ, P., GOURDON, E. & ARNAUD, L. 2011. Acoustical properties of materials made of vegetable particles with several scales of porosity. *Applied Acoustics,* 72**,** 249-259.

GLÉ, P., GOURDON, E. & ARNAUD, L. 2012. Modelling of the acoustical properties of hemp particles. *Construction and Building Materials,* 37**,** 801-811.

GONG, A., KAMDEM, D. & HARICHANDRAN, R. 2004. Compression tests on wood-cement particle composites made of CCA-treated wood removed from service. *Environmental Impacts Of Preservative-Treated Wood Conference.*

GOODHEW, S. 2016. *Sustainable construction processes: A resource text*, John Wiley & Sons.

GOURLAY, E. 2008. Caractérisation de la chènevotte et influence des caractéristiques de la chènevotte sur celles des bétons de chanvre-chaux Rapport de Stage MSP.

GROSS, C. D. 2013. *Structural enhancement of timber framing using hemp-lime.* PhD, University of Bath.

GÜMÜŞKAYA, E., USTA, M. & BALABAN, M. 2007. Carbohydrate components and crystalline structure of organosolv hemp (Cannabis sativa L.) bast fibers pulp. *Bioresource technology,* 98**,** 491-497.

HAMMOND, G. & JONES, C. 2008. *Inventory of Carbon & Energy: ICE*, Sustainable Energy Research Team, Department of Mechanical Engineering, University of Bath.

HAMZAH, M., VON, W. & ABDULLAH, N. 2013. Effects of Compactor Types on Aggregate Orientation of Asphalt Mixtures. *International Journal of Engineering-Transactions A: Basics,* 26**,** 677.

HAN, J. 2015. *Garbage mountain of Mumbai* [Online]. FT Photo Diary: Financial Times Available: http://blogs.ft.com/photo-diary/tag/landfill/ 2017].

HANKINSON, R. 1921. Investigation of crushing strength of spruce at varying angles of grain. *Air service information circular,* 3**,** 130.

HASNAIN, S. M. 1998. Review on sustainable thermal energy storage technologies, Part I: heat storage materials and techniques. *Energy Conversion and Management,* 39**,** 1127-1138.

HILL, R. 1965. A self-consistent mechanics of composite materials. *Journal of the Mechanics and Physics of Solids,* 13**,** 213-222.

HIRST, E., WALKER, P., PAINE, K. & YATES, T. 2010. Characterisation of low density hemp-lime composite building materials under compression loading. *Second international conference on sustainable construction materials and technologies.*

HIRST, E., WALKER, P., PAINE, K. & YATES, T. 2012. Characteristics of low-density hemp-lime building materials. *Construction Materials,* 165**,** 15 - 23.

HIRST, E. A. J. 2013. *Characterisation of hemp-lime as a composite building material.* PhD, University of Bath.

HOLMBERG, H. 2000. Influence of grain angle on Brinell hardness of Scots pine (Pinus sylvestris L.). *Holz als Roh- und Werkstoff,* 58**,** 91-95.

HUOVILA, P. 2007. *Buildings and climate change: status, challenges, and opportunities*, UNEP/Earthprint.

HUSTACHE, Y. & ARNAUD, L. 2008. Synthèse des connaissances sur les bétons et mortiers de chanvre. Construire en Chanvre.

IP, K. & MILLER, A. 2012. Life cycle greenhouse gas emissions of hemp–lime wall constructions in the UK. *Resources, Conservation and Recycling,* 69**,** 1-9.

JIA, X., ANSELL, M., HUSSAIN, A., LAWRENCE, M. & JIANG, Y. 2017. Physical characterisation of hemp shiv: Cell wall structure and porosity. *ICBBM & ECOGRAFI 2017.* Leeds.

JIANG, S., KANG, Y. & SUN, Z. 2009. A digital image method for analysis of soil pores. *In:* LI, D. & ZHAO, C. (eds.) *Computer and Computing Technologies in Agriculture II, Volume 2: The Second IFIP International Conference on Computer and Computing Technologies in Agriculture (CCTA2008), October 18-20, 2008, Beijing, China.* Boston, MA: Springer US.

JOHNSON, R. 2010. Hemp as an Agricultural Commodity. Library of Congress Washingto DC Congressional Research Service.

KANG, S.-T. & KIM, J.-K. 2011. The relation between fibre orientation and tensile behaviour in an Ultra High Performance Fiber Reinforced Cementitious Composites (UHPFRCC). *Cement and Concrete Research,* 41**,** 1001-1014.

KAOUACHE, B., ADDIEGO, F., HIVER, J.-M., FERRY, O., TONIAZZO, V., et al. 2013. In Situ Mechanical Characterization of Short Vegetal Fibre-Reinforced High-Density

Polyethylene Using X-Ray Tomography. *Macromolecular Materials and Engineering,* 298**,** 1269-1274.

KARUS, M. 2005. European hemp industry 2001 till 2004: Cultivation, raw materials, products and trends. European Industrial Hemp Association.

KASHTANJEVA, A., SONEBI, M. & AMZIANE, S. 2015. Investigation of the mechanical performance and drying shrinkage of hemp concrete. *First International Conference of Bio-based Building materials* Clermont-Ferrand, France.

KASTNER, J., KICKINGER, R. & SALABERGER, D. 2011. High-resolution X-ray computed tomography for 3D microstructure characterization of a cellulose particle filled polymer foam. *Journal of Cellular Plastics,* 47**,** 567-578.

KAZEMI NAJAFI, S., ABBASI MARASHT, A. & EBRAHIMI, G. 2007. Prediction of ultrasonic wave velocity in particleboard and fiberboard. *Journal of Materials Science,* 42**,** 789-793.

KHAZMA, M., GOULLIEUX, A., DHEILLY, R.-M., ROUGIER, A. & QUÉNEUDEC, M. 2014. Optimization of flax shive-cementitious composites: Impact of different aggregate treatments using linseed oil. *Industrial Crops and Products,* 61**,** 442-452.

KIDALOVA, L., STEVULOVA, N., TERPAKOVA, E. & SICAKOVA, A. 2011. Use of magnesium oxide-cement binder in composites based on hemp shives. *Journal of Environmental Science and Engineering,* 5.

KIDALOVA, L., STEVULOVA, N., TERPAKOVA, E. & SICAKOVA, A. 2012. Utilization of alternative materials in lightweight composites. *Journal of Cleaner Production,* 34**,** 116-119.

KIOY, S. 2013. *Lime-hemp composites: compressive strength and resistance to fungal attacks. .* MEng University of Bath.

KRISCHER, O. & KAST, W. 1978. *Die wissenschaftlichen Grundlagen der Trocknungstechnik,* Berlin, Springer-Verlag.

KUTAY, M. E., ARAMBULA, E., GIBSON, N. & YOUTCHEFF, J. 2010. Three-dimensional image processing methods to identify and characterise aggregates in compacted asphalt mixtures. *International Journal of Pavement Engineering,* 11**,** 511-528.

LAIDOUDI, B., FLAMIN, C., CRIGNY, A., FERRARI, J., et al. 2015. Bio based concrete with crushed rape straw, a good alternative to develop an affordable bio based concrete for

construction and regeneration. *First international conference on bio-based building materials* Clermont-Ferrand, France.

LANAS, J. & ALVAREZ-GALINDO, J. I. 2003. Masonry repair lime-based mortars: factors affecting the mechanical behaviour. *Cement and Concrete Research,* 33**,** 1867-1876.

LANGER, W. H. & ARBOGAST, B. F. 2002. Environmental Impacts Of Mining Natural Aggregate. *In:* FABBRI, A. G., GAÁL, G. & MCCAMMON, R. B. (eds.) *Deposit and Geoenvironmental Models for Resource Exploitation and Environmental Security.* Dordrecht: Springer Netherlands.

LANOS, C., COLLET, F., LENAIN, G. & HUSTACHE, Y. 2013. Formulation and Implementation. *Bio-aggregate-based Building Materials.* John Wiley & Sons.

LAWRENCE, M. 2013. The use of bio-based materials to reduce the environmental impact of construction. *Civil and Environmental Research,* 5**,** 136-141.

LAWRENCE, M. & JIANG, Y. 2017. Porosity, Pore Size Distribution, Micro-structure. *In:* AMZIANE, S. & COLLET, F. (eds.) *Bio-aggregates Based Building Materials : State-of-the-Art Report of the RILEM Technical Committee 236-BBM.* Dordrecht: Springer Netherlands.

LAWRENCE, M., SHEA, A., WALKER, P. & DE WILDE, P. 2011. Hygrothermal perfomance of bio-based insulation materials. *Construction Materials,* 166**,** 257 - 263.

LAWRENCE, R. 2006. *A study of carbonation in non-hydraulic lime mortars.* PhD, University of Bath.

LAWRENCE, R. M., MAYS, T. J., RIGBY, S. P., WALKER, P. & D'AYALA, D. 2007. Effects of carbonation on the pore structure of non-hydraulic lime mortars. *Cement and Concrete Research,* 37**,** 1059-1069.

LE, A. T., GACOIN, A., LI, A., MAI, T. H. & EL WAKIL, N. 2015. Influence of various starch/hemp mixtures on mechanical and acoustical behaviour of starch-hemp composite materials. *Composites Part B: Engineering,* 75**,** 201-211.

LE, A. T., GACOIN, A., LI, A., MAI, T. H., REBAY, M., et al. 2014. Experimental investigation on the mechanical performance of starch–hemp composite materials. *Construction and Building Materials,* 61**,** 106-113.

LE TROËDEC, M., DALMAY, P., PATAPY, C., PEYRATOUT, C., SMITH, A., et al. 2011. Mechanical properties of hemp-lime reinforced mortars: influence of the chemical treatment of fibers. *Journal of Composite Materials,* 45**,** 2347-2357.

LI, D., VELDE, B. & ZHANG, T. 2004. Observations of pores and aggregates during aggregation in some clay-rich agricultural soils as seen in 2D image analysis. *Geoderma,* 118**,** 191-207.

LIU, J., LI, C., LIU, J., CUI, G. & YANG, Z. 2013. Study on 3D spatial distribution of steel fibers in fiber reinforced cementitious composites through micro-CT technique. *Construction and Building Materials,* 48**,** 656-661.

LOG, T. & GUSTAFSSON, S. E. 1995. Transient plane source (TPS) technique for measuring thermal transport properties of building materials. *Fire and Materials,* 19**,** 43-49.

LUX, J., AHMADI, A., GOBBÉ, C. & DELISÉE, C. 2006. Macroscopic thermal properties of real fibrous materials: Volume averaging method and 3D image analysis. *International Journal of Heat and Mass Transfer,* 49**,** 1958-1973.

MAGNIONT, C. & ESCADEILLAS, G. 2017. Chemical Composition of Bio-aggregates and Their Interactions with Mineral Binders. *In:* AMZIANE, S. & COLLET, F. (eds.) *Bio-aggregates Based Building Materials : State-of-the-Art Report of the RILEM Technical Committee 236-BBM.* Dordrecht: Springer Netherlands.

MAGNIONT, C., ESCADEILLAS, G., COUTAND, M. & OMS-MULTON, C. 2012. Use of plant aggregates in building ecomaterials. *European Journal of Environmental and Civil Engineering,* 16**,** s17-s33.

MAROULIS, Z. B., KROKIDA, M. K. & RAHMAN, M. S. 2002. A structural generic model to predict the effective thermal conductivity of fruits and vegetables during drying. *Journal of Food Engineering,* 52**,** 47-52.

MAZHOUD, B., COLLET, F., PRETOT, S. & LANOS, C. 2017. Development and hygric and thermal characterization of hemp-clay composite. *European Journal of Environmental and Civil Engineering***,** 1-11.

MEYER, C. 2009. The greening of the concrete industry. *Cement and Concrete Composites,* 31**,** 601-605.

MICALES, J. A. & SKOG, K. E. 1997. The decomposition of forest products in landfills. *International Biodeterioration & Biodegradation,* 39**,** 145-158.

MICHEL, A. & BILLINGTON, S. 2014. Nonlinear Constitutive Model for Anisotropic Biobased Composite Materials. *Journal of Engineering Mechanics,* 140.

MILLER, A. & IP, K. 2013. Sustainable Construction Materials. *In:* YAO, R. (ed.) *Design and Management of Sustainable Built Environments.* Springer London.

MILUTIENĖ, E., STANIŠKIS, J., KRUČIUS, A., AUGULIENĖ, V. & ARDICKAS, D. 2012. Increase in buildings sustainability by using renewable materials and energy. *Clean Technologies and Environmental Policy,* 14**,** 1075-1084.

MING-KUEI, H. 1962. Visual pattern recognition by moment invariants. *Information Theory, IRE Transactions on,* 8**,** 179-187.

MOM, S., DARTOIS, S., HAMIDA, A. B., DUMONTET, H. & BOUSSA, H. 2012. Non linear micromechanical modeling of hemp concretes. *15th European conference on composite materials (ECCM15).* Venice.

MOSQUERA, M. J., SILVA, B., PRIETO, B. & RUIZ-HERRERA, E. 2006. Addition of cement to lime-based mortars: Effect on pore structure and vapour transport. *Cement and Concrete Research,* 36**,** 1635-1642.

MOUNANGA, P., POULLAIN, P., BASTIAN, G., GLOUANNEC, P. & KHELIFI, H. 2009. Influence de la composition et du mode de mise en œuvre sur le développement des propriétés mécaniques du béton de chanvre. *Rencontres de l'AUGC*.

MULCHRONE, K. F. & CHOUDHURY, K. R. 2004. Fitting an ellipse to an arbitrary shape: implications for strain analysis. *Journal of Structural Geology,* 26**,** 143-153.

MURPHY, F., PAVIA, S. & WALKER, R. 2010. An assessment of the physical properties of lime-hemp concrete. *Proceeding of the bridge and concrete research in Ireland, Cork*.

NAZAR, A. M., SILVA, F. A. & AMMANN, J. J. 1996. Image processing for particle characterization. *Materials Characterization,* 36**,** 165-173.

NGUYEN-SY, T., TRAN-LE, A. D., NGUYEN-THOI, T. & LANGLET, T. 2017. A multi-scale homogenization approach for the effective thermal conductivity of dry lime–hemp concrete. *Journal of Building Performance Simulation***,** 1-11.

NGUYEN, S. T., TRAN-LE, A. D., VU, M. N., TO, Q. D., DOUZANE, O., et al. 2016. Modeling thermal conductivity of hemp insulation material: A multi-scale homogenization approach. *Building and Environment,* 107**,** 127-134.

NGUYEN, T.-T., PICANDET, V., AMZIANE, S. & BALEY, C. 2009. Influence of compactness and hemp hurd characteristics on the mechanical properties of lime and hemp concrete. *European Journal of Environmental and Civil Engineering,* 13**,** 1039-1050.

NGUYEN, T. T. 2010. *Contribution à l'étude de la formulation et du procédé de fabrication d'éléments de construction en béton de chanvre.* Université de Bretagne Sud.

NGUYEN, T. T., PICANDET, V., CARRE, P., LECOMPTE, T., AMZIANE, S., et al. 2010. Effect of compaction on mechanical and thermal properties of hemp concrete. *European Journal of Environmental and Civil Engineering,* 14**,** 545-560.

NING, L. & BING, C. 2015. Experimental Investigation Concrete Using Magnesium Phosphate Cement, Fly Ash, and Rape Stalk. *Journal of Materials in Civil Engineering,* 28**,** 04015163.

NISHIMURA, T. & ANSELL, P. M. Monitoring fiber orientation in OSB during production using filtered image analysis. *Wood Science and Technology,* 36**,** 229-239.

NIYIGENA, C. 2015. Statistical analysis of the variability of the mechanical properties of hemp concrete. *First International Conference on Bio-based Building Materials.* Clermont-Ferrand.

NIYIGENA, C., AMZIANE, S. & CHATEAUNEUF, A. 2017. Investigating Hemp Concrete Mechanical Properties Variability Due to Hemp Particles. *In:* RALPH, W. C., SINGH, R., TANDON, G., THAKRE, P. R., ZAVATTIERI, P., et al. (eds.) *Mechanics of Composite and Multi-functional Materials, Volume 7 : Proceedings of the 2016 Annual Conference on Experimental and Applied Mechanics* Cham: Springer International Publishing.

NORDBY, A. S. & SHEA, A. D. 2013. Building Materials in the Operational Phase. *Journal of Industrial Ecology,* 17**,** 763-776.

NOZAHIC, V. & AMZIANE, S. 2013. Environmental, Economic and Social Context of Agro-Concretes. *Bio-aggregate-based Building Materials.* John Wiley & Sons, Inc.

NOZAHIC, V., AMZIANE, S., TORRENT, G., SAÏDI, K. & DE BAYNAST, H. 2012. Design of green concrete made of plant-derived aggregates and a pumice–lime binder. *Cement and Concrete Composites,* 34**,** 231-241.

OSANYINTOLA, O. F. & SIMONSON, C. J. 2006. Moisture buffering capacity of hygroscopic building materials: Experimental facilities and energy impact. *Energy and Buildings,* 38**,** 1270-1282.

OXFORD ENGLISH DICTIONARY 2010. *"sustainable, adj."*, Oxford University Press.

PAVIA, S., WALKER, R. & MCGINN, J. 2015. Effect of testing variables on the hydration and compresive strength of lime-hemp concrete. *First International Conference on Bio-based Building Materials.* Clermont-Ferrand, France.

PÉREZ-LOMBARD, L., ORTIZ, J. & POUT, C. 2008. A review on buildings energy consumption information. *Energy and Buildings,* 40**,** 394-398.

PICANDET, V. 2013. Characterization of Plant-Based Aggregates. *Bio-aggregate-based Building Materials.* John Wiley & Sons, Inc.

PICANDET, V. 2017a. Bulk Density and Compressibility. *In:* AMZIANE, S. & COLLET, F. (eds.) *Bio-aggregates Based Building Materials : State-of-the-Art Report of the RILEM Technical Committee 236-BBM.* Dordrecht: Springer Netherlands.

PICANDET, V. 2017b. Particle Size Distribution. *In:* AMZIANE, S. & COLLET, F. (eds.) *Bio-aggregates Based Building Materials : State-of-the-Art Report of the RILEM Technical Committee 236-BBM.* Dordrecht: Springer Netherlands.

PICANDET, V. T., P;COLINART, T; LECOMPTE, T; CHOINSKA, M 2015. Permeability and thermal conductivity of pre-cast lime and hemp concrete. *First international conference on bio-based building materials.* Clermont Ferrand, France.

PIERRE, T., COLINART, T. & GLOUANNEC, P. 2014. Measurement of Thermal Properties of Biosourced Building Materials. *International Journal of Thermophysics,* 35**,** 1832-1852.

PIOTROWSKI, S. & CARUS, M. 2011. Ecological benefits of hemp and flax cultivation and products. Nova Institute.

PRETOT, S., COLLET, F. & GARNIER, C. 2014. Life cycle assessment of a hemp concrete wall: Impact of thickness and coating. *Building and Environment,* 72**,** 223-231.

PRITCHETT, I. 2009. Hemp and lime composites in sustainable construction. *Proceedings of the 11th international conference on non-conventional materials and technologies (NOCMAT 2009).*

RAHIM, M., DOUZANE, O., LE, A. T., PROMIS, G., LAIDOUDI, B., et al. 2015. Characterization of flax lime and hemp lime concretes: Hygric properties and moisture buffer capacity. *Energy and Buildings,* 88**,** 91-99.

RANASINGHE, A. 2008. Multi Scale Segmentation Techniques In Object Oriented Image Analysis. *Asian Conference on Remote Sensing.*

ROOHI SEFIDMAZGI, N. & BAHIA, H. U. 2014. Effect of compaction conditions on aggregate packing using 2-dimensional image analysis and the relation to performance of HMA. *Materials and Structures,* 47**,** 1313-1324.

ROULAC, J. W. 1997. *Hemp horizons: the comeback of the world's most promising plant,* White River Junction, Chelsea Green Publishing Company.

SASSONI, E., MANZI, S., MOTORI, A., MONTECCHI, M. & CANTI, M. 2014. Novel sustainable hemp-based composites for application in the building industry: Physical, thermal and mechanical characterization. *Energy and Buildings,* 77**,** 219-226.

SCHINDELIN, J., ARGANDA-CARRERAS, I., FRISE, E., KAYNIG, V., LONGAIR, M., et al. 2012. Fiji: an open-source platform for biological-image analysis. *Nature methods,* 9**,** 676-682.

SCHULGASSER, K. 1985. Fibre orientation in machine-made paper. *Journal of Materials Science,* 20**,** 859-866.

SHAFIEE, S. & TOPAL, E. 2009. When will fossil fuel reserves be diminished? *Energy Policy,* 37**,** 181-189.

SHERIDAN, J., SONEBI, M., TAYLOR, S. & AMZIANE, S. 2017. Effect of viscosity modifying agent on the mechanical and transport properties of hemp and rapeseed straw concrete.

SHI, B., MURAKAMI, Y. & WU, Z. 1998. Orientation of aggregates of fine-grained soil: quantification and application. *Engineering Geology,* 50**,** 59-70.

SINGLETON BIRCH. 2017. *Lime Cycle* [Online]. Singleton Birch. Available: https://www.singletonbirch.co.uk/lime/cycle 2017].

SINKA, M., RADINA, L., SAHMENKO, G., KOIJAKINS, A. & BAJARE, D. 2015. Enhancement of lime-hemp concrete properties using different manufacturing technologies. *First International Conference on Bio-based Building Materials.* Clermont-Ferrand, France.

SINKA, M. & SAHMENKO, G. 2013. Sustainable Thermal Insulation Biocomposites from Locally Available Hemp and Lime. *Environment. Technology. Resources,* 1**,** 73-77.

STANDFEST, G., KRANZER, S., PETUTSCHNIGG, A. & DUNKY, M. 2010. Determination of the Microstructure of an Adhesive-Bonded Medium Density Fiberboard (MDF) using 3-D Sub-micrometer Computer Tomography. *Journal of Adhesion Science and Technology,* 24**,** 1501-1514.

STANWIX, W. & SPARROW, A. 2014. *The Hempcrete Book: Designing and Building with Hemp-lime*, Green Books.

STEVULOVA, N., CIGASOVA, J., TERPAKOVA, E., JUNAK, J., SICAKOVA, A., et al. 2014. Properties testing of lightweight composites based on hemp hurds. *16th European conference on composite materials.* Seville, Spain.

STEVULOVA, N., KIDALOVA, L., CIGASOVA, J., JUNAK, J., SICAKOVA, A., et al. 2013. Lightweight Composites Containing Hemp Hurds. *Procedia Engineering,* 65**,** 69-74.

STEVULOVA, N., KIDALOVA, L., JUNAK, J., CIGASOVA, J. & TERPAKOVA, E. 2012. Effect of hemp shive sizes on mechanical properties of lightweight fibrous composites. *Procedia Engineering,* 42**,** 496-500.

STOREY, J. B. 2008. *Construction Materials Stewardship: The Status Quo in Selected Countries: CIB W115*, Centre For Building Performance Research, Victoria University of Wellington.

SUTTON, A., BLACK, D. & WALKER, P. 2011. *Hemp Lime: An Introduction to Low-impact Building Materials*, BRE Press.

TEAGUE, M. R. 1980. Image analysis via the general theory of moments. *Journal of the Optical Society of America,* 70**,** 920-930.

THE ENGINEERING TOOLBOX. 2017. *Air properties* [Online]. Available: http://www.engineeringtoolbox.com/air-properties-d_156.html 2017].

TRADICAL®. 2015. *Building lime innovation* [Online]. Available: http://www.tradical.com/ [Accessed 29/06/2015 2015].

TRAN LE, A., MAALOUF, C., MAI, T., WURTZ, E. & COLLET, F. 2010. Transient hygrothermal behaviour of a hemp concrete building envelope. *Energy and Buildings,* 42**,** 1797-1806.

TRONET, P., LECOMPTE, T., PICANDET, V. & BALEY, C. 2014. Study of lime hemp composite precasting by compaction of fresh mix — An instrumented die to measure friction and stress state. *Powder Technology,* 258**,** 285-296.

TRONET, P., LECOMPTE, T., PICANDET, V. & BALEY, C. 2016. Study of lime hemp concrete (LHC) – Mix design, casting process and mechanical behaviour. *Cement and Concrete Composites,* 67**,** 60-72.

VEJMELKOVÁ, E., KEPPERT, M., KERŠNER, Z., ROVNANÍKOVÁ, P. & ČERNÝ, R. 2012. Mechanical, fracture-mechanical, hydric, thermal, and durability properties of lime–metakaolin plasters for renovation of historical buildings. *Construction and Building Materials,* 31**,** 22-28.

VELDE, B., MOREAU, E. & TERRIBILE, F. 1996. Pore networks in an Italian Vertisol: quantitative characterisation by two dimensional image analysis. *Geoderma,* 72**,** 271-285.

VIGNON, M. R., DUPEYRE, D. & GARCIA-JALDON, C. 1996. Morphological characterization of steam-exploded hemp fibers and their utilization in polypropylene-based composites. *Bioresource Technology,* 58**,** 203-215.

WAGH, A. S. 1993. Porosity dependence of thermal conductivity of ceramics and sedimentary rocks. *Journal of Materials Science,* 28**,** 3715-3721.

WAGH, A. S., SINGH, J. P. & POEPPEL, R. B. 1993. Dependence of ceramic fracture properties on porosity. *Journal of Materials Science,* 28**,** 3589-3593.

WALKER, R. & PAVIA, S. 2012. Impact of water retainers in the strength, drying and setting of lime hemp concrete. *Bridge and Concrete Research in Ireland (BCRI).* Dublin.

WALKER, R. & PAVÍA, S. 2014. Moisture transfer and thermal properties of hemp–lime concretes. *Construction and Building Materials,* 64**,** 270-276.

WALKER, R., PAVIA, S. & MITCHELL, R. 2014. Mechanical properties and durability of hemp-lime concretes. *Construction and Building Materials,* 61**,** 340-348.

WANG, J., CARSON, J. K., NORTH, M. F. & CLELAND, D. J. 2006. A new approach to modelling the effective thermal conductivity of heterogeneous materials. *International Journal of Heat and Mass Transfer,* 49**,** 3075-3083.

WEHRHAUSEN, M., LAUDON, N., BRÜCHERT, F. & SAUTER, U. H. 2012. Crack Detection in Computer Tomographic Scans of Softwood Tree Discs. *Forest Products Journal,* 62**,** 434-442.

WIJAYASUNDARA, M., CRAWFORD, R. H. & MENDIS, P. 2017. Comparative assessment of embodied energy of recycled aggregate concrete. *Journal of Cleaner Production,* 152**,** 406-419.

WILLIAMS, J., LAWRENCE, M. & WALKER, P. 2016a. The influence of the casting process on the internal structure and physical properties of hemp-lime. *Materials and Structures,* 50**,** 108.

WILLIAMS, J., LAWRENCE, M. & WALKER, P. 2016b. A method for the assessment of the internal structure of bio-aggregate concretes. *Construction and Building Materials,* 116**,** 45-51.

WILLIAMS, J., LAWRENCE, M. & WALKER, P. 2017. Projection formed and precast hemp-lime: Better by design? *2nd International Conference on Bio-based Building Materials.* Clermont-Ferrand.

WOLOSZYN, M., KALAMEES, T., OLIVIER ABADIE, M., STEEMAN, M. & SASIC KALAGASIDIS, A. 2009. The effect of combining a relative-humidity-sensitive ventilation system with the moisture-buffering capacity of materials on indoor climate and energy efficiency of buildings. *Building and Environment,* 44**,** 515-524.

YANG, Y., BOOM, R., IRION, B., VAN HEERDEN, D.-J., KUIPER, P., et al. 2012. Recycling of composite materials. *Chemical Engineering and Processing: Process Intensification,* 51**,** 53-68.

YATES, T. 2002. Final report on the construction of the hemp houses at Haverhill, Suffolk. Building Research Establishment.

YONAVJAK, L. 2013. *Industrial Hemp: A Win-Win For The Economy And The Environment* [Online]. Forbes online. Available: https://www.forbes.com/sites/ashoka/2013/05/29/industrial-hemp-a-win-win-for-the-economy-and-the-environment/#4cf37296289b 2017].

YOUSSEF, A., LECOMPTE, T., PICANDET, V. & CHALLAMEL, N. 2015. Compressive and shearing behaviour of lime and hemp concrete. *First international conference on bio-based building materials.* Clermont-Ferrand, France.

YUE, Z. Q. & MORIN, I. 1996. Digital image processing for aggregate orientation in asphalt concrete mixtures. *Canadian Journal of Civil Engineering,* 23**,** 480-489.

8 Appendices

8.1 Published journal papers

A method for the assessment of the internal structure of bio-aggregate concretes

Joseph Williams *, Mike Lawrence, Pete Walker

BRE Centre for Innovative Construction Materials, Department of Architecture and Civil Engineering, University of Bath, Bath BA2 7AY, UK

HIGHLIGHTS

- A novel method for assessing bio-aggregate composites is proposed.
- 2D and 3D image analysis used to assess aggregate orientation.
- Specimens of hemp-lime found to have a strong anisotropic internal structure.

ARTICLE INFO

Article history:
Received 20 January 2016
Received in revised form 21 April 2016
Accepted 22 April 2016
Available online 3 May 2016

Keywords:
Bio-aggregate
Hemp-lime
Image analysis
Internal structure

ABSTRACT

The thermal and mechanical properties of bio-aggregate concretes are known to be anisotropic. This is assumed to be the result of an orientated internal arrangement of particles; the internal structure of other aggregate composite materials is known to be a determiner of physical properties and has been the focus of much study. Despite this the internal structure of bio-aggregate concretes has to date only been considered qualitatively. This work presents a novel method for the assessment of the internal structure of bio-aggregate concretes through the application of image analysis. Results are presented for the assessment of hemp-lime specimens and demonstrate a significant anisotropy within the material. These results account for anisotropic thermal and mechanical behaviour observed elsewhere and demonstrate the importance of the internal structure in determining the properties of these materials. This innovative technique represents a significant breakthrough in the search for optimisation of the performance of renewable, low carbon insulation materials. This class of materials is critical to the sustainable future of the construction industry.

1. Introduction

Bio-aggregate concretes (BAC) are formed by combining crop based aggregate, mineral binder and water. Hemp-lime, produced from the chopped up stalk (shiv) of the hemp plant, is one of the most best known but other examples include wood chips, sunflower plant stems [1] and flax plant stems [2]. As a result of the photosynthetically used carbon dioxide embodied within the plant materials, BACs have very low embodied carbon [3–5] as well as favourable thermal properties for use in building envelopes, including low thermal conductivity and high heat capacity [6–9].

To produce BACs the mixed constituents are cast into formwork or spray applied onto a substrate. Both processes apply a unidirectional compacting force to the wet material: tamping or deliberate compaction in the case of cast and force of projection in the case of sprayed. As bio-aggregate particles are often elongated in form, this compacting force is considered by most to have significant influence on their arrangement, the elongated particles tending towards stratified planes that are perpendicular to compacting force [10,11].

The anisotropic arrangement concept is supported by observations of some physical properties. Nguyen [12] measured the thermal conductivity of cast-compressed hemp-lime specimens both parallel and perpendicular to the compacting force and found up to a 30% higher thermal conductivity in the perpendicular direction. Other work has reported similar findings for cast-tamped material [13] and sprayed material [14]. In all cases the observations were attributed to the internal structure, in which the stratified planes are opposing the transverse heat transfer.

The compressive behaviour of BACs has also been studied with respect to orientation of the bio-aggregates. Previous studies have observed that the peak compressive strength of these materials is higher when loaded parallel to the compacting force however the

* Corresponding author.
E-mail address: J.P.Williams@bath.ac.uk (J. Williams).

http://dx.doi.org/10.1016/j.conbuildmat.2016.04.088
0950-0618/

Nomenclature

Symbols

x_i, y_i, z_i	the location of a given pixels/voxels within any given shape comprising n connected pixels/voxels
m_{pqr}	the global image moments of a given shape comprising n connected pixels/voxels
u_{pqr}	the central image moments of a given shape comprising n connected pixels/voxels
$\bar{x}$, $\bar{y}$, $\bar{z}$	the location of the centroid of any given shape comprising n connected pixels/voxels
θ_{xy}, θ_{yz}, θ_{zx}	the orientation of the principle axis of the best fit ellipse for any given shape comprising n connected pixels/voxels
f	the frequency of particles observed at a given orientation
n	experimentally derived constant

compressive stiffness is lower [15–17]. Additionally the material has been observed to fail in a more brittle manner when loaded perpendicularly. Fig. 1 shows the average compressive stress/strain plots of three 150 mm cube specimens of hemp lime and highlights this difference in behaviour that can be attributed to the internal structure – the strata providing differing transverse and parallel load paths.

Studies of other particulate composite materials such as asphalt [18,19] and soil [20], have demonstrated that the arrangement of the internal structure in these cases is one of the contributing factors for the global properties and a cause of anisotropic behaviour. Despite this, and the observation of anisotropic properties, there has, to the authors' knowledge, been no attempt to measure the internal structure of bio-aggregate concretes, for orientation or for any other parameter.

In order to test the hypothesis of compaction generating strata within bio-aggregate concretes, this paper outlines an image analysis method for the statistical assessment of particle orientation within cast material. The method is based on established methods for other materials as well as image analysis methods already in use for the study of the size distribution of bio-aggregate particles. Results are reported from the application of this method to three variants of the bio-aggregate concrete hemp-lime.

2. Methodology

2.1. Materials and specimen production

All the specimens considered in this work were produced using hemp shiv grown in the UK the properties of which are presented in Table 1. The particle size distribution of bio-aggregates length and width can be determined by two dimensional digital image analysis as established by others [21]. A 20 g sample of shiv was assessed in this way with the results presented in Fig. 2. The results presented in Table 1 and Fig. 2 indicate that the material used in this study is comparable to that used widely elsewhere in the literature and that the shiv particles can be considered to be of elongated form.

The binder used was pre-formulated for hemp-lime construction. The specific formulation of the binder is not declared by the manufacturer, however it is believed to be mainly hydrated lime with additional pozzolanic additives and cement.

To produce the composite material the constituents were mixed in a revolving pan mixer by first slaking the binder with the water and then adding the hemp and further mixing until uniformly combined. For each specimen a set mass of material was tamped into a 150 mm cube mould fitted with a collar to allow for initial overfilling. Three variations of material, standard, light weight and compact, were used in the study Table 2. The standard mix represents an industry standard hemp-lime formulation for walling applications. The light weight mix represent a material with the same proportion of hemp per unit volume but a lower binder content; the compacted mix represents a higher density version of the standard mix but with the same binder to aggregate ratio.

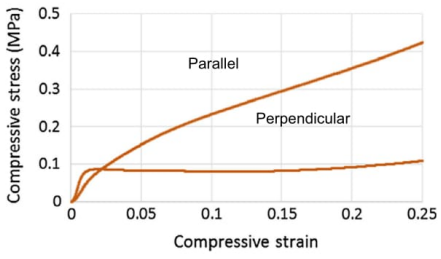

Fig. 1. Stress strain plots for perpendicular and parallel loaded hemp-lime cubes produced with a ratio of 16% hemp, 36% binder and 48% water and cast in three layers of 0.66 kg with vertical compaction applied between each layer.

2.2. Image analysis

Image analysis is the process of imaging a material either in two or three dimensions and then using analysis conducted on the image to extract meaningful data. In this application the required outcome was to gauge if a preference of orientation is present in the particles of the material and the process utilised was as follows:

Table 1
Properties of hemp shiv.

Bulk density (kg m^{-3})	Particle length (mm)		Particle width (mm)	
	Mean particle length (mm)	Standard deviation	Mean	Standard deviation
108	5.56	5.49	1.55	1.33

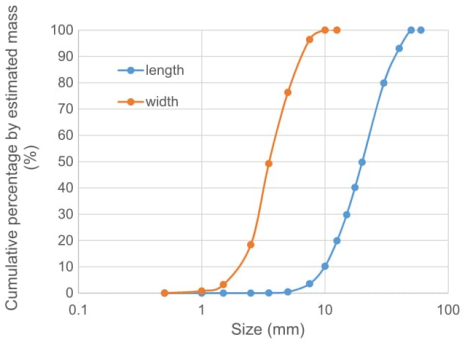

Fig. 2. Particle size distribution of hemp shiv as obtained by two dimensional image analysis of a 20 g sample.

Table 2
Hemp-lime mixture variations.

Mixture	Aggregate (bulk%)		Binder (bulk%)		Water (bulk%)		Paste (%)		Wet mass of specimen (kg)	Estimated Porosity (Fresh state%)	Average dry density (kgm^{-3})
	Mass	Vol	Mass	Vol	Mass	Vol	Mass	Vol			
Standard	16	56	36	23	48	21	84	32	2.00	66	284
Light weight	21	64	36	20	43	16	79	25	1.48	84	353
Compacted	16	56	36	23	48	21	84	32	2.41	60	422

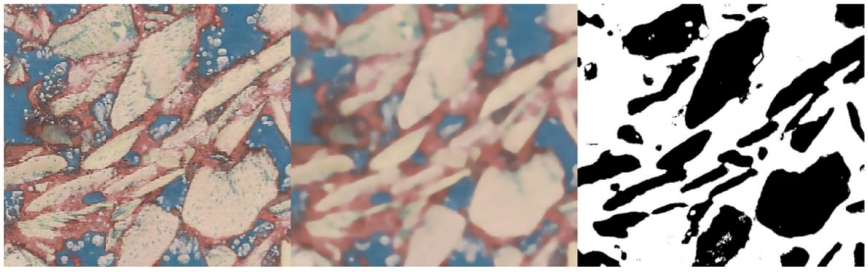

Fig. 3. Left to right: original VD image, image passed through median filter, image passed through threshold filter.

Table 3
Image enhancement and filtering settings trialled, those deemed most appropriate identified in bold.

Process	ImageJ settings	Avizo® Fire 8 settings
Median filter	Radius (pixels): 5, 10, 15, **20**, 25, 30	Iterations: 5, **6**, 7
Colour threshold lower boundary	8 bit hue value: 10, 12, **14**, 16, 18, 20	32 bit float intensity value: **4**, 5, 6 (basic mix) 4, 4.5, **5** (light mix) 6, **7**, 8 (compacted mix)
Colour threshold upper boundary	8 bit hue value: **50**	32 bit float intensity value: 28, **29**, 30 (basic mix) 8, 8.5, **9** (light mix) 28, **29**, 30 (compacted mix)
Opening algorithm	Iterations: 1, 2, **3**, 5, 10, 15, 20, 25	Radius (voxels) 1, 2, **3**

- image the material;
- segregate out the shiv;
- identify and measure the orientation of the particles;
- perform a frequency analysis of the population.

Similar methods, but for the study of other materials, have already been developed and were used as a reference for application to bio-aggregate concretes. These include asphalt [22,23], soil [20], fibre reinforced concrete [24,25] and fibre board [26,27]. Image analysis has also been applied to investigate the size distribution of bio-aggregate particles [21] and was used as an additional reference. Two methods of imaging were considered within the study in order to provide comparison and validate results: visual digital imaging (VD imaging) and computer tomography scanning (CT scanning).

VD imaging is conducted by taking physical sections of the material and imaging the exposed face using a digital camera or flat-bed scanner. An advantage of this method is its low cost however it is a destructive method and requires imaging in several orientations in order to assess the three dimensional topology. Further disadvantages specific to use with BACs are the similar colouring of the particles and binder and the large number of voids that makes visual differentiation of components difficult.

In this study, pairs of specimens were VD imaged, one parallel to compacting force and one perpendicular. Each specimen was sectioned into six 150 mm square slices using a band saw. To improve the visual contrast between material and voids, the slices were submerged in a low viscosity coloured resin. Once cured, the faces were sanded to remove excess and scanned with a flatbed scanner at a resolution of 2400 dpi. To improve contrast between the binder and the hemp, a coloured pigment was added to the binder during the specimen production at a dose of 10 g per specimen.

CT scanning is an established method of imaging the internal structure of materials producing a map of the X-ray absorbance within the material, a property closely linked to density. Advantages of this method are that it is non-destructive and produces a three dimensional image of the material. It is however expensive in comparison to VD imaging and the contrast within the parameters it measures cannot be enhanced by physical pre-treatments.

Within this study all CT scans were taken using a Nikon XTEK, XTH 225 ST CT scanner set to 165 kV and 165 μA. The data were recompiled into a three dimensional volume using Avizo® Fire 8.

2.3. Segregation

To identify the shiv within the images, two image filters with successful precedents for other materials [23,28,29] were applied: a median filter and a threshold filter. The same processes were implemented for both two dimensional and three dimensional images, however differing programs and settings were used due to the differing image formats. ImageJ and Avizo® Fire 8 were used for the two dimensional and three dimensional images respectively.

A median filter replaces each two dimensional pixel's, or three dimensional voxel's, value with the median of those within a specified radius [30,31]. This has the result of smoothing the image and removing anomalies Fig. 3. A threshold filter is used to segregate the smoothed image. Each pixel/voxel is in turn assessed against a set of criteria in order to produce a binary image [30,31]. Careful selection of the criteria enables the identification of a single component and in this case was used to identify the shiv Fig. 3.

Both the median filter and threshold filter applied by each program are controlled by operator assigned settings. The nature of these settings differs between the two programs used, however, in both cases their selection will have a bearing on the analysis results. To assess the sensitivity of the analysis to the choice of settings used, a sensitivity analysis was undertaken on a single image from each imaging method. The range of settings considered for each of the imaging methods is presented in Table 3.

2.4. Identification and measuring orientation

Within the binary images, particles are considered to be regions of interconnected positive pixel/voxels. Due to the close proximity of particles and the limited resolution of the images, there are regions where several aggregates may be

Fig. 4. Left to right: thresholded image, image passed through opening algorithm, image assessed for particles and represented as best fitting ellipses.

misinterpreted as a single particle due to touching areas. To help mitigate the extent of misinterpreted particle groups, an opening algorithm was applied to the images prior to final assessment Fig. 4.

Opening algorithms selectively remove and then add additional positive pixels or voxels based on the values of those around it [30,31]. These are commonly used at this stage of image analysis in order to clean the images and help remove bridges between adjoining particles. As the opening algorithm in both cases was controlled by a user assigned setting, again a range of settings was trialled with details given in Table 3.

To measure the orientation of the identified particles, inbuilt tools within the respective programs were used. The process in both cases is based on calculation and interpretation of the first and second order image moments and is detailed fully elsewhere [32,33]. For each group of n connected pixels/voxels, the global first and second moments are calculated:

$$m_{pqr} = \sum_{i=1}^{n} x_i^p y_i^q z_i^r \tag{1}$$

The central second moments: u_{200}, u_{020}, u_{002}, u_{011}, u_{101}, and u_{110} and the centroid coordinates can then be determined:

$$u_{pqr} = m_{pqr} - \frac{m_{100}^p m_{010}^q m_{001}^r}{m_{000}} \tag{2}$$

$$\bar{x} = \frac{m_{100}}{m_{000}} \tag{3}$$

$$\bar{y} = \frac{m_{010}}{m_{000}} \tag{4}$$

$$\bar{z} = \frac{m_{001}}{m_{000}} \tag{5}$$

By equalising the second moments and centroid of the particle with that of an ellipse or ellipsoid, the best fitting ellipse or ellipsoid can be determined Fig. 4. This enables a consistent measurement of geometrical properties of particles despite their irregular shapes. The orientation of the principal axis of the ellipse or ellipsoid was used as the measure of particle orientation and can be found in each 2D plane:

$$\theta_{xy} = \frac{1}{2}\tan^{-1}\left(\frac{2u_{110}}{u_{200}u_{020}}\right) \tag{6}$$

$$\theta_{yz} = \frac{1}{2}\tan^{-1}\left(\frac{2u_{011}}{u_{020}u_{002}}\right) \tag{7}$$

$$\theta_{zx} = \frac{1}{2}\tan^{-1}\left(\frac{2u_{101}}{u_{002}u_{200}}\right) \tag{8}$$

2.5. Frequency analysis

For visual digital imaging, twelve images were produced for each mix: six taken parallel to compaction and six perpendicular. For each mix a cumulative frequency distribution was produced in each direction for the total particle population from all six slices. In the case of CT scanning, one image was taken per mix with two values of particle orientation measured that equate to the same parallel and perpendicular viewpoints. For each mix a cumulative frequency distribution was produced in each direction for the total particle population of the image. In both cases only particles above a minimum size of 1 mm^2 and 1 mm^3 respectively were considered. The data from both imaging methods were manipulated to give an orientation scale of between 0° and 90° which represent horizontal and vertical alignment in the image plane respectively.

3. Results

3.1. Sensitivity to image enhancement parameters

The perpendicular frequency distributions obtained from one image but using the range of parameters provided in Table 3 were compared. In each instance a version of the Hankinson equation [34], Eq. (9), was fitted to the distribution using a least squares approach and the determined values of f_0, f_{90} and n used as indicators by which to compare the distributions. Hankinson's equation was originally developed for modelling the compressive stress of spruce with respects to orientation of the grain but has since been developed for modelling other properties of timber as well as wood based particle composite boards [35–37]. Hankinson's equation was selected due to strong similarities between distribution forms observed in this study and those where the equation has been previously applied. In addition the boundary criteria, f_0 and f_{90}, enable the distribution to be applied both to the 2D images, where a lower bound frequency can be observed, as well as the 3D images. To the author's knowledge Hankinson's equation has not previously been used to model frequency of orientated particles/fibres however the

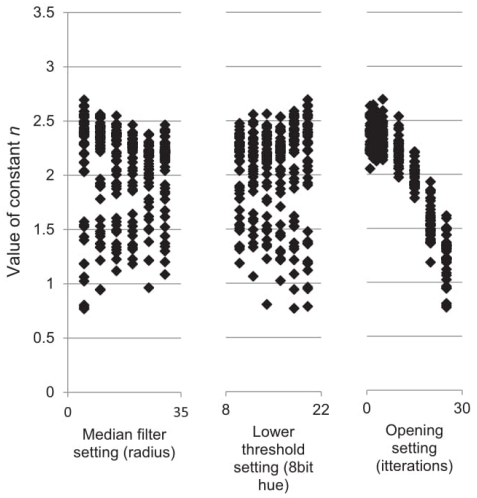

Fig. 5. The value of the constant n obtained using differing enhancement setting with 2D images.

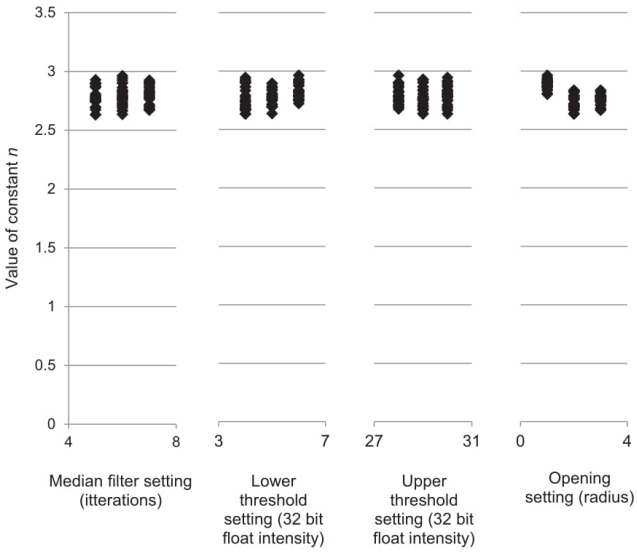

Fig. 6. The value of the constant n obtained using differing enhancement setting with 3D images.

wrapped Cauchy distribution that can be manipulated into the same "Hankinson" form has been used successfully [38].

$$f = \frac{f_0 f_{90}}{f_0 \sin^n \theta + f_{90} \cos^n \theta} \tag{9}$$

The values of n, for differing enhancement parameters, are presented for the standard mix in Figs. 5 and 6. for two dimensional and three dimensional images respectively. The values of f_0 and f_{90} with respect to the enhancement parameters, while not shown, exhibit similar patterns and the same pattern was found in all three mix designs.

In Figs. 5 and 6 it is evident that the enhancement parameters can have a significant influence on the value of n and therefore the distribution produced; for the visual digital imaging method it was determined that the range of parameters considered was able to effect a 10% variation in the peak frequency of the distribution. The opening algorithm can be seen to be the most onerous process and the smaller number of opening algorithm variations considered in the CT data is the likely reason for the smaller spread of results in this case. When the opening algorithm iterations are restricted to under three iterations for the digital visual image data, the variation in peak frequencies is reduced to 2.4% and is comparable to the variation in the CT images.

In order to select appropriate parameters to use for the full assessment, the enhanced images from the sensitivity study were compared against the original images by eye. This was conducted using a "winner stays on" system whereby two images were compared to the original with the one judged least effective at identifying hemp particles being replaced. The process was continued until all permutations had been considered. The parameters identified as most appropriate by this method are identified in Table 3.

3.2. Particle orientation frequency analysis

The particle orientation frequency distributions from VD imaging using the enhancement and filtering setting identified in Table 3 are presented in Fig. 7. The resulting distributions, viewing both perpendicularly and parallel to the direction of compacting

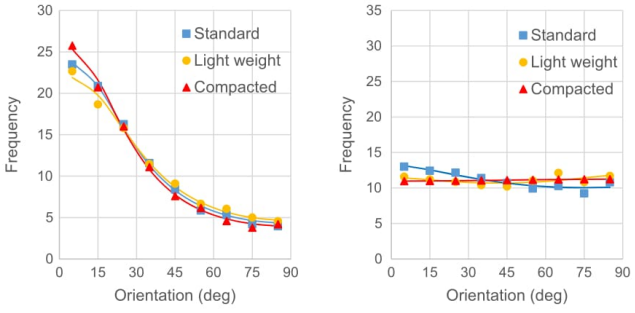

Fig. 7. Frequency distribution of particle orientation produced using two dimensional imaging. Perspective perpendicular to compaction, left, and parallel to compaction, right.

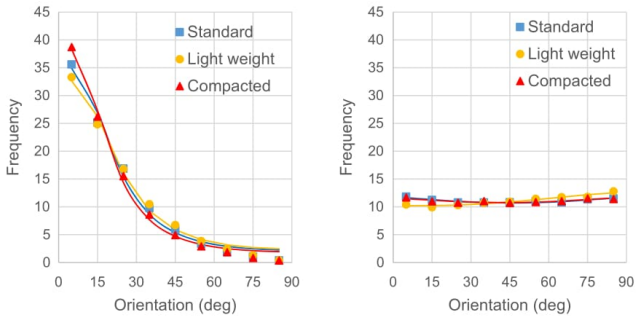

Fig. 8. Frequency distribution of particle orientation produced using CT imaging. Perspective perpendicular to compaction, left, and parallel to compaction, right.

force, are shown as are the distributions produced from all three mixes. Eq. (9) has been fitted to the data in using a least squares approach each case to aid comparison. The equivalent distributions produced using CT imaging are presented in Fig. 8.

4. Discussion

4.1. Comparison of material in opposing directions

From Figs. 7 and 8 it can be seen that the frequency distribution of particle orientations viewed parallel to compacting force is flat: indicative of a random distribution and suggests the structure is isotropic in this plane. Conversely, in the perpendicular plane, the frequency distribution of particle orientations is strongly swayed. This indicates a preference of orientation within the population and is therefore suggestive that the material's structure is anisotropic in this plane.

The finding of both an anisotropic and isotropic distributions in contrasting directions is supportive of the hypothesis that compaction force produces a preferential orientation [10,12]. A clear tendency is observed in all specimens for the major axis of the particles to tend towards horizontal planes, perpendicular to the compaction force. This observation concurs with, and provides an explanation for the observations of others that several physical properties of bio-aggregate composites exhibit anisotropic behaviour with respect to the direction of compaction force [15–17].

4.2. Comparison of materials produced using differing formation variables

In the perpendicular perspective, a consistent difference between distributions produced from the differing mixes is present in the results from both methods. The light mix is observed to have the lowest maximum frequency and highest minimum frequency; the compacted mix is observed to have the highest maximum frequency and lowest minimum frequency.

A possible interpretation is that the overall degree of orientation is higher in the compacted material and lower in the low density material compared to the standard mix. This is logical in the case of the compacted mix where the ratio of constituents was the same but level of compaction was known to be higher. For the light weight mix, the density of hemp in the material was controlled to be the same as the standard mix and this was assumed to indicate a similar compaction level and thus the cause of the apparently lower degree of orientation in the case of the lightweight mix can therefore not be attributed to compaction. Alternately it is proposed that the aggregate volume fraction may be a determining factor in the degree of orientation; a lower volume of aggregates producing a higher level of inter-particle porosity and increasing the ability of particles to rotate under compaction. It is considered likely therefore that both compaction and aggregate volume fraction will impact the degree of orientation and further experiments to investigate the impact of both variables on the internal structure are proposed.

The observed difference between the frequency distributions from the three mixes is noted to fall within the difference obtained using differing image enhancement settings and highlights the importance of using consistent settings for comparing material. A consistent set of enhancement settings was used across all specimens analysed with VD imaging and so removes this as a source of uncertainty in this case. The variation observed in the perpendicular perspective was also noted to be of greater magnitude than those observed in the parallel perspective. This indicates that the observations in the perpendicular perspective are within the natural variation of the population and therefore the observation that there are differing degrees of orientation, while promising, is statistically insignificant and undermines any firm conclusions at this stage.

4.3. Comparison of digitisation methods

The frequency distributions produced by the VD imaging Fig. 7, are observed to be of the same general form of those produced using CT images Fig. 8. In each case the parallel perspective has produced a relatively level distribution with all frequencies approximately between 9% and 14%. In the perpendicular perspective both methods have indicated a swayed distribution towards the horizontal with a similar form in both cases. In both cases the ordering of the mixes, least to most orientated, is the same. A smoother frequency distribution was found using the CT images as opposed to the VD imaging and is attributed to the larger overall population of particles measured.

In the perpendicular view, the CT generated images have, in all variations of material, yielded distributions with a consistently higher frequency range. This difference is attributed to the differing nature of the methods; VD imaging analysis measures a random section through each particle while CT scan analysis measures the whole particle and indicates that a consistent method must be adopted for the comparison of material.

The strong correlation between the results from both methods provides a high level of confidence in the results. VD imaging conducted in two planes is considered sufficient to infer the three dimensional structure of the material and, due to the lower costs,

is considered to be the more practical of the two methods for larger samples of material.

5. Conclusion

In this work the novel application of image analysis methodology for the assessment of the internal structure of bio-aggregate concretes was trialled. It was shown that similar results are obtainable using two differing methods of imaging: CT scanning and VD imaging. This indicates that both procedures are capable of producing reliably analysable images and that image analysis is a suitable method for the assessment of these materials.

The results in this study support the established theory that these materials have an orientated internal structure that is determined by the direction of any compacting force. A consistent difference was also observed between materials constructed in differing ways and, while this was within the natural variation of the results, indicates that the production method is likely to determine the degree of orientation.

This study demonstrates that image analysis is a reliable and repeatable method of assessing the internal structure of bio-aggregate concretes. This will facilitate the development of models which will better predict the impact of construction processes on the mechanical and hygrothermal properties of these materials, leading to the potential optimisation of their performance. Additional work is required to establish the exact way in which construction processes influence the internal structure of bio-aggregate concretes in order to utilise this aspect of the material.

Acknowledgements

The authors gratefully acknowledge the financial support provided by the Engineering and Physical Sciences Research Council – United Kingdom, EP/L016869/1.

References

[1] V. Nozahic, S. Amziane, G. Torrent, K. Saïdi, H. De Baynast, Design of green concrete made of plant-derived aggregates and a pumice–lime binder, Cement Concr. Compos. 34 (2) (2012) 231–241.
[2] A. Korjenic, V. Petránek, J. Zach, J. Hroudová, Development and performance evaluation of natural thermal-insulation materials composed of renewable resources, Energy Build. 43 (9) (2011) 2518–2523.
[3] M. Boutin, C. Flamin, S. Quinton, G. Gosse, Analyse du Cycle de Vie de Mur en Béton Chanvre Banché sur Ossature en Bois, INRA, Lille, France, 2005.
[4] K. Ip, A. Miller, Life cycle greenhouse gas emissions of hemp–lime wall constructions in the UK, Resour. Conserv. Recycl. 69 (2012) 1–9.
[5] S. Pretot, F. Collet, C. Garnier, Life cycle assessment of a hemp concrete wall: Impact of thickness and coating, Build. Environ. 72 (2014) 223–231.
[6] L. Arnaud, D. Samri, É. Gourlay, Hygrothermal Behavior of Hempcrete. Bio-aggregate-based Building Materials, John Wiley & Sons, 2013, pp. 179–242.
[7] F. Collet, S. Pretot, Experimental highlight of hygrothermal phenomena in hemp concrete wall, Build. Environ. 82 (2014) 459–466.
[8] M. Lawrence, E. Fodde, K. Paine, P. Walker, Hygrothermal performance of an experimental hemp-lime building, Key Eng. Mater. 517 (2012) 413–421.
[9] F. Collet, S. Prétot, Thermal conductivity of hemp concretes: variation with formulation, density and water content, Constr. Build. Mater. 65 (2014) 612–619.
[10] Y. Hustache, L. Arnaud, Synthèse des connaissances sur les bétons et mortiers de chanvre, Construire en Chanvre, 2008.
[11] S. Elfordy, F. Lucas, F. Tancret, Y. Scudeller, L. Goudet, Mechanical and thermal properties of lime and hemp concrete ("hempcrete") manufactured by a projection process, Constr. Build. Mater. 22 (10) (2008) 2116–2123.
[12] T.T. Nguyen, V. Picandet, P. Carre, T. Lecompte, S. Amziane, C. Baley, Effect of compaction on mechanical and thermal properties of hemp concrete, Eur. J. Environ. Civ. Eng. 14 (5) (2010) 545–560.
[13] T. Dinh, C. Magniont, M. Coutand, G. Escadeillas, Hemp concrete using innovative pozzolanic binder, in: First International Conference on Bio-based Building Materials, 2015. Clermont-Ferrand, France.
[14] T. Pierre, T. Colinart, P. Glouannec, Measurement of thermal properties of biosourced building materials, Int. J. Thermophys. 35 (9–10) (2014) 1832–1852.
[15] S. Amziane, V. Nozahic, M. Sonebi, Design of mechanically enhanced concrete using hemp shiv, in: First International Conference on Bio-based Building Materials, 2015. Clermont-Ferrand, France.
[16] A. Kashtanjeva, M. Sonebi, S. Amziane, Investigation of the mechanical performance and drying shrinkage of hemp concrete, in: First International Conference of Bio-based Building Materials Clermont-ferrand, France, 2015.
[17] A. Youssef, T. Lecompte, V. Picandet, N. Challamel, Compressive and shearing behaviour of lime and hemp concrete, in: First International Conference on Bio-based Building Materials, 2015. Clermont-Ferrand, France.
[18] M. Hamzah, W. Von, N. Abdullah, Effects of compactor types on aggregate orientation of asphalt mixtures, Int. J. Eng. Trans. A Basics 26 (7) (2013) 677.
[19] E. Sanchez-Alonso, A. Vega-Zamanillo, D. Castro-Fresno, Effect of type of compaction on mechanical properties in warm-mix asphalts, J. Mater. Civ. Eng. 24 (8) (2012) 1043–1049.
[20] B. Shi, Y. Murakami, Z. Wu, Orientation of aggregates of fine-grained soil: quantification and application, Eng. Geol. 50 (1) (1998) 59–70.
[21] V. Picandet, Characterization of Plant-Based Aggregates. Bio-aggregate-based Building Materials, John Wiley & Sons, 2013, pp. 27–74.
[22] M.E. Kutay, E. Arambula, N. Gibson, J. Youtcheff, Three-dimensional image processing methods to identify and characterise aggregates in compacted asphalt mixtures, Int. J. Pavement Eng. 11 (6) (2010) 511–528.
[23] N. Roohi Sefidmazgi, H.U. Bahia, Effect of compaction conditions on aggregate packing using 2-dimensional image analysis and the relation to performance of HMA, Mater. Struct. 47 (8) (2014) 1313–1324.
[24] Y. Akkaya, S. Shah, B. Ankenman, Effect of fiber dispersion on multiple cracking of cement composites, J. Eng. Mech. 127 (4) (2001) 311–316.
[25] J. Liu, C. Li, J. Liu, G. Cui, Z. Yang, Study on 3D spatial distribution of steel fibers in fiber reinforced cementitious composites through micro-CT technique, Constr. Build. Mater. 48 (2013) 656–661.
[26] E. Badel, C. Delisee, J. Lux, 3D structural characterisation, deformation measurements and assessment of low-density wood fibreboard under compression: the use of X-ray microtomography, Compos. Sci. Technol. 68 (7–8) (2008) 1654–1663.
[27] G. Standfest, S. Kranzer, A. Petutschnigg, M. Dunky, Determination of the microstructure of an adhesive-bonded medium density fiberboard (MDF) using 3-D sub-micrometer computer tomography, J. Adhes. Sci. Technol. 24 (8–10) (2010) 1501–1514.
[28] I. Bessa, V. Castelo Branco, J. Soares, Evaluation of different digital image processing software for aggregates and hot mix asphalt characterizations, Constr. Build. Mater. 37 (2012) 370–378.
[29] A.R. Coenen, M.E. Kutay, N.R. Sefidmazgi, H.U. Bahia, Aggregate structure characterisation of asphalt mixtures using two-dimensional image analysis, Road Mater. Pav. Design 13 (3) (2012) 433–454.
[30] FEI Visualization Sciences Group, Avizo 8, Avizo User's Guide, English, Konrad-Zuse-Zentrum für Informationstechnik, Berlin, Germanry, 2014.
[31] T. Ferreira, W. Rasb, ImageJ user guide, 2012.
[32] H. Ming-Kuei, Visual pattern recognition by moment invariants, IRE Trans. Inform. Theory 8 (2) (1962) 179–187.
[33] M.R. Teague, Image analysis via the general theory of moments*, J. Opt. Soc. Am. 70 (8) (1980) 920–930.
[34] R. Hankinson, Investigation of crushing strength of spruce at varying angles of grain, Air Serv. Inform. Circ. 3 (259) (1921) 130.
[35] H. Holmberg, Influence of grain angle on Brinell hardness of Scots pine *(Pinus sylvestris L.)*, Holz als Roh- und Werkstoff 58 (1) (2000) 91–95.
[36] S. Kazemi Najafi, A. Abbasi Marasht, G. Ebrahimi, Prediction of ultrasonic wave velocity in particleboard and fiberboard, J. Mater. Sci. 42 (3) (2007) 789–793.
[37] T. Nishimura, P.M. Ansell, Monitoring fiber orientation in OSB during production using filtered image analysis, Wood Sci. Technol. 36 (3) (2002) 229–239.
[38] K. Schulgasser, Fibre orientation in machine-made paper, J. Mater. Sci. 20 (3) (1985) 859–866.

Materials and Structures (2017)50:108
DOI 10.1617/s11527-016-0976-4

ORIGINAL ARTICLE

The influence of the casting process on the internal structure and physical properties of hemp-lime

Joseph Williams · Mike Lawrence · Pete Walker

Received: 27 September 2016 / Accepted: 28 November 2016

Abstract Bio-aggregate composites such as hemp-lime offer a more sustainable alternative to traditional walling infill material. Hemp-lime, whether in situ or prefabricated, is generally either cast or sprayed, which results in a directionally dependent, typically layered, physical structure. This paper considers the impact of compaction and layering on the directional thermal conductivity, compressive strength and internal structure of the material through use of a novel image analysis method. The results presented indicate that production variables have a significant, and crucially, directionally dependent impact on the thermal and mechanical properties of cast hemp-lime.

Keywords Hemp-lime · Bio-aggregate · Image analysis · Compressive strength · Thermal conductivity · Directional modeling

1 Introduction

Hemp-lime is a bio-aggregate composite material produced by combining the chopped woody core of the hemp plant (shiv), a lime-based binder and water. The resulting mixture can be cast or sprayed into place and cures to form a rigid but highly voided structure. The large proportion of bio-sourced material means that hemp-lime is a net absorber of carbon dioxide that is essentially sustainable to produce [1–3]. The multi scaled porous structure within hemp-lime produces a high thermal resistivity alongside a high thermal storage capacity and moisture buffering properties, making it a desirable infill insulation material for use in building envelopes [4–7].

The most common method used to manufacture hemp-lime is to mix the components into a wet mix that is cast within formwork or block moulds. The process of casting is usually conducted in layers that are individually placed by tamping. The depth of layers, the degree of compaction and the direction of compaction with respect to the direction of thermal and mechanical loading are all variables within this process. The distribution of density within cast material is known to be dependent on depth within a single layer and globally a function of compaction [8, 9]; it is also known that the casting process produces an orientated internal structure [10]. Taken together these variables will in part determine the internal topology of the material and thus have an influence on the physical properties.

The effect of compaction of hemp-lime on the mechanical and thermal properties has been studied previously. Nguyen et al. [8, 9] found that static load compaction of fresh hemp-lime during casting can

J. Williams (✉) · M. Lawrence · P. Walker
BRE Centre for Innovative Construction Materials, Department of Architecture and Civil Engineering, University of Bath, Bath BA2 7AY, UK
e-mail: J.P.Williams@bath.ac.uk

Published online: 09 December 2016

improve the peak compressive strength and stiffness of the material; the thermal conductivity was also seen to increase but to a lesser extent. The results are attributed to a reduction of inter particle voids that would reduce the volume fraction of thermally resistive air and increase the volume fraction of structural binder. It is proposed elsewhere [11–16] and widely accepted that compressive strength and thermal conductivity of hemp-lime follows an approximate linear relation to density for this reason.

The density distribution through specimens of sprayed hemp-lime has been assessed previously and found to vary with depth [15]. In addition it has been observed elsewhere that cylinders of hemp lime cast in three layers will tend to fail in compression in the top third [17], suggesting of a lower density of material in this area. It is known from the study of other aggregate material that self-weight and boundary friction will impact density profile of a compacted layer. As these are both a result of the layer size then it is appropriate that for cast material, the layer size may influence the density distribution of the composite and impact on the physical properties. To the authors' knowledge, no preceding study exists that directly assesses how the size of layers used to cast hemp-lime influences the physical properties.

The aggregate used for hemp-lime comes from the stem of the plant and is therefore generally of an elongated form. The application of any compaction has been shown to produce a preferential orientation of the particles towards stratified planes perpendicular to the compacting force [10] that is widely considered to produce observed anisotropic behaviour [8, 18–21]. The compressive strength, compressive stiffness and failure mode of compacted hemp lime have been shown to depend on whether testing is conducted parallel or perpendicular to the compaction force [21] as has thermal conductivity [8, 20].

This paper considers how the variables of layer size and compaction affect the directional compressive behaviour and thermal conductivity of hemp-lime. Results are presented from uniaxial heat flow test and uniaxial compressive test for five permutations of cast material in two orientations (perpendicular and parallel with respect to casting). Additional information about the internal structure, obtained using a recently developed method of image analysis, is also presented.

2 Methodology

2.1 Specimen production

A single mixture of hemp-lime was used to investigate the influence of the internal structure on its properties, with the method of specimen casting the primary variable. The hemp shiv used was produced in France and the bulk properties and particle size distribution are reported in Table 1 and Fig. 1 respectively. The binder used was a commercially available formulated binder for use with hemp, containing mainly a high surface area natural hydraulic lime with the addition of pozzolanic additives. The ratio of binder, hemp and water used throughout the study was 2.25:1.0:3.0 (by mass), which is representative of the ratios widely used for walling applications [22, 23].

Mixing of the constituent materials was carried out in a revolving pan mixer. The binder and water were first combined to form a uniform slurry prior to the addition of the hemp shiv. Subsequent mixing was then conducted until a uniform mixture was achieved, paused occasionally to break up any clumps forming by hand. Pre-determined quantities of mixture were weighed out into oiled moulds and tamped to height successively to build up each specimen in the required number of layers. The specimens were left uncovered and transferred to a conditioning room at 20 °C and 70% relative humidity with the moulds being removed after six days.

Specimens were produced using a range of three layer sizes: 25, 50 and 150 mm; and three compaction levels: 30, 45 and 60% volumetric decrease from the uncompact state. Two sets, one to be tested parallel to compaction and one to be tested perpendicular to compaction, were produced for each variant of layer size and compaction level; the full range of permutations considered is detailed in Table 2 and diagrammatically explained in Fig. 2. For each of these permutations, three 150 mm cube specimens were produced for compressive testing with a further three produced for assessment of the internal structure. In addition a single 400 mm by 400 mm by 50 mm specimen was produced for thermal conductivity testing for all permutations except variant 6 where a 150 mm layer would exceed the required 50 mm specimen thickness.

Table 1 Hemp shiv properties

Country of origin	Bulk density (kg m^{-3})	Mean particle length (mm)	Length standard deviation (mm)	Mean particle width (mm)	Width standard deviation (mm)
France	122	3.34	3.51	1.06	0.987

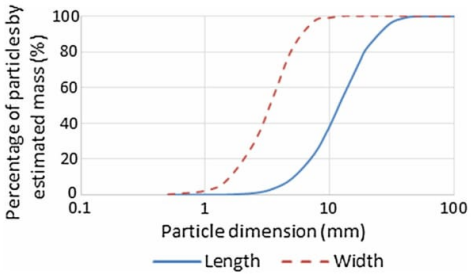

Fig. 1 Particle size distribution, length and width, from 2D image analysis

2.2 Experimental procedure

The methods and specimen ages from casting were chosen based on combination of the British Standards for compressive strength testing of concrete and insulation products [24, 25], as well as preceding studies on hemp-lime [8, 11, 15, 17]. All specimens were removed from the temperature and humidity controlled curing room and tested at 28 days after casting. Specimen masses and dimensions were measured to obtain 28 day densities as well as geometric parameters required for the calculation of stress and strain. Compressive tests were conducted using an Instron 50 KN testing rig at a controlled displacement of 3 mm/min; the inbuilt instrumentation was used to both record load and platen displacement at a resolution of one data point per 0.1 s.

Thermal conductivity measurements were conducted on the 50 mm × 400 mm × 400 mm specimens following oven drying for 48 h at 105°. Mass and dimensions were recorded for all specimens to determine density and for use in calculation of thermal conductivity. The thermal conductivity tests were undertaken using a Fox 600 heat flow meter with a temperature gradient of 10 to 30 °C. Prior to testing the specimens were wrapped with a single layer of clear shrink wrap food packing material in order to both protect the instrument and prevent moisture loss from the specimens during testing.

Assessment of each internal specimen structure was conducted using an original method developed by the authors [10]. In brief it comprises cutting six slices from each specimen using a band saw with the cuts made in the perpendicular plane to the direction of thermal and mechanical loading. The cut faces of each slice were then cast within a low viscosity colored

Table 2 The design permutations of hemp-lime specimens produced

Variant number	Direction of testing in relation to casting	Compaction (%vol reduction of uncompact)	Size of layers (mm)	Green density (kg m^{-3})	Ave 28 day density (kg m^{-3})
1	Parallel	45	150	649	423
2	Parallel	30	50	577	374
3	Parallel	45	50	649	412
4	Parallel	60	50	721	462
5	Parallel	45	25	649	406
6	Perpendicular	45	150	649	408
7	Perpendicular	30	50	577	355
8	Perpendicular	45	50	649	399
9	Perpendicular	60	50	721	450
10	Perpendicular	45	25	649	411

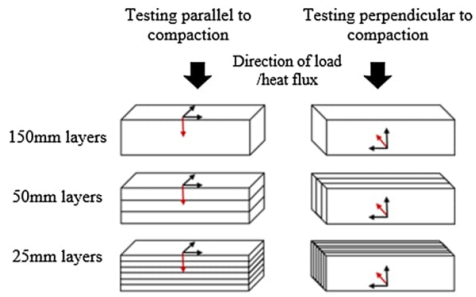

Fig. 2 Layering and testing direction arrangements for parallel and perpendicular loading with direction of compaction and preferred plane of orientation of particles indicated by the *red* and *black axis* respectively. (Color figure online)

resin, used to highlight the voids within the material, and sanded to reveal a section through the material; the prepared surfaces were 'imaged' with a flatbed scanner at a resolution of 1200 dpi. To enhance the contrast of the images produced, a red pigment was added to the slaked binder used in the production of the specimens to enable easier computer recognition of the differing parts of the image: voids (blue resin) binder (red) and hemp shiv (natural yellow).

Analysis of the images was carried out using ImageJ primarily using the measure and partial analysis tools. Prior to analysis the images were smoothed using a median filter to remove noise and then a threshold analysis was undertaken to identify a single constituent and binaries the image. Following this the binary image was further cleaned by use of an opening algorithm to help segregate touching particles and finally a partial analysis was conducted to identify and measure the discreet binary objects (shiv particles) within each image. The orientation of each particle within the image plane was assessed by means of an ellipse fitting process, as described in [10] and the results were combined into frequency analysis of the whole population to give an assessment of global orientation within the plane.

3 Results

3.1 Density

The 28 day average density of the different variations of material is given in Table 2 while the dry densities obtained after 48 h oven drying at 105 °C are given in Table 3. From table two it is apparent that the density at 28 days varies with orientation of casting as well as compaction but not layer thickness; the parallel compaction direction is found to be on average 2.6% higher than the parallel direction. From the dry densities, Table 3 again the dry densities are found to be higher in the parallel direction however in this case the average increase is only 1.5% and of comparable magnitude to the average variation found between similar specimens of 1.0%. It is suggested therefore that the casting orientation has bearing on the drying hysterics of the material and thus the 28 day density but negligible impact on the dry density of the material, considered to be solely a result of the compaction where the constituents are kept constant.

3.2 Compressive behaviour

The average stress–strain graphs for three specimens tested parallel (variant 3) and perpendicular (variant 8), with the median layer size and compaction, are shown in Fig. 3. As observed previously the failure mode exhibited when loaded parallel to the casting compaction direction was different to that when loaded perpendicular. A difficulty therefore arises in selecting a definition of compressive strength that can be compare performance in both directions. This is made harder still by the lack of a definable peak stress observed in parallel loading of cube specimens, but rather strain hardening, and a variable initial period of material settling, Fig. 3.

As insulation materials typically have much lower stiffness compared to structural materials, the compressive resistance of insulation materials, such as rigid foam, is commonly defined as the stress attained at a given strain level [24]. A similar approach has also previously been adopted in the study of bio-aggregate composites [26–28]. As the strain level that defines resistance is somewhat arbitrary, combined with the variable initial settling period for hemp-lime, an alternative approach was proposed for parallel loaded material by Tronet et al. based on a model developed for FRP-confined concretes [16]. This approach uses a repeatable method for the calculation of a yield stress that is both independent of initial displacement (settling) and compatible with prolonged strain hardening. However, whilst this approach is a development from that that of preceding studies, it is not applicable

Table 3 Volumetric proportion of air obtained by 2D image analysis of hemp-lime at different compaction levels

Variant number	Direction of testing in relation to casting	Compaction (%vol reduction of uncompact)	Size of layers (mm)	Volume of air (%macroscopic level)	Dry density (kg m^{-3})
1	Parallel	45	150	30.8	345
2	Parallel	30	50	40.7	319
3	Parallel	45	50	32.7	338
4	Parallel	60	50	23.5	379
5	Parallel	45	25	31.6	338
6	Perpendicular	45	150	35.8	336
7	Perpendicular	30	50	41.7	304
8	Perpendicular	45	50	35.6	337
9	Perpendicular	60	50	23.8	372
10	Perpendicular	45	25	31.6	346

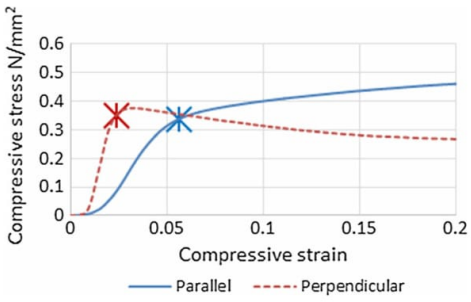

Fig. 3 The stress strain relationship for parallel and perpendicular loaded hemp lime cube specimens with the rupture stress indicated

for material loaded in the perpendicular direction that do exhibit a peak stress and no strain hardening post yielding and so was not applicable to this study.

An alternative parameter is proposed in this study to compare hemp-lime material performance in both loading orientations. The composite rupture stress has been defined in this study thus: the stress at the strain where the tangent Young's Modulus of the material, taken from a moving sample of twenty consecutive data points, falls to 25% of its peak value. While the selection of the proportion is in itself arbitrary, the threshold strain value is determined by the material's behaviour. The proposed approach accounts for both the initial low stiffness (settling) and the different apparent stiffness of the hemp-lime in each direction, while being insensitive to post yielding behaviour.

The effect of compaction and layer size on compressive rupture stress in both the parallel and perpendicular directions is shown in Fig. 4. The compressive rupture stress of hemp-lime increases with increasing casting compaction effort in both the perpendicular and parallel loaded directions, Fig. 4 (left). For a 30% increase in compaction the rupture stress increased by 200 and 175% in the perpendicular and parallel directions respectively. The average coefficient of variance from the results represented in Fig. 4 (left) was found to be 7.0%, indicating that while the natural variance in these materials is high, the increase from compaction in both cases is a significant result.

The compressive rupture stress of hemp-lime is generally independent of casting layer thickness within the range of 150to 25 mm, in both the parallel and perpendicular directions with respect to casting [Fig. 4 (right)]. There is a small apparent increase in compressive rupture strength in the perpendicular direction of 17 and 30% respectively for casting in 25 and 150 mm layers compared to 50 mm. While the average coefficient of variance for these results, 6.6%, indicates these increases may be significant, it is noted that they are of significantly lower magnitude that those observed in altering compaction, and have come from a relatively small sample size.

3.3 Thermal conductivity

The thermal conductivity results for the hemp-lime materials considered are presented in Fig. 5. On

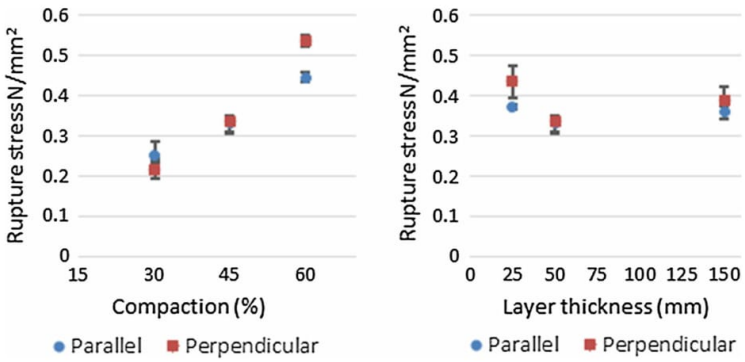

Fig. 4 The parallel and perpendicular compressive rupture stress of hemp-lime at different compaction levels (*left*) and different layer thicknesses (*right*)

average the perpendicularly tested specimens exhibited a 16% higher thermal conductivity than the parallel tested specimens. While this is lower than the results reported by Pierre [20], who found a 33% directional difference in thermal conductivity, it is in line with the results of several others [29, 30]. It is observed from Fig. 5 (left) that compaction has a strong positive correlation with thermal conductivity. There is no evidence of a correlation between layer thickness and thermal conductivity in the perpendicular direction and the omission of a result for a 150 mm thick layer means no conclusive statements can be drawn in the parallel direction.

3.4 Internal structure

The results for the frequency analysis of particle orientation are presented in Fig. 6 and the volumetric proportions of air voids obtained and the 28 day density presented in Table 3. A clear difference is observed in the frequency diagrams between the perpendicular and parallel orientations, which is indicative of an anisotropic internal structure, consistent with previous results presented previously by the authors [10].

Neither compaction nor layer thickness affect the particle distribution in the parallel direction, which remained consistent in all cases (Fig. 6). The shape of the graph in this instance suggests an even and thus random distribution of particles as would be expected in planes perpendicular to the compacting force. The slightly higher frequencies at the extremes, 0° and 90°, are believed to be a result of the mould edges.

In the perpendicular direction there is again consistency in the distributions across compaction and layer thickness indicating a minimal impact. Variant 7, the lowest compaction level, appears to have the flattest graph and thus lowest degree of orientation. A relationship between compaction and degree of orientation is, however, not observed as the

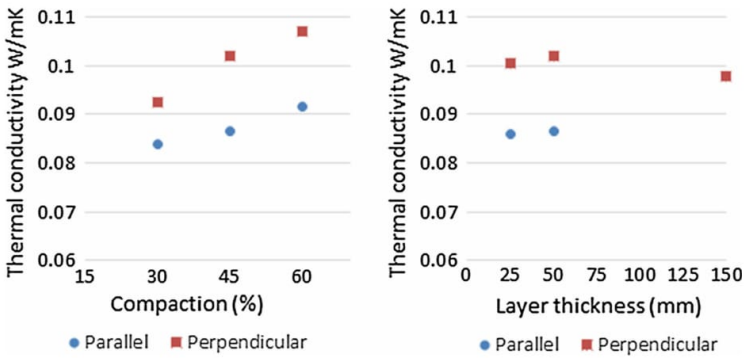

Fig. 5 The parallel and perpendicular thermal conductivity of dry hemp-lime at different compaction levels (*left*) and different layer thicknesses (*right*)

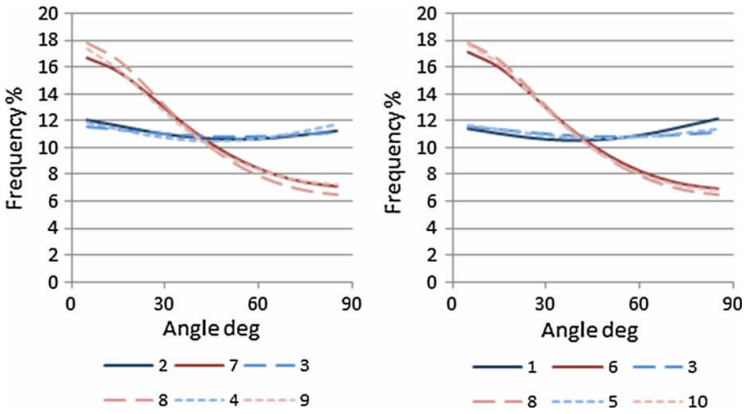

Fig. 6 The parallel and perpendicular particle orientation frequency distributions obtained by 2D image analysis of hemp-lime at different compaction levels (*left*) and different layer thicknesses (*right*)

most compact (variant 9), is observed to have a flatter graph than the median compaction (variant 8). From Fig. 6 (right) the variant with the largest layer sizing (variant 6) appears to have a flatter graph than the similar variants of smaller layer sizes. Variations in all cases are however small and comparable to the natural variation that is assumed to be exhibited in the perpendicular distributions.

4 Discussion

It is evident from the results presented in Fig. 6 that an anisotropy in the particle arrangement of the hemp in hemp-lime composites produces anisotropic thermal and mechanical behavior (Figs. 3, 5). The anisotropic arrangement of the particles is attributed to the casting process, where the application of even the lowest amount of compaction force will tend the particles into stratified planes in the perpendicular direction. As the orientation of the particles is evenly distributed in the other two axes, the result is a material with a bidirectional internal structure and physical properties.

Increasing compaction was found to produce higher compressive rupture stress and thermal conductivity in both orientations, and can be generally attributed to a reduction in the proportion of air voids in the composite, Table 3. The impact of compaction is however not global but instead is observed to have greater bearing in the perpendicular direction; a 30% increase in compaction resulting in an increase in the rupture stress of 200% in the perpendicular direction compared to 175% in the parallel directions. A differing increase of dry density for the two directions was observed, 21.7 and 18.8% respectively, put down to natural variations in the material and casting that may at least in part account for this.

To ascertain to what extent variation in density might explain the seemingly directionally dependent influence of compaction, the dry density can be plotted against compressive rupture stress, Fig. 7. It can be seen from Fig. 7 that the relation of dry density to compressive rupture strength is not consistent across the two directions. The differing increases of density with compaction observed in the two directions is therefore insufficient alone to account for apparent directionally dependent influence of compaction and a further explanation is needed. A logical reason would be greater compaction producing a greater degree of orientation, however, this is not supported by the image analysis that showed a lower degree of orientation present in the most compact variant. As has been found in similar analysis of other materials [31] it is possible that high compaction could increase the misidentification of touching particles, as single particles, and thus this discrepancy, may be explained by a limitation of the method used.

The layer sizes used in the casting process were not observed to influence either the thermal conductivity or the rupture stress of the material within the range of 25 to 150 mm. It had been thought that the layer size would influence the local distribution of material during casting with smaller layers leading to a more

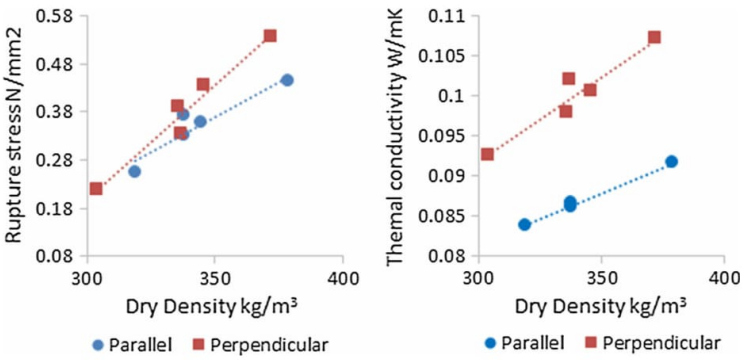

Fig. 7 The parallel and perpendicular rupture stress (*left*) and dry thermal conductivity (*right*) with respect to density

homogenous material. This in turn could reduce possible stress concentrations or thermal bridges through the material thus influencing behaviour. The results indicate that this is not the case for the range of layer sizes considered here, however, the results of others who have plotted density with depth of larger specimens indicate that it may still have bearing at larger layer sizes [8].

A common way to model the thermal conductivity and compressive strength of hemp-lime is as a linear function of dry density [12], as this is both easy to control on site and has been shown to be accurate for most cases. While a linear relationship between density and these properties is a good fit for the results obtained in this study it is also apparent that a single global linear function is not sufficient and different functions are required in the perpendicular and parallel direction respectively, Fig. 7. If it is assumed that the parallel and perpendicular functions are the bounding conditions, then a global model can be produced for thermal and physical loading in any direction by combining them into a weighted function of orientation.

To provide a form for the orientation function a comparison can be made to timber, where the compressive strength is modelled with respect to grain direction by the Hankinsons distribution [32]. As this distribution has already been found by the authors to be an appropriate form for the particle distribution within hemp-lime [10] and thus its internal structure, it is likely that it may also be appropriate for the modelling of thermal conductivity and rupture stress with respect to orientation. By substituting in the linear equations for rupture stress and thermal conductivity as found from the experimental data, Fig. 7, into the Hankinsons form, the following is derived:

$$\text{Rupture stress} = \frac{(0.0029\rho - 0.66)(0.0048\rho - 1.2)}{(0.0029\rho - 0.66)\sin^n\theta + (0.0048\rho - 1.2)\cos^n\theta}, \quad (1)$$

$$\text{Thermal conductivity} = \frac{(0.00013\rho + 0.043)(0.00021\rho + 0.028)}{(0.00013\rho + 0.043)\sin^n\theta + (0.00021\rho + 0.028)\cos^n\theta}, \quad (2)$$

where ρ is the dry density of the composite, θ is the direction of thermal or mechanical loading with respect to the direction of casting compaction and n is a constant that can be derived by fitting to experimental data. The four linear functions fitted to the data in Fig. 7 and used in Eqs. 1 and 2 have R-squared values of 0.878, 0.959, 0.996 and 0.920 respectively indicating a good level of fit of these functions and justifying there use in the model.

5 Conclusions

This paper considers the influence of the casting process on the thermal and mechanical properties of hemp-lime and applies a newly developed method of image analysis to investigate the role of the internal structure in the manifestation of these properties.

A clear anisotropy in the material's structure is observed through the image analysis for all variations

considered in this study. This is attributed to the compaction produced in casting causing the elongated particles of hemp to tend towards perpendicular strata. The influence of this on the physical properties of thermal conductivity and compressive behaviour is shown to be profound and so necessitates that further study into bio-aggregate composites accounts for it.

The thickness of the layering used to cast the material was found to have no clear impact on the internal structure or the mechanical properties for the range of layer sizes considered. An initial assumption that a larger layer size would create a less homogenous material was shown not to be the case within the range of this study, however, it is considered likely that this may not apply to larger layer sizes. From a commercial standpoint it can be stated that there is no benefit to using layer sizes smaller than 150 mm during the manufacture of hemp-lime.

The degree of compaction used in casting was found to influence both the internal structure and in turn the physical properties of the composite. Increasing compaction was found to decrease the proportion of air voids in the material and thus increase both the compressive rupture stress and the dry thermal conductivity; in both cases this was found to be more pronounced in the perpendicular direction. It is considered possible that this is due to a higher level of orientation being produced at higher compaction however this was not confirmed by the image analysis possibly due to a limitation of the method.

The finding that compaction does not have a global impact on the properties of hemp-lime, but rather a directionally dependent one, is of high significance in the modelling of properties and development of the material. A new form of directionally weighted linear model for thermal conductivity and compressive strength is suggested based on a previously established model for timber, although further work is required to ascertain if the Hankinsons form of the weighting equation is more generally applicable.

Acknowledgements This study was funded by the Engineering and Physical Sciences Research Council (grant number EP/L016869/1).

Compliance with ethical standards

Conflict of interest The authors declare that they have no conflict of interest.

References

1. Boutin M et al (2005) Analyse du Cycle de Vie de Mur en Béton Chanvre Banché sur Ossature en Bois. INRA, Lille
2. Ip K, Miller A (2012) Life cycle greenhouse gas emissions of hemp–lime wall constructions in the UK. Resour Conserv Recycl 69:1–9
3. Hustache Y, Arnaud L (2008) Synthèse des connaissances sur les bétons et mortiers de chanvre. Construire en Chanvre, Quebec City
4. Evrard A, De Herde A (2010) Hygrothermal performance of lime-hemp wall assemblies. J Building Phys 34(1):5–25
5. Collet F, Pretot S (2014) Experimental highlight of hygrothermal phenomena in hemp concrete wall. Build Environ 82:459–466
6. Lawrence M et al (2012) Hygrothermal performance of an experimental hemp-lime building. Key Eng Mater 517:413–421
7. Le Tran A et al (2010) Transient hygrothermal behaviour of a hemp concrete building envelope. Energy Build 42(10):1797–1806
8. Nguyen TT et al (2010) Effect of compaction on mechanical and thermal properties of hemp concrete. Eur J Environ Civil Eng 14(5):545–560
9. Nguyen T-T et al (2009) Influence of compactness and hemp hurd characteristics on the mechanical properties of lime and hemp concrete. Eur J Environ Civil Eng 13(9):1039–1050
10. Williams J, Lawrence M, Walker P (2016) A method for the assessment of the internal structure of bio-aggregate concretes. Constr Build Mater 116:45–51
11. Arnaud L et al (2013) Mechanical behavior. bio-aggregate-based building materials. Wiley, New York, pp 153–178
12. Cerezo V (2005) Propriétés mécaniques, thermiques et acoustiques d'un matériau à base de particules végétales: approche expérimentale et modélisation théorique. L'Institut National des Sciences Appliquées de Lyon, Villeurbanne
13. Collet F, Prétot S (2014) Thermal conductivity of hemp concretes: variation with formulation, density and water content. Constr Build Mater 65:612–619
14. Balčiūnas G et al (2013) Physical properties and structure of composite made by using hemp hurds and different binding materials. Procedia Eng 57:159–166
15. Elfordy S et al (2008) Mechanical and thermal properties of lime and hemp concrete ("hempcrete") manufactured by a projection process. Constr Build Mater 22(10):2116–2123
16. Tronet P et al (2016) Study of lime hemp concrete (LHC)—mix design, casting process and mechanical behaviour. Cem Concr Compos 67:60–72
17. Hirst EAJ (2013) Characterisation of hemp-lime as a composite building material. University of Bath, Bath

18. Magniont C et al (2012) Use of plant aggregates in building ecomaterials. Eur J Environ Civil Eng 16(sup1):s17–s33
19. Gross C et al. (2012) Structural enhancement of timber stud framing using renewable insulation materials. In: 12th world conference on timber engineering, p 19
20. Pierre T, Colinart T, Glouannec P (2014) Measurement of thermal properties of biosourced building materials. Int J Thermophys 35(9–10):1832–1852
21. Nozahic V et al (2012) Design of green concrete made of plant-derived aggregates and a pumice–lime binder. Cem Concr Compos 34(2):231–241
22. Bevan R et al (2008) Hemp Lime Construction: a guide to building with hemp lime composites. BRE Press, Berkshire
23. Lanos C et al (2013) Formulation and implementation. In: Arnaud L, Amziane S (eds) Bio-aggregate-based building materials. Wiley, New York, pp 117–152
24. British Standards (2013) BS EN 826:2013—thermal insulating products for building applications. Determination of compression behaviour. Wärmedämmstoffe für das Bauwesen. Bestimmung des Verhaltens bei Druckbeanspruchung
25. British Standards (2009) BS EN 12390-3:2009—testing hardened concrete. Compressive strength of test specimen
26. Sinka M, Sahmenko G (2013) Sustainable thermal insulation biocomposites from locally available hemp and lime. Environ Technol Resour 1:73–77
27. Sassoni E et al (2014) Novel sustainable hemp-based composites for application in the building industry: physical, thermal and mechanical characterization. Energy Build 77:219–226
28. Youssef A et al. (2015) Compressive and shearing behaviour of lime and hemp concrete. In: First international conference on bio-based biulding materials, Clermont-Ferrand, France
29. Amziane S, Nozahic V, Sonebi M (2015) Design of mechanically enhanced concrete using hemp shiv. In: First international conference on bio-based building materials, Clermont-Ferrand, France
30. Dinh T et al. (2015) Hemp concrete using innovative pozzolanic binder. In: First international conference on bio-based building materials, Clermont-Ferrand, France
31. Kutay ME et al (2010) Three-dimensional image processing methods to identify and characterise aggregates in compacted asphalt mixtures. Int J Pavement Eng 11(6):511–528
32. Hankinson R (1921) Investigation of crushing strength of spruce at varying angles of grain. Air Serv Inf Circ 3(259):130

8.2 Papers under review

Submitted to Construction and Building Materials March 2017:

The influence of constituents on the properties of the bio-aggregate composite hemp-lime

Joseph Williams*, Mike Lawrence, Pete Walker

BRE Centre for Innovative Construction Materials, Department of Architecture and Civil Engineering, University of Bath, Bath, BA2 7AY, UK

* J.P.Williams@bath.ac.uk

Abstract

Composites made of bio-aggregate particles and lime based binder can be used as a low embodied energy alternative to traditional walling systems and can provide several performance advantages. As the ratio and nature of constituents used in bio-aggregate composites will have bearing on the properties, it is necessary for these to be capable of being optimised to meet specific design requirements. In addition, as these materials are known to be anisotropic, it is required that any impact of constituents is assessed with respect to orientation. In this paper, the influence of the binder to aggregate ratio and aggregate particle size distribution on the compressive strength, flexural strength and thermal conductivity of hemp-lime composites in two directions of loading have been assessed. A newly developed image analysis method was also employed to study the topology of the internal structure. The results show that the material is anisotropic in both behaviour and internal structure and that both binder/aggregate ratio and aggregate particle size distribution affect composite properties. In the case of binder to aggregate ratio, the impact is shown to be directionally dependent and indicative of differing governing factors controlling the failure mode in opposing loading directions.

Key words

Hemp-lime, mechanical properties, thermal conductivity, anisotropic structure

1. Introduction

Bio-aggregate composites are formed from a mineral binder and bio-aggregate particles such as hemp [1-3], sun flower [4-6] or rape stalk [7, 8]. The wet mixture can be cast or projection formed around a structural frame as an insulating infill [9] with such walls exhibiting lower embodied energy than traditional alternatives [10-12]. In

addition composites of hemp and lime have been shown to offer a beneficial compromise between thermal conductivity and thermal inertia, enabling the passive moderation of building climate [13-15]. Despite these advantages the application and utilisation of bio-aggregate composites remains low in construction due in part to the high variability of a bio-sourced product and in part to the conservative nature of the industry. A better understanding of the material's performance, leading to control and optimisation of physical properties, is a necessary step in addressing these issues.

As composite materials, alterations to the ratio and nature of the constituents are logical avenues of material development. The ratio of binder to aggregate and its influence on thermal conductivity and mechanical strength of hemp-lime have been studied extensively [4, 16-18] with unanimous agreement that an increase in the binder quantity increases the compressive strength, flexural strength and thermal conductivity. This is attributed to an increasing binder content tending the behaviour of the composite to that of the binder, [19, 20] and several models for thermal conductivity and compressive strength have been proposed based broadly on this assessment. Mechanical properties and thermal conductivity have been modelled simplistically as a function of density [3, 21], considered an indicator of binder content, and more recently, through multi-phase models that specifically accounts for the ratio of constituents [18]. While such models are logical, it should be noted that they assume an isotropic relationship in a material that is known to have an anisotropic structure and behaviour [22].

The influence of the particle size distribution of the bio-aggregates used has also been studied previously [23-25]. While in all studies reviewed, particle size distribution has been shown to impact on the physical properties of materials, although there has been limited consensus between studies as to the relationship. It has been observed by some that a finer grade of particles provides an increase in mechanical strength and a smaller increase in thermal conductivity [23, 24], attributable to a closer packing of the particles [19]. Contrastingly, others found that a coarser grade of particles yielded better mechanical properties, attributed to a greater overlap of particle [25]. A possible reason for the disagreement of these conclusions may be the small fluctuations in properties reported compared to relatively large natural variation. Alternatively it may also be argued that previous studies tend to express bio-aggregate grades simply as finer or coarser based on average length; other potentially significant factors such as the spread of the distribution or aspect ratio of particles may thus have been overlooked.

Within the body of previous work it is noticeable that the effect of changing these variables is often only reported in one orientation but the observed relationships are assumed to apply globally. It is now known that the internal structure of the bio-aggregate composite hemp-lime is orientated [22] as a result of the production method chosen and the elongated form of the particles. It has also been identified from a number of sources that the mechanical behaviour and thermal conductivity of bio-aggregate composites are anisotropic [19, 26-28] that may be attributed to the structure and presumed to apply in all cases where the bio-aggregates are elongated. It is therefore necessary to consider any influence of constituent variables within this context meaning it cannot be assumed that constituent variables have an isotropic effect. To the author's knowledge it has not previously been ascertained if changing the binder concentration or the particle size distribution has a global or directionally dependant influence on physical properties.

This paper considers the thermal conductivity, compressive strength and flexural strength of hemp-lime specimens produced with three ratios of hemp to binder and three distinct grades of hemp aggregate; the particle distribution of the hemp aggregate fully characterised in each instance by means of two dimensional imaging. In order to ascertain if any effects are directionally dependent, thermal and mechanical tests were conducted in two directions: parallel to the direction of casting force and perpendicular to it. A recently developed method for assessment of the internal structure of bio-aggregate composites was also used in each case to provide an insight into the internal topology and to help inform any conclusions drawn about the mechanisms involved.

2. Method

2.1 Specimen production

Five mixtures of hemp-lime were considered in the study covering a range of three distinct grades of hemp aggregate and three hemp to binder ratios, (table 1). Hemp lime was chosen due to it being the most prominently assessed bio-aggregate composite within the literature and indeed industry. In order to minimise the total amount of material used, single sets of rectangular prism specimens were produced for all mechanical tests as well as the internal structure assessment. The prisms produced were all 400mm x 150mm x 150mm for testing in three point bending. Following the flexural test, one half was resized to a 150mm cube used for compressive testing and one half sliced into 150mm x 150mm x 25mm slices for the analysis of the internal structure. For thermal conductivity tests, 400mm x 400mm x 50mm specimens were

produced of each mixture. In all cases two sets of specimens were cast, one for testing parallel to the casting compaction and one perpendicular.

The specimens were produced by first combining water and the binder in a revolving pan mixer to produce a uniform slurry. Once uniform, the hemp aggregate was added and further mixing conducted until a homogenous mixture was observed. The total mixing time was under 5 minutes in each case. The binder used throughout the study was a commercially available pre-formulated binder for use with bio-aggregates produced by Tradical®. The hemp aggregate used was grown and processed in France and supplied by the producer in four grades 7,8,12 and 14. The three grades used for this study were 7 (referred to herein as fine), 14 (referred to herein as coarse) and 1:1 by mass mixture of 8 and 12 (referred to herein as medium). The rationale of mixing two of the manufactures' grades to produce the medium grade was to ensure a wider distribution of particle sizes in this grade compared to the fine and coarse grades.

The combined mixture was weighed out into the moulds prepared with release oil in 50mm layers with light tamping between each layer. The amount of material weighed out in each case was predetermined in order to produce a similar compaction state across the specimens. In this study this was set at 45% densification of loose-state density, determined for each mix by weighing a set volume of un-compacted material placed carefully by hand, (table 1). The specimens were stored after production in a conditioned room at 20°C and 70% relative humidity, uncovered in the moulds for 6 days and uncovered out of the moulds thereafter.

Table 1 Variations of hemp-lime produced

Variation ID	Grade of hemp aggregate	Binder to aggregate ratio (by mass)	Hemp / Binder / Water (by mass)	Loose density (kgm^{-3})	Target wet density (kgm^{-3})	Mean measured 28 day density (kgm^{-3})
F 2.2	Fine	2.2 : 1	16% / 36% / 48%	459	666	422
M 1.8	Medium	1.8 : 1	17%/ 32%/ 51%	407	590	374
M 2.2	Medium	2.2 : 1	16% / 36% / 48%	433	628	406
M 2.6	Medium	2.6 : 1	15% / 39% /	470	682	432

C 2.2	Coarse	2.2 : 1	46% 16% / 36% / 48%	411	596	382

2.2 Material classification

The three grades of aggregate used in this study: fine, medium and coarse were assessed for particle size distribution by a method of two dimensional image analysis developed by Picandet [29]. This was selected over a simple sieving method in order to provide data about both particle length and width. The analysis was conducted on a 20g sample of each grade removed from a 20kg bag by a process of quartering. Scanning was conducted by arranging a small amount of particles with their largest surface face down on the surface of a flatbed scanner by hand in order to segregate them. This was then scanned against a blue background at a resolution of 1200dpi and the process repeated until the full 20g was imaged.

All image processing and measurements were conducted using the program ImageJ and the method used follows that described by Picandet [29] and reported here in brief. In each case a colour threshold was applied to the image to produce a binary image of the hemp. The binary images were then enhanced using three iterations of an opening algorithm to remove noise and dust. Assessment of each image was conducted using the particle analysis tool that identifies the primary and secondary axis of each discrete binary object. This is done though equalising the particle's second moments of area to that of an ellipse whose axes are then used to provide a measure of length and width.

To produce a distribution comparable to a sieving analysis, an estimated volume for each particle is calculated based on the area of the particles and an assumption that average thickness is proportional to particle width. Assuming uniform density, this can then provide an estimated mass of the particle allowing for the production of an estimated mass distribution of the sample for both particle length and width. The particle size distributions for the three grades of aggregate are presented in figure 1 while bulk density and particle size distribution parameters are presented in table 2. The mean aspect ratio is the unweighted average value of a particles length divided by width for the population and provided a numerically comparable value of particle elongation while the interquartile range of mass may be used to compare the spread of distributions.

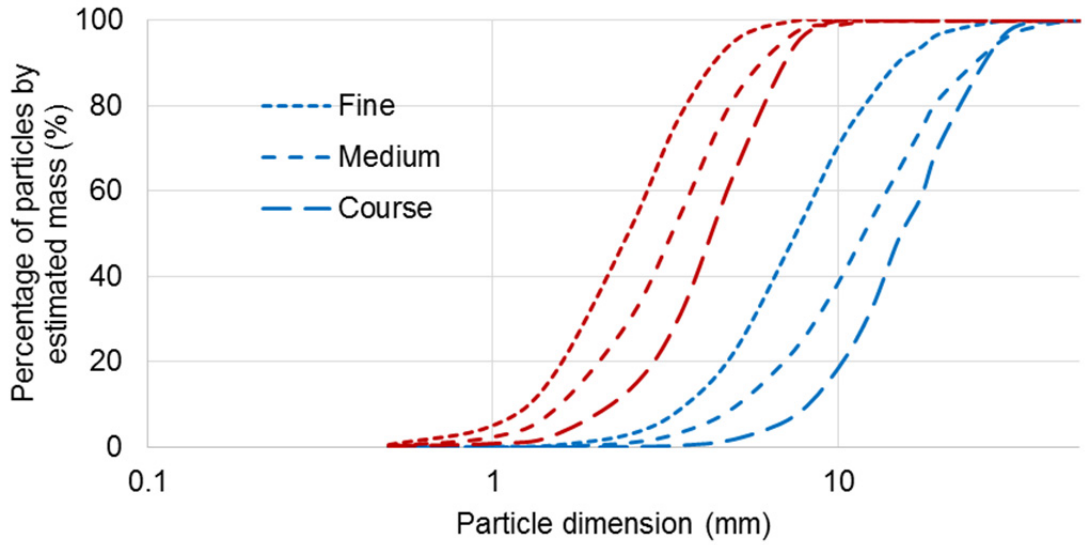

Figure 1 Particle size distribution length (blue) and width (red) by image analysis of 20g sample

Table 2 Properties of hemp shiv grades

Hemp Grade	Bulk Density (kgm^{-3})	Median particle length (mm)	Median particle width (mm)	Particle length interquartile range (mm)	Particle width interquartile range (mm)	Mean aspect ratio (length /width)
Fine	129	7.54	2.47	5.54	1.60	3.04
Medium	122	11.88	3.31	9.80	2.26	3.27
Coarse	119	15.27	4.30	9.42	2.44	3.66

2.3 Physical testing

Flexural tests were conducted at 28 days after casting by means of a three point bending test over a span of 300mm.Tests were conducted at a constant displacement of 3mm per minute on an Instron 50KN testing frame with inbuilt instrumentation and large diameter dowel supports were used to minimise any local crushing, figure 2. Each variation was tested in two directions: the load applied parallel to the direction of casting force and with the load applied perpendicular to the direction of casting force by rotating the specimen 90° about the major axis, figure 2. All data were collected using inbuilt instrumentation at a sampling rate of 10Hz. Each test was repeated three times.

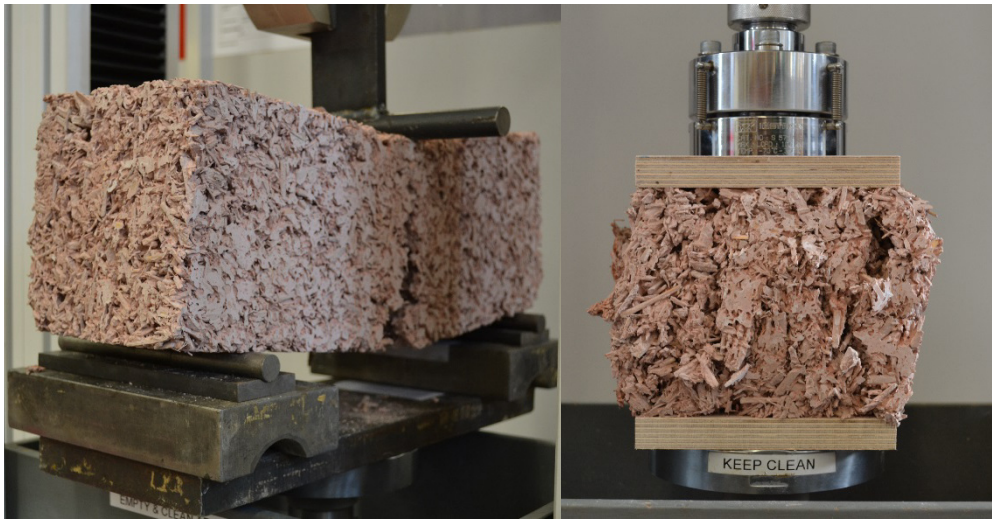

Figure 2 Flexural and compressive testing setup

Compressive tests were conducted immediately following the flexural tests at to provide 28 day values in both cases. One half of the specimen was reduced to a 150mm cube prior to testing by using a band saw fitted with a fine blade to minimise damage. All the tests were carried out on an Intron 50KN testing frame using the same test parameters and in the same loading direction as the flexural tests, figure 2 and 3. As the compressive failure modes of the material are known to be different in the differing testing directions, a parameter that is universally applicable to both conditions is required in order to compare the results. In this case failure of the material is considered to occur at a point of rupture, defined as when the instantaneous stiffness falls to 25% of its recorded maximum based on a 20 point moving average. All mechanical tests were conducted in triplicate with the presented results being the mean value.

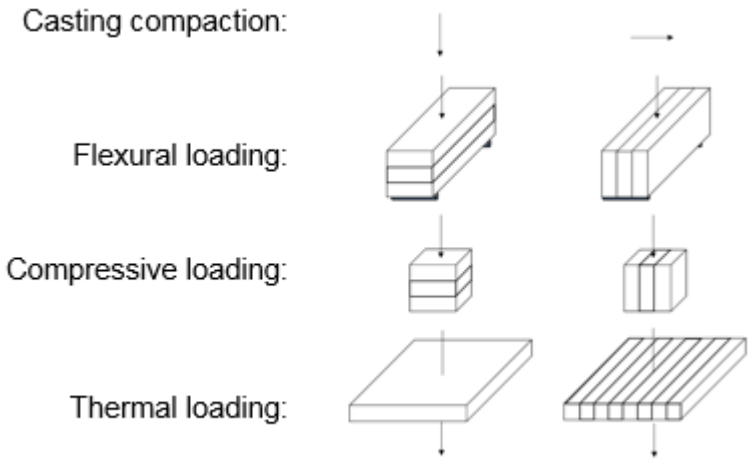

Figure 3 The mechanical and thermal loading arrangements with respects to casting compaction for parallel loaded specimens left and perpendicular loaded specimens right

Thermal conductivity tests were conducted after a minimum of 28 days and after oven drying of the specimens at 105° for 48 hours. All tests were conducted using a Fox 600 heat flow meter at a temperature gradient of 10-30°C and in the orientations indicated in figure 3. The specimens were wrapped in a single layer of Clingfilm to protect the machine and limit moisture incursion.

2.4 Image analysis of internal structure

Two dimensional image analysis of the internal structure was conducted on 150mm square slices taken from each of the flexural specimens after testing. The method used was developed in previous work by the authors and fully detailed elsewhere [22]. Six slices were produced in each case in planes perpendicular to the direction of compressive loading, (figure 2). The slices were encased in a blue casting resin prior to being sanded to reveal a cross section for analysis. The resin has the effect of both stabilising the face, that may be fragile, as well as improving the contrast of voids in the images. Imaging was conducted of the cross sections using a flatbed scanner at a resolution of 1200dpi providing a pixel size of 0.0213mm square.

Enhancement and analysis of the images was conducted in several stages using the software ImageJ. A 10px median filter was first applied to all images to remove noise and smooth outlying pixels by replacing each pixel with the median value of those within the specified radius, the selection of which was based on previous work. Following this, a series of colour threshold filters were used to produce binary images of the air, binder and aggregate and measure their perspective proportions visible at this scale. To assess orientation, the binary images of the aggregates were enhanced with three iterations of a binary opening algorithm to help segregate adjacent particles and analysed using the inbuilt particle analysis tool. The particle analysis tool identifies and measures the discrete binary objects visible within an image, including the length, width and orientation of a fitted ellipse of the same second moments and area. To provide an indication of the overall orientation of the material, orientations of each particle for the full population of all 6 images were combined into a frequency distribution. Based on preceding work where a sensitivity study into the impact of the processing was conducted, the process was controlled with values used based on the proceeding study.

3. Results

3.1 The impact of binder content

The compressive rupture stress, flexural strength, thermal conductivity and particle orientation distribution for specimens tested with differing binder ratios are presented in figure 4 a, b, c and d respectively.

In the parallel direction of loading a strong positive correlation is observed between binder content and the three assessed properties: compressive rupture stress, peak flexural stress and thermal conductivity. In each of these cases the impact of the binder ratio was found to be of greater magnitude compared to the natural variation found in similar specimens indicating the significance of the hemp to binder ratio in determining these properties in this direction. These findings are in agreement with the previous findings of others who also observed a similar correlation for tests in this direction [4, 16-18].

In the perpendicular direction of loading, a positive correlation to binder content is again seen for flexural strength and thermal conductivity. The compressive rupture stress is also seen to have a positive correlation to binder ratio between the ratios of 1:1.8 and 1:2.2 however it is not observed for the higher 1:2.6 binder ratio where there is no significant difference from 1:2.2 and a perception of a slight decrease. In all the results a clear and significant difference can be seen in all three properties between the loading directions, which is in line with results of others [26-28]. There are no known existing studies that consider directly the impact of hemp to binder ratio on perpendicular performance of the material for these results to be compared to.

It is observed that the distributions of particle orientations in these two directions are of noticeably differing form: an even distribution imaged in the parallel direction compared to a swayed distribution imaged in the perpendicular direction. The material may be considered to have no preferential orientation in planes perpendicular to initial casting compaction and orientated in parallel planes. In the perpendicular direction this sway of orientation is observed to be greatest in the low binder ratio specimens compared to the higher binder ratio specimens. The degree of orientation therefore appears to be inversely proportional to binder content however the trend is only slight and may not be significant in the reflection of the natural variance observed in the parallel direction imaging.

Figure 5 presents the average stress strain plots from the three specimens of material tested of each binder ratio in both parallel and perpendicular compression and flexure.

Figure 5 reiterates many of the findings observed in figure 4 but gives additional insight into the failure modes exhibited. It is noted that in compression the failure mode occurring in loading parallel to the casting compaction is of a change in stiffness and high ductility associated with the failure of the binder structure and subsequent densification of the material. In the perpendicular direction of loading the failure mode is more brittle with a clearly defined peak. In flexure it is noticed that the direction of loading has little to no bearing on the failure mode or stiffness however the form of the plots do imply that binder ratio may have an impact on both the compressive and flexural stiffness.

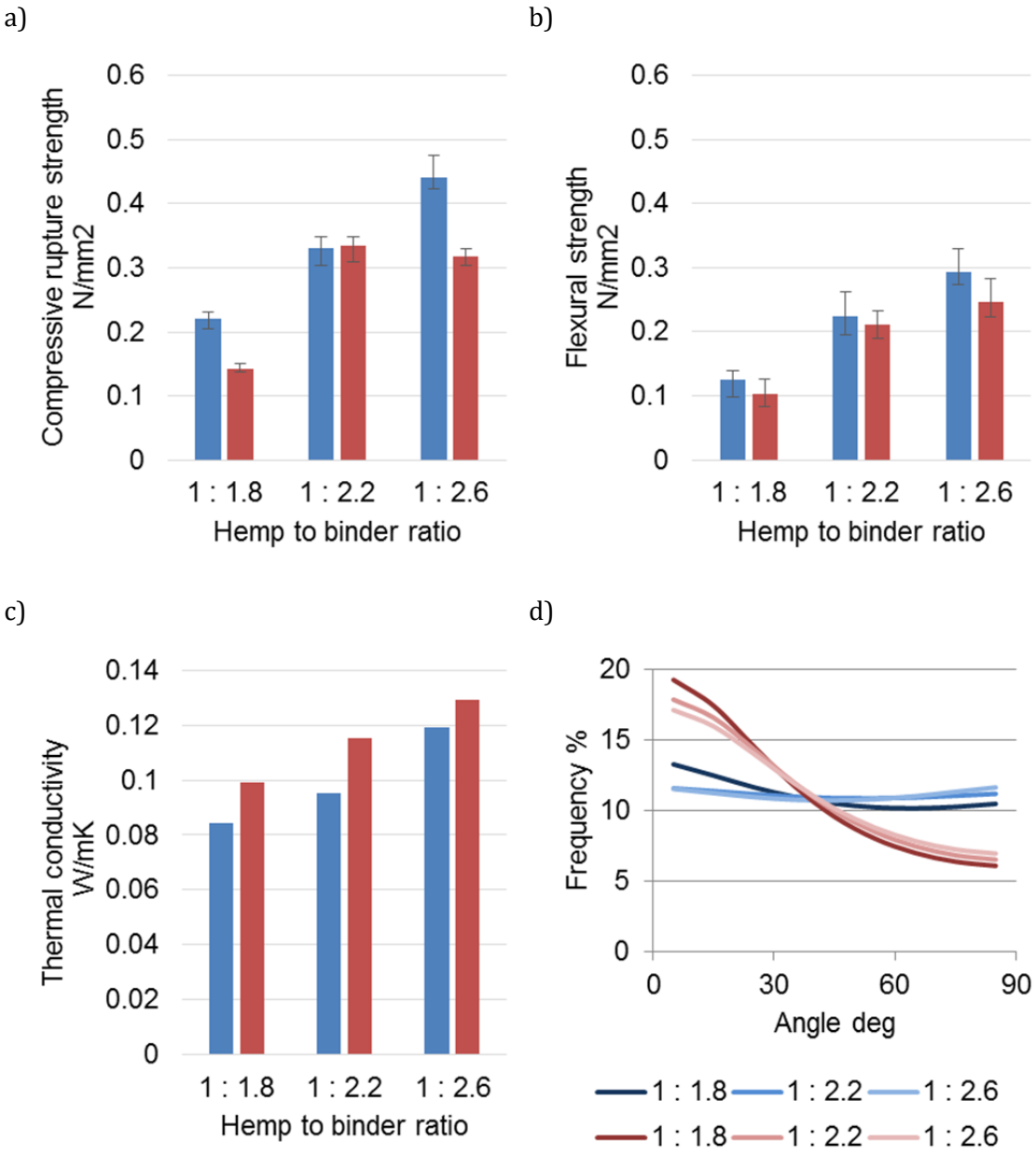

Figure 4 the influence of binder ratio on the compressive rupture stress (top left), flexural strength (top right), thermal conductivity (bottom left) and distribution of

particle orientation (bottom right) obtained from testing/imaging parallel and perpendicular to casting compaction, blue and red respectively.

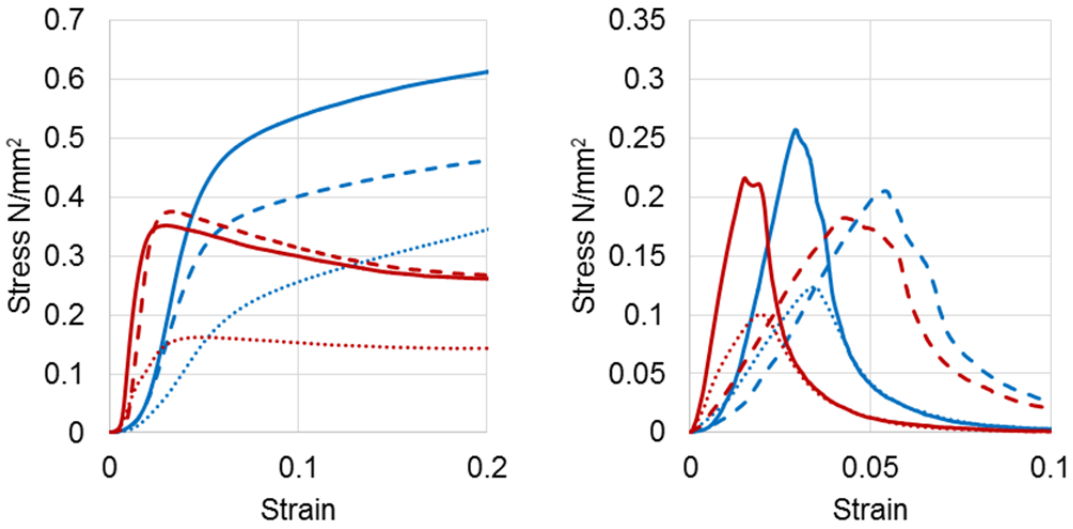

Figure 5 the average stress strain plots of three specimens tested in compression (left) and flexure (right) made with three binder to hemp ratios of 1 : 1.8 (dotted), 1 : 2.2 (dashed) and 1 : 2.6 (solid). Results are presented for both parallel loading (blue) and perpendicular loading (red) with respects to casting compaction.

3.2 The impact of particle size distribution

The compressive rupture stress, flexural strength, thermal conductivity and particle orientation distribution for specimens tested with differing grades of hemp shiv are presented in figure 6 a, b, c and d respectively.

In both the perpendicular and parallel directions there is no correlation between the particle size of hemp aggregates and either the compressive rupture stress, flexural strength or thermal conductivity. Previous studies, often considering only two grades of aggregate, have found both a positive and negative correlation between particle sizes and various physical properties and so in this respect the results can be seen to broadly be in line with previous work. There is however still a distinct and significant difference in both the compressive rupture strength and flexural strength obtained from differing grades of aggregate used: the medium grade is observed to consistently have both the lowest compressive rupture strength and flexural strength in both testing directions. The thermal conductivity in the perpendicular direction was found to be approximately 20% higher than in the parallel direction but again this is independent of grade of aggregate.

For all grades considered, the particle orientation distribution is again observed to be even imaged in the parallel to compaction direction and swayed in the perpendicular orientation. In the perpendicular orientation the sway of the distribution is found most pronounced in the coarse grade and least in the fine grade indicating a possible correlation between shiv grade and degree of particle orientation in the material.

Figure 7 presents the average stress strain plots from the three specimens of material tested of shiv grade in both parallel and perpendicular compression and flexure. From figure 7 the same difference in failure mode between parallel and perpendicular compressive loading is noticed as in figure 5 indicating that this may be independent of both constituent ratio and particle size distribution; again the failure mode in flexure is observed to be consistent in both directions of loading. It can be inferred from figure 7, as was observed in figure 5, that the material has a greater stiffness when loaded perpendicular to initial casting compaction, both in flexure and in compression. In compression it appears that the fine grade of shiv provides the highest stiffness although in general the grade of shiv seems to have limited correlation to this property. In flexure it is observed that the medium grade of shiv provided the lowest stiffness as well as strength and a general trend between stiffness and strength seems to occur.

a)

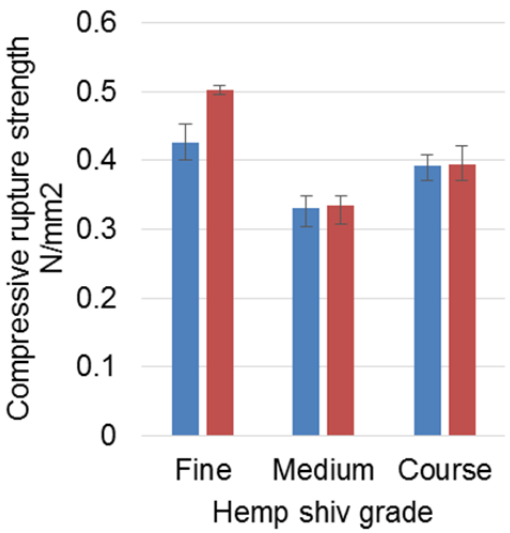

b)

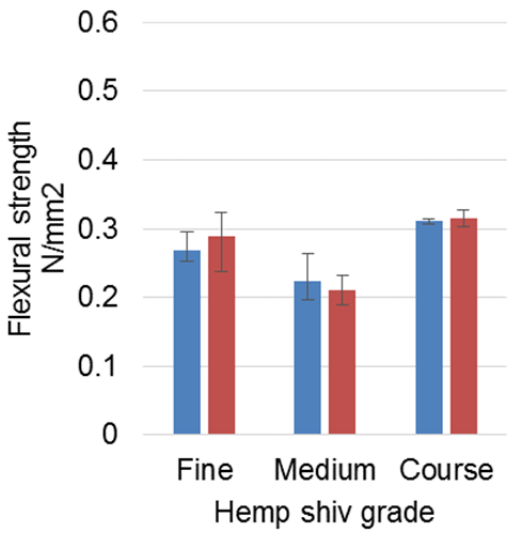

c) d)

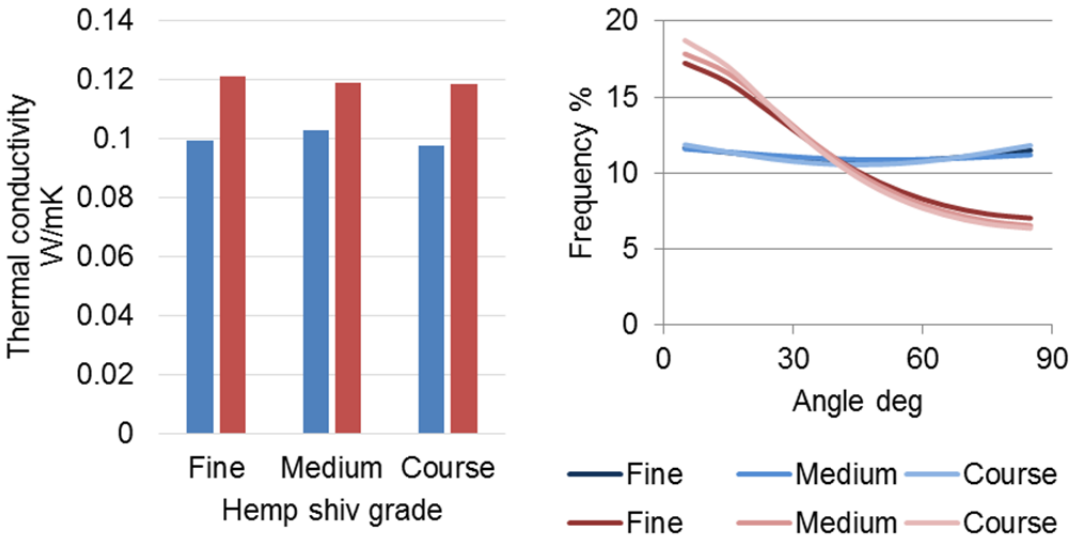

Figure 6 the influence of shiv grade on the compressive rupture stress (top left), flexural strength (top right), thermal conductivity (bottom left) and distribution of particle orientation (bottom right) obtained from testing/imaging in parallel and perpendicular to casting compaction, blue and red respectively.

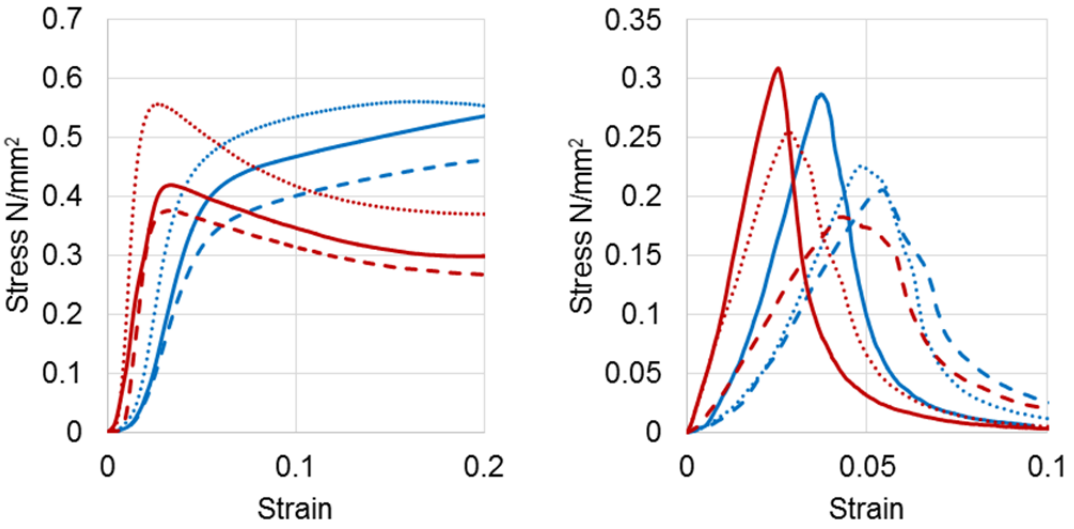

Figure 7 the average stress strain plots of three specimens tested in compression (left) and flexure (right) made with three shiv grades fine (dotted), medium (dashed) and coarse (solid). Results are presented for both parallel loading (blue) and perpendicular loading (red) with respects to casting compaction.

4. Discussion

In the imaging parallel to the direction of casting compaction, the particle orientation distribution was consistently found to be even across all variations of binder content and hemp grade. In contrast, in the perpendicular direction the distribution was consistently found to be swayed towards a horizontal alignment. This is attributed to the compaction applied during the casting process directing the elongated particles of hemp towards stratified planes transverse to compaction. This observation is in line with previous work and also indicated that the process occurs irrespective of binder content or aggregate grade. It can be assumed that all observations of anisotropic properties, present across all specimens, are as a result of this orientated structure.

The degree of orientation can be assessed by how prominent the curve of the graph is for the particle orientation distribution in the perpendicular to compaction imaging direction. In the case of binder content an increasing ratio of binder is observed to seemingly reduce the level of particle orientation. It is questionable however if this trend is significant or just natural variation, the extent of which may be indicated in the results from parallel imaging. In addition there are limited explanations for such an occurrence, the most probable being an increased binder content increasing the separation between particles and limiting the effect of compaction in rotating them.

In the case of aggregate grade, a finer grade was found to also produce a perceived reduction in the level of particle orientation. It can be seen, (table 1), that the mean aspect ratio of the shiv particles is also a product of the shiv grade and thus a finer grade can be considered to produce not only smaller particles but also more rounded ones. This reduction of the aspect ratio is almost certainly likely to lessen the extent to which particles are rotated under compaction and thus offers explanation of the perceived lower degree of orientation.

In all cases the anisotropic internal structure of the material accounts for the clear variation in both mechanical and thermal properties of the material with testing direction. This is found to be most consistent in the thermal conductivity with a significantly lower thermal conductivity for all variations of hemp-lime in the parallel loading direction. As the thermal conductivity is arguably the most important property out of those studied, it can clearly be seen from these results that it is advantageous to have compaction in the same direction as thermal loading. Traditional vertical casting processes are therefore not advantageous in this respect while pre-casting in a perpendicular direction offers a likely benefit.

In the parallel direction, the impact of binder ratio on the thermal conductivity and both the compressive rupture stress and flexural strength can be considered in-line

with previous studies: an increased proportion of binder enhancing the structural skeleton of the material but providing a global densification and increase in thermal conductivity. In the perpendicular direction it is logical to expect a similar trend between increasing binder content and an enhancement of physical properties, and indeed this is observed for the thermal conductivity. For the flexural strength and compressive strength a similar pattern is observed in increasing the binder content from 1:1.8 to 1:2.2 however it is not possible to extrapolate these results. An additional increase to 1:2.6 is found to have a lower than expected improvement in flexural strength, compared to the parallel direction, and a negligible impact on compressive rupture strength. It is likely that at very high binder contents the behaviour will tend to reflect that of the binder in all directions indicating that sensitivity to orientation plateaus.

As particles of hemp are generally elongated in line with the stem of the plant, their porous structure and mechanical properties will also be aligned. Hemp particles and indeed most bio-aggregates could then be considered isotropic themselves with a greater stiffness along the main axis. Parallel to compaction compressive loading hemp-lime can thus be considered as transfer through the binder skeleton, the hemp particles offering limited contribution along their highly compressible secondary axis. This rupture limit would be dependent on the quantity of binder alone. In contrast, in the perpendicular direction, load is likely to be transferred in a more composite action, utilising the stiffer axis of the particles. Rupture in this case can be attributed to a failure of bond between the particles and the binder allowing localised rotational or sheering failure. As the available surface area of the hemp particles is limited, an increase to the binder content once the surface is fully utilised would have a negligible impact on the compressive strength. Such a differing behavioural model may then explain the apparently differing impact of binder content in the different loading directions.

The impact of particle size distribution on the thermal conductivity can be seen from figure 6 to be negligible in both directions. The density of the specimens produced with differing particle size distributions were mostly consistent, (table 2), and so the total porosity may be assumed to be similar and account for this.

The mechanical tests conducted on material of differing particle size distributions show a general correlation between flexural rupture stress and compressive rupture stress although no clear trend between median particle size and the mechanical properties. This is consistent with the mixed results found within the literature that report in

separate studies increasing coarseness having a positive and negative impact on mechanical properties.

The properties of hemp-lime and other bio-aggregate composites are often presented with respect to weight of material as it is a general trend observed widely in the literature that mechanical resistance as well as thermal conductivity increase with density. Figure 8 plots the results from both mechanical tests and the thermal conductivity test against material average dry density values. Lines of best fit added to the data confirm the positive correlation between the properties mentioned and density that is in line with results elsewhere in the literature.

In general the binder ratio is found to fit closely to the line of best fit in all cases, figure 8, in both parallel and perpendicular measurements with the exception of perpendicular loading. This is indicative of the observed increases in these properties being broadly associated to the increase in density of the material and thus effective structure as well as the previously discussed consideration that the perpendicular compressive strength exhibits a plateau as a certain binder content due to the mechanism of load transfer in the material.

The grading of the particle size is seen from figure 8 to have a more complex relation to density and to other physical properties. It is noticeable that the coarse aggregate is consistently producing stronger and more thermally conductive material than would be obtained at a similar density produced using the medium aggregate and a lower ratio of binder. This may be attributed to the larger aggregates providing a more direct thermal path and continuous loading path. The coarse particles produced a naturally less dense material while the fine grade of shiv a naturally more dense material. This might be accounted for by the improved natural packing of particles with a lower average aspect ratio. When considered against the line of best fit, the fine grade of shiv gives no obvious benefit in terms of mechanical behaviour and so the observed benefits found in figure 5 can be attributed to the increase in density. Conversely it may also be noted that finer particles might give a lower thermal conductivity than may be expected for equivalent density material with a medium grade of shiv and higher binder content. This is likely attributed to the inverse of the coarser particles providing higher thermal conductivity suggesting a link between thermal conductivity and average particle size.

From table 2 and figure 1 it is not obviously apparent what aspect of the coarse grade of shiv might account for the seeming mechanical over performance. What is considered likely in light of these results is that a combination of factors inherent to the particle size distribution combine to determine the impact on mechanical performance.

It is considered likely that this will include the mean length of particles, mean aspect ratio of particles and spread of distribution. Further study where such variables are isolated and assessed is required to establish this and could lead to easily obtainable performance increases.

A possible limitation of the presented results is the omission of testing at other material ages beyond 28 days. It is known that hemp-lime can continue to develop strength past 28 days due to the continued carbonation of the lime binder although this has been shown to vary in magnitude according to the binder and conditions of material storage. It has been previously suggested in other studies that the particle size distribution may alter the permeation of carbon dioxide into the materials and thus alter the rate of carbonation. In this particular case, in light of the binder being known to have a significant hydraulic set and being comparable to some other previously studied binders, the potential strength gains through ongoing carbonation are considered likely to be negligible; the results are therefore considered likely to be applicable to materials tested at greater ages. It is not clear and indeed unlikely that this would be replicated for pure lime binders and further work on the combined impact of aging and particle size distribution would be a useful topic for future study.

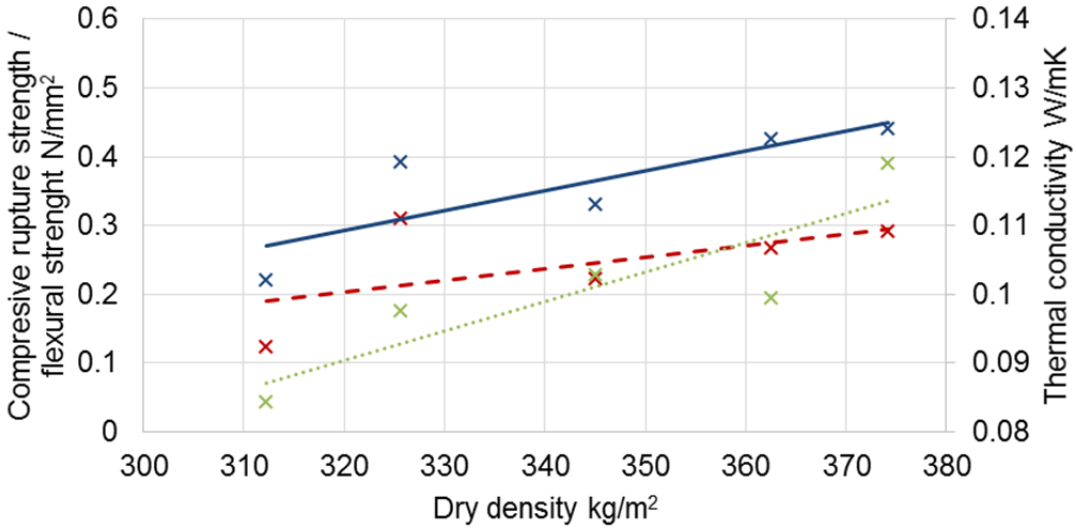

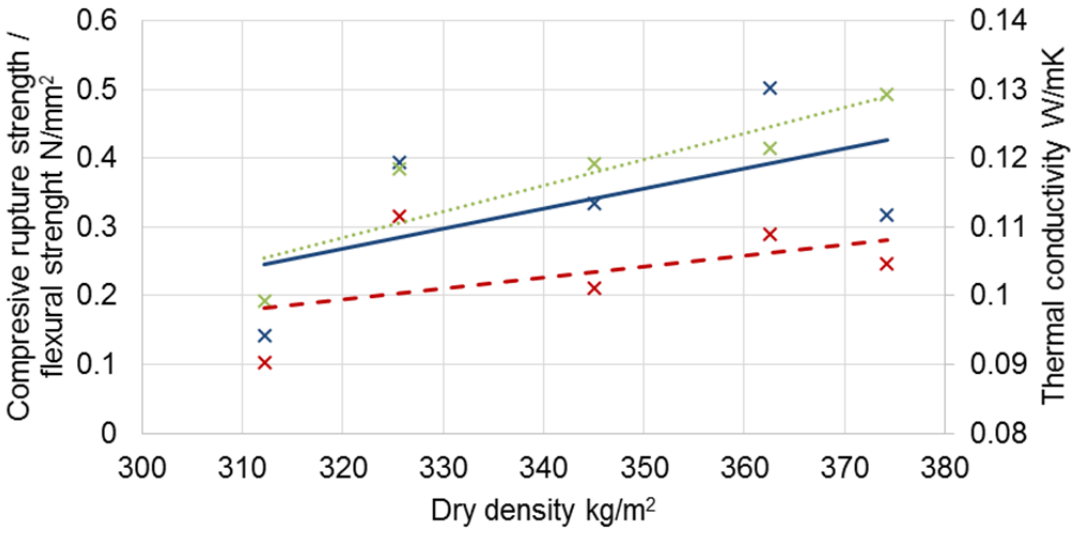

Figure 8 the compressive rupture strength (blue solid line), flexural strength (red dashed line) and thermal conductivity (green dotted line) plotted against dry density for parallel and perpendicular load to casting compaction, top and bottom respectively.

5. Conclusion

Compressive and flexural tests were carried out on hemp-lime specimens produced with a range of hemp to binder ratios and particle size distributions. In all cases the internal structure of the material was also assessed by means of two dimensional image analysis. A general anisotropy was observed in all the specimens by means of this method indicating the production process used imparts a preferential direction to the particle and thus structure of the material. The results further indicate that the degree of orientation may be linked to both the particle size distribution and the aggregate to binder ratio. Given that most bio-aggregates have a similar elongated form to hemp particles, the trends identified in this respect are considered likely to be repeated across other bio-aggregates and merits additional investigation.

Increasing the binder ratio was, as expected, found to increase the thermal conductivity globally as well as the flexural strength in both the perpendicular and parallel directions, attributed to an increase of the stiffer, denser and more thermally conductive component. The compressive strength was observed to follow this trend in the parallel direction however in the perpendicular direction the beneficial effect of the binder was seen to plateau above a hemp to binder ratio of 1:2.2. This is considered to be a result of a different load transfer mechanism in this direction. This finding has

implications for both manufacturers as well as future research as most behavioural models and rules of thumb assume isotropic impacts of binder content.

Where previous studies have provided contradictory results as to how the particle size influences the mechanical properties of hemp-lime composites, this study has identified no clear relation between median length of particle and any physical properties. Rather it was observed that uniformity of particle sizes has a beneficial influence on the mechanical properties, independent of the average particle size and may account for the mixed results of others. This may have an implication for manufacturers of bio-aggregate particles and the development of more engineered products.

6. References

[1] Arizzi A, Cultrone G, Brümmer M, Viles H. A chemical, morphological and mineralogical study on the interaction between hemp hurds and aerial and natural hydraulic lime particles: Implications for mortar manufacturing. Construction and Building Materials. 2015;75:375-84.

[2] Walker R, Pavia S, Mitchell R. Mechanical properties and durability of hemp-lime concretes. Construction and Building Materials. 2014;61(0):340-8.

[3] Elfordy S, Lucas F, Tancret F, Scudeller Y, Goudet L. Mechanical and thermal properties of lime and hemp concrete ("hempcrete") manufactured by a projection process. Construction and Building Materials. 2008;22(10):2116-23.

[4] Magniont C, Escadeillas G, Coutand M, Oms-Multon C. Use of plant aggregates in building ecomaterials. European Journal of Environmental and Civil Engineering. 2012;16(sup1):s17-s33.

[5] Nozahic V, Amziane S, Torrent G, Saïdi K, De Baynast H. Design of green concrete made of plant-derived aggregates and a pumice–lime binder. Cement and Concrete Composites. 2012;34(2):231-41.

[6] Chabannes M, Nozahic V, Amziane S. Design and multi-physical properties of a new insulating concrete using sunflower stem aggregates and eco-friendly binders. Materials and Structures. 2015;48(6):1815-29.

[7] Ning L, Bing C. Experimental Investigation Concrete Using Magnesium Phosphate Cement, Fly Ash, and Rape Stalk. Journal of Materials in Civil Engineering. 2015;28(4):04015163.

[8] B Laidoudi CF, A Crigny, J Ferrari, G Glazy, B Dupre. Bio based concrete with crushed rape straw, a good alternative to develop an affordable bio based concrete for construction and regeneration. First international conference on bio-based building materials Clermont-Frrrand, France. 2015.

[9] Bevan R, Woolley T, Pritchett I, Carpenter R, Walker P, Duckett M. Hemp Lime Construction: a guide to building with hemp lime composites: BRE Press; 2008.

[10] Boutin M, Flamin C, Quinton S, Gosse G. Etude des caractéristiques environnementales du chanvre par l'analyse de son cycle de vie Ministère de l'agriculture et de la pèche, Paris. 2006.

[11] Ip K, Miller A. Life cycle greenhouse gas emissions of hemp–lime wall constructions in the UK. Resources, Conservation and Recycling. 2012;69(0):1-9.

[12] Pretot S, Collet F, Garnier C. Life cycle assessment of a hemp concrete wall: Impact of thickness and coating. Building and Environment. 2014;72(0):223-31.

[13] Arnaud L, Samri D, Gourlay É. Hygrothermal Behavior of Hempcrete. Bio-aggregate-based Building Materials: John Wiley & Sons; 2013. p. 179-242.

[14] Collet F, Pretot S. Experimental highlight of hygrothermal phenomena in hemp concrete wall. Building and Environment. 2014;82(0):459-66.

[15] Evrard A. Transient hygrothermal behaviour of lime-hemp materials [PhD]: Universite catholique de louvain; 2008.

[16] Benfratello S, Capitano C, Peri G, Rizzo G, Scaccianoce G, Sorrentino G. Thermal and structural properties of a hemp–lime biocomposite. Construction and Building Materials. 2013;48(0):745-54.

[17] Murphy F, Pavia S, Walker R. An assessment of the physical properties of lime-hemp concrete. Proceeding of the bridge and concrete research in Ireland, Cork. 2010.

[18] Tronet P, Lecompte T, Picandet V, Baley C. Study of lime hemp concrete (LHC) – Mix design, casting process and mechanical behaviour. Cement and Concrete Composites. 2016;67:60-72.

[19] Arnaud L, Amziane S, Nozahic V, Gourlay E. Mechanical Behavior. Bio-aggregate-based Building Materials: John Wiley & Sons; 2013. p. 153-78.

[20] Hustache Y, Arnaud L. Synthèse des connaissances sur les bétons et mortiers de chanvre. Construire en Chanvre; 2008.

[21] Balčiūnas G, Vėjelis S, Vaitkus S, Kairytė A. Physical Properties and Structure of Composite Made by Using Hemp Hurds and Different Binding Materials. Procedia Engineering. 2013;57(0):159-66.

[22] Williams J, Lawrence M, Walker P. A method for the assessment of the internal structure of bio-aggregate concretes. Construction and Building Materials. 2016;116:45-51.

[23] Cigasova J, Stevulova N, Junak J. Properties monitoring of fibrous composites based on hemp hurds with different mean particle size. Pollack Periodica. 2013;8(2):41-6.

[24] Stevulova N, Kidalova L, Cigasova J, Junak J, Sicakova A, Terpakova E. Lightweight Composites Containing Hemp Hurds. Procedia Engineering. 2013;65:69-74.

[25] Ceyte I. Béton de chanvre, définition des caractéristiques mécaniques de la chènevotte (Hemp concrete , definition of mechanical characteristics). Travail de Fin d'Études, ENTPE. 2008;155:2008.

[26] Pierre T, Colinart T, Glouannec P. Measurement of Thermal Properties of Biosourced Building Materials. Int J Thermophys. 2014;35(9-10):1832-52.

[27] Youssef A, Lecompte T, Picandet V, Challamel N. Compressive and shearing behaviour of lime and hemp concrete. First international conference on bio-based building materials. Clermont-Ferrand, France. 2015.

[28] Nguyen TT, Picandet V, Carre P, Lecompte T, Amziane S, Baley C. Effect of compaction on mechanical and thermal properties of hemp concrete. European Journal of Environmental and Civil Engineering. 2010;14(5):545-60.

[29] Picandet V. Characterization of Plant-Based Aggregates. Bio-aggregate-based Building Materials: John Wiley & Sons, Inc.; 2013. p. 27-74.

8.3 Image sequences

8.3.1 Flexure

8.3.1.1 Cast 25 45

Parallel	Strain	Perpendicular
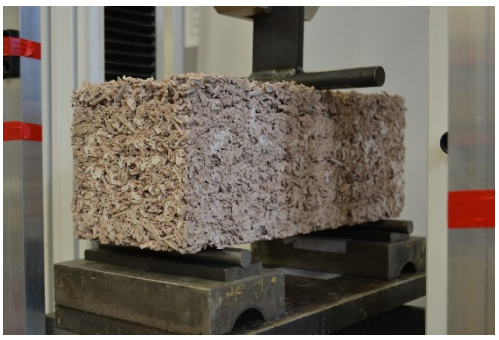	0%	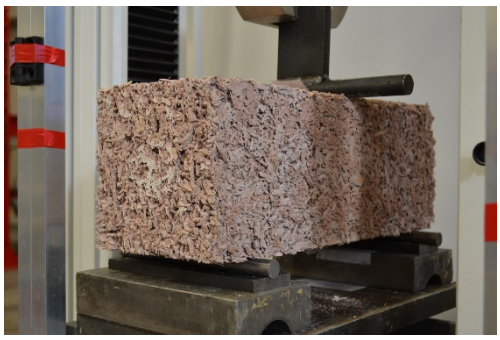
	5%	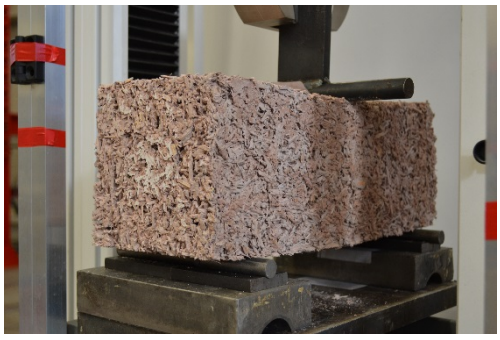
	10%	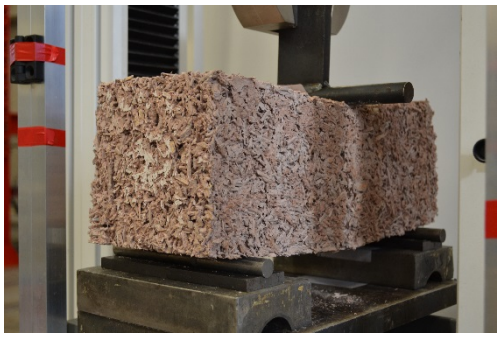
	15%	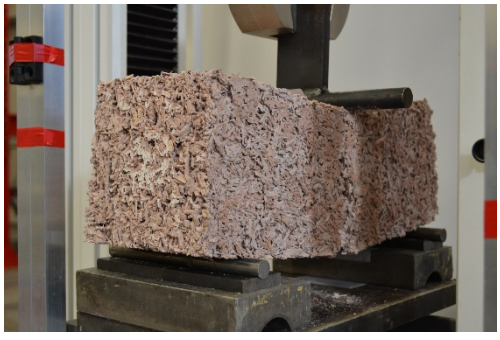

8.3.1.2 Cast 50 30

Parallel	Strain	Perpendicular
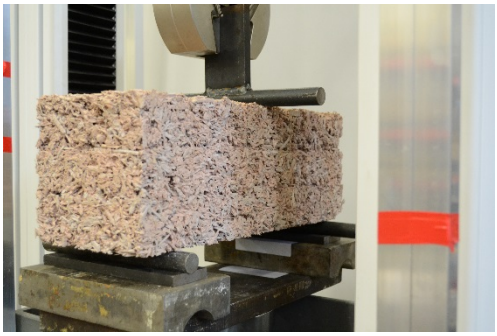	0%	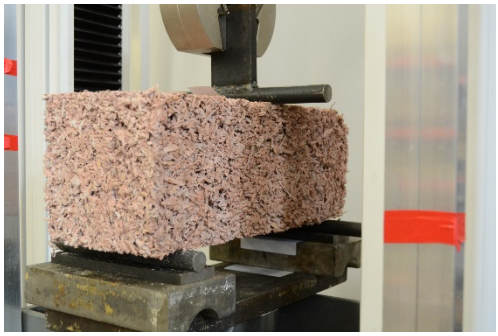
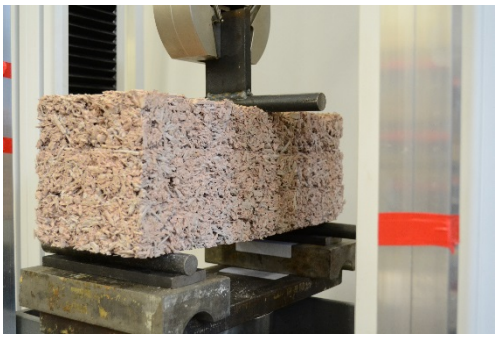	5%	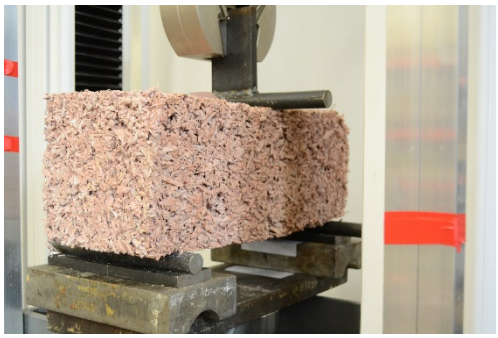
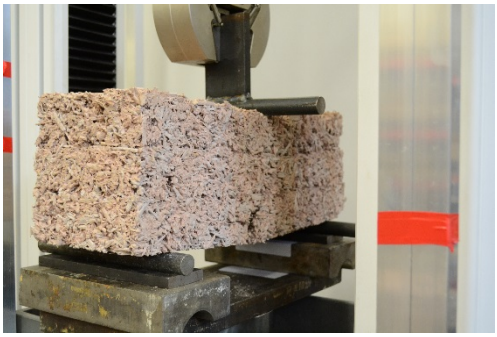	10%	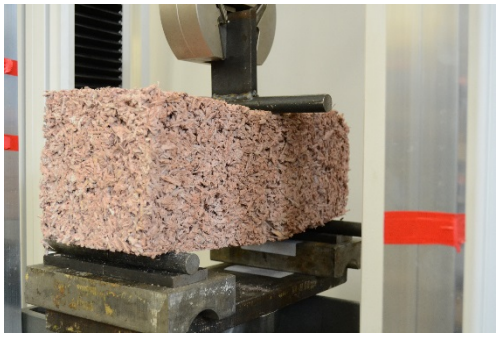
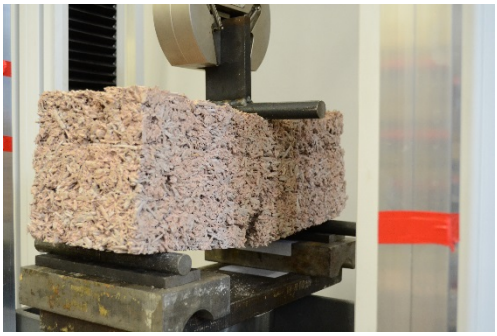	15%	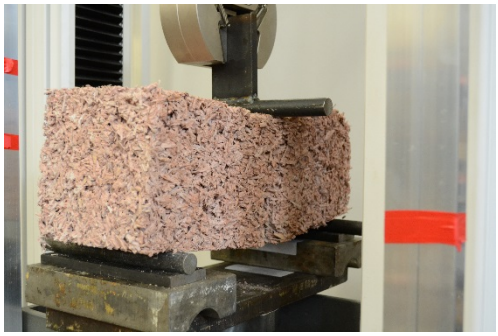

8.3.1.3 Cast 50 60

Parallel	Strain	Perpendicular
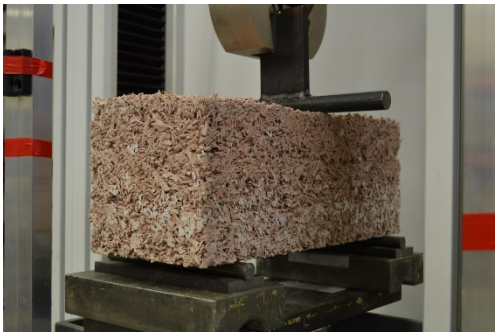	0%	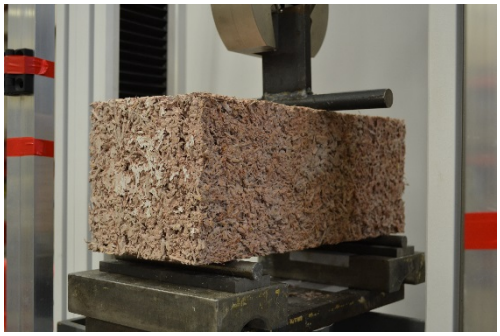
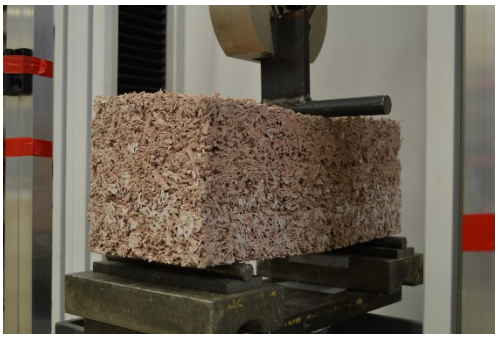	5%	
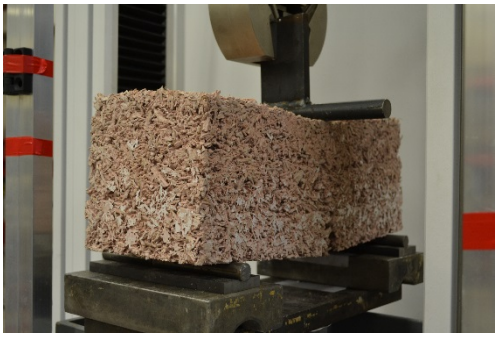	10%	
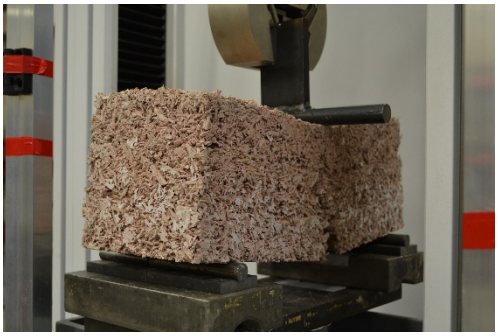	15%	

8.3.1.4 Cast 150 45

Parallel	Strain	Perpendicular
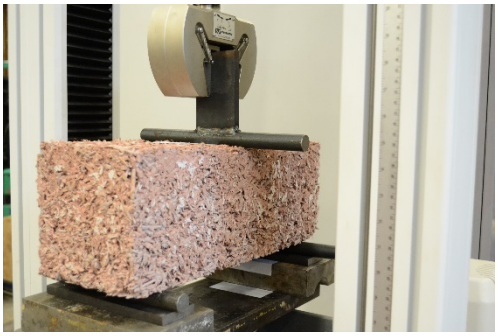	0%	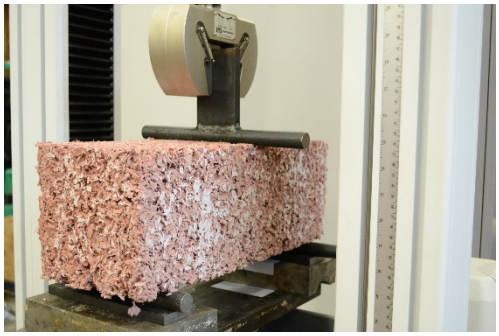
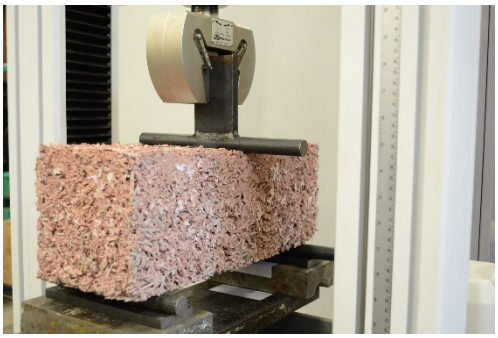	5%	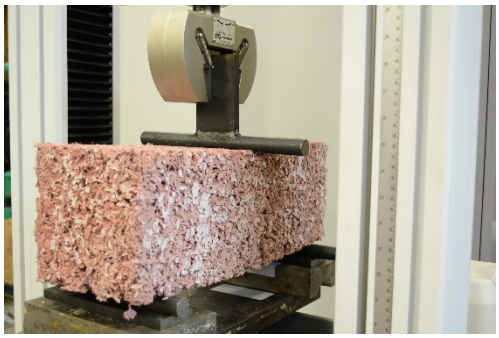
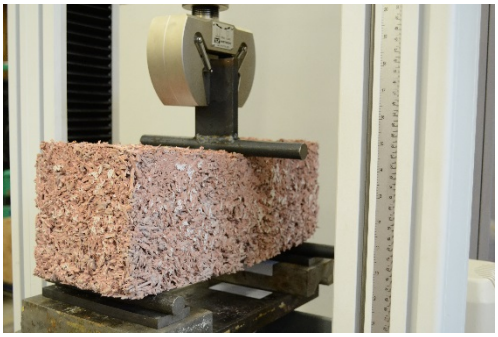	10%	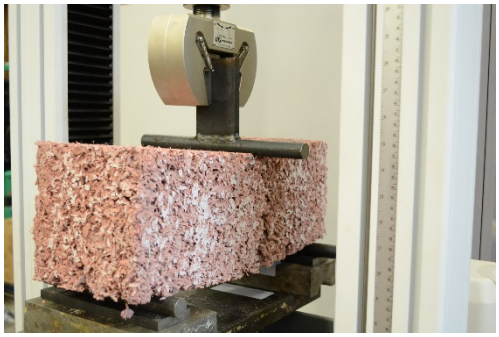
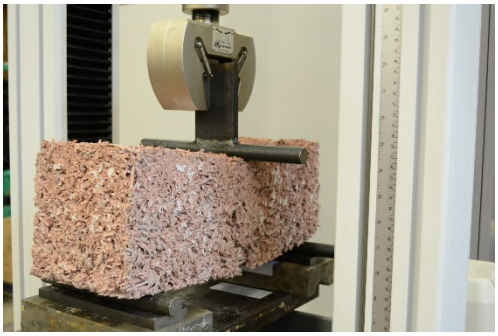	15%	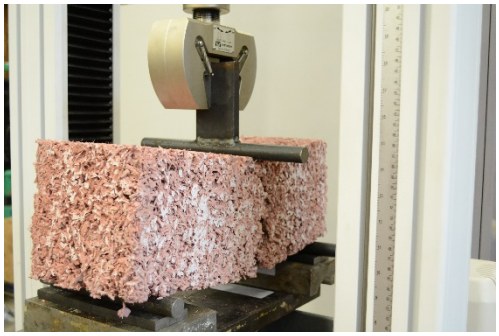

8.3.1.5 Coarse 2.2

Parallel	Strain	Perpendicular
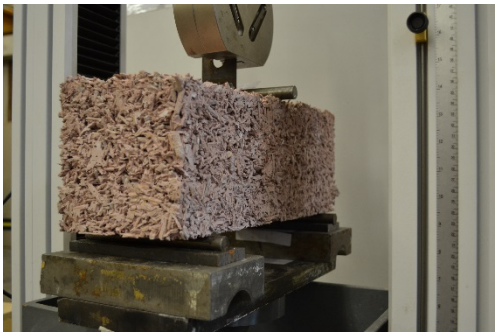	0%	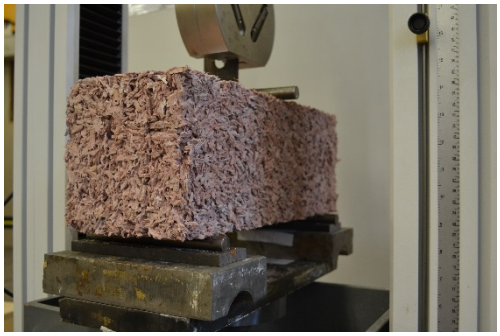
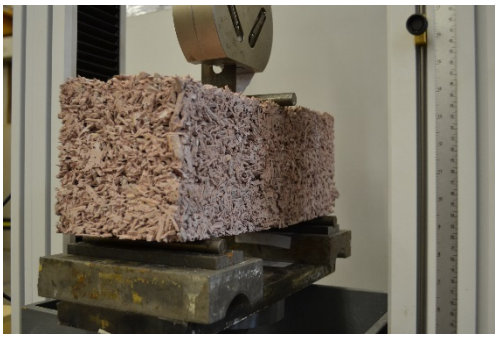	5%	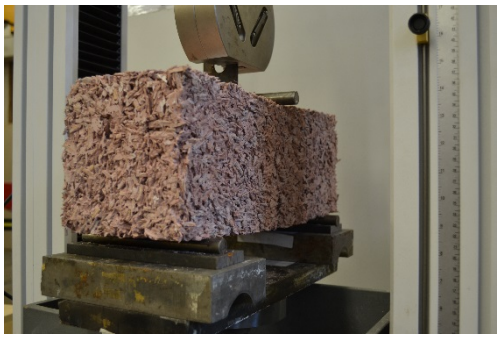
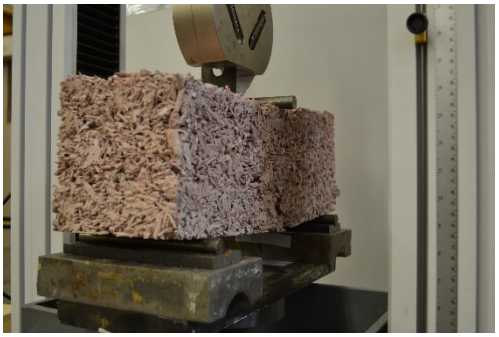	10%	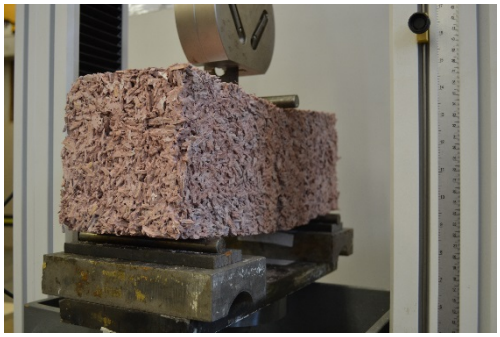
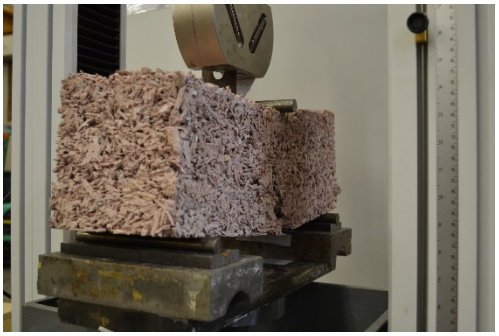	15%	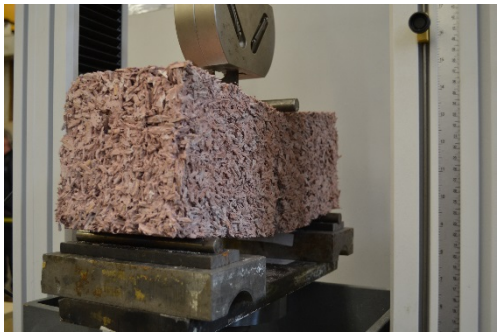

8.3.1.6 Fine 2.2

Parallel	Strain	Perpendicular
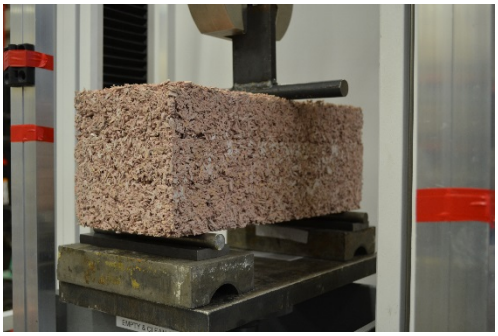	0%	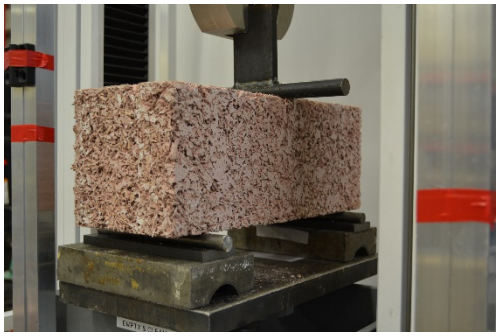
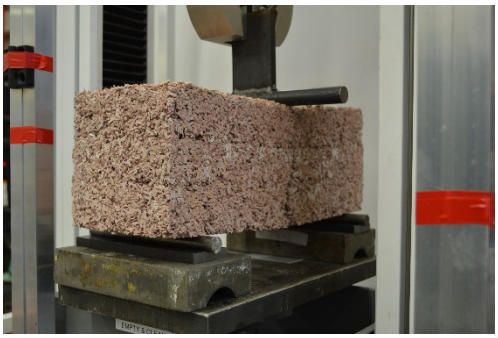	5%	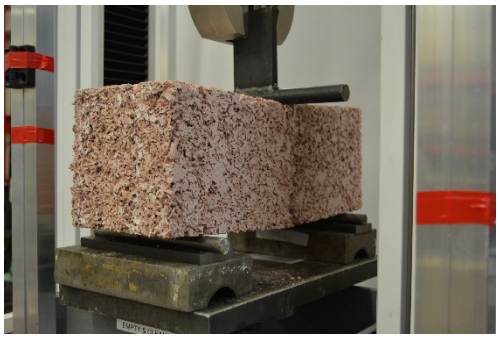
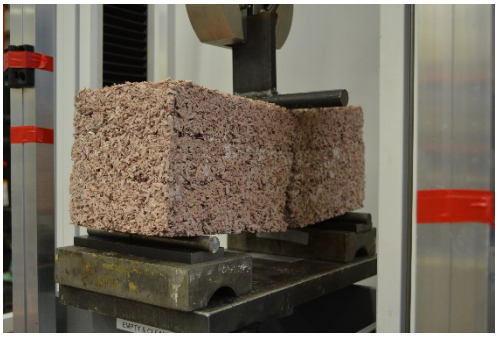	10%	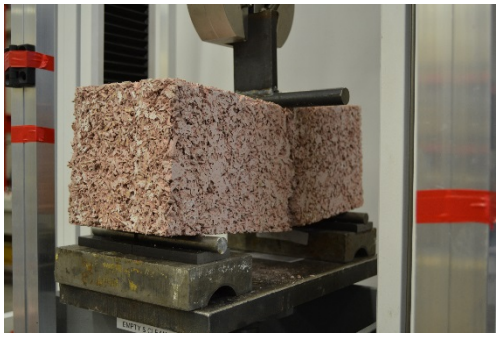
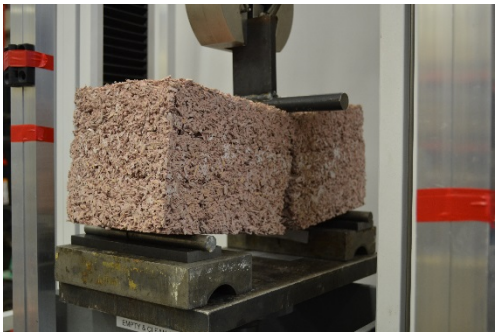	15%	

8.3.1.7 Medium 1.8

Parallel	Strain	Perpendicular
	0%	
	5%	
	10%	
	15%	

8.3.1.8 Medium 2.6

Parallel	Strain	Perpendicular
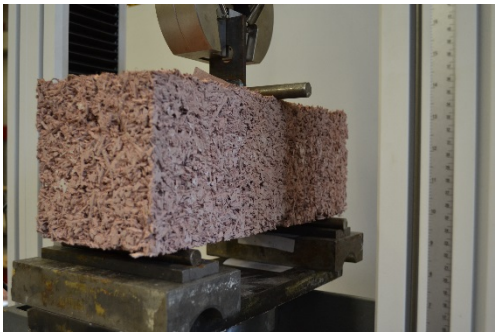	0%	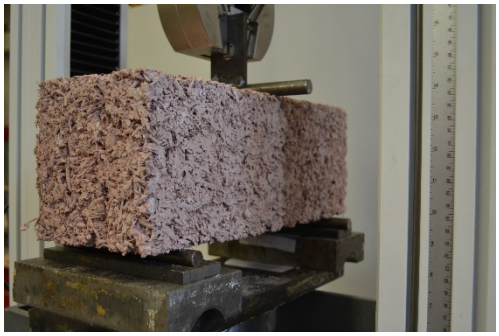
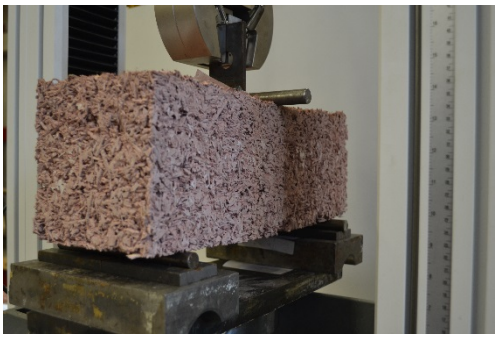	5%	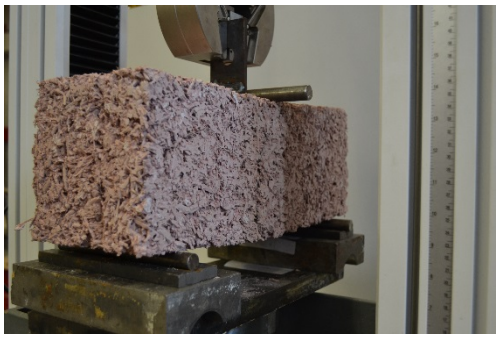
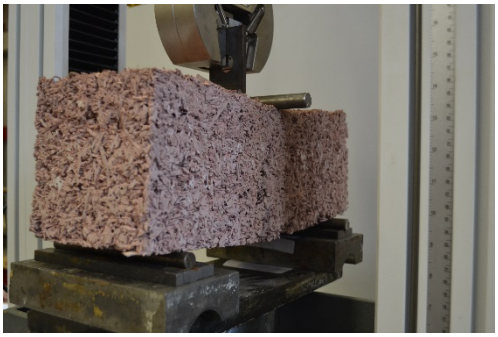	10%	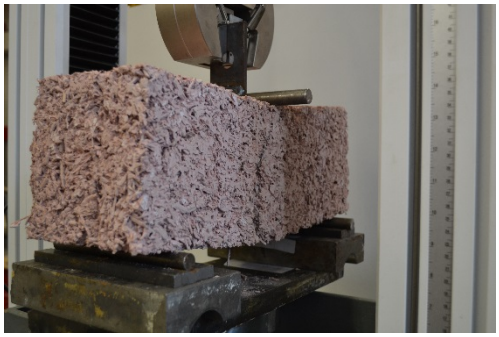
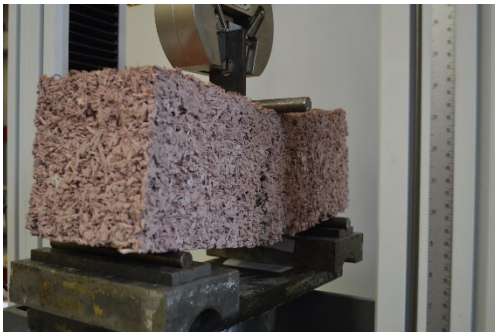	15%	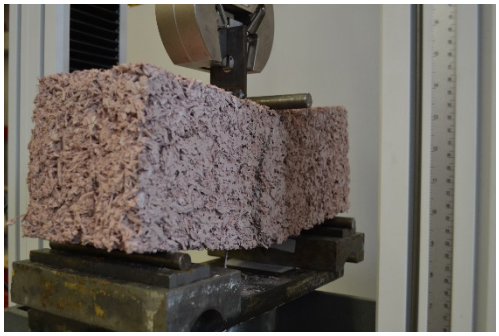

8.3.2 Compression

8.3.2.1 Cast 25 45

Parallel	Strain	Perpendicular
	0%	
	5%	
	10%	
	15%	

8.3.2.2 Cast 50 30

Parallel	Strain	Perpendicular
	0%	
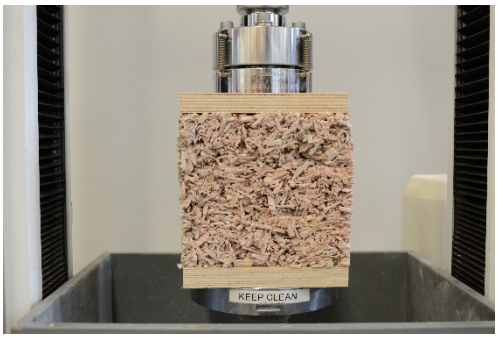	5%	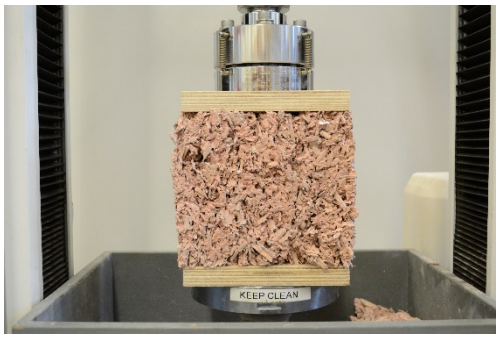
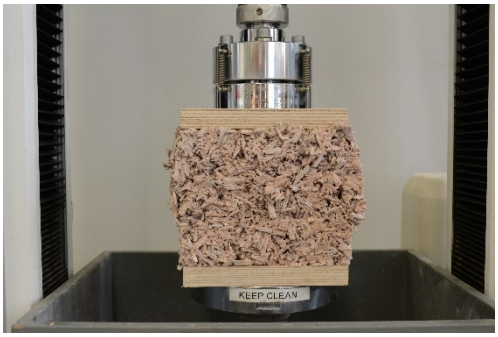	10%	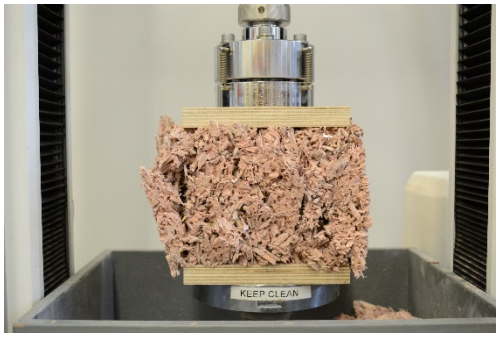
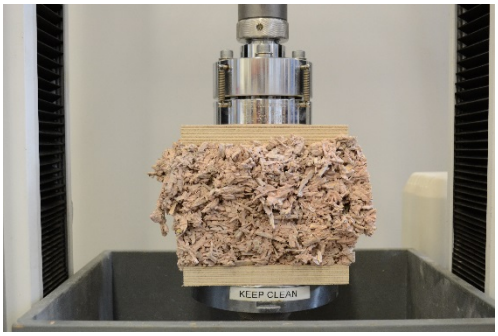	15%	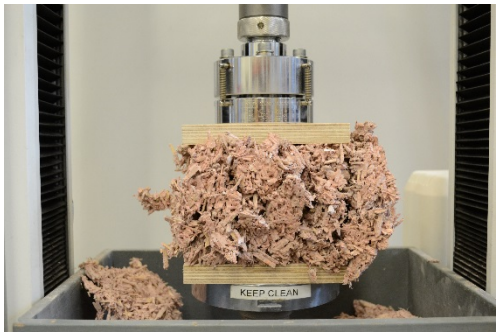

8.3.2.3 Cast 50 60

Parallel	Strain	Perpendicular
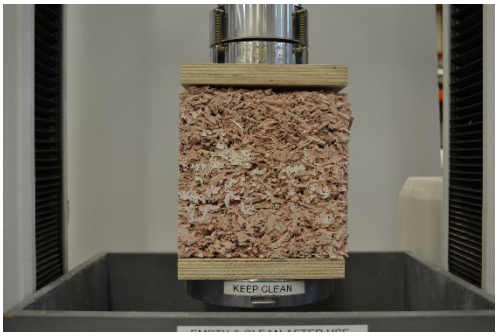	0%	
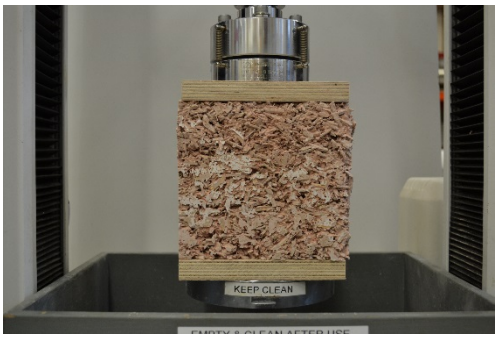	5%	
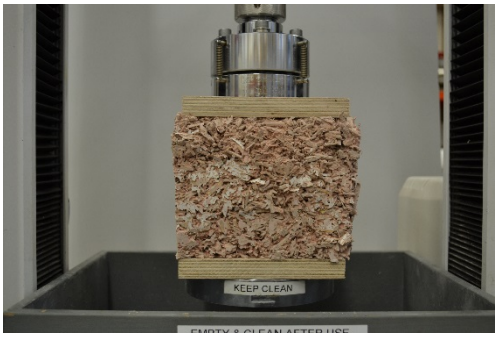	10%	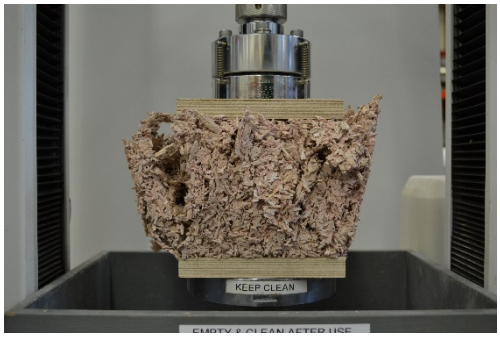
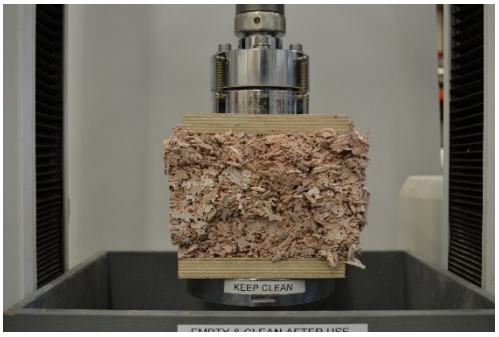	15%	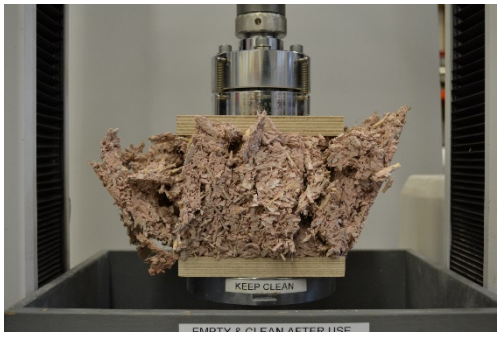

8.3.2.4 Cast 150 45

Parallel	Strain	Perpendicular
	0%	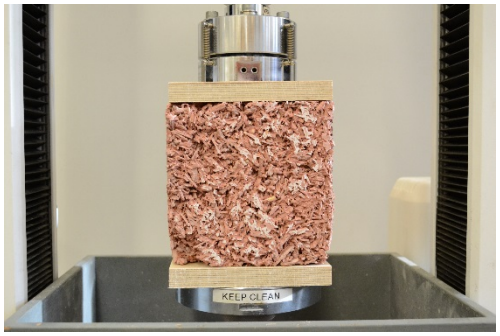
	5%	
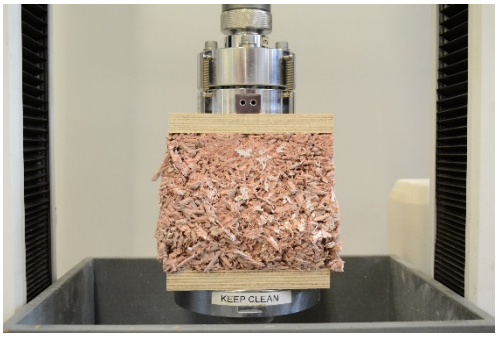	10%	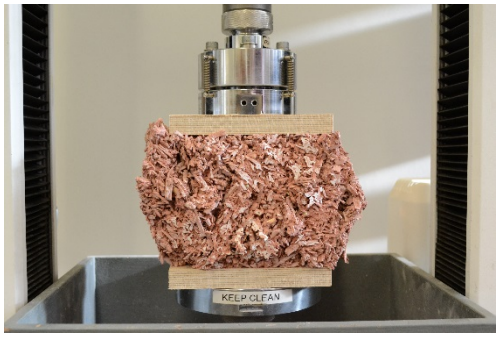
	15%	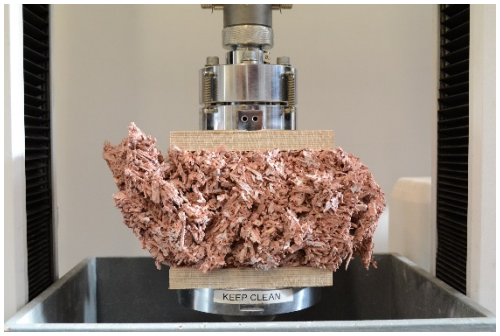

8.3.2.5 Coarse 2.2

Parallel	Strain	Perpendicular
	0%	
	5%	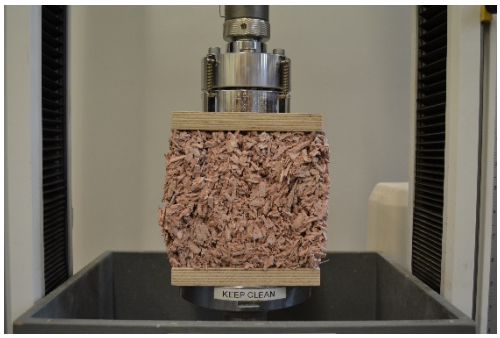
	10%	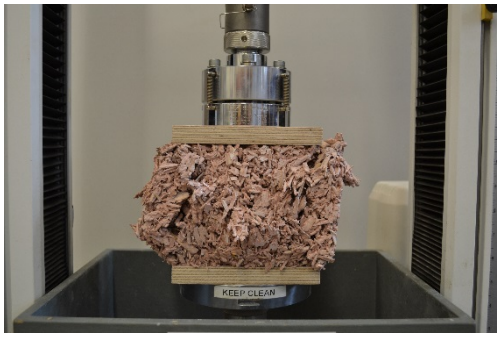
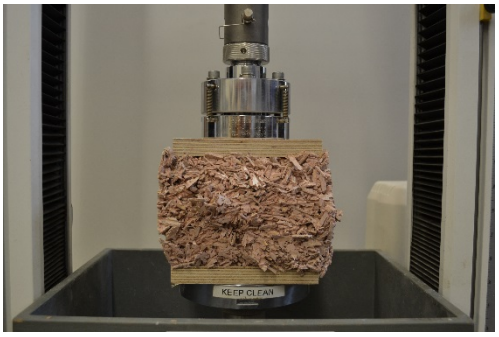	15%	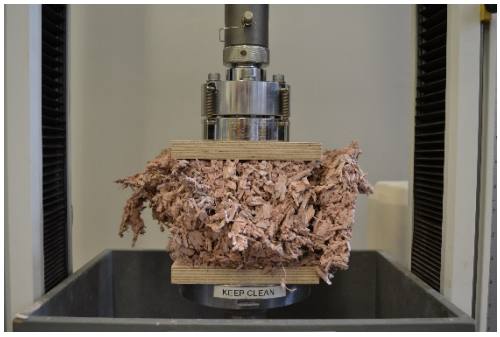

8.3.2.6 Fine 2.2

Parallel	Strain	Perpendicular
	0%	
	5%	
	10%	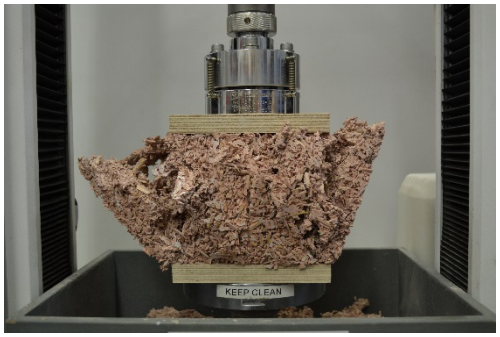
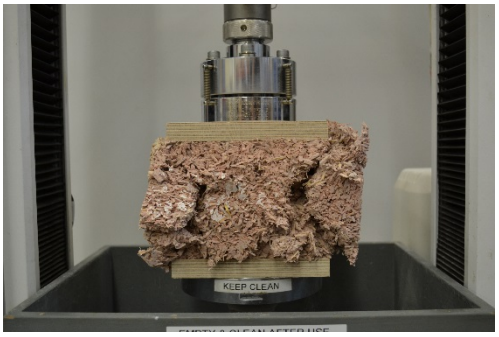	15%	

8.3.2.7 Medium 1.8

Parallel	Strain	Perpendicular
	0%	
	5%	
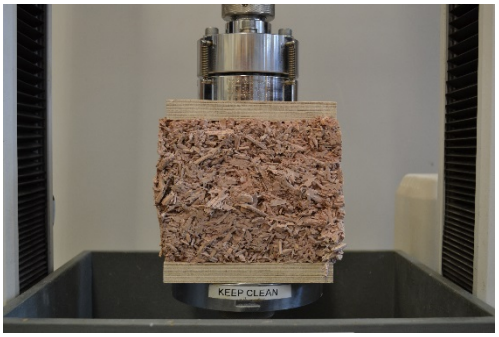	10%	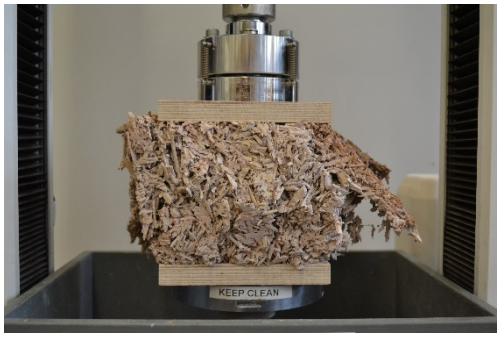
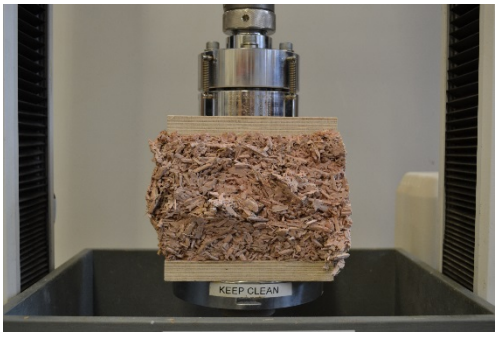	15%	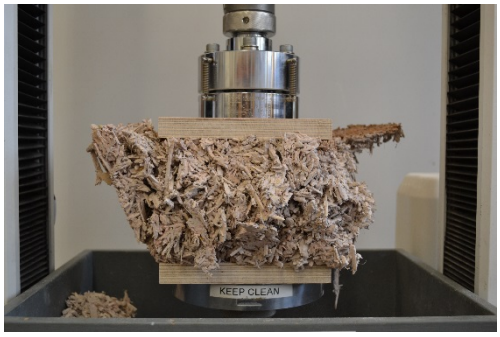

8.3.2.8 Medium 2.6

Parallel	Strain	Perpendicular
	0%	
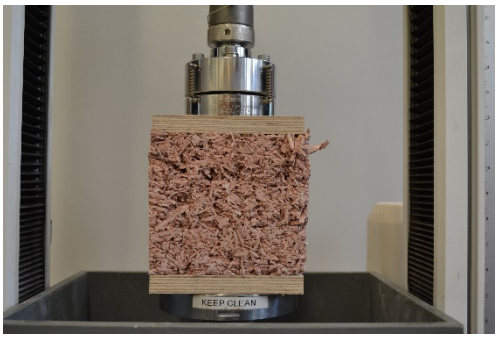	5%	
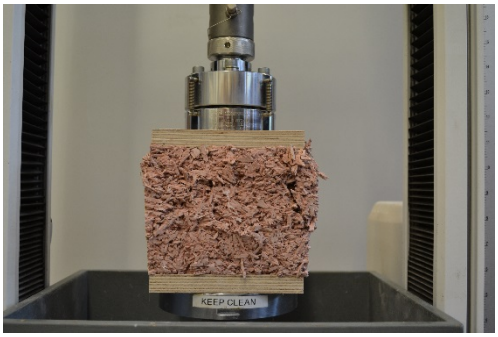	10%	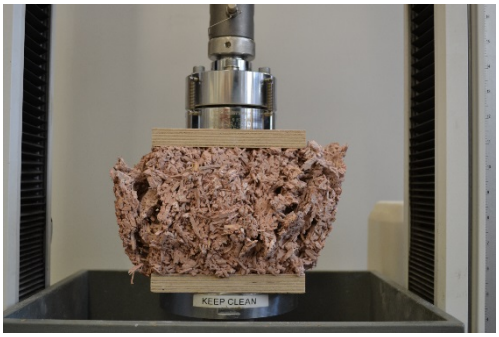
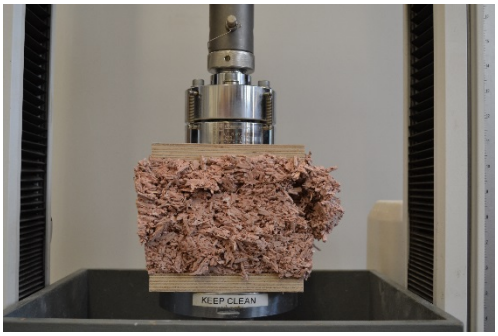	15%